COMPLEX FORMATION OF 1,4-DIAZABICYCLO[2.2.2]OCTANE WITH COPPER(II) TETRASULFOPHTHALOCYANINE IN AQUEOUS SOLUTION

Alena Voronina, Natalya Litova, Ilya Kuzmin, Mihail Razumov, Artur Vashurin, Maxim Shepelev and Svetlana Pukhovskaya

Keywords: water-soluble phthalocyanine, solution, complex formation, DABCO, spectroscopy

The self-association in the formation of copper tetrasulfophthalocyanine complex and 1,4-diazabicyclo[2.2.2.]octane (DABCO) in aqueous solution are reported. Formation of phthalocyanine π-π dimers and a CuPc-DABCO complex could be confirmed, however, formation of sandwich-type dimers could not be detected.

* Corresponding Authors
E-Mail: asvashurin@mail.ru
[a] Ivanovo State University of Chemistry and Technology, Ivanovo, 153000 Sheremetevsky str. 7, Russia

Introduction

Transition metal complexes of water-soluble phthalocyanine derivatives are used as high-performance catalyst in different oxidation processes in organic chemistry,[1-4] as photosensitizers in photodynamic therapy of cancer[5-7] and as inactivators of bacteria and virus.[8,9] Mechanisms of catalytic and biological action of such compounds are based on processes of molecular ligands coordination with central metal cation.[10,11]

Association of macromolecules in aqueous medium is the main trouble while using water solution of metalophthalocyanine. That process reduces their useful properties.[12-14] Linked π-electron system, that is located above and below the plane of the molecule, plays the main role in aggregation of metalophthalocyanines.[15,16] The central metal cation forming π-π dimer becomes isolated for ligand coordination. The second important factor affecting the associative balance is solvation.

It is possible to control the balance of monomer-dimer forms in water solution of metalophthalocyanines by changing the molecular complexation processes and solvating ability of medium.

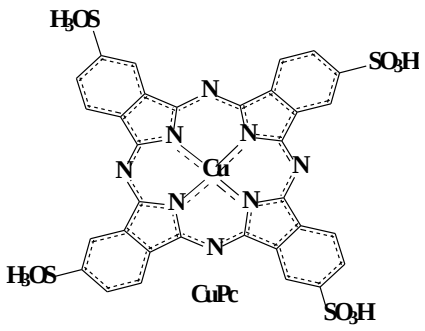

Scheme 1. Structure of copper tetrasulfophthalocyanine complex

Associated form of copper metalophthalocyanine complex in water solution and its molecular complexation with 1,4-diazobisyclo[2.2.2]octane are reported.

Materials

Copper tetrasulfophthalocyanine (CuPc) is synthesized and purified by a known "direct sulfonation" method.[17] Its composition and structure is confirmed by electron-absorbtion spectroscopy, IR spectroscopy and elemental analyzes. IR-spectra were recorded on the Avatar 360 FT-IR spectrophotometer using KBr tablets. , There are intense bands at 700, 1032-1035, 1192-1197 cm^{-1}, it is caused by presence of sulfonic groups. Oscillation in 839-855 cm^{-1} is caused by C-H vibrations of three-substituted benzene nuclei connecting with porfirazine ring. IR-spectra matched with literature data.[18] UV-Vis spectra were recorded in the frequency range 400 – 4000 cm^{-1}.

Commercial product (DABCO) 1,4-diazabicyclo[2.2.2]octane (Sigma-Aldrich) with 99.98% purity was used without additional purification. Degased bidistilled water was used for preparing the solutions.

The coordination process of DABCO was studied spectrophotometrically. Electronic absorption spectra were recorded on a double-beam Shimadzu UV 1800 spectrophotometer. Investigations were carried out at 298.15 K using 10 mm quartz cuvettes, placed in a thermostatic cell.

Results and discussion

Association of metalophthalocyanine sulfonated derivatives in water solution is reported in the literature, which suggests[19-23] its ability to aggregate through the formation of dimers due to the overlap of π-electron systems of macrocycles. The thermodynamic parameters of associative monomer-dimer equilibrium in water-organic environment are also studied in this works.

UV-Vis spectra of CuPc at different dilutions in water

$$2CuPc \overset{K}{\rightleftarrows} (CuPc)_2 \qquad (1)$$

(Fig.1), suggests dimerization of CuPc (c $2\cdot10^{-7}$ to $2\cdot10^{-4}$ mol L^{-1}) in water.

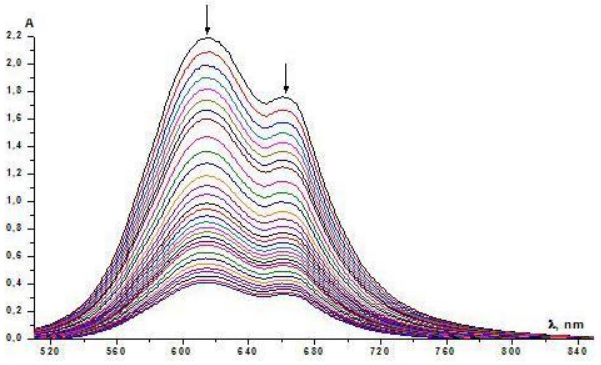

Figure 1. UV-Vis spectra's changing upon diluting of CuPc water solution ($c = 8\cdot10^{-4}$ to $2\cdot10^{-7}$ mol L^{-1}) at 298.15 K

Both dimeric and high-order associations are observed in aqueous solution. Associated forms of CuPc absorbs light in the 615-620 nm, monomeric forms (*Q*-band) in the 662-665 nm.[19,24] Changing ratio of intensities $\lambda_{620}/\lambda_{665}$ has a non-linear character. At the first stage there is a consistent increase of the ratio, it reflects the shift of equilibrium (1) to the monomerization of macrocycle. When the concentration of CuPc reaches about $3\cdot10^{-5}$ mol L^{-1}, the ratio becomes constant. This fact indicates equilibrium between monomeric and associated forms in process (1).

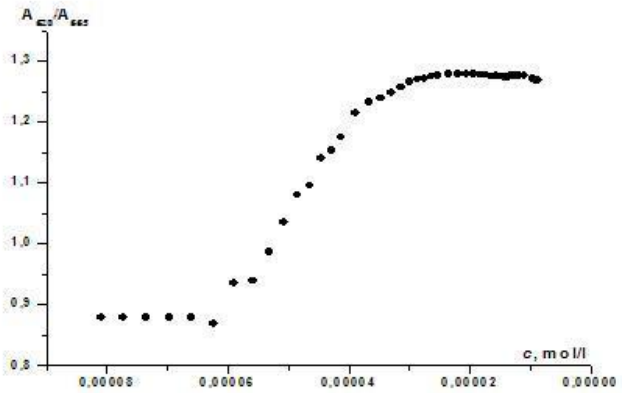

Figure 2. Ratio's changing of absorbing intensity of monomeric and dimeric forms of CuPc at 298.15 K

Analysis of literature data[15,16,20,24] and CuPc structure suggests formation of dimers due to the overlap of π-electron systems of two molecules. Formation of other types of associations , for example, due to coordinating interaction of distal substituent of phthalocyanine molecule with other macromolecule or μ-oxo-dimerization is unlikely because of coordinating features of central copper cation which is a part of macrocycle.

The molar extinction coefficient for the dimeric form of CuPc is ε_D = 5000 ± 80 L mol^{-1} cm^{-1} and that of monomeric is ε_M = 5900 ± 80 L mol^{-1} cm^{-1}. The closeness of the values of molar extinction coefficients suggests similarity in the light-absorbing source of macrocycle. It confirms π-π-dimerization. Coordination of ligand by molecule of dimer will promote a redistribution of electron density in the molecule of dimer, which, depending on the donor ability of the ligand, will have a significant effect on the association.

There are significant spectral changes during the titration of water solution of CuPc with solution of DABCO (Fig. 3). There is increase of *Q*-band absorption intensity and its bathochromic shift of 5 nm, although width of band stays wide enough. Intensity of absorption band of dimeric form (620 nm) is reduced.

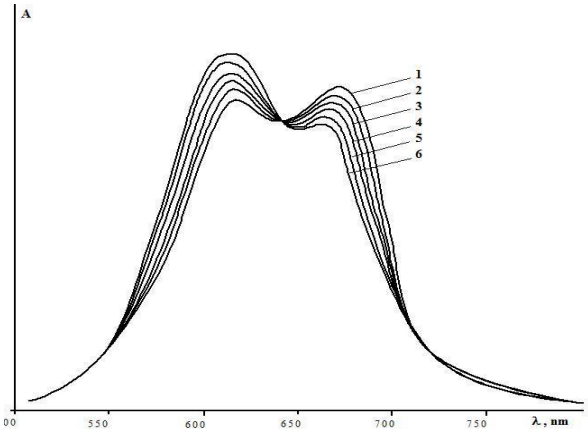

Figure 3. UV-Vis spectra's changing during titration of water solution of CuPc (c = $6.99\cdot10^{-5}$ mol L^{-1}) with solution of DABCO (c=4.98·10-2 mol L^{-1})

It is known that tetrapyrrolic macroheterocyclic compounds are able to coordinate additional ligands, depending on the denticity. Formation of 1:1, 1:2, 2:1complexes is possible which can cause various spectral changes.[25-27]

In the present case, in addition to (1) the following equilibria can also be present.:

$$CuPc + L \overset{K_2}{\rightleftarrows} CuPcL \qquad (2)$$

$$CuPcL + L \overset{K_3}{\rightleftarrows} CuPcL_2 \qquad (3)$$

$$CuPcL + CuPc \overset{K_4}{\rightleftarrows} (CuPc)_2 L \qquad (4)$$

In case of tetrapyrrolic macroheterocyclic compounds it is known that metal atom comes out of the plane of coordination node towards extra ligand when ligand is attached. Change in the geometry of the complex leads to a bathochromic shift in *Q*-band. There is a hypsochromic shift when the second ligand is coordinated. As a result of these factors, total shift of the *Q*-band of absorption could be small.[28]

The obtained spectral data indicates that the equilibrium (1) shifts towards monomeric form when DABCO (L) is added due to the formation of monomolecular complex in (2). According the equation (5), the calculated stability constant (K_2) of molecular complex was 210 L mol^{-1}.

$$K_2 = \frac{[MPcL]}{[MPc]\cdot[L]} = \frac{1}{[L]}\cdot\left(\frac{\Delta A_{1,\lambda_1}\cdot\Delta A_{0,\lambda_2}}{\Delta A_{0,\lambda_1}\cdot\Delta A_{1,\lambda_2}}\right), \quad (5)$$

where λ_1 = decreasing wavelength, λ_2 = increasing wavelength, [L]= equilibrium concentration of the ligand, ΔA_0 = maximum change in the optical density of solution at a given wavelength, ΔA_i = change of the optical density of solution at a given wavelength and given concentration.

Increase of DABCO concentration in solution to molar ratio CuPc:DABCO 1:50 does not lead to the formation of sandwich-type dimers (4).

According to the value of K_2, the molecular complex is not stable enough and equilibrium is shifted toward associated macrocyclic form that confirms the view of electronic absorption spectra. Formation of sandwich-type dimers requires a sufficient amount of phthalocyanine monomers. Therefore, the obtained data confirms the formation of CuPc dimers by π-π type.

π-π Dimers are formed due to π-σ-contraction effects and π-π-repulsion of electronic systems of two macromolecules. Coordination of DABCO should increase polarization of macrocycle π-system. It causes domination of π-π-repulsion processes over process of π-σ-contraction and shifts equilibrium (1) toward monomeric form, but there was no significant shift of associative equilibrium.

This fact may be explained in terms of competing of solvation interaction of water molecules with macrocycle and DABCO molecules. It is known,[29-31] that coordinated molecule of water, thanks to additional hydrogen bonds, could form solvation shell around macrocyclic molecule. After DABCO molecules enter in this shell, there is, probably, a resolvation, that is why CuPc dimer – DABCO coordination interaction is prevented.

Acknowledgments

The reported study was supported by Russian Foundation for Basic Research, research project No. 13-03-00615-a.

References

[1]Saka, E. T., Bıyıklıoğlu, Z., *J. Organomet. Chem.*, **2013**, *745-746*, 50.

[2]Sorokin, A. B., Kudrik, E. V., *Cat. Today*, **2011**, *159*, 37.

[3]Sorokin, A. B., *Chem. Rev.*, **2013**, *113*, 8152.

[4]Ghasemi, M., Wan Daud, R., Rahimnejad, M., Rezayi, M., Fatemi, A., Jafari, Ya., Somalu, M.R., Manzour, A., *Int. J. Hydrogen Energy*, **2013**, *22*, 9533

[5]De Filippis, M. P., Die, D., Fantetti, L., Roncucci, G., *Tetrahedron Lett.*, **2000**, *41*, 9143.

[6]Horne, T. K., Abrahamse, H., Cronjé, M. J., *Photodiagn. and Photodynam. Therapy*, **2012**, **9**, 215.

[7]Zorlu, Yu., Dumoulin, F., Bouchu, D., Ahsen, V., Lafont, D., *Tetrahedron Lett.*, **2010**, *51*, 6615.

[8]Bayrak, R., Akçay, H. T., Beriş, F. Ş., Şahin, E., Bayrak, H., Demirbaş, Ü., *Spectrochim. Acta A*, **2014**, *133*, 272.

[9]Chen, Z., Zhou, Sh., Chen, J., Li, L., Hu, P., Chen, S., Huang, M., *J. Luminescence*, **2014**, *152*, 103.

[10]Konarev, D. V., Khasanov, S. S., Lyubovskaya, R. N., *Coord. Chem. Rev.*, **2014**, *262*, 16.

[11]Rawling, T., Donagh, A., *Coord. Chem. Rev*., **2007**, *251*, 1128.

[12]Vashurin, A. S., Badaukaite, R. A., Futerman, N. A., Puhovskaya, S. G., Shaposhnikov, G. P., Golubchikov, O. A., *Petrol. Chem*., **2013**, *53*, 197.

[13]Iliev, V., Alexiev, V., Bilyarska, L., *J. Molec. Cat. A*, **1999**, *137*, 15.

[14]Iliev, V., Mihaylova, A., *J. Photochem. Photobiol. A*, **2002**, *149*, 23.

[15]Palewska, K., Sworakowski, J., Lipiński, J., *Opict. Mat.*, **2012**, *34*, 1717.

[16]Tong, Sh.-L., Zhang, J., Yan,Ya., Hu, Sh., Yu, J., Yu, L., *Solid State Sci*., **2011**, *13*, 1967.

[17]Kulinich, V. P., Shaposhnikov, G. P., Badaukaite, R. A., *Macroheterocycles*, **2010**, *3*, 23.

[18]Przywarska – Boniecka, H., *Rocz. Chem.*, **1967**, *41*, 1703.

[19]Camp, Ph. J., Jones, A. C., Neely, R. K., Speirs, N. M., *J. Phys. Chem. A*, **2002**, *106*, 10725.

[20]Snow, A. W., Jarvis, N. L., *J. Am. Chem. Soc.*, **1984**, *106*, 4706.

[21]Kuznetsova, N. A., Gretsova N. S., Derkacheva, V. M., Kaliya, O. L., Lukyanets, E. A., *J. Porphyrins and Phthalocyanines*, **2003**, *7*, 147.

[22]Palewska, K., Sworakowski, J., Lipinski, J., Nespurek, S., *J. Photochem. Photobiol. A*, **2011**, *223*, 149.

[23]Schelly, Z. A., Harward, D. J., Hemmes, P., Eyring E. M., *J. Phys. Chem.*, **1970**, *74*, 3040.

[24]Snow, A. W., *The Porphyrin Handbook. Phthalocyanines: Properties and Materials, Elsevier Science*, **2003**, *17*, 129.

[25]Mauzerall, D., *Biochem*., **1965**, *4*, 1801.

[26]Mamardashvili, G. M., Mamardashvili, N. Zh., Koifman, O. I., *Russ.Chem. Rev.*, **2008**, *77*, 59.

[27]Mamardashvili, N. Zh., Mamardashvili, G. M., Weiss, J. *Russ. J. Inorg. Chem.*, 2005, 50, 218.

[28]Kasha, M., Rawls, H. R., Ashraf El-Bayoumi M., *Pure Appl. Chem.*, **1965**, *11*, 371.

[29]Blagrove, R. J., *Aust. J. Chem.*, **1973**, *26*, 1545.

[30]Blagrove, R. J., Gruen, L. C., *Aust. J .Chem.*, **1972**, *25*, 2553.

[31]Blagrove, R. J., Gruen, L. C., *Aust. J. Chem.*, **1973**, *26*, 225.

Received: 11.07.2014.
Accepted: 14.08.2014.

LIQUID–SOLID EXTRACTION OF Hg(II) FROM AQUEOUS SOLUTION BY CHELATING RESIN CHELEX-100

Afaf Amara-Rekkab[a] and Mohamed Amine Didi[a]*

Keywords: mercury(II); Chelex 100; adsorption; ion exchange; optimization.

The sorption of mercury(II) from aqueous medium on a chelating resin Chelex 100 has been studied in batch mode. Since the extraction kinetic was obtained, with a mixture of 0.1 g of resin and 5 mL of mercury(II) at 200.59 mg L^{-1} of initial concentration, extraction equilibrium was reached within 180 min of mixing. The influence of some parameters such as initial mercury(II) ion concentration, initial pH of aqueous solution, ion strength and the amounts of resin have been studied at fixed temperature (20±1 °C). The optimum pH value level for quantitative sorption was 5.7. The best performance obtained was 98.0 % of extraction yield equivalent to 14.19 mg g^{-1} of resin. The pseudo-first- order equation, pseudo-second-order equation, the intra-particle diffusion model and Boyd's diffusivity model were used to describe the kinetics data and rate constants were evaluated. The Freundlich and Langmuir adsorption models were applied to describe the equilibrium isotherms.

*Corresponding Author
Fax: +213 43216378
E-Mail: madidi13@yahoo.fr
[a] Laboratory of Separation and Purification Technologies, Department of Chemistry — Faculty of Sciences, Box 119, Tlemcen University — 13000, Algeria

Introduction

Mercury is a carcinogenic heavy metal and poses a potential threat to human health even at very low concentrations (0.47 µg kg^{-1} of p.w. day^{-1}. (p.w. = Physical weight). It has been well documented that mercury may cause brain damage, dysfunction of liver, kidney, gastrointestinal tract and central nervous system, as well as induce cellular toxicity by binding to intracellular sulfhydryl groups. Inorganic mercury is the most prevalent form of mercury in aquatic ecosystems.[1] The other hand, mercury recovery is important from the economical point of view because it has a wide range of applications like dental amalgams, anti-fouling paints, electrodes for some types of electrolysis, batteries, fluorescent lamps, catalysts, etc.[2] Several methods can be applied to remove mercury from aqueous solutions such as ion exchange,[3] carbon adsorption,[4] sequential injection extractions,[5] liquid– liquid (LLE)[2,6] and solid phase extraction (SPE).[1,7-18]

In this paper, the extraction of mercury(II) by liquid–solid extraction use resin Chelex 100 as extractant agent. Chelating resins have seen considerable application in speciation studies, particularly the commercially available Chelex-100 resin, which is a polystyrene divinylbenzene copolymer incorporating iminodiacetate chelating groups. The iminodiacetate groups coordinate metals by means of oxygen and nitrogen bonds and the resins have a particularly strong affinity for trace metals. It was proposed firstly to use Chelex-100 for the preconcentration of total trace metals from seawater. After, she is used to differentiate labile from non-labile fractions of trace metals. Chelex-100 retains free metal ions and loosely bound trace metals.[19]

Chelex 100 finds application in many fields, it was effective in binding several metal ions (Cr^{3+}, Ni^{2+}, $Cu^{2+}$and Zn^{2+}, Tl^{3+}, La^{3+} and Al^{3+}).[20-23]

Therefore, the objectives of this study are to investigate the best performance of mercury(II) extraction by Chelex 100, by varying diverse parameters as the initial mercury(II) ion concentration, initial pH of aqueous solution, ion strength and the amounts of resin.

Materials and methods

Characteristics of Chelex 100

Chelex -100 (Bio-Rad Laboratories, CA, USA) is a chelating resin which uses ion exchange to bind transition metal ions. The resin is composed of polystyrene divinylbenzene copolymers containing paired iminodiacetate ions, which act as chelators for polyvalent metal ions (see Table 1).[24] This group can interact via its nitrogen and oxygen atoms with the mercury according a tridentate interaction.

Table 1. General description and some properties of resin

Type	Chelex 100
Ionic form	Na^+
Functional group	iminodiacetic acid
Matrix	polystyrene-divinylbenzene
Structure	macroporous
pH range	0–14
Bead size	0.3-1.0 mm
Capacity	0.4 mmol mL^{-1}
Appearance	white, translucent

Metal salt and other chemicals

Mercury(II) chloride is procured from Sigma (St. Louis, MO, USA). Buffer is obtained from Riedel-de-Haen (Seelze, Germany), while sodium chloride is from PANREAC (Phillipsburg, USA). Pyridylazonaphtol PAN used for mercury analysis were from Sigma (St. Louis, MO, USA). Hydrochloric acid and sodium hydroxide used for adjusting pH of mercury(II) solutions were from Stinnes chemicals (Deutscland), Sigma (St. Louis, MO, USA), respectively.

Batch studies

Effect of the agitation time

Kinetic experiments were carried out by agitating 5.0 mL of mercury(II) solution at initial concentration, 1 mmol L^{-1}, with 0.1 g of chelating resin Chelex 100 in a 10 mL Erlen at 20±1 °C at pH=5.7 and at a constant agitation speed of 1000 rounds per minute (rpm) for a time ranging from 2 to 180 min and the amount of mercury(II) remaining in solution was measured. All experiments were made at pH=5.7 without adjustment. The samples were collected from the shaker, filtered and the filtrates were analyzed for mercury(II) concentration with a SPECORD 210 plus spectrophotometer at 590 nm using pyridylazonaphtol PAN and buffer at pH=13.0 as reagents.

The percent Hg(II) extraction, (%) was determined as follows:

$$\text{Yield}(\%) = 100\frac{C_0 - C}{C_0} \quad (1)$$

The adsorption amount was calculated as follows:

$$q_t = \frac{V(C_0 - C)M}{w} \quad (2)$$

where

q_t is the adsorption amount (mg g^{-1}),

w the weight of the Chelex 100 (g),

M molar mass (g mol^{-1}),

V the volume of solution (L), and

C_0 and C are the concentrations (mol L^{-1}) of mercury ions before and after adsorption, respectively.

Effect of initial solution pH

The effect of solution pH on the equilibrium uptake of mercury(II) from aqueous solution by the Chelex 100 resin investigated between pH 1.6 and 10.0. The experiments were performed by adding a known weight of resin (0.1 g) into eight 10 mL Erlenmeyer containing 5 mL of mercury(II) solution. Dilute nitric acid or sodium hydroxide was used to adjust the pH of mercury solutions using a pH meter (model WTW, PH 3310 SET 2, Germany). The flasks were shaken at 1000 rpm at 20±1 °C for 180 min.

Effect of initial mercury(II) concentration

Kinetic experiments were carried out by agitating 5.0 mL of mercury(II) solution of concentration ranging from 0.01 to 1 mmol L^{-1} with 0.1 g of Chelex 100 resin in a 10 mL Erlen at 20±1 °C at pH=5.7 and at a constant agitation speed of 1000 rpm for 180 min.

Effect of the amount of resin

The effect of the adsorbent amount was studied with a 5 mL solution of 1 mmol L^{-1} mercury(II) solution and varying amounts of adsorbent from 0.05 to 0.2 mg.

Effect of ionic strength

The effect of ionic strength of aqueous media on the equilibrium uptake of mercury(II) from the aqueous solution by the Chelex 100 resin (0.1 g) was investigated by adding, in a 10 mL Erlen, a known weight of solid NaCl to 5 mL of 1 mmol L^{-1} mercury(II) solution at 20±1 °C at pH =5.7 and at a constant agitation speed of 1000 rpm for 180 min. Flame Photometer Jenway Models PFP7 spectrometer was used for the measurements of free sodium before and after extractions of mercury(II) by Chelex 100 resin.

Adsorption kinetic model

In an attempt to express the mechanism of mercury adsorption onto the surface and pores of the resin, the following kinetic model equations are used to analyze the adsorption experimental data for determination of the related kinetic parameters.

Pseudo-first order model (PFO)

The PFO rate expression based on solid capacity is the most widely used rate equation for assigning the adsorption rate of an adsorbate from a liquid phase and is known as the Lagergren rate equation.[25] It is represented as:

$$\frac{dq}{dt} = k_f(q_e - q_t) \quad (3)$$

where

q_e (mg g^{-1}) and q_t (mg g^{-1}) are the adsorption capacity at equilibrium and time t respectively and

k_f (min^{-1}) is the rate constant of the PFO adsorption reaction.

On integration and applying boundary conditions as $q_t = 0$ at $t = 0$ and $q_t = q_e$ at $t=t_e$, Eq. (3) becomes:

$$\log(q_e - q_t) = \log q_e - k_f\frac{t}{2.303} \quad (4)$$

Pseudo- second order model (PSO)

The PSO kinetic expression was developed by Ho[35] to describe the adsorption of metal ions onto adsorbent. The rate expression is represented as:

$$\frac{dq_t}{dt} = k_S\left(q_e - q_t\right)^2 \qquad (5)$$

where

q_e and q_t (mg g^{-1}) are the adsorption capacities at equilibrium and time t respectively and

k_s (g mg^{-1} min^{-1}) is the rate constant for the PSO adsorption reaction.

The nonlinear form of PSO model (Eq. (5)) can be rearranged into four different linear forms, of which the most popular one is:[26]

$$\frac{t}{q_t} = \frac{1}{k_S q_e^2} + \left(\frac{t}{q_e}\right) \qquad (6)$$

The product $k_2 q_e^2$ (mg g^{-1} min^{-1}) is the initial sorption rate (h).

Applying Eq. (6) for the analysis of kinetic data is usually based on the plotting of t/q_t versus t which should give a linear relationship; whereas, $1/q_e$ and $1/k_2 q_e^2$ are the slope and the intercept of obtained line, respectively.

Intra-particle diffusion model (IDM)

The intra-particle diffusion model is represented as follows:

$$\frac{q_t}{q_e} = 1 - \frac{6}{\pi^2}\sum_{n=1}^{\infty}\frac{1}{n^2}\exp\left(-\frac{D_e n^2 \pi^2}{r^2}t\right) \qquad (7)$$

where

D_e is the intra-particle diffusion coefficient and

r is the particle radius.

For short times (when q_t/q_e is less than 0.3), Eq. (7) can reduce to the following expression:

$$q_t = k_{ID}\sqrt{t} \qquad (8)$$

where k_{ID} is the intra-particle diffusion constant. The significant property of this equation is that, if the intra-particle diffusion is the only rate-limiting step, then the linear plot of q_t versus $t^{0.5}$ should pass through the origin. On the other hand, if the intercept of plots do not equal zero, then it indicates that the intra-particle diffusion is not the sole rate determining step.[26]

Then Eq. (8)[27] is modified to:

$$q_t = k_{ID}\sqrt{t} + S \qquad (9)$$

where S is a constant and reflects the boundary layer effect.

Investigation of various reports about the sorption rate shows that the intra-particle diffusion model is the most popular one for the diffusion rate-controlling step that has been used in conjunction with the surface reaction models to recognize the adsorption kinetics.

Boyd's diffusivity model (BDM)

Boyd's kinetic model[27] for adsorption reaction is based on diffusion through the boundary liquid film, considering adsorption kinetics as a chemical phenomenon. The simplified form of the rate equation can be expressed as:

$$\ln\left[\frac{1}{1-F^2(t)}\right] = \pi^2 D_e \frac{t}{R_a^2} \qquad (10)$$

where

$F(t) = q_t/q_e$ is the fractional attainment of equilibrium at time t,

D_e (m^2 s^{-1}) is the rate constant and

R_a (m) is the radius of the spherical adsorbent particle.

A linear plot of $\ln[1/(1-F^2(t))]$ versus t will give the value of D_e.

Results and discussion

Effect of contact time on mercury(II) adsorption

The influence of contact time on the percent Hg (II) extraction (%) (Eq. (1)) and the uptake (mg g^{-1}) (Eq. (2)) from aqueous solution of Hg(II), 1 mmol L^{-1}, is investigated at 20±1 °C (Fig. 1).

Based on Fig. 1, we can divide the sorption process into three steps. During the first step (2 min < t ≤ 30 min) sorption is fast and percent Hg(II) extraction increase from 0 to 62.2 % for Hg(II). The reason is that the driving force for mercury(II) is higher, which permits to overcome all the external mass transfer resistances and the active sites with higher affinity are first occupied, thus Hg(II) ions might enter easily the accessible pore sites and bind with the chelating ligands.[28]

During the second step (t=30 min to t=120 min), it is slower and percent Hg(II) extraction increases from 62.2 to 91.2 % , which could be due to that some Hg(II) ions might be hampered to diffusion into the deeper pores and to the existence of different sorption mechanisms.[28]

 DOI: 10.17628/ecb.2014.3.860-868

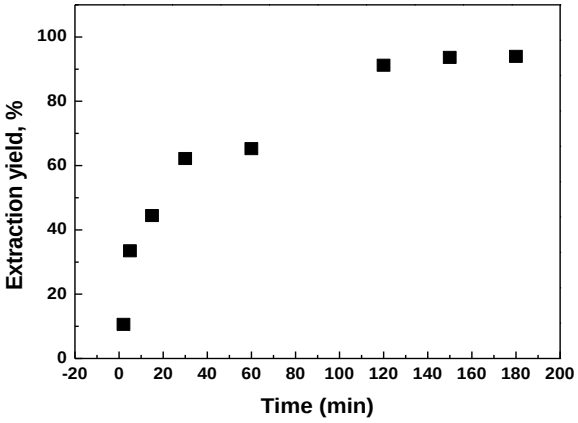

Figure 1. Effect of contact time on the ion exchange of Hg(II) using Chelex-100. Initial concentration of Hg(II) 1 mmol L^{-1}, amount of resin 0.1 g, volume of ion-exchange medium 5 mL, T=20±1 ◦C, stirring = 1000 rpm and initial pH 5.7

In the third phase ($t \geq 120$ min), the sorption process ceases, indicating the attainment of equilibrium and percent Hg(II) extraction became constant. The maximum percent Hg(II) extraction is 93.9 % obtained at 180 min which is used as a suitable contact time for mercury(II) adsorption. It is found that the concentration of Hg^{2+} in aqueous solutions decrease more rapidly in the early stage of operation (0–30 min), and the exchange is virtually completed within 30–180 min. That is, the decrease of the concentration of Hg^{2+} in the solution demonstrates that higher exchange rates (dC_M/dt) of Hg^{2+} with Na-form chelating resins is obtained at the onset; and the plateau is reached gradually within 150 min. This time is half that obtained by Manouchehri in the extraction of cadmium, copper and lead, which was of 300 minutes and the maximum of extraction of copper and zinc at 240 and 300 minutes respectively by Chelex 100.[21,29]

Kinetics of adsorption

In this study, batch sorption kinetics of Hg (II) ions at initial concentration, 1 mmol L^{-1}, with the chelating resin Chelex 100 has been studied. The different values of constants from the slopes and intercepts of linear plots of Eq. (4) (shown in Fig. 2), Eq. (6) (shown in Fig. 3), are summarized in Table 2.

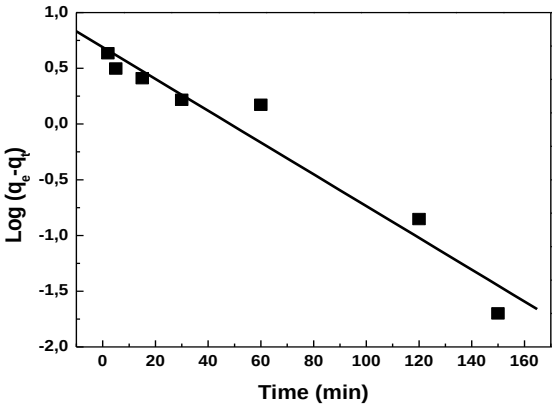

Figure 2. Lagergren plots for the adsorption of Hg(II) using Chelex-100. Amount of resin 0.1 g, volume of ion-exchange medium 5 mL, *T*= 20±1°C, stirring = 1000 rpm, initial pH 5.7 and initial concentration of Hg(II) 1 mmol L^{-1}.

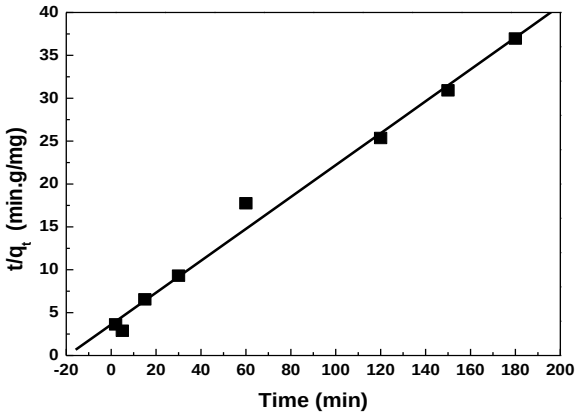

Figure 3. Pseudo-second order kinetic models for the adsorption of Hg(II) onto Chelex 100**.** Amount of resin 0.1 g, volume of ion-exchange medium 5 mL, *T* = 20±1°C, stirring = 1000 rpm, initial pH 5.7 and initial concentration of Hg(II) 1 mmol L^{-1}.

Table 2. Kinetic parameters for adsorption of mercury by Chelex 100

Models	Parameters	[Hg(II)]=1 mmol L^{-1}
Pseudo first order	k_f (min^{-1})	0.032
	q_e* (mg g^{-1})	4.88
	q_e ** (mg g^{-1})	4.87
	R^2	0.949
Pseudo second order	k_s (g mg^{-1} min^{-1})	68.74
	q_e *(mg g^{-1})	0.281
	q_e ** (mg g^{-1})	4.87
	R^2	0.9996

*calculated, **experiment

As shown in Table 2, the obtained coefficients values of the pseudo-second-order model (> 0.999) were better than those of the first-order model for the adsorption of Hg(II) at the considered concentration, suggesting that the pseudo-second-order model was more suitable to describe the adsorption kinetics of Chelex 100 for Hg (II).This suggests that the rate limiting step may be a chemical process involving valence forces through sharing or exchange of electrons.[25] Similar results have been observed in the adsorption of Hg (II) by an extracellular biopolymer poly (γ-glutamic acid)[1] and on bamboo leaf powder.[17]

Diffusivity study

The mercury(II) ions transport from the solution phase to the surface of the Chelex 100 occurs in several steps. The overall adsorption process may be controlled either by one or more steps (e.g., film or external diffusion, pore diffusion, surface diffusion and adsorption on the pore surface). Besides adsorption at the outer surface of the resin, there is also a possibility of intra-particle diffusion of Hg (II) from the bulk of outer surface into the pores adsorbent. The possibility of intra-particle diffusion was studied using the Morris–Weber equation (Eq. (9)).

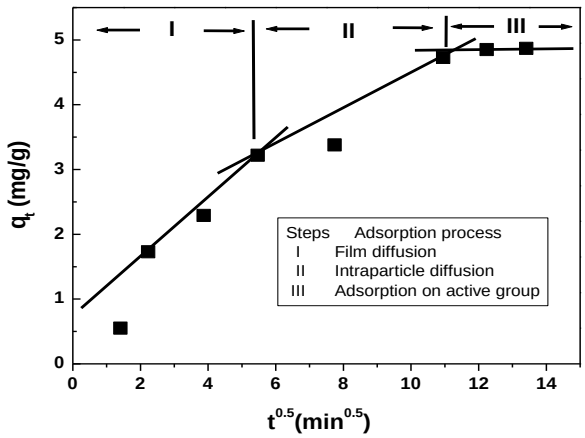

Figure 4. Intra-particle diffusion Kinetic models for the adsorption of Hg(II). Amount of resin 0.1 g, volume of ion-exchange medium 5 mL, T= 20±1°C, stirring = 1000 rpm, initial pH 5.7 and initial concentration of Hg(II) 1 mmol L^{-1}.

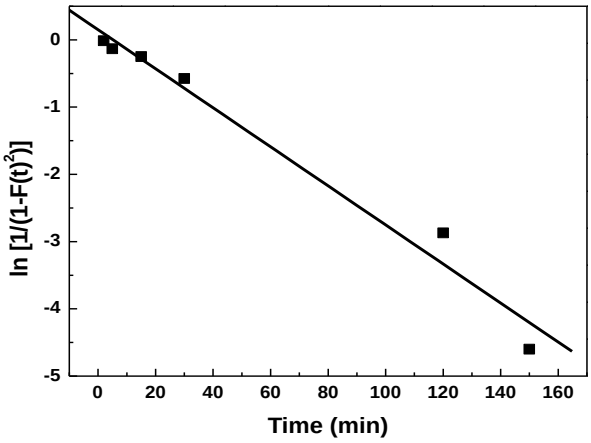

Figure 5. Boyd's diffusivity plot for adsorption of Hg(II) onto Chelex 100**.** Amount of resin 0.1 g, volume of ion-exchange medium 5 mL, *T* = 20±1°C, stirring 1000 rpm, initial pH 5.7 and initial concentration of Hg (II) 1 mmol L^{-1}.

The plot of the Morris–Weber relationship for the sorption of Hg (II), at initial concentration equal to 1 mmol L^{-1}, by the resin is shown in Fig. 4. Based on this figure, it may be seen that the intra-particle diffusion of Hg(II) within the resin occurred in 3 stages.

The first linear portion included the adsorption period from 0 to 60 min, representing the external mass transfer or film diffusion (boundary layer) and the rapid distribution of Hg(II) ions onto the outer surface of Chelex 100. The second linear portion corresponded to the adsorption period of 60–180 min, which represents the intra-particle diffusion and binding of Hg(II) ions into the internal active sites of the biomass. Finally, the third linear portion (from 150 min on) indicated a saturation of the adsorption process. The intra-particle diffusion constants and regression coefficients for these three stages (k_{ID} and R^2) are given in Table 3.

Table 3. Intra-particle diffusion model parameters and effective pore diffusivities for mercury adsorption onto Chelex 100

Intra-particle diffusion	k_{ID} **(mg $g^{-1}$$min^{0.5}$)**	***S***	R^2
Stage 1	0.45938	0.641	0.9778
Stage 2	0.28517	1.48	0.89612
Stage 3	0.05753	4.115	0.87392
Effective pore diffusivities	D_e **(m^2s^{-1})**	R_a **(m)**	R^2
	$2.94.10^{-9}$	10^{-3}	0.976

The plot of $\ln[1/1-F^2(t)]$ versus t (Fig. 5) is a line whose slope,$(2/R_a^2)D_e$, thus diffusion coefficient, D_e can be calculated. The value of diffusion coefficient as calculated from Eq. (10) is shown in Table 3. The values of D_e falls well within the values reported in literature, especially for chemisorptions system (10^{-9} to 10^{-17} m^2 s^{-1}).[30]

Effect of mercury concentration

Sorption capacity

The percentage uptake is highly dependent upon the initial concentration of the Hg(II) ion and the resin. The initial Hg(II) concentrations tested were 0.01, 0.1, 0.2, 0.5, 0.8 and 1 mmol L^{-1} at an amount of adsorbent of 0.1 g (Fig. 6). The data indicates that the initial metal concentration determines the equilibrium concentration, and also determines the uptake rate of metal ion and the kinetic character of the process.

In the case of low concentrations, the ratio of the initial number of moles of Hg(II) ion to the available surface area is larger and subsequently, the fractional ion exchange becomes independent of initial concentrations. The rapid metal extraction has significant practical importance, as this will facilitate with the small amount of resins to ensure efficiency and economy.

The amount of Hg(II) ions adsorbed per unit mass of the resin increased with the initial metal concentration as expected. This is due to the fact that sorption sites took up the available metal ions more quickly at low concentration, but metal needed to diffuse to the inner sites of the sorbent for high concentration. The extraction of mercury sorbed after equilibrium is 13.03 mg g^{-1}, at an initial concentrations between 0.5 and 1 mmol L^{-1}. The initial rate of sorption was greater for higher initial mercury concentration, because the resistance to the metal uptake decreased as the mass transfer driving force increased.

It is also noticed that an increase in the initial mercury concentration leads to a decrease in the metal removal.

This effect can be explained as follows: at low metal/sorbent ratios, there are a number of sorption sites in Chelex 100 structure. As the metal/sorbent ratio increases, sorption sites are saturated, resulting in decreases in the sorption efficiency.

 DOI: 10.17628/ecb.2014.3.860-868

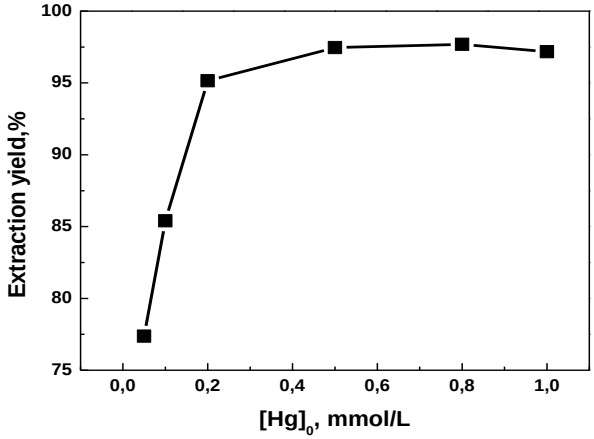

Figure 6. Effect of initial concentration of Hg(II) on the ion exchange using Chelex-100. Amount of resin 0.1 g, volume of ion-exchange medium 5 mL, *T*= 20±1°C, stirring = 1000 rpm, initial pH 5.7 and contact time 180 min.

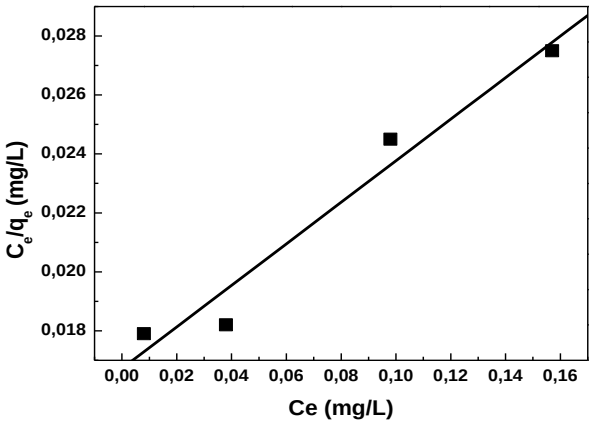

Figure 7. Langmuir plot for the adsorption of mercury(II). Resin quantity 0.1 g, aqueous volume 5 mL, initial pH 5.7, time of contact 180 min.

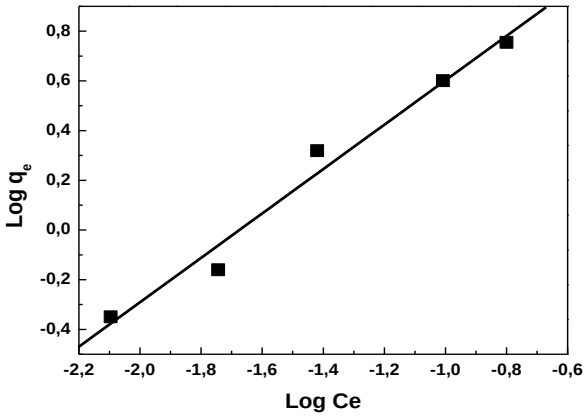

Figure 8. Freundlich plot for the adsorption of mercury(II). Resin quantity 0.1 g, aqueous volume 5 mL, initial pH 5.7, time of contact 180 min.

Adsorption isotherm modeling

For the interpretation of the adsorption data, the Langmuir and Freundlich isotherm models were used (Eqs. (11) and (12)).[27,31]

$$\frac{C_e}{q_e} = \frac{1}{q_{max} K_L} + \frac{C_e}{q_{max}} \quad (11)$$

$$\log q_e = \log k_f + \left(\frac{1}{n}\right) \log C_e \quad (12)$$

where

C_e is the equilibrium concentration of mercury (mmol L^{-1}),

q_e is the amount of mercury sorbed on the Chelex 100 (mg g^{-1}),

k_L is the Langmuir adsorption constant (L mg^{-1}),

q_{max} is the maximum amount of mercury that can be sorbed by the resin,

k_F is the Freundlich adsorption constant and n is a constant that indicates the capacity and intensity of the adsorption, respectively.

Table 4. Isotherm parameters for mercury adsorption on Chelex 100.

Models	Parameters	[Hg(II)]=1 mmol L^{-1}
Langmuir constants	q_{max} (mg.g^{-1})	14.19
	k_L (L.mg^{-1})	4.214
	R^2	0.9607
	R_L	0.00118
Freundlich constants	1/n	0.89318
	k_f (L.mg^{-1})	31.304
	R^2	0.978

For the two studied systems, the Langmuir (C_e/q_e versus C_e) plot was found to be linear in the concentration range of 0.008– 0.197 mg L^{-1} and the correlation coefficients were extremely high (R^2 > 0.96). In this concentration range, the Freundlich isotherm correlated better than Langmuir (R^2 > 0.98) isotherm with the experimental data from adsorption equilibrium of mercury ions by chelating resin, suggested a monolayer adsorption.

The maximum adsorption values were 14.19 (mg g^{-1}) which is acceptable accordance with experimentally obtained values (13.03 mg g^{-1}).

Initial pH effect

The retention of mercury(II) on resin was studied in the pH range from 1.66 to 10.0 and the results obtained are shown in Fig. 10.

From Fig. 10, it was observed that the sorption was strongly pH-dependent. The maximum sorption capacity takes place at pH 5.7.

Table 5. Comparison of maximum capacities of various sorbents materials for Hg(II) ions sorption

Sorbent	q_{max}, mg g^{-1}	Reference
BLP	27.11	Mondal., 2013[32]
Triton X-100 modified BLP	28.1	Mondal., 2013[32]
Charcoal-immobilized papain (CIP)	4.70	Dutta et al., 2009[33]
Camel bone charcoal	28.24	Hassan et al., 2008[34]
Treated sawdust (*Acacia arabica*)	20.6	Meena et al., 2008[35]
Eucalyptus bark	33.11	Ghodbane , 2008[36]
3-Mercaptopropyl functionalized silica gel	66.0	Gao et al., 2011[37]
Chelex 100	14.19	In this study

The equilibrium sorption capacity was minimum at pH 1.6 (1.48 mg g^{-1}) and increased up to pH 2.6 (11.83 mg g^{-1}), reached maximum (13.03 mg g^{-1}) at pH 5.7. This sorption trend can likely be ascribed to the effect of competitive binding between Hg(II) and hydrogen ions for the binding sides on the surface of the resins. At low pH, an excess of hydrogen ions can compete effectively with Hg(II) for bonding sites, resulting in a lower level of Hg(II) uptake. This increase is rational for Chelex-100 because the exchanger being weakly acidic, is practically in the hydrogen form at pH 2 and is gradually converted into metal form as the pH was increasing.[20] The percentage of ion exchange decreases rapidly when the pH is increased above 6.0 due to the formation of of soluble hydroxilated compound ($Hg(OH)_2$), at higher pH values.[38] Several authors have reported maximum biosorption of mercury by different biomasses at pH 5.7 or near values.[38,39]

Figure 9 give, the functional group of the resin is present in four forms depending on the pH. A pH_i = 5.7 is the shape (c) predominates. The complex formed between the resin and mercury(II) is shown in (Fig. 11).

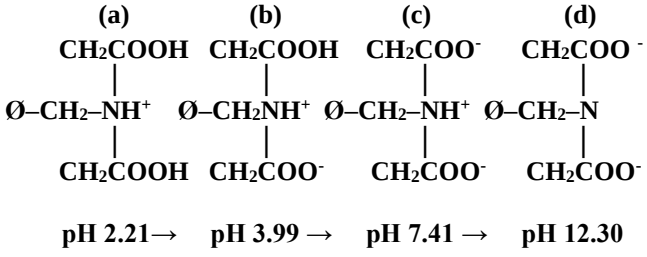

Figure 9. Different forms of the resin Chelex 100 depending on the pH

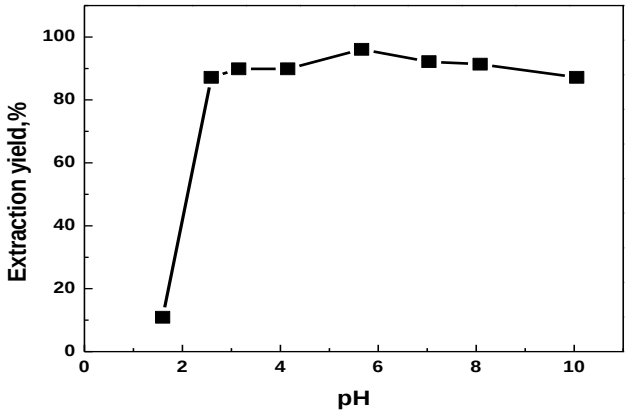

Figure 10. Effect of initial pH for efficient extraction of mercury ion. Amount of resin 0.1 g, volume of ion-exchange medium 5 mL, *T*= 20±1°C, stirring = 1000 rpm, initial concentration of Hg(II) 1 mmol L^{-1} and contact time 180 min.

Iminodiacetic acid is diprotic in nature and in the resin has two different exchange sites in its acetate groups with different selectivity for hydrogen. At initial pH=5.7, the form (c) (Fig.8) was predominant. For this, mercury(II) forms 1:1 complex with Chelex-100 and releases two hydrogens (see Fig.10).

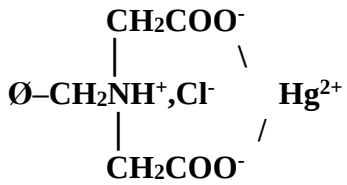

Figure 11. Complex structure " Chelex-Hg". Initial pH = 5.7.

Amount of resin

The effect of varying doses of the adsorbent Chelex 100 was investigated using 1 mmol L^{-1} of mercury(II) concentration. Fig. 12 shows an increase in the percentage of extraction of mercury with the increase in dose of the adsorbents up to certain limit and then the rate of change in increase becomes negligible.

The increase in the adsorption with increasing doses of adsorbent is likely due to increase in adsorbent surface area and availability of more adsorption sites. The optimum adsorbent dose is found to be 0.125 g of resin, the optimal amount of resin will be choosen at 0.1 g for ameliorate the extraction by the another effects.

Effect of ionic strength

The effect of ionic strength on mercury(II) sorption was studied by stirring 0.1 g of Chelex 100 resin with increasing NaCl amount, in the aqueous solutions, from 0.001 to 0.073g. Results are summarized in Fig. 13 and shows that the influence of the ionic strength on sorption of mercury is important.

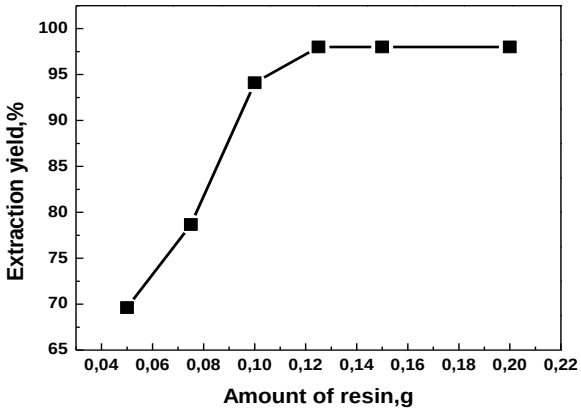

Figure 12. Effect of amount of resin on the ion exchange of Hg(II) using Chelex-100. Initial concentration of Hg(II) 1 mmol L^{-1}, volume of ion-exchange medium 5 mL, *T*= 20±1 °C, stirring = 1000 rpm, initial pH 5.7 and contact time 180 min.

The calibration graph was established using standard solutions of sodium. The graph is linear (not showed) in the range between 0.029 and 4.0 mg L^{-1}. The calibration equation of standard sodium is:

$$Abs = 17.25[Na] + 2.1705$$

It is evident in Fig. 13, that there is a positive impact on increasing of extraction yield of Na^+ at concentration from 0 to 0.03 g. Before this concentration, the quantity of Na^+ after extraction decreased in solution. It seems that the presence of Na^+ at concentration lower than 0.03 g has a negative effect on Hg^{2+} adsorption.

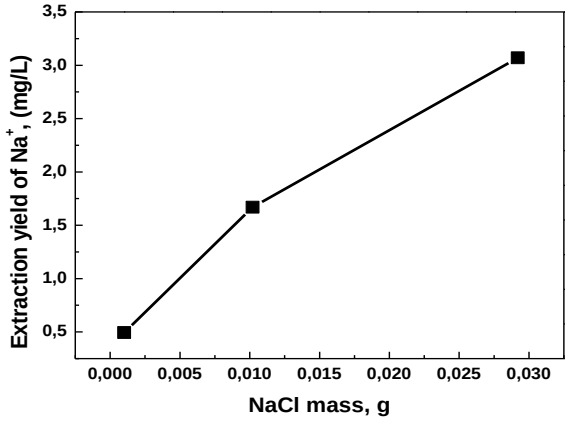

Figure 13. Effect of NaCl concentration on the extraction yield. Initial concentration of Hg(II) 1 mmol L^{-1}, amount of resin 0.1 g, volume of ion-exchange medium 5 ml, *T*= 20±1°C, stirring = 1000 rpm, initial pH 5.7 and contact time 180 min.

The form of sodium complex at a higher concentration of sodium chloride is agreement with the one given by the CHEAQS V.L20.1. In fact, the increase of NaCl concentration, shows that the free sodium passes from 99.95 % to 93.96 % (ratio = 0.94) and the free Hg^{2+} passes from 91.67 % to 13.72 % (ratio = 0.15). The quantity of free sodium is higher than the quantity of free mercury (Na^+/Hg^{2+} = 6.26), so the sodium is extracted.

Conclusions

A commercial resin the Chelex 100 was tested on mercury(II) extraction. The extraction efficiency was determined as a function of various parameters such as time, pH, mercury concentration, amount of resin and ionic strength effect. The experimental capacity obtained is 14.19 mg g^{-1}.

The kinetics of mercury(II) adsorption on resin follows the pseudo-second order kinetic model. The equilibrium isotherm for sorption of the investigated metal ions has been modeled successfully using the Langmuir and Freundlich isotherm.

Kinetics of Hg(II) adsorption from the solution of $HgCl_2$ on Chelex 100 resin is controlled by the film and particle-diffusion process. The effective diffusivity of Hg(II) removal for all the adsorbent was of the order of 10^{-9} m^2 s^{-1} which suggested chemisorption of the process.

The maximum sorption of mercury(II) took place in the initial pH at 5.7 and the mercury(II) concentration range of 0.5 and 1 mmol L^{-1}, the presence of NaCl (above 0.05 mmol L^{-1}) increases the extraction efficiency.

The results of this study show that the Chelex 100 is an effective's adsorbant for extraction of mercury(II) from aqueous solution.

References

[1]Inbaraj, S. B., Wang, J. S., Lu, J. F., Siao, F. Y., Chen, B. H., *Bioresour. Technol.*, **2009**, *100*, 200–207.

[2]Fábrega, D. M. F., Mansur, B. M., *Hydrometallurgy*, **2007**, *87*, 83–90.

[3]Chiarle, S., Ratto, M., Rovatti, M., *Water Res*, **2000**, *34(11)*, 2971-2978.

[4]Starvin, A. M., Rao, P. T., *J Hazard Mater*, **2004**, *B113*, 75–79.

[5]Staden, V. J. F., Taljaard, R. E., *Talanta*, **2004**, *64*, 1203–1212.

[6]Meera, R., Francis, T., Reddy, M. L. P., *Hydrometallurgy*, 2001, 61, 97–103.

[7]Costa Luciana, C., Gomes Ailton, S., Coutinho Fernanda M. B., Teixeira, V. G., *React. Funct. Polym.*, **2010**, *70*, 738–746.

[8]Takagai, Y., Shibata, A., Kiyokawa, S., Takase, T., *J. Colloid Interfac. Sci.*, **2011**, *353*, 593–597.

[9]Xiong, C., Yao, C., *Chem. Eng. J.*, **2009**, *155*, 844–850.

[10]Hakim, L., Sabarudin, A., Oshita, K., *Talanta*, **2008**, *76*, 1256–1260.

[11]Neagu, V., Cornelia, L., Simina, S., Ştefan, M., I. Untea, I., *React. Funct. Polym.*, 2007, *67*, 1433–1439.

[12]Maa, N., Yang, Y., Chen, S., Zhang, Q., *J. Hazard. Mater.*, **2009**, *171*, 288–293.

[13]Ji, C., Song, S, Wang, C., Sun,C., Qu, R., Wang, C., Chen, H., *Chem. Eng. J.*, **2010**, *165*, 573-580.

[14]Soliman M .E., Saleh, B. M., Ahmed, A. S., *Anal. Chim. Acta*, **2004**, *523*, 133- 140.

[15]Rajesh, N., Gurulakshmanan, G., *Spectrochim. Acta A*, **2008**, *69*, 391–395.

[16]Zhang, Y., Kogelnig, D., Morgenbesser, C., Stojanovic, A., Jirsa, F., Lichtscheidl-Schultz, I., Krachler, R., Li, Y., Keppler, B. K., *J. Hazard. Mater.*, **2011**, *196*, 201-209.

[17]Mondal, D. K., Nandi, B. K., Purkait, M.K., *J Environ Chem Eng*, 2013, *1(4)*, 891-898.

[18]Sarwghadi, M., Nedaie, M., Taherian, A., Ghaznavia, A., Eftekhari, A., Bandegharaei, A. H., Hosseini, M. S., Jalalabadi, Y., *Chem Eng J*, 2011, *168*, 1163–1173.

[19]Wen, L-S., Jiann, K-T., Santschi, P. H., *Marine Chem.*, **2006**, *101*, 104–129.

[20]Gode, F., Pehlivan, E., *J. Hazard. Mater.*, **2006,** *B136*, 330–337.

[21]Lin, L-C., Juang, R-S., *Chem Eng J*, 2007, *132*, 205–213.

[22]Wu. R. S. S., Lam, K. H., Lee, J. M. N., Lau, T. C., *Chemosphere*, **2007**, *69*, 289–294.

[23]Etou, A., Bai, S., Saito, T., Noma, H., Okaue, Y., Yokoyama, T., *J. Colloid Interfac. Sci.*, **2009**, *337*, 606–609.

[24]Kirsty, P., McCallum, N., Welch, L., *Forensic Sci. Int.*, **2012**, *6*, 282–285.

[25]Ho, Y-S., *Scientometrics*, 2004, *59 (1)*, 171-177.

[26]Haerifar, M and Azizian, S., *J. Phys. Chem.* C, **2013**, *117*, 8310−8317.

[27]Barkakati, P., Begum, A., Das, M. L., *Chem. Eng. J.*, **2010**, *161*, 34–45.

[28]Ferrah, N., Abderrahim, O., Didi, M.A., Villemin, D., *Desalination*, **2011**, *269*, 17–24.

[29]Manouchehri, N., Bermond, A., *Anal. Chim. Acta*, **2006**, *557*, 337–343.

[30]Biswajit, S., Sudip, K, D., *Colloid Surface B*, **2011**, *84*, 221–232.

[31]Kadous, A., Didi, M. A., Villemin, D., *J. Radioanal. Nucl. Chem.*, **2011**, *288(2)*, 553 – 561.

[32]Mondal, B. C., Das, A. K., *Anal. Chim. Acta*, **2003**, *477*, 73-80.

[33]Dutta, S., Bhattacharyya, A., De, P., Ray, P., Basu, S., *J. Hazard. Mater.*, **2009**, *172*, 888–896.

[34]Hassan, S. S. M., Awwad, N. S., Aboterika, A. H. A., *J. Hazard. Mater.*, **2008**, *154*, 992–997.

[35]Meena, A. K., Kadirvelu , K., Mishra, G. K., Rajagopal, C., Nagar, P. N., *J. Hazard. Mater.*, **2008**, *150*, 604–611.

[36]Ghodbane, I., Hamdaoui, O., *J. Hazard. Mater.*, **2008**, *160*, 301–309.

[37]Gao,Y., Canck, E. D, Leermakers, M., Baeyens, W., Van Der Voort, P., *Talanta*, **2011**, *87*, 262– 267.

[38]Sari, A., Tuzen, M., *J. Hazard. Mater.*, **2009**, *171*, 500–507.

[39]Bayramoğlu, G., Tuzun, I., Celik G., Yilmaz, M., Yakup Arica, M., *Int. J. Miner. Process*, **2006,** *81*, 35–43.

Received: 07.07.2014.
Accepted: 14.08.2014.

METHANOLYSIS OF *N*-ACETOXY-*N*-*n*-PROPYLOXY-*N*',*N*'-DIMETHYLUREA IN DIFFERENT CONDITIONS

Vasiliy Georgievich Shtamburg,[a] Alexandr Valerievich Tsygankov,[b] Victor Vasilievich Shtamburg,[c] Andrey Alexandrovich Anishchenko,[a]* Alexander Vladimirovich Mazepa[d] and Remir Grigorievich Kostyanovsky[e]

Keywords: nucleophilic substitution at nitrogen; *N*-acyloxy-*N*-alkoxyureas; *N*,*N*-dialkoxyureas; methanolysis.

The methanolysis of *N*-acetoxy-*N*-*n*-propyloxy-*N',N'*-dimethylurea in the presence of strong acids at room temperatures or in the boiling methanol yields *N*,*N*-dimethoxy-*N',N'*-dimethylurea as final product. Primarily the nucleophilic substitution acetoxy group at nitrogen on methoxy group arises. At second stage the transesterification of *N*,*N*-dialkoxyamino group of formed *N*-methoxy-*N*-*n*-propyloxy-*N',N'*-dimethylurea take place.

* Corresponding Authors
Tel: +**380**-68-410-41-79
E-Mail: Koloxai@gmail.com
[a] Ukrainian State Chemico-Technologycal University, 49038 Ukraine, Dnepropetrovsk, Mostovaya st., 2/6.
[b] State Flight Academy of National Aviation University, 25013 Ukraine, Kirovograd, 50 Let Octiabrya,22/127
[c] Ukrainian State Chemico-Technologycal University, 61050 Ukraine, Kharkov, Moskovsky pr., 31/56.
[d] Bogatsky Physiko-Chemical Institute of NAS of Ukraine, 65063 Odessa, Armeyskaya st. 21 .107.
[e] Semenov Institute of Chemical Physics, Russian Academy of Sciences, 119991, Russian Federation, Moscow, Kosygina st., 4.

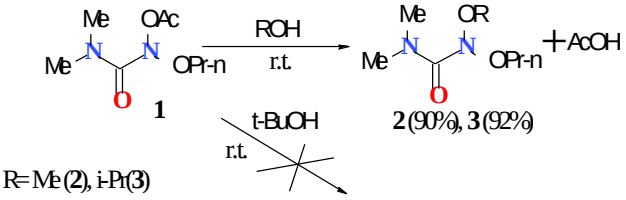

Scheme 1

INTRODUCTION

Amides,[2-9] carbamates,[10,11] and ureas,[10-15] having at nitrogen atom two electronegative substituents, one of them is alkoxy group and other substituent may be alkoxy group, acyloxy group, chlorine atom, 1-pyridinium group, are called "anomeric amides" due to $n_{O(Alk)} \rightarrow \sigma^*_{N-X}$ (X= OC(O)R, Cl, OAlk, $N^+C_5H_5$) anomeric effect domination. In X−N−O(R) group amide nitrogen is sp^3 hybridized and has pyramidal configuration, (Alk)O−N bond is shortened and N−X bond is elongated and destabilized. Due to this N−X bond destabilization the S_N2 nucleophilic substitution at amide nitrogen atom becomes possible.[2,4,6]

Earlier we had found that alcoholysis of *N*-acyloxy-*N*-alkoxyureas by primary and secondary alcohols at room temperatures (18-25 °C) yields the proper *N*,*N*-dialkoxyureas[7] (Scheme 1). If the methanolysis of *N*-acetoxy-*N*-*n*-propyloxy-*N',N'*-dimethylurea **1** arises during 55 hours, the final isopropanolysis of compound **1** occurs during 1224 hours.[10] The *tert*-butanolysis of compound **1** no take place at room temperature because steric hindrances to the nucleophilic substitution at nitrogen,[10] realized, probably, via S_N2 mechanism.[2,4,6-8,10]

By alcoholysis at room temperatures *N*-acetoxy-*N*-*n*-propyloxy-*N',N'*-dimethylurea **1** selectively converts in *N*,*N*-dialkoxyureas **2**,**3** and acetic acid. In these conditions acetic acid is indifferent to *N*,*N*-dialkoxyureas **2**,**3**.

But the influence of alcoholysis temperature and the presence of strong acids on the alcoholysis process remained practically unstudied.

EXPERIMENTAL

^{1}H NMR spectra were recorded on a Varian VXP-300 spectrometer (300 MHz, internal standard – Me_4Si), chemical shifts in σ-scale (ppm), coupling constants in Hz). Mass spectra were recorded on a VG-70EQ 770 mass spectrometer in FAB mode (FAB) and on Kratos MS 890 mass spectrometer electron impact mode (EI) and chemical ionization mode (CI), gas-reagent isobutane. MeOH was dried by boiling and distillation over Ca.

N-Acetoxy-N-n-propyloxy-N',N'-dimethylurea (1).[10]

Yellowish oil, n_D^{20} 1.4561. ^{1}H NMR (300 MHz, $CDCl_3$): 0.95 (t, 3H, $OCH_2CH_2\underline{Me}$, ^3J = 7.2 Hz), 1.68 (sex, 2H, $OCH_2C\underline{H_2}Me$, ^3J = 7.2 Hz), 2.15 (s, 3H, NO_2CMe), 3.04 (s, 6H, NMe_2), 4.04 (t, 2H, $OC\underline{H_2}CH_2Me$, ^3J = 7.2 Hz), IR (ν, $см^{-1}$): 1784 (C=O), 1732 (C=O). MS (CI, m/z (I_{rel}(%)): 206 $[M+2H]^+$ (17.3); 205 $[M+H]^+$ (100), 204 M^+ (9.4), 203 (11.9), 174 (15.3), 160 (16.0), 148 (10.8), 132 (25.8). Found (%): C 47.12, H 8.02, N 13.65. Calc. for $C_8H_{16}N_2O_4$ (%): C 47.05, H 7.90, N 13.72.

 DOI: 10.17628/ecb.2014.3.869-872

Methanolysis of *N*-acetoxy-*N*-*n*-propyloxy-*N',N'*-dimethylurea (1) in boiling MeOH.

The solution of *N*-acetoxy-*N*-*n*-propyloxy-*N',N'*-dimethylurea **1,**[10] (3.95 mmol, 0.81 g) in MeOH (6 ml) was boiled for 4 h, than reaction mixture was evaporated *in vacuo*, the residue was distilled at 1 Torr, yielding 0.45 g (76 %) of *N*,*N*-dimethoxy-*N',N'*-dimethylurea **4**, colorless liquid, bp. 98 – 99.5 °C (7 Torr), n_D^{20} 1.4470, identified with the reference sample of **2,**[10] by ^{1}H NMR. ^{1}H NMR (300 MHz, $CDCl_3$): 3.00 (s, 6H, NMe_2), 3.75 (s, 6H, $N(OMe)_2$).

***N*,*N*-Dimethoxy-*N',N'*-dimethylurea (4)**

N,N-dimethoxy-N',N'-dimethylurea (the reference sample) was obtained by methanolysis of *N*-acetoxy-*N*-methoxy-*N',N'*-dimethylurea,[10] at 20 °C for 34 h with yield 67 %.

***N*-Methoxy-*N*-*n*-propyloxy-*N',N'*-dimethylurea (2)**.

Colorless oil, bp. 95-95.5 °C (1 Torr); n_D^{26} 1.4449, obtained by the methanolysis of *N*-acetoxy-*N*-*n*-propyloxy-*N',N'*-dimethylurea **1** at 20 °C for 55 h with yield 80 %[10] and *n*-propanolysis of *N*-acetoxy-*N*-methoxy-*N',N'*-dimethyl-urea,[10] at 30 °C for 264 h with yield 82 %. ^{1}H NMR (300 MHz, $CDCl_3$): 0.96 (t, 3H, $CH_2CH_2\underline{Me}$, ^3J = 7.1 Hz), 1.67 (sex, 2H, $CH_2C\underline{H_2}Me$, ^3J = 7.1 Hz), 3.00 (s, 6H, NMe_2), 3.73 (s, 3H, NOMe), 3.91 (t, 2H, $NOCH_2$, ^3J = 7.1 Hz). MS (CI, m/z (I_{rel}(%)): 177 $[M+H]^+$ (7.7), 175 (6.4), 174 (9.9), 161 (32.8), 160 (11.0), 146 (14.0), 145 (19.0), 133 (11.2), 118 (13.9), 117 (46.5), 116 (29.3), 105 (12.9), 104 (24.3), 103 (40.2), 90 (14.3), 89 (100);, 73 (20.7), 72 (23.5). Found (%): C 47.82, H 9.17, N 15.63. Calc. for $C_7H_{16}N_2O_3$ (%): C 47.71, H 9.15, N 15.90.

Transesterification of *N*-methoxy-*N*-*n*-propyloxy-*N',N'*-dimethylurea (2) by MeOH in the presence of AcOH.

The solution of *N*-methoxy-*N*-*n*-propyloxy-*N',N'*-dimethylurea **2** (0.500 mmol, 0.085 g) and AcOH (0.500 mmol, 0.030 g) in MeOH (1 ml) was boiled for 1 h, then MeOH was evaporated *in vacuo*, the residue was kept at 5 Torr and 23 °C, yielding 0.052 g (72 %) *N*,*N*-dimethoxy-*N',N'*-dimethylurea **4**, identified by ^{1}H NMR.

Methanolysis of *N*-acetoxy-*N*-*n*-propyloxy-*N',N'*-dimethylurea (1) in the presence of CF_3CO_2H.

N-Acetoxy-*N*-*n*-propyloxy-*N',N'*-dimethylurea **1** (1.474 mmol, 0.301 g) was added to solution of CF_3CO_2H (0.79 mmol, 0.09 g) in MeOH (4 ml). The reaction mixture was kept at 15 °C for 5 h, then MeOH was evaporated *in vacuo*, the residue was extracted by Et_2O (6 ml). Et_2O-Extract was evaporated *in vacuo*, the residue was kept at 2 Torr and 20 °C, yielding 0.214 g yellowish oil, which was identified by ^{1}H NMR as mixture of *N*-methoxy-*N*-*n*-propyloxy-*N',N'*-dimethylurea **2,**[10] and *N*,*N*-dimethoxy-*N',N'*-dimethylurea **4** in molar ratio 69.8 %:30.2 % (molar). It means 60.5 % yield of urea **2** and 26.1 % yield of urea **4**.

Methanolysis of *N*-acetoxy-*N*-*n*-propyloxy-*N',N'*-dimethylurea (1) in the presence of oxalic acid.

N-Acetoxy-*N*-*n*-propyloxy-*N',N'*-dimethylurea **1** (2.34 mmol, 0.60 g) was added to solution of oxalic acid (0.29 mmol, 0.03 g) in MeOH (4 ml). The reaction mixture was kept at 18-20 °C for 100 h, then MeOH was evaporated *in vacuo*, the residue was extracted by Et_2O (10 ml). Et_2O-Extract was evaporated *in vacuo*, the residue was kept at 1 Torr and 20 °C, yielding 0.31 g (71 %) *N*,*N*-dimethoxy-*N',N'*-dimethylurea **4**, identified by ^{1}H NMR.

Transesterification of *N*-methoxy-*N*-*n*-propyloxy-*N',N'*-dimethylurea (2) by MeOH in the presence of oxalic acid.

The mixture of *N*-methoxy-*N*-*n*-propyloxy-*N',N'*-dimethylurea **2,**[10] (0.466 mmol, 0.081 g), oxalic acid (0.052 mmol, 0.005 g) and MeOH (1 ml) was kept at 20 °C for 73 h, then MeOH was evaporated *in vacuo*, the residue was extracted by Et_2O (3 ml). Et_2O-Extract was evaporated *in vacuo*, the residue was extracted mixture of Et_2O (4 ml) and hexane (1 ml), the extract was evaporated *in vacuo*, the residue was kept at 5 Torr and 20 °C, yielding 0.045 g (66 %) of *N*,*N*-dimethoxy-*N',N'*-dimethylurea **4**, identified by NMR ^{1}H.

Ethanolysis of *N*-acetoxy-*N*-methoxyurea (5) in boiling EtOH.

The solution of *N*-acetoxy-*N*-methoxyurea **5,**[11,16] (0.1601 mmol, 0.0237 g) in EtOH (4 ml) was boiled for 1 h, then EtOH was evaporated *in vacuo*, the residue was extracted by CH_2Cl_2 (3 ml), the CH_2Cl_2-extract was evaporated *in vacuo*, the residue was kept at 2 Torr and 20 °C, yielding 0.0172 g (80 %) of *N*-ethoxy-*N*-methoxyurea **6,** colourless oil**,** n_D^{20} 1.4493, identified by ^{1}H NMR and MS. ^{1}H NMR (300 MHz, $CDCl_3$): 1.33 (t, 3H, $NOCH_2\underline{Me}$, ^3J = 6.9 Hz), 3.84 (s, 3H, NOMe), 4.13 (q, 2H, $NO\underline{CH_2}Me$, ^3J = 6.9 Hz), 5.64 (br. s, 1H, NH), 5.96 (br. s, 1H, NH). MS (FAB, NaI, m/z (I_{rel} %)): 157 $[M+Na]^+$ (22), 89 $H_2NC(O)N^+OMe$ (25), 72 (77), 58 (100). Found (%): C 35.93, H 7.80, N 20.69. Calc. for $C_4H_{10}N_2O_3$ (%): C 35.82, H 7.51, N. 20.88. Also, *N*-ethoxy-*N*-methoxyurea **6** was obtained by ethanolysis of *N*-acetoxy-*N*-methoxyurea **5** at 15 °C for 69 h with yield 88 %.

Methanolysis of *N*-acetoxy-*N*-ethoxyurea (7) in boiling MeOH.

The solution of *N*-acetoxy-*N*-ethoxyurea **7,**[10,11] (0.925 mmol, 0.150 g) in MeOH (3.5 ml) was boiled for 4 h, then MeOH was evaporated *in vacuo*, the residue was extracted by CH_2Cl_2 (6 ml),the CH_2Cl_2-extract was evaporated *in vacuo*, the residue was kept at 2 Torr and 20 °C, yielding 0.089 g (72 %) of *N*-ethoxy-*N*-methoxyurea **6,** identified by ^{1}H NMR.

RESULTS AND DISCUSSION

This work is devoted to study of the influence of conditions of alcoholysis of *N*-acyloxy-*N*-alkoxyureas on the nature of formed products. As we found the main product of methanolysis *N*-acetoxy-*N*-*n*-propyloxy-*N',N'*-dimethylurea **1** in boiling methanol (4 h) was *N*,*N*-dimethoxy-*N',N'*-dimethylurea **4** (Scheme 2).

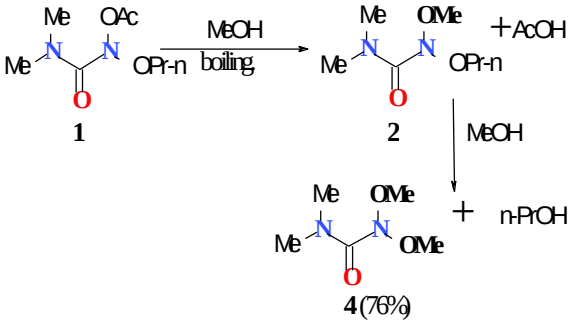

Scheme 2

Probably, at the first stage *N*-methoxy-*N*-*n*-propyloxy-*N',N'*-dimethylurea **2** forms by nucleophilic substitution of acetoxy group at nitrogen in compound **1**. The weak signals of protons of urea **2** can be observed in ^{1}H NMR of reaction mixture. Then, at second stage, the transesterification of *N*,*N*-dialkoxyamino group of *N*,*N*-dialkoxyurea **2** by methanol arises yielding *N*,*N*-dimethoxy-*N',N'*-dimethylurea **4**. Presumably the other product of propanolysis *N*-acetoxy-*N*-*n*-propyloxy-*N',N'*-dimethylurea **1**, acetic acid, catalyses this transesterification but only at boiling temperature (64 °C), not at room temperatures.[10] As was found earlier,[17,18] transesterification of *N*,*N*-dialkoxyamino group of *N*,*N*-dialkoxy-*N',N'*-dimethylureas,[17] and *N*,*N*-dialkoxy-*N*-*tert*-alkylamines,[18] took place by catalysis of more strong acids, such as TsOH.

This presumption is supposed by the independent transesterification of *N*-methoxy-*N*-*n*-propyloxy-*N',N'*-dimethylurea **2** to *N*,*N*-dimethoxy-*N',N'*-dimethylurea **4** by the boiling of methanolic solution of compound **2** in the presence of acetic acid during 4 hours (Scheme 3)

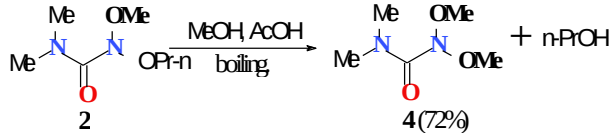

Scheme 3

We suggested that in the presence of acid, which is more strong than acetic aced, the secondary trasesterification will be occur at methanolysis of *N*-acetoxy-*N*-*n*-propyloxy-*N',N'*-dimethylurea **1** at room temperature. Actually, it methanolysis in presence of trifluoroacetic acid at 15 °C for 5 hour yields the mixture of *N*,*N*-dialkoxyureas **2** and **4** in molar ratio 69.8 %:30.2 %. Respectively, yield of **2** is 61 %, yield of **4** is 26 %.

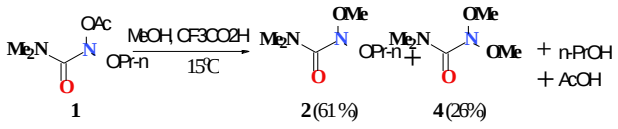

Scheme 4

In the presence of oxalic acid *N*-acetoxy-*N*-*n*-propyloxy-*N',N'*-dimethylurea **1** converted by the methanolysis at 20 °C for 100 hour selectively in *N*,*N*-dimethoxy-*N',N'*-dimethylurea **4** (Scheme 5). The traces of *N*,*N*-dialkoxyurea **2** are absent in the reaction mixture.

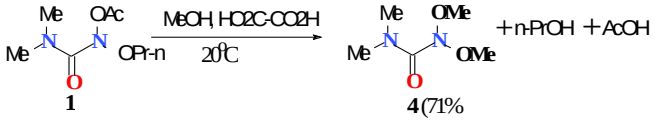

Scheme 5

Indeed, *N*-methoxy-*N*-*n*-propyloxy-*N',N'*-dimethylurea **2** easily react with MeOH on the presence of oxalic acid (20 °C, 73 h), yielding *N*,*N*-dimethoxy-*N',N'*-dimethylurea **4** (Scheme 6)

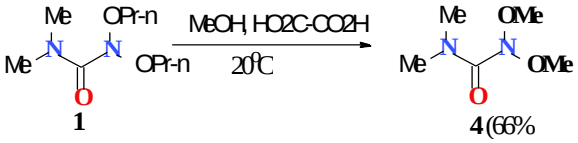

Scheme 6

Interestingly that for "unsubstituted" *N*-acetoxy-*N*-alkoxyureas **5**,**7** tranesterication of *N*,*N*-dialkoxyamino group in boiling alcohols in the presence of acetic acid don't take place (Scheme 7).

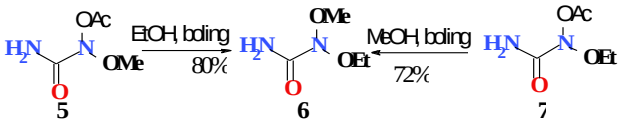

Scheme 7

This difference in the reactivity of *N*-acetoxy-*N*-*n*-propyloxy-*N',N'*-dimethylurea **1** and *N*-acetoxy-*N*-alkoxyureas **5**,**7** can be understood on the assumption of S_N1 mechanism of transesterification *N*,*N*-dialkoxyamino group (Scheme 8). Earlier Glover has found that *N*-acetoxy-*N*-alkoxybenzamides underwent acid-catalyzed solvolysis by the $A_{Al}1$ (S_N1) mechanism.[2,4,19]

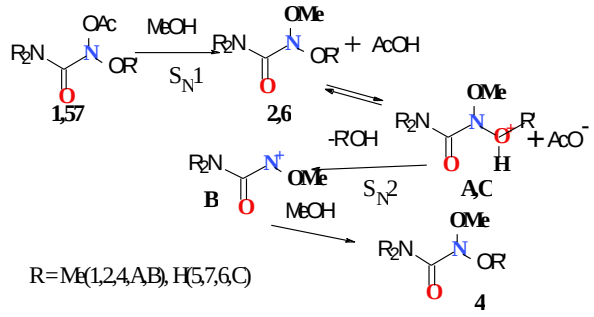

Scheme 8

At the first stage the nucleophilic substitution of acetoxy group by S_N2 mechanism,[2,4,6] take place. Then reversible O-protonation *N*,*N*-dialkoxyureas **2**,**6** arises. At the methanol boiling temperature protonated intermediate **A** (R=Me)

dissociates to nitrenium cation **B**, which reacts with methanol yielding *N,N*-dimethoxyurea **4**. The dimethylcarbamoyl moiety is only weakest electron-withdrawing substituent than methoxynitrenium cation **B** destabilization arises.

In the case of protonated intermediate **C** (R = H) it further dissociation to unstable methoxynitrenium cation becomes impossible because it carbamoyl moiety has substantial electron-withdrawing effect.

Thus methanolysis of *N*-acetoxy-*N*-*n*-propyloxy-*N',N'*-dimethylurea in the presence of strong acids at room temperatures or in the boiling methanol proceeds as two stage process yielding *N,N*-dimethoxy-*N',N'*-dimethylurea as final product.

Acknowledgement

This work was supported by the Russian Foundation for Basic Research (grant no. 13-03-90460) and Ukrainian Foundation for Fundamental Research (Grant no. F-53/105-2013).

References

[1]Shtamburg, V. G., Shishkin, O. V., Zubatyuk ,R. I., Shtamburg, V. V., Tsygankov, A. V., Mazepa, A. V., Kadorkina, G. K., Kostyanovsky, R. G., *Mendeleev Commun.*, **2013**, *23*, 289-291.

[2]Glover, S. A., *Tetrahedron*, **1998**, *54*, 7229-727.

[3]Gerdes, R. G., Glover, S. A., Ten Have, J. F., Rowbottom, C. A., *Tetrahedron Lett.*, **1989**, *31*, 5377-5380.

[4]Glover, S. A. Chapter 18. "*N-Heteroaton-substituted hydroxamic esters*" in "*The Chemistry of Hydroxylamines, Oximes and Hydroxamic Acids*", ed. Rappoport Z. and Liebman J. F., **2009**, John Wiley & Sons, Ltd.

[5]Gillson, A-M. E., Glover, S. A., Turner, D. J., Turner, P. *Org. Biomol. Chem.*, **2003**, *1*, 3430-3437.

[6]Cavanach, K. L., Glover, S. A., Price, H. L. Schumacher, R. R., *Aust. J. Chem.*, **2009**, *62*, 700 – 710.

[7]Digianantonio, K. M., Glover, S. A., Johns, J. P., Rosser, A. A., *Org. Biomol. Chem.*, **2011**, *9*, 4116-4126.

[8]Glover, S. A., White, J. M., Rosser, A. A., Digianantonio, K. M., *J. Org. Chem.*, **2011**, *76*, 9757 – 9763.

[9]Shtamburg, V. G., Tsygankov, A. V., Shishkin, O. V., Zubatyuk, R. I., Uspensky, B. V., Shtamburg, V. V., Mazepa, A. V., Kostyanovsky, R. G., *Mendeleev Commun.*, **2012**, *22*, 164-166.

[10]Shtamburg, V. G., Klots, E. A., Pleshkova, A. P., Avramenko, V. I., Ivonin, S. P., Tsygankov, A. V., Kostyanovsky, R. G., *Russ. Chem. Bull*, **2003**, *52*, 2251 – 2260.

[11]Shishkin, O. V., Zubatyuk, R. I., Shtamburg, V. G., Tsygankov, A. V., Klots, E. A., Mazepa, A. V., Kostyanovsky, R. G., *Mendeleev Commun.*, **2006**, *16*, 222-223.

[12]Shtamburg, V. G., Shishkin, O. V., Zubatyuk, R. I., Kravchenko, S. V., Tsygankov, A. V., Mazepa, A. V., Klots, E. A., Kostyanovsky, R. G., *Mendeleev Commun.*, **2006**, *16*, 323-325.

[13]Shtamburg, V. G., Shishkin, O. V., Zubatyuk, R. I., Kravchenko, S. V., Shtamburg, V. V., Distanov, V. B., Tsygankov, A. V., Kostyanovsky, R. G., *Mendeleev Commun.*, **2007**, *17*, 178-180**.**

[14]Shtamburg, V. G., Tsygankov, A. V., Gerasimenko, M. V., Shishkin, O. V., Zubatyuk, R. I., Mazepa, A. V., Kostyanovsky, R. G., *Mendeleev Commun.*, **2011**, *21*, 50-52**.**

[15]Shtamburg, V. G., Tsygankov, A. V., Shishkin, O. V., Zubatyuk, R. I., Shtamburg, V. V., Gerasimenko, M. V., Mazepa, A. V., Kostyanovsky, R. G., *Mendeleev Commun.*, **2012**, *22*, *92-94.*

[16]Shishkin, O. V., Shtamburg, V. G., Zubatyuk, R. I., Olefir, D. A., Tsygankov, A. V., Prosyanik, A. V., Mazepa, A. V., Kostyanovsky, R. G., *Chirality*, **2009**, *21*, 642 - 647.

[17]Rudchenko, V. F., Shevchenko, V. I., Kostyanovskii, R. G., *Bull. Acad. Sci. USSR Div. Chem. Sci.*, **1986**, *37*, 1436 – 1440.

[18]Rudchenko, V. F., Shtamburg, V. G., Pleshkova, A. P., Nasibov, Sh. S., Chervin, I. I., Kostyanovskii, R. G., *Bull. Acad. Sci. USSR Div. Chem. Sci.*, **1981**, *30*, 2100 – 2109.

[19]Campbell, J. J., Glover, S. A., Hammond, G. P., Rowbottom, C. A., *J. Org. Chem. Perkin Trans. 2*, **1992**, 2067 – 2079.

Received: 27.07.2014.
Accepted: 14.08.2014.

SULFATE FREE RADICALS –A KINETIC APPROACH FOR OXIDATION OF L-ASCORBIC ACID IN AQUEOUS ACID MEDIUM

N. K. Soni, Riya Sailani,[a]* Anita Meena,[a] Vinita K. Gupta,[a] C. L. Khandelwal[a] and P. D. Sharma[a]

Keywords: sulfate free radicals; ascorbic acid; peroxodisulfate; radical kinetics; acid aqueous medium.

The kinetics of oxidation of L-ascorbic acid in absence and presence of silver(I) as catalyst has been studied in aqueous acid medium. The stoichiometry corresponds to the reaction as represented by eqn: $S_2O_8^{2-} + C_6H_8O_6 \rightarrow 2SO_4^{2-} + C_6H_6O_6 + 2H^+$. The order with respect to ascorbic acid is unity in uncatalyzed reaction where as it is zero order in silver (I) catalyzed reaction. The reaction mechanism has been suggested in both the conditions delineating the role of sulfate radical ion.

Corresponding Authors
Tel:+91-9928194174
E-Mail: l.p_riya@yahoo.co.in
[a] Department of Chemistry, University of Rajasthan, Jaipur-302055 (India)A

Introduction

Numerous studies on uncatalyzed and silver(I) catalyzed oxidations of various types of substrates by peroxodisulfate have been reported.[1-11] The rate of silver(I) catalyzed reactions was generally found to be independent of substrate(s) concentration in oxidation reactions of persulfate. However, certain questions still remain to be replied.

The thermal decomposition of peroxodisulfate is first order whereas the reaction is second order in the presence of certain substrate(s). Therefore, such observations are not only interesting but help in understanding chemistry of the oxidant owing to the formation of sulfate free radicals.

Similar is the situation in silver(I) catalyzed oxidation of the substrate which is also a second order reaction and the rate is still controlled by the interaction of catalyst and oxidant. However, no firm evidence is provided to discriminate between catalyst redox cycles viz. Ag^{I}/Ag^{II} or Ag^{I}/Ag^{III}.

Ascorbic acid (vitamin C) has played an essential role as a water soluble vitamin in diet. Survey is developed in a person due to its deficiency vitamin C is also known to help in cardiovascular and cancer diseases.[12] Interestingly plants and some animals make their own vitamin C but it is not in case of human bodies and is, therefore, sought from other sources.[13] It is added as a supplementary source in pharmaceutical preparations. Also, it is a known anti-oxidant in large number of biological processes. The kinetic based determinations in analytical chemistry have been exploited owing to its strong reducing properties.[14] The spectrofluorometric methods are based on vanadium(V) catalysed and ascorbic acid activated oxidation of rhodamine[15,16] or Saframine T[17] by bromate. Such were the observations that tempted us to undertake the title study to gain detailed insight of the reaction events *viz.* to *viz*. the role of sulfate free radicals in both silver (I) catalyzed and uncatalyzed oxidations of l-ascorbic acid by peroxodisulfate.

Experimental

Material and method

All the reagents employed in the kinetics study were either of AnalaR or guaranteed reagent grade and were employed as supplied. Silver nitrate (BDH) solution was prepared by dissolving requisite amount of the salt in doubly distilled water. The solution of silver nitrate, however, was kept in bottles painted black from the outside at refrigerated temperature (~ 5 ˚C) to check photochemical decomposition. Nevertheless, afresh solution of the catalyst was employed.

Twice distilled water was employed throughout the study; the second distillation was from an alkaline potassium permanganate solution in an all glass apparatus. Other reagents were employed as received.

Kinetic procedure

The reaction was conducted in Corning glass vessels painted black from the outside. These flasks were immersed in a water-bath thermostated at ± 0.1 °C unless stated otherwise. All other reaction ingredients of requisite concentrations except peroxodisulfate were taken in these flasks, the reaction was initiated by adding temperature pre-equilibrated peroxodisulfate solution and the time of initiation of the reaction was recorded when the pipette was half-emptied. An aliquot sample (5 cm^3) of the reaction mixture was withdrawn at different time intervals and then discharged into an ice-cold dil. H_2SO_4 (~1.0 mol dm^{-3}), the remaining ascorbic acid was then estimated by titrating

against cerium(IV) solution using n-phenylanthranilic acid as an indicator. The results in triplicate were reproducible within ± 6 %. Initial rates (k_i, mol dm^3 s^{-1}) were computed by employing plane mirror method.

Stoichiometry

The stoichiometry was determined by conducting reactions taking excess of ascorbic acid (H_2A) over peroxodisulfate (heretofore written as PDS) in glass stoppered vessels along with other reaction ingredients. The reaction mixtures were thermostated in a water-bath maintained at 40 ± 0.1 °C for ca. 4 h. The excess ascorbic acid was determined ceremetrically. The results correspond to the stoichiometry of the reaction as represented by Eqn. 1.

$$S_2O_8^{2-} + C_6H_8O_6 \xrightarrow{Ag^I} 2SO_4^{2-} + C_6H_6O_6 + 2H^+ \quad (1)$$

where $C_6H_6O_6$ is dehydroascorbic acid. Similar stoichiometry has earlier been reported.[18,19]

Results

Peroxodisulfate dependence

The concentration of peroxodisulfate varied fixing constant concentrations of other reaction ingredients. Initial rates (k_i, mol dm^{-3} s^{-1}) were calculated and a plot of initial rate against the concentration of the oxidant [PDS] yielded a straight line passing through the origin conforming first order with respect to peroxodisulfate in uncatalyzed and catalyzed reactions respectively.

L-Ascorbic acid dependence

The concentration of l-ascorbic acid also varied at constant concentrations of other reaction ingredients under pseudo first order conditions ([H_2A] << 10 [PDS]) and pseudo first order plots were made. However, rate was independent of gross initial concentrations of ascorbic acid in silver(I) catalyzed reaction ascribing rate to be first order with respect to substrate concentrations. Nevertheless, rate exhibited first order dependence with respect to ascorbic acid also in uncatalyzed reaction.

Silver(I) dependence

The concentration of silver (I) varied from 1.0x10^{-4} to 1.0x10^{-3} mol dm^{-3} at fixed concentrations of other reaction ingredients. A plot of initial rate against [Ag(I)] yielded a straight line passing through the origin conforming first order with respect to the catalyst.

If one takes into account these kinetic orders with respect to peroxodisulfate, ascorbic acid (H_2A) in uncatalyzed and silver(I) in catalyzed reactions respectively, following empirical rate Eqns. 2 and 3 are obeyed.

$$-\frac{d[S_2O_8^{2-}]}{dt} = k[S_2O_8^{2-}][H_2A] \quad (2)$$

$$-\frac{d[S_2O_8^{2-}]}{dt} = k_{Ag}[S_2O_8^{2-}][Ag^I] \quad (3)$$

where k and k_{Ag} are the second order rate constants in uncatalyzed and catalysed reactions respectively.

Hydrogen ion dependence

The concentration of hydrogen ion varied by employing perchloric acid at fixed concentrations of other reaction ingredients and also at constant ionic strength (I). (Ionic strength (I) was adjusted to be 0.5 mol dm^{-3} by employing lithium perchlorate). The rate, however, remains unchanged on varying ionic strength. The rate decreases with increasing hydrogen ion concentration in uncatalyzed reaction whereas rate is independent of hydrogen ion concentration in silver(I) catalyzed reactions.

Persulfate reactions normally show the presence of free radicals if the oxidant interacts with one-equivalent substrate. Free radicals were, therefore, tested in the reaction mixture by adding acrylic acid during the progress of the reaction. The monomer of this unsaturated acid changes to polymer yielded white solid material which after some time settles. This conforms participation of $SO_4^{\bullet -}$ free radicals. However, none of the reactants polymerized when the monomer was added in these reactant solutions respectively under identical experimental conditions of the reaction.

Discussion

Mechanism of uncatalyzed reaction

An important observation in uncatalyzed oxidation of L-ascorbic acid is the retardation of the rate by the addition of acrylic acid with the formation of white precipitate. Acrylic acid is known to be an efficient scavenger of sulfate free radicals in reactions of peroxodisulfate. Whether it is the initial interaction of the oxidant and the substrate to generate free radicals or simply the latter is generated by thermal decomposition of persulfate. Since the reaction is second order *viz*. first order with respect to each reactant, following mechanism consisting of Eqns. 4-9 can be envisaged involving role of free radicals.

$$H_2A \underset{}{\overset{K}{\rightleftharpoons}} HA^- + H^+ \quad (4)$$

$$S_2O_8^{2-} + HA^- \xrightarrow{K_1} SO_4^{2-} + SO_4^{\bullet -} + HA \quad (5)$$

$$SO_4^{\bullet -} + HA^- \xrightarrow{K_2} SO_4^{2-} + HA \quad (6)$$

$$HA + HA \xrightarrow{K_3} \text{Products} \quad (7)$$

$$SO_4^{\bullet -} + H_2O \xrightarrow{K_4} HSO_4^- + OH \quad (8)$$

$$OH + HA^- \xrightarrow{K_5} H_2O + A^{\bullet -} \quad (9)$$

where HA is the ascorbate radical.

Applying steady state to free radicals such as $SO_4^{\bullet -}$, HA and OH respectively which are in steady-state concentrations, Eqns. 10, 11 and 12 are obtained.

$$\frac{d[SO_4^{-}]}{dt} = k_1[S_2O_8^{2-}][HA^-] - k_2[HA^-][SO_4^{-}] - k_4[SO_4^{-}] = 0 \quad (10)$$

$$\frac{d[HA]}{dt} = k_1[S_2O_8^{2-}][HA^-] - k_2[HA^-][SO_4^{-}] - k_5[OH][HA^-] - k_3[HA^-]^2 = 0 \quad (11)$$

and

$$\frac{d[OH]}{dt} = k_4[SO_4^{-}] - k_5[OH][HA^-] = 0 \quad (12)$$

The rate of the reaction is given by Eqn. 13

$$-\frac{d[H_2A]}{dt} = k_3[HA]^2 \quad (13)$$

Eqn. 14 is obtained from Eqns. 11 and 13,

$$\frac{d[H_2A]}{dt} = k_1[S_2O_8^{2-}][HA^-] - k_2[HA^-][SO_4^{-}] - k_5[OH][HA^-] \quad (14)$$

The concentrations of free radicals ($SO_4^{\bullet -}$) and (OH) are obtained from Eqns. 10 and 12 as in Eqns. 15 and 16 respectively

$$[SO_4^{-}] = \frac{k_1[S_2O_8^{2-}][HA^-]}{k_2[HA^-] + k_4} \quad (15)$$

and

$$[OH] = \frac{k_4[SO_4^{-}]}{k_5[HA^-]} \quad (16)$$

If Eqns. 14, 15 and 16 are simultaneously considered, Eqn. 17 or 18 is obtained after accounting for an inequality $k_2[HA^-] >> k_4$.

$$\frac{d[H_2A]}{dt} = 2k_1[S_2O_8^{2-}][HA^-] \quad (17)$$

or

$$-\frac{d[H_2A]}{dt} = \frac{2k_1K[S_2O_8^{2-}][H_2A]}{[H^+]} \quad (18)$$

where $k=2k_1K$ is an observed composite second order rate constant.

The rate Eqn. 18 is in agreement with the rate equation obtained earlier[18] but slightly differing from other.[19] A plot of $(-d[H_2A]/dt)[S_2O_8^{2-}][H_2A] = k_{obs}$ was made against $[H^+]^{-1}$ that yielded a straight line passing through the origin (Fig 1).

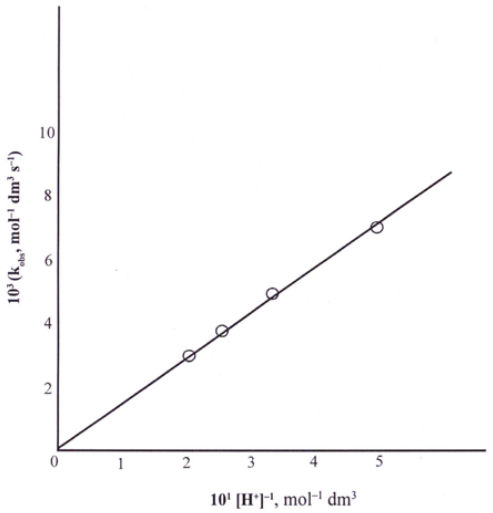

Figure 1. Plot of k_{obs} versus $[H^+]$ in ascorbic acid and peroxodisulphate reaction, [PDS]=5.0x10^{-2} M; [H_2A]=2.0x10^{-3} M; I=0.5 M; 40 °C

Mechanism of silver(I) catalyzed oxidation of ascorbic acid

The role of silver(I) as a catalyst in peroxodisulfate reactions is reported through the catalyst redox cycle of either Ag^I/Ag^{II} or Ag^I/Ag^{III}. Since the rate is independent of the substrate concentration, there is every possibility that higher valent silver(III) is obtained through the interaction of silver(I) and peroxodisulfate that oxidizes substrate in a fast step. An interaction of Ag(I) with persulfate to form Ag(II) is probably responsible for formation of sulphate free radical. Moreover, if the redox potential of Ag(II)/Ag(I) or Ag(III)/Ag(I) redox couples is any guide, the reactions of Ag(II) or Ag(III) with ascorbic acid must be very fast.

Considering these aspects, a plausible reaction mechanism for Ag(I) catalyzed oxidation of ascorbic acid can be envisaged as follows:

$$S_2O_8^{2-} + Ag(I) \xrightarrow{K_1} SO_4^{2-} + SO_4^{\bullet -} + Ag(II) \quad (19)$$

$$Ag(II) + H_2A \xrightarrow{K_2} HA + Ag(I) + H^+ \quad (20)$$

$$SO_4^{\bullet -} + H_2A \xrightarrow{K_3} HSO_4^- + HA \quad (21)$$

$$HA + HA \xrightarrow{K_4} \text{Product} \quad (22)$$

$$SO_4^{\bullet -} + H_2O \xrightarrow{K_5} HSO_4^- + OH \quad (23)$$

$$OH + H_2A \xrightarrow{K_6} H_2O + HA \quad (24)$$

Applying steady – state treatment to all intermediates such as $SO_4^{\bullet -}$, Ag^{II}, OH and HA, the following Eqns. 25-28 are obtained

$$\frac{d[SO_4^-]}{dt} = k'_1[S_2O_8^{2-}][Ag(I)] - k_3[SO_4^-][H_2A] - k_5[SO_4^-] = 0 \quad (25)$$

$$\frac{d[Ag(II)]}{dt} = k'_1[S_2O_8^{2-}][Ag(I)] - k_2[Ag(II)][H_2A] = 0 \quad (26)$$

$$\frac{d[(OH)]}{dt} = k_5[SO_4^-] - k_6[(OH)][H_2A] = 0 \quad (27)$$

$$\frac{d[HA]}{dt} = k'_2[Ag(II)][H_2A] - k_3[SO_4^-][H_2A] - k_6[OH][H_2A] - k_4[HA]^2 = 0 \quad (28)$$

The rate of the reaction is represented by Eqn. 29

$$\frac{d[(H_2A)]}{dt} = k'_2[Ag(II)][H_2A] + k_3[SO_4^-][H_2A] - k_6[(OH)][H_2A] \quad (29)$$

Combining Eqn. 29 with Eqns. 26 and 27, Eqn. 30 is obtained:

$$\frac{d[H_2A]}{dt} = k'_1[S_2O_8^{2-}][Ag(I)] \quad (30)$$

Such a rate Eqn. 30 accounts for first order dependence with respect to persulfate and silver(I) respectively and rate independence of ascorbic acid concentration.

Since the catalysed reaction does not exhibit any hydrogen ion dependence, an important question in silver(I) catalysed oxidation of ascorbic acid is whether the catalyst operates via a Ag^I/Ag^{II} or Ag^I/Ag^{III} redox cycle and needs discrimination between Ag^{II} or Ag^{III}. Since an evidence for formation of complexes such as $[FeSO_4]^+$ and $[FeSO_4]^{2+}$ has been adduced[20] in the reaction of $[Fe(II)\text{-}SO_4^{\bullet -}]$

If a similar complex such as $[Ag^I\text{-}SO_4^{\bullet -}]$ is also a possibility between Ag^I and $SO_4^{\bullet -}$ as in Eqn. 31, Ag^{II} is expected to be formed in a one-equivalent reaction 32 through the redox rupturing of such a complex. Ag^{II} formation interacts with ascorbic acid in a fast step 33

$$Ag^I + SO_4^{\bullet -} \rightleftharpoons [Ag^I.\ SO_4^{\bullet -}] \quad (31)$$

$$[Ag^I.\ SO_4^{\bullet -}] \rightleftharpoons Ag^{II} + SO_4^{2-} \quad (32)$$

$$2Ag^{II} + C_6H_8O_6 \xrightarrow{fast} 2Ag^I + C_6H_6O_6 + 2H^+ \quad (33)$$

However, the possibility of formation of such a complex $[Ag^{II}.\ SO_4]^+$ and then to rupture oxidatively also cannot be ruled out as in Eqn. 34

$$[Ag^{II}.\ SO_4]^+ \rightleftharpoons Ag^{III} + SO_4^{2-} \quad (34)$$

$$Ag^{III} + C_6H_8O_6 \xrightarrow{fast} Ag^I + C_6H_6O_6 + 2H^+ \quad (35)$$

Such an alternative proposal explains the kinetics of the reaction but requires an evidence[21,22] for the formation of Ag^{III}. If redox potential[23] of this sulphate radical ion (2.5-3.1 V) is taken into account, Ag^{II} should further be oxidized to Ag^{III}. Nevertheless, addition of 2,2′-bipyridine in the reaction mixture exhibits an orange coloured species of transient life time that negates formation of Ag^{III}. Such a colored test might not be positive in the light of the fact that Ag^{III} as soon as is formed it is consumed by ascorbic acid oxidant leaving no chance for its indication. Nevertheless, following observations if taken into account, the formation of Ag^{III} can be ruled out.

The oxidation of Ag^I to Ag^{II} is energetically more facile as $SO_4^{\bullet -}$ radical ion is one electron oxidant. One electron transfer processes are more facile than two electron transfer process energetically.

Since ascorbic acid being a strong reducing agent, it will not allow $SO_4^{\bullet -}$ to interact with Ag^{II}. There is every possibility of competition between Ag^{II} and ascorbic acid for $SO_4^{\bullet -}$ in which ascorbic acid appears to score over. Ag^{II} minimising the chances of formation of Ag^{III} significantly.

If silver(III) is formed through fast disproportionation of initially formed silver(II) as in step 36 under experimental conditions, the presence of Ag(I)

$$2Ag(II) \rightleftharpoons Ag(I) + Ag(III) \quad (36)$$

will push back this equilibrium 36 significantly minimizing the chances of formation of Ag(III).

Also, Ag(III) is not stable in acid medium in absence of any complexing ligand. The complexing ligand even in alkaline medium is required to stabilize it.

Such arguments are logically and adequately account for the possibility of operation of Ag^{I}/Ag^{II} catalyst redox cycle in preference to Ag^{I}/Ag^{III} catalyst redox cycle in the oxidation of ascorbic acid by peroxodisulfate in the presence of silver(I).

Conclusions

Silver(I) catalyzed oxidation of ascorbic acid by peroxodisulfate is second order reaction. The rate in Ag^{I} catalyzed reaction does not show hydrogen ion dependence as in case of uncatalyzed oxidation of ascorbic acid by peroxodisulfate in a manner characterized in other oxidations. Since the rate in catalyzed reaction is independent of ascorbic acid, it is established that the rate dependence on hydrogen ion in uncatalyzed reaction comes from ascorbic acid. Since rate is independent of ascorbic acid, in silver(I) catalysed oxidation, silver(I) catalyst redox cycle operates via Ag^{II}/Ag^{I} in preference to Ag^{III}/Ag^{I}.

Acknowledgement

This work was supported in part by the University Grant Commission, New Delhi, India through senior research fellowship for financial support. Acknowledgment is also made to the co-authors and Head of Department of Chemistry, UOR, Jaipur, Rajasthan, India.

References

[1]Wilmarth, W. K., Haim, A., *Peroxide Reaction Mechanisms*, Edwards, J.O. (Ed.) Interscience, New York, pp. 186, **1962**.

[2]House, D. A., *Chem. Rev.*, **1962**, *62*, 185.

[3]Anderson, J. M., Kochi, J. K., *J. Am. Chem. Soc.*, **1970**, *92*, 1651.

[4]Walling, C., Camaioni, D. M., *J. Org. Chem.*, **1978,** *43*, 3266.

[5]Prakash, A., Mehrotra, R. N., Kapoor, R. C., *Ind. J. Chem.*, **1982**, *21A*, 906.

[6]Sengar, H. G. S., Gupta, Y. K., *J. Ind. Chem. Soc.*, **1966**, *43*, 223.

[7]Prakash, A., Mehrotra, R. N., Kapoor, R. C., *J. Chem. Soc. Dalton Trans.*, **1976**, *16*, 1578.

[8]Mohanty, N. K., Panda, B. P., Pani, S., *Ind. J. Chem.*, **1988**, *27A*, 347.

[9]Dash, A. C., Nanda, R. K., Mohanty, P., *Ind. J. Chem.*, **1984**, *23A*, 11.

[10]Thusius, D. D., Taube, H., *J. Phys. Chem.*, **1967,** *71*, 3845.

[11]Gupta, K. S., Bhargava, P., Manoj, S. V., *Ind. J. Chem.*, **1999**, *38A*, 692.

[12]Carr, C., Frei, B., *Am. J. Clin. Nutr.*, **1999**, *69*, 1086.

[13]Guclu, K., Sozgen, K., Tutem, E., Ozyurek, M., Apak, R., *Talanta*, **2005**, *65*, 1226.

[14]Rustoiu-Csadari, A., Nickel, U., *Anal. Bioanal. Chem.*, **2002**, *374*, 1113.

[15]Li, S., Huang, L., Cen, X., *Xiangtan Daxue Ziran Kexue Xuebao*, **2000**, *22*, 73.

[16]Bao, S., Li, S., Hu, H., Shi, S., *Fenxi Shiyanshi*, **2001**, *20*, 4.

[17]Nickel, U., Peris, C. V., Ramminger, U., *J. Phys. Chem. A*, **2002**, *106*, 3773.

[18]Mehrotra, U. S., Mushran, S. P., *J. Ind. Chem. Soc.*, **1970**, *47*, 41.

[19]Kimura, M., Kobayashi, A., Boku, K., *Bull. Chem. Soc. Jpn.*, **1982**, *55*, 2068.

[20]McElroy, W. J., Waygood, S. J., *J. Chem. Soc. Faraday Trans.*, **1990**, *86*, 2557.

[21]Gogolev, A. V., Makarov, I. E., Fedoseev, A. M., Pikaev, A. K., *High Energy Chem.*, **1986**, *20*, 229.

[22]Kumar, A., Neta, P., *J. Am. Chem. Soc.*, **1980**, *102*, 7284.

[23]Neta, P., Huie, R. E., Ross, A. B., *J. Phys. Chem. Ref. Data*, **1988**, *17*, 1027.

Received: 03.07.2014.
Accepted: 16.08.2014.

SYNTHESIS, CHARACTERIZATION AND BIOLOGICAL ACTIVITY OF SOME METAL COMPLEXES OF BENZOYLACETONE SCHIFF BASE

T. I. Kashar[a,b]

Keywords: Schiff base; synthesis; IR; thermal analyses; biological activity.

N-Anilinoacetohydrazobenzoylacetone (H_2L) and their manganese(II), cobalt(II), nickel(II), copper(II) and zinc(II) complexes have been synthesized and characterized by IR, electronic spectra, molar conductivities, thermal analyses and magnetic susceptibilities. Binuclear complexes with molar ratios of M:L=2:1 are formed. IR spectra show that the ligand (H_2L) coordinates to the metal ions in a tetradentate manner with O_2N_2 donor sites in Mn(II), Co(II), Ni(II) and Zn(II) complexes while in the Cu(II) complexes the ligand coordinates as bidentate via N and O donor atoms. The electronic absorption spectra and magnetic susceptibility measurements show that all the complexes have octahedral structure. The copper(II) complexes shows higher antibacterial activity towards G^+ bacteria (*Bacillus subtilis*) than the ligand and other complexes while Mn(II) complex shows higher antifungal activity than the free ligand.

Corresponding Author
E-Mail: tahanikashar@yahoo.com
[a] Department of Chemistry, Faculty of Science, Menoufia University, Shebin El-Kom, Egypt .
[b] Department of Chemistry, Faculty of Science, Qassim University,Saudia Arabia

Introduction

Schiff bases have wide applications in many fields such as biological, inorganic and analytical chemistry[1,2] and are used in optical and electrochemical sensors, as well as in various chromatographic methods, to enable detection of enhanced selectivity and sensitivity.[3-5] Transition metal complexes of Schiff base have been widely studied because of their industrial, antifungal, antibacterial, anticancer, antiviral and herbicidal applications.[6-10] Complexes of Ni(II), Co(II) and Cu(II) with Schiff base ligands derived from β-diketones and *p*-anisidine have been studied,[11] these complexes have antimicrobial activity and show higher activity than the free ligands. There has been increasing interest in the synthesis and characterization of unsymmetrical Schiff base ligands and their metal complexes of biological interest. Phenylaminoacetic acid ethyl acetoacetate-2-ylmethylenehydrazone and its Mn(II), Fe(III), Co(II), Ni(II), Cu(II) and Zn(II) complexes have been synthesized and characterized by elemental analyses, IR, UV-vis, electrical conductivity, magnetic moment and thermal analyses (DTA, TGA).[12] The ligands behave as di- or tridentate mono or dibasic acid in these mononuclear complexes. Density functional theory (DFT) calculations indicated that the diketo form is the most stable tautomer and the agreement between the calculated and experimental vibrational frequencies is very good.[12] In this work N-anilinoacetohydrazobenzoylacetone (H_2L) and their metal complexes were synthesized and studied.

Experimental

All compounds and solvents used were resorced from BDH or Aldrich and used as received. The ligand was prepared by mixing ethanolic solutions of N-anilino-acetohydrazide (0.05 mol) and benzoylacetone (0.05 mol) with reflux for 3 h. The resulting product was filtered off and crystallized from ethanol. The complexes were prepared by the following general method. To a hot ethanolic solution of β-diketone hydrazone (0.05 mol) of metal salts (MCl_2) were added where [M=Mn(II), Co(II), Ni(II), Cu(II) and Zn(II)] or $Cu(NO_3)_2$ in (2:1) metal: ligand stoichiometric ratio. The reaction mixture was refluxed on a water bath for 4 hours. The formed complexes were filtered off, washed several times with pure dry methanol and dried in vacuum over anhydrous $CaCl_2$.

Measurements

Elemental analyses (C, H, N and Cl) were carried out at the microanalytical Unit of the University of Cairo. Metal ions were determined using atomic absorption with a Perkin Elmer (model 2380) spectrophotometer. The IR spectra were measured as KBr discs using a Perkin-Elmer 1430 infrared spectrometer (4000-200 cm^{-1}). Electronic absorption spectra were recorded in the 200-900 nm region on a Perkin-Elmer 550 spectrophotometer. The magnetic susceptibilities were measured at room temperature using the Gouy method with mercury(II) tetrathiocyanato-cobaltate(II) as magnetic susceptibility standard, diamagnetic corrections were made using Pascal's constants.[13] A Bibby conductimeter MCl was used for conductance measurements. The thermal analyses (TGA) were carried out on a Shimadzu TG-50 thermal analyzers in the 27-800 ^oC range at a heating rate of 10 ^oC min^{-1}.

Bacteria media

Nutrient agar medium was prepared by standard method.[14] The antibacterial activity of the ligand and its complexes were tested using the paper disc diffusion method[15] against Gram positive bacteria (*Bacillas Subtilis*) and Gram negative bacteria (*Nesseria gonorrleer*). The test compounds, in measured quantities, were dissolved in DMF to a concentration of 1000 ppm of compounds. Nutrient Agar media was poured in each Petri dish. After solidification, 0.1

cm^3 of the tested bacteria was spread over the medium using a spreader. Discs of Whatman No.1 filter paper having diameter of 5.00 mm, containing compounds were placed in the inoculated Petri plates. The plates were incubated at 28 °C for 24–48 h and the zone of inhibition was calculated in millimetres.

Fungus media

The test compounds in measured quantities were dissolved in DMF to a concentration of 1000 ppm of compounds. Czapek dox agar medium was prepared by a standard method.[14] *Penicillum notatum* was spread over each dish by using a sterile bent loop rod. Disks were cut by a sterilised cork borer and then taken by sterilised needle. The resulting pits were sites for the test compounds, the plates are sites for the test compounds. The plates were incubated at 30 °C for 24–48 h and any clear zones present were detected, the zone of inhibition was calculated in millimetres.

Results and Discussion

A new polydentate Schiff base (H_2L) was synthesized from the condensation of N-anilinoacetohydrazide with benzoylacetone in EtOH in 1:1 molar ratio. The ligand formed was characterized by elemental analysis,[1] HNMR and IR spectral analyses. The results of elemental analyses with molecular formula and the melting point are presented in Table 1. The results obtained are in a good agreement with those calculated for the suggested formula and the melting point is sharp indicating the purity of the prepared Schiff base (Scheme 1)

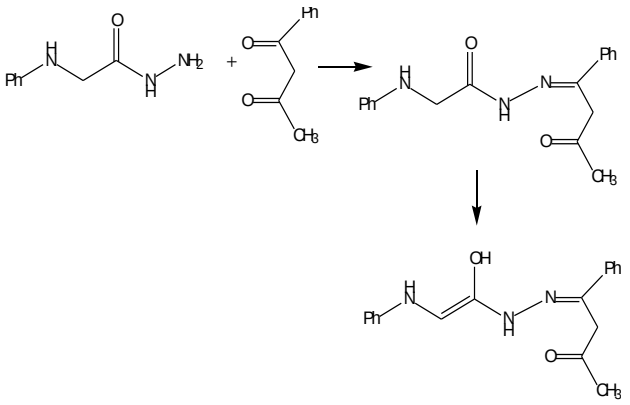

Scheme 1

IR Spectra

The data of the IR spectra of Schiff base ligand (H_2L) and its complexes are listed in Table 2. The ligand (H_2L) has tautomeric forms as shown in Scheme 1. The IR spectrum of the ligand shows a broad band in the 3400–3100 cm^{-1} ranges which may be assigned to stretching vibration of hydroxyl groups associated through inter- and intramolecular hydrogen bonds.[1] The spectrum shows strong bands at 3059, 1654 and 1600 cm^{-1} are assigned to the ν_{NH}, $\nu_{C=O}$ and $\nu_{C=N}$ respectively.[17-21] The IR spectra of the complexes are compared with the free ligand in order to determine the coordination sites that may be involved in chelation. New peaks are also guide peaks as well as ν_{OH} of water of coordination, and these characteristic peaks are listed in Table 2. The spectra of the metal complexes reveals that the presence of lattice water molecules in the prepared complexes, except C-1 and C-6. It is assigned by the broad band around 3400 cm^{-1} which is usually assigned to OH stretching modes of lattice water. However the broad band due to the coordinated water molecules appears in the 3400–3200 cm^{-1} range.[22,23] Two weaker bands around 950 and 800 cm^{-1} could be assigned to out of plane deformation modes of OH bands stretching, rocking and wagging modes of vibrations. In complexes C-4 and C-5 the ν_{NH} appears as strong band at 3243 and 3059 cm^{-1}.[22,23] All the complexes show a strong band at 1654 – 1651 cm^{-1} Table 2 which is assigned to $\nu_{C=O}$ of β-diketone moiety.[24] In complexes C-4 and C-5 $\nu_{C=O}$ of hydrazide moiety appeared as strong band at 1728 and 1726 cm^{-1}. The $\nu_{C=N}$ and ν_{N-N} bands are shifted to lower or higher wave length indicating that these groups participate in coordination.[25,26] All the complexes showing new medium and weak bands at 694–602 and 514–504 cm^{-1} ranges due to ν_{M-O} and ν_{M-N} vibrations, respectively[27,28] indicated that the bonding of the metal ions to the H_2L is through the oxygen and nitrogen atoms. All the complexes show a medium band at 450–400 cm^{-1} range except C-5 corresponding to terminal and bridging chloride atoms.[27]

Therefore from the IR spectra it is concluded that H_2L behaves as monobasic or neutral tri or bidentate ligand coordinated to the metal ion via carbonyl oxygen of benzoylacetone and enolic oxygen of hydrazide moiety and azomethine nitrogen atom.

^{1}H NMR spectra

The ^{1}H NMR spectrum of the ligand H_2L in DMSO-d_6 confirmed the proposed structure. The peaks at 6.3 and 4.6 are assignable to the protons of NH group (s, 1H, NH).[29] Multiplet signals at 7.8–7.2 ppm range are observed due to aromatic protons (m, 5H, Ar-H). The resonances at 2.1-2.3 ppm correspond to CH_2 groups. The methyl group signal is appeared as a single peak at 1.3 ppm. The OH group signal is appeared at 3.8 ppm as broad peak. ^{1}H NMR spectrum of the Zn(II) complex reveals the following signals: 7.5–7.3 ppm (m, 5H, Ar-H), 7.8 and 4.5 ppm (s, 1H, NH), 2.5 ppm (s, 2H, CH_2), 1.9 ppm (s, 3H, CH_3). The comparison of the spectrum of Zn(II) complex with the parent Schiff base shows that the peak of OH which appeared at 3.8 ppm in the ligand has disappeared in the spectrum of Zn(II) complex indicating that the coordination occurs through enolic oxygen of hydrazide moiety.[12]

Electronic spectra

The electronic spectral data of the ligand (H_2L) and its complexes are listed in Table 3. The ligand shows four bands at 340, 320, 280 and 240 nm which may be due to n-π* and π-π* transitions. All the complexes show two bands in the 350–300 and 300–240 nm ranges which are assigned to intra-ligand transitions.[30] The binuclear complexes of Mn(II), Co(II) and Ni(II) show two bands at 550–530 nm and 400–350 nm due to $^3T_1 \rightarrow {}^3T_2$ and $^3T_1(F) \rightarrow {}^3T_2(P)$ d-d transitions.[31] The copper(II) complexes show different bands at 600, 480 and 620, 430 nm are assigned to ligand metal charge transfer $^2B_1 \rightarrow {}^2E$ and $^2B_1 \rightarrow {}^2B_2$ transition respectively indicating a distorted octahedral structure.

Table 1. Elemental analyses of the ligand H_2L and its complexes .

No.	Compound	Mp., C°	Colour	M.wt	C % Found calc.	H % Found calc.	N % Found calc.	Cl % Found calc.	M % Found calc.
	H_2L	235	yellow	309	69.3	6.3	13.5	-	-
					69.9	6.1	13.6	-	-
C-1	$[HLMn_2Cl(H_2O)_5]Cl_2$	>310	pale brown	614	35.3	5.5	6.5	11.4	18
					35.2	5.0	6.8	11.6	17.9
C-2	$[HLCo_2Cl(H_2O)_5]Cl_2.H_2O$	>310	Pale brown	639.8	33.9	5.2	6.7	11.7	19
					33.7	5.2	6.6	11.1	18.4
C-3	$[HLNi_2Cl(H_2O)_5]Cl_2.H_2O$	>310	Pale green	639.4	32.9	5.3	6.4	11.0	18.2
					33.7	5.2	6.6	11.1	18.4
C-4	$[(H_2L)_2CuCl(H_2O)]Cl.H_2O$	>310	dark brown	788.5	54.7	5.4	10.2	9.7	9.0
					54.8	5.3	10.7	9.0	8.0
C-5	$[(H_2L)_2CuNO_3(H_2O)]NO_3.3H_2O$	>310	green	813.5	54.0	5.4	11.8	-	8.0
					54.0	5.4	12.0	-	7.9
C-6	$[HLZn_2Cl(H_2O)_5]Cl_2$	270	pale yellow	617	35.2	4.2	6.9	11.1	21.1
					35.0	4.5	6.8	11.5	20.4

Table 2. Important IR spectral bands of the ligand H_2L and its complexes.

No.	Compound	υOH (H_2O)	υNH,CH		$\upsilon_{C=O}$ β-diketone	$\upsilon_{C=O}$ hydrazide	$\upsilon_{C=N}$	υ_{N-N}	υ_{M-O}
	H_2L	3400 (br)	3059 (s)	2951 (s)	1654 (s)	-	1592 (s)	1075 (s)	-
C-1	$[HLMn_2Cl(H_2O)_5]Cl_2$	3431 (br)			1651 (s)	-	1558 (s)	1100 (m)	507 (s)
C-2	$[HLCo_2Cl(H_2O)_5]Cl_2H_2O$	3551 (br)			1651 (s)	-	1555 (s)	1100 (w)	510 (s)
C-3	$[HLNi_2Cl(H_2O)_5]Cl_2.H_2O$	3430 (br)			1652 (s)	-	1591 (s)	1100 (m)	510(m)
C-4	$[(H_2L)_2CuCl(H_2O)]Cl.H_2O$	3350 (br)	3243 (br)		1654 (s)	1726 (s)	1595 (s)	1100 (m)	507 (s)
C-5	$[(H_2L)_2CuNO_3(H_2O)]NO_3.3H_2O$	3300 (br)	3059 (s)		1651 (s)	1728 (s)	1593 (s)	1100 (m)	514 (s)
C-6	$[HLZn_2Cl(H_2O)_5]Cl_2$	3440 (br)			1651 (s)	-	1590 (s)	1100 (m)	504 (s)

Magnetic moments

The room temperature magnetic moments of the complexes are shown in Table 3. The magnetic moment values of manganese(II) complex are 3.53 BM[33] while for the copper(II) complexes these are 1.8 and 2.3 BM[33] indicating octahedral structure. The zinc (II) complex show diamagnetic value .

Molar conductance measurements

The chelates are dissolved in DMF and the molar conductivities of 10^{-3} M solutions are measured. Table 3 shows the molar conductance values of the complexes. It is concluded from the results that the Mn(II), Co(II), Ni(II) and Zn(II) complexes have molar conductivity values in the range 130.8–167.3 Ω^{-1} mol^{-1} cm^2 indicating 1 : 2 electrolyte while copper(II) complexes have a molar conductance values of 61.6 and 86.6 Ω^{-1} mol^{-1} cm^2 which indicates 1:1 electrolyte.[34]

TGA Thermal Analyses

Thermogravimetric analyses (TGA) of the ligand and their complexes are used to: (i) get information about the thermal stability of these complexes (ii) decide whether the water molecules are inside or outside the inner coordination sphere of the central metal ion. In the present investigation, heating rates were suitably controlled at 10 °C min^{-1} under nitrogen atmosphere, and the weight loss was measured from the ambient temperature up to 800 °C. The results of the thermogravimetric analysis of the metal complexes show that the metal complexes lost their lattice water in the range 100-180 °C while some coordinated water is lost within the temperature range 110-240 °C[35] and then displayed the loss of other coordinated water and decomposition of the organic ligand within the temperature range from 220-300 °C. The coordinated water is lost in two steps in all complexes except C-4 and C-5 which is lost in one step. In C-1, C-2, C-4 and C-6 complexes the coordinated water is lost with one aniline molecule with percentage weight loss of 24.5 %, 22.9 % and 34.1 %, respectively, while in C-3 complex the coordinated water is lost with one HCl molecule with percentage weight loss of 14.2 %. One coordinated water and two HNO_3 are lost in C-5 complex with percentage weight loss of 17.7 %.

Antibacterial and antifungal screening

The aim of the producing and synthesising of any antimicrobial compound is to inhibit the microbe without any side effects on the patients The antimicrobial screening data, Table 4, show that the compounds exhibit antimicrobial properties, the metal chelates exhibiting a

Table 3. Electronic spectra, coductivity and magnetic moments of the ligand H_2L and its complexes .

No.	Compound	λ_{max}, nm	Λ, Ω^{-1} mol^{-1} cm^2	μ_{eff}, B.M
	H_2L	340, 320, 280, 240	10	-
C-1	$[HLMn_2Cl(H_2O)_5]Cl_2$	550, 393, 350, 301, 288, 243	167.3	3.53
C-2	$[HLCo_2Cl(H_2O)_5]Cl_2H_2O$	530, 399, 350, 327, 310, 302, 288, 240	167	3.43
C-3	$[HLNi_2Cl(H_2O)_5]Cl_2.H_2O$	543, 400, 350, 320, 313, 290, 240	139	3.04
C-4	$[(H_2L)_2CuCl(H_2O)]Cl.H_2O$	600, 480, 345, 309, 303, 240	61.6	1.86
C-5	$[(H_2L)_2CuNO_3(H_2O)]NO_3.3H_2O$	620, 430, 350, 310, 300, 240	86.6	2.36
C-6	$[HLZn_2Cl(H_2O)_5]Cl_2$	393, 351, 302, 292, 245	130.8	Dia

Table 4. Antimicrobial activity of the ligand H_2L and its complexes.

No. of compound	Compound	*Bacillas subtilis*	*Nesseria gonorrleer*	*Penicillum notatum*
	H_2L	3	3	4
C-1	$[HLMn_2Cl(H_2O)_5]Cl_2$	6	4	12
C-2	$[HLCo_2Cl(H_2O)_5]Cl_2H_2O$	12	-	10
C-3	$[HLNi_2Cl(H_2O)_5]Cl_2.H_2O$	3	18	4
C-4	$[(H_2L)_2CuCl(H_2O)]Cl.H_2O$	20	-	11
C-5	$[(H_2L)_2CuNO_3(H_2O)]NO_3.3H_2O$	20	12	11
C-6	$[HLZn_2Cl(H_2O)_5]Cl_2$	5	3	3

greater inhibitory effect than the parent ligand. From the data obtained, it is observed that the inhibition zone area is much larger for metal complexes against the gram positive bacteria, gram-negative bacteria and fungi.

The increased activity of the metal chelates can be explained on the basis of chelation theory.[36] It is known that chelation tends to make ligands act as more powerful and potent bactericidal agents and antifungal agents, thus killing more of the bacteria than the ligand. It is observed that, in a complex, the positive charge of the metal is partially shared with the donor atoms present in the ligand, and there may be π-electron delocalisation over the whole chelate.[36] This increases the lipophilic character of the metal chelate and favours its permeation through the lipoid layer of the bacterial membranes. Also, there are other factors which also increase the activity, such as solubility, conductivity and bond length between the metal and the ligand.

The mode of action may involve the formation of a hydrogen bond through the azomethine nitrogen and oxygen atom with the active centres of the cell constituents, resulting in interference with the normal cell process. The variation in the effectiveness of different compounds against different organisms depend either on the impermeability of the cells of the microbes or the difference in ribosomes of microbial cells.

There is a marked increase in the bacterial activities of the ligand and complexes for gram positive bacteria. The results showed that the copper(II) complexes have higher antibacterial activity towards Gram-positive bacteria (*Bacillus subtilis*) than the other complexes.

Ni(II) complex shows higher antibacterial activity towards Gram-negative bacteria (*Nesseria gonorrleer*). Mn(II) complex shows higher antifungal activity than the other complexes.

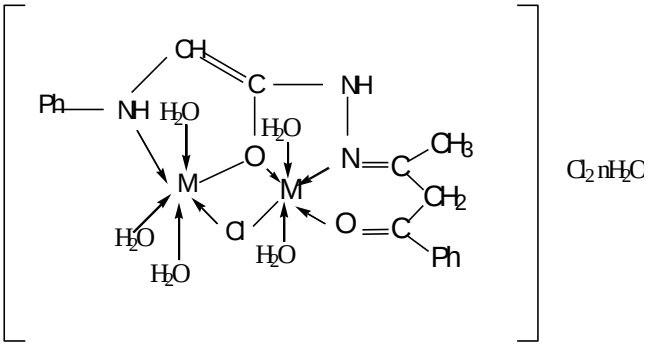

M = Mn^{2+}, Co^{2+}, Ni^{2+} or Zn^{2+}; n=1 for $Co^{2+}$and Ni^{2+} complexes

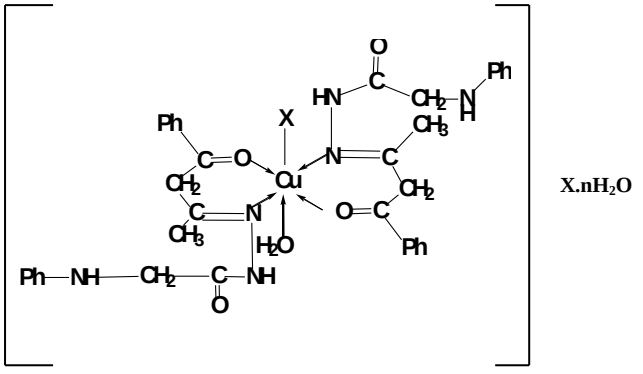

X = Cl^- or NO_3^-; n = 1 when X = Cl^- ; n = 3 when X = NO_3^-

Figure 1. Proposed structure of the complexes

 DOI: 10.17628/ecb.2014.3.878-882

Conclusion

N-Anilinoacetohydrazobenzoylacetone and its Mn(II), Co(II), Ni(II), Cu(II) and Zn(II) complexes have been synthesized and characterized. The structural characterization showed that the hydrazone ligand is coordinated to the metal ions as monobasic tetradentate manner with O_2N_2 donor sites in Mn(II), Co(II), Ni(II) and Zn(II) complexes while in the Cu(II) complexes the ligand is coordinated as bidentate. The copper(II) complexes show higher antibacterial activity towards G^+ bacteria (*Bacillus subtilis*) than the ligand and other complexes while Mn(II) complex shows higher antifungal activity than the free ligand.

References

[1]Cimerman, Z., Miljanic, S., Galic, N., *Croat. Chem. Acta*, **2000**, *73*, 81.

[2]Elmali, A., Kabak, M., Elerman, Y., *J. Mol. Struct.*, **2000**, *477*, 151.

[3]Valcarcel, M., Laque de Castro, M. D., *Flow-Through Biochemical Sensors*, Elsevier, Amsterdam., **1994**.

[4]Spichiger-Keller, U., *Chemical Sensors and Biosensors for Medical and Biological Applications*, Wiley-VCH, Weinheim, **1998**.

[5]Lawrence, J. F., Frei, R. W., *Chemical Derivatization in Liquid Chromatography*, Elsevier, Amsterdam, **1976**.

[6]Brown, D. In: *Insect Ecology*, Chapmann and Hall, London, **1990**.

[7]Singh, K., Barwa, M. S., Tyagi, P., *Eur. J. Med. Chem.*, **2007**, *42*, 394.

[8]Ferrari, M. B., Capacchi, S., Pelosi, G., Reffo, G., Tarasconi, P., Albertini, R., Pinelli, S., Lunghi, P., *Inorg. Chim. Acta*, **1999**, *286*, 134.

[9]Canpolat, E., Kaya, M., *J. Coord. Chem.*, **2004**, *57*, 1217.

[10]Yildiz, M., Dulger, B., Koyuncu, S. Y., Yapici, B. M., *J. Indian Chem. Soc.*, **2004**, *81*, 7.

[11]Atkins, R., Brewer, G. A., Kokot, E., Mockler, G. M., Sinn, E., *Inorg. Chem.*, **1985**, *24*, 127.

[12]Kashar, T. I., El-Nahas, A., El-Mughamsi, A. M., *Asian J. Chem.*, **2011**, *23(1)*, 159-165.

[13]El-Tabl, A. S., *Transit. Metal Chem.*, **1996**, *21*, 428.

[14]El-Tabl, A. S., El-Saied, F. A. and Al-Hakimi, A., *Transit. Metal Chem.*, **2007**, *32*, 689.

[15]Tang, H. A., Wang, L. F. and Yang, R. D., *Transit. Metal Chem.*, **2003**, *28*, 395.

[16]Kashar, T. I., *Thermochim. Acta*, **2010**, *507*, 66-70.

[17]El-Tabl, A. S., Kashar, T. I., El-Bahnaswy, R. M., Ibrahim, A. E., *Polish. J. Chem.*, **1999**, *73*, 245.

[18]Kashar, T. I., El-Magams, A. M., *Egypt. J. Chem.*, **2006,** *49(2)*, 261-268.

[19]Singh, K., Singh, R.V., Tandon, J. P., *Polyhedron*, **1988**, *7*, 151.

[20]El–Boraey, H. A., El–Tabl, A .S., *Pol. J. Chem.*, **2003**, *77*, 1759 .

[21]Mishra, L. A., Yadaw, K. T., *Transit. Met. Chem.*, **1997**, *22*, 406.

[22]El-Tabl, A. S., El-Baradie, K., Issa, R. M., *J. Coord. Chem.*, **2003**, *56*, 1113 .

[23]Hegazy, W. H ., *Monatsh. Chem.*, **2001**, *132*, 639

[24]Raman, N., Kulanadai Ssmy, A., Thangaraia, C. Manisankar, P. S., Swanathan, V., Vedhi, C., *Transit. Met. Chem.*, **2004**, *29*, 129 .

[25]Abdou El-Enein, S. A., El-Saied, F. A., Kasher, T. I., Wardany, A. H., *Spectrochimica Acta, Part A,* **2007**, *67*, 737-743.

[26]Athappan, P., Rajagopal, G., *Trans. Met. Chem.*, **1997**, *22*, 84.

[27]El-Tabl, A .S., *J . Chem . Res.*, **2002**, 529 .

[28]Ramadan, A. E. M., Sawodny, W., El-Baradie, G, M., *Transit. Met. Chem.*, **1997**, *22*, 211 .

[29]Gudasi, K. B., Patil S. A., Vadvav, R. S., Shenoy, R . V., Nethagi, M., *Transit. Met. Chem.*, **2006**, *31*, 586 .

[30]Praakar, B., Reddy, K., Lingaiant, P., *Indian J. Chem.*, **1988**, *27A*, 217 .

[31]Chiumia, G. C., Phillips, D. J., Rae, A. D., *Inorg. Chim. Acta*, **1995**, *238*, 197 .

[32]El-Shereafy, E., El-Tabl, A. S., Bahnasawy, R. M., Issa, Y. M., Kashar, T. I., *Polish. J. Chem.*, **1999**, *73(12)*, 1952.

[33]Gudasi, K. B., Patil, S. A., Vadvavi, R. S., Shenoy R. V. and Nethaji, M., *Transit. Metal Chem.*, **2006**, **31**, 586.

[34]Hegazy, W.H., *Monatsh. Chem.*, **2001**, *132*, 639

[35]Rao, M. S. and Reddy, K. H., *Indian J. Chem. Sect. A –Inorg. Bio-Inorg. Phys. Theor. Anal. Chem.*, **1999**, *38*, 262-266.

[36]Sengupta, S. K., Pandy, O. P., Srivastava B. K. and Sherma, V. K., *Transit. Met. Chem.*, **1998**, *23(4)*, 349

Received: 08.07.2014.
Accepted: 20.08.2014.

A STUDY OF THE DYNAMICS OF COPPER(II) IONS UPTAKE FROM AQUEOUS SOLUTIONS BY HUMAN HAIR USING CONDUCTIVITY AND pH MEASUREMENTS

Mosotho J. George[a]* and Nthako Ramollo[a]

Keywords: Human hair; Amberlite; copper ions; extraction; conductivity; ion exchange.

As the search for renewable resources for removal of pollutants from the environment grows, the use of biological sorbents has received a great deal of attention. Biological sorbents such as human hair have been explored due to their ready availability, renewability and effectiveness. This manuscript reports a study of the dynamics of copper(II) ions uptake by human hair using conductivity and pH measurements. The adsorption of these ions demonstrated a logarithmic behaviour, resembling first order kinetics, although the analysis showed a deviation from the first order kinetics. The maximum uptake of 288 μg $g^{-1}$was reached after about 120 minutes of static equilibration using a solution of 100 ppm. Interestingly the adsorption seems to be intermediate between a simple chemisorption and ion exchange as evidenced by a deviation from the linearity when conductivity was plotted against the pH measurements. However there was a significant correlation (R^2 = 0.9926) between conductivity and pH in the case of a classical ion exchange resin – Amberlite CG 50.

Corresponding Authors
Tel: +266 5221 3502,
Fax: +266 2234 0000
E-Mail: jm.george@nul.ls; maluti2005@gmail.com
[a] Department of Chemistry and Chemical Technology, National University of Lesotho, P.O. Roma 180, Lesotho – Southern Africa.

Introduction

Heavy metals are metallic elements that have a relatively high density and toxic or poisonous at lowconcentrations.[1] They are metals of relative densities of 5 g mL^{-1}. Despite this, some of the heavy metals are vital for cell metabolism on living systems. However, the threat is posed when they accumulate high concentrations in the environment. Accumulation occurs when organisms take-up ions of heavy metals and store them in a rate which is faster than they are oxidised and/or reducedso that they be excreted.[2] The natural biogeochemical cycles are disrupted by various human activities causing increased deposition of heavy pollutants which without proper treatment poses significant threat to both environment and public health as they are non-biodegradableand therefore are persistent.[3]

In recent years, the need for safe and economic methods for elimination of heavy metals from wastewater has necessitated the research for low cost available methods and materials.[4] The inorganic adsorbing materials that have been found effective for removal of heavy metals from aqueous samples in include fly ash,[5] zeolites,[6] natural clays such as montmorillonite,[7] just to name a few. Biological materials have recently received a great deal of attention not only due to their renewability but also because they are highly efficient with some taking up heavy metals up to 50 % of the biomass dry weight.[8] The ability of living organisms to take in and accumulate heavy metals has been employed in phytoremediation.[9] Following the death of the organism, most of the body structure can be used as solid biomass to prepare biosorbentssuch as saw dust[10,11] potatohusk,[12] rice husks,[13] pine cones,[14] corn cobs,[15] just to mention a few. Most of the generated biological waste reportedly has some degree of ability to bind most metal ions.[16] The uptake in most of these sorbents is mainly due to the sugar-based polymers such as cellulose that form oxygen-rich moieties that chelate these metal ions.

The other biological systems such as human hair, human nails have been used for analysis of heavy metals poisoning as they tend to trap and concentrate these metals and other chemicals.[17,18] Apart from the above mentioned types of adsorbents, human hair has also been used to absorb heavy metals.[19] The ability of hair to bind metals is due to the keratin proteins that contain nitrogen, oxygen and sulphur all possessing high electron density.[20] The adsorption of Pb^{2+} and Zn^{2+} from aqueous solutions by human hair has been found to be endothermic and spontaneous process.[21] A recent study showed that a perm-lotion-treated hair binds ions more strongly than a natural hair.[22]

This manuscript presents the study the dynamics of adsorption of copper(II) ions on human hair using simple conductivity and pH measurements. The study was aimed at exploring the applicability of these simple measurements in studies of metal analyses. However the results obtained as reported herein were astounding as they revealed the nature of the interaction being not a simple chemisorption that was expected but rather a combination of this and ion exchange process. This, to the best knowledge of the authors, is the first time that such simple approach is used for such studies; as well as determining the type of interactions of the metal ions with human hair.

Experimental

Reagents and apparatus used

Anhydrous Copper Nitrate (AR) was obtained from [brand, City and Country) and used as a stock solution using distilled water. Sulphuric acid [ACE, Johannesburg, South

Africa] was used to treat the hair. Amberlite CG-50, No. A-3894 Wet Mesh 100-200 (SIGMA-Aldrich, Johannesburg, South Africa) was used in place as an alternate sorbent for comparison of the adsorption behaviour of the ions on hair.

Preparation of the adsorbent (human hair)

The sample of human hair with average length of 5 mm was obtained from one of the researchers (black African). This sample was washed with distilled water followed by ethanol to remove surface oils. Thereafter it was soaked in 10% v/w of H_2SO_4 acid for a period of one hour to remove any surface metal ions. Then it was rinsed with distilled water until the conductivity of the rinsing water becomes less 10 µS cm^{-1} and the hair was dried in the oven 130 °C. Portions of 1g of dried hair sample were used as adsorbent at room temperature. These portions were suspended in the solution of copper ions for the requisite time and the conductivity and pH of the supernatant liquid measured appropriately.

Measurements of conductivity and pH of the solutions

An HI 8033 Hanna conductivity meter (HANNA Instruments, Romania) was used to measure conductivity. The probe of the conductivity meter was submerged in 50 mL aliquots of the 100 ppm Cu^{2+} solution and allowed to equilibrate for about 15 seconds before the reading was recorded. A longer equilibration time could not be allowed as it would affect the time dependent measurements. The pH were measurements were made with a Hanna pH-meter (HANNA Instruments,Romania) with an average 15 seconds equilibration time as well.

Quantitative analysis of copper uptake by human hair using AAS spectrometer

Different copper standard solutions were prepared and their absorbances measured using Spectra AAS 100 Spectrometer (Varian, USA) to determine correlation of absorbance to the concentration of the copper ions in the concentration range of 50–150 ppm. Thereafter, a suspension of hair and copper solution was made by suspending 10 g of hair in 500 mL of the 100 ppm Cu^{2+} solution. The supernatant solution was drawn using a pipette every 30 minutes to measure absorbances. The remaining solution was replaced immediately after the analyses.

Results and Discussions

Determination of conductivity of the copper solution after suspended of human hair

As a preliminary experiment, it was prudent to assess the degree of correlation between conductivity and concentration of Cu^{2+}. To this end, the conductivity of 50 mL aliquots of Cu^{2+} ion at concentration range 100 to 500 ppm was measured at 25 °C using conductivity metre.These data demonstrated significant correlation with regression coefficient (R^2) value of 0.9637.

To assess the uptake of the Cu^{2+}, 1 g of pre-treated hair was suspended in 50 mL of a 100 ppm solution for 30 minutes following which the conductivity of the supernatant liquid was measured and compared to the initial conductivity. The conductivity seemed to increase contrary to the expectation of a decrease. Further measurements were taken after 60, 90 and 120 min and the increase was consistent. Subsequently, a time-dependence profile was determined for between 30 and 120 min (Figure 1).

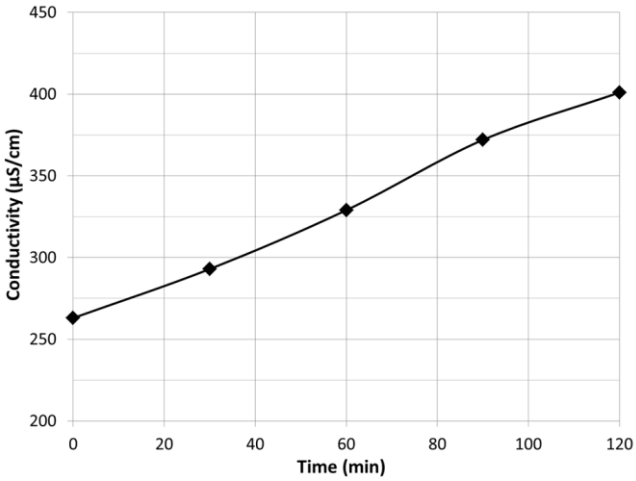

Figure 1. The plot of conductivity of solution suspending hair against time

Consistently, these results confirmed that conductivitydoes increases with time, implying that as more Cu^{2+} ions are taken up, conductivity increases. This was startling since conductivity would have been expected to drop as the number of ions is depleted through the adsorption process. This lead to the thinking, perhaps the adsorption could be due to some ion exchange behaviour. This would explain the observed increase in conductivity being due to the release of more conducting ions as Cu ions are being adsorbed.

Correlation between conductivity to pH of the copper solution in the hair suspension

Suspecting thatthe increase *K* is due to the release of hydrogen ions, it was prudent to determine difference of $[H^+]$ in the resulting solution.The experiment was repeated again and this time both conductivity and pH were measured simultaneously. Figure 2 shows the combined results obtained by measuring conductivity and the pH of the solution as the time allowed for hair to remain in suspension increases. While the conductivity of the solution increases, the pH of the solution decreasesimplying the increase in H^+ ions in the supernatant solution.

Assessment of correlation between conductivity and $[H^+]$ yielded a somewhat logarithmic behaviour (see Figure 3). However as expected, the plot of concentration of hydrogen ions as a function of pH resulted in a significantly linear (R^2 = 9805).

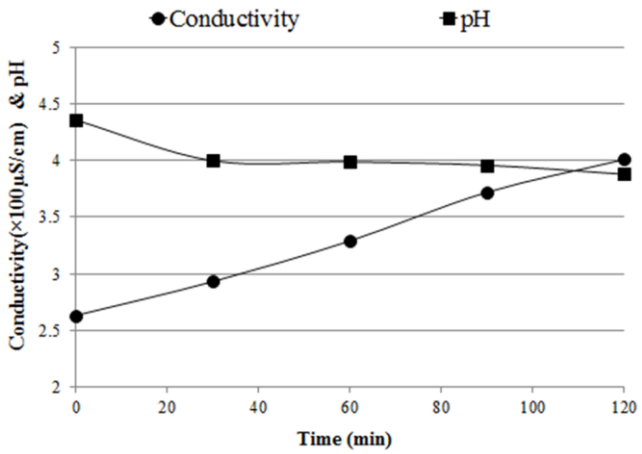

Figure 2. Conductivity and pH of the supernatant solution as a function of suspension time in human hair

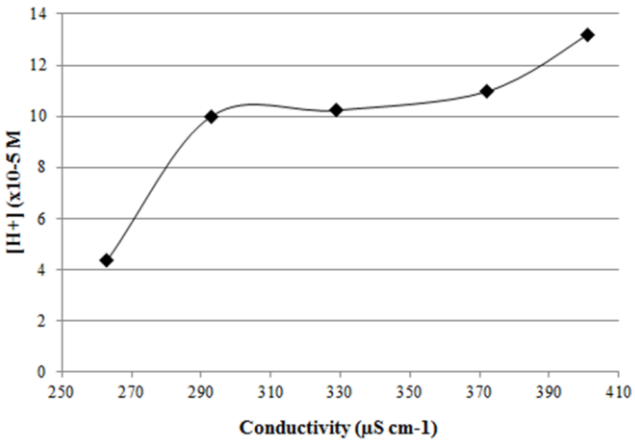

Figure 3. The plot of conductivity against concentration of hydrogen ions released

Quantitative determination of Cu $^{2+}$ uptake by AAS

The consistent increase in conductivity led to the thought that perhaps Cu^{2+} ions were not being taken up by the hair sample, so the quantitative analysis was performed using atomic absorption spectrophotometry. Figure 4 shows the combined absorbance and the Cu^{2+} ions uptake as well as the relative concentrations. The absorbance values noted are the actual values obtained from the spectrophotometer. The relative mass uptake was taken as a difference in the mass of Cu^{2+} in solution at any time relative to t=0 which was taken as unity. The actual mass uptake ranged from 171 µg g^{-1} (at t=30 min) to 288 µg g^{-1} (at t=480 minutes, 8 h) as demonstrated in Figure 5.

As can be seen there is significant complementarity between the relative concentration of the remaining solution and the relative mass uptake. The lower amounts of copper ions uptake (micro-gramme range) could be due to the poor optimisation of the hair such as carrying out static instead of dynamic equilibration. Since no quantitative checks were made to rid the hair of any pre-trapped metal ions was performed, it could be that the sample already had a significant amounts of other metal ions that competed with the analyte.

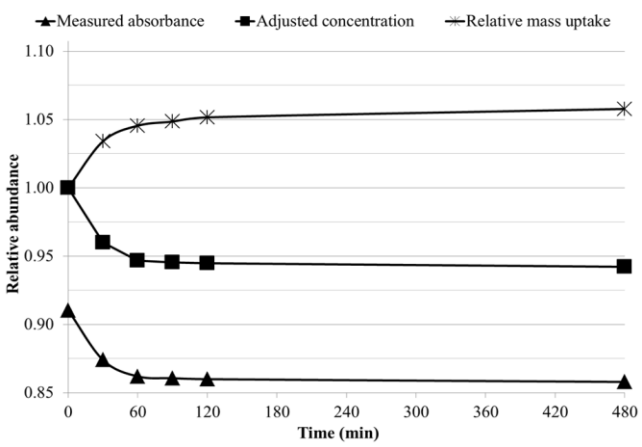

Figure 4. Measured absorbance, adjusted concentration and relative Cu^{2+} uptake

The other issue could be the fact that the hair was not ground into a fine powder but was rather used as short strands of about 5 mm length. This is consistent with the report that the hair sample treated with mineral acids can be soaked up to 48 h but do not show considerable "softening of the fibres" and hence "exhibit negligible adsorption capacity for Cu^{2+} [ions]" below 0.1 mg g^{-1} of hair.[23]

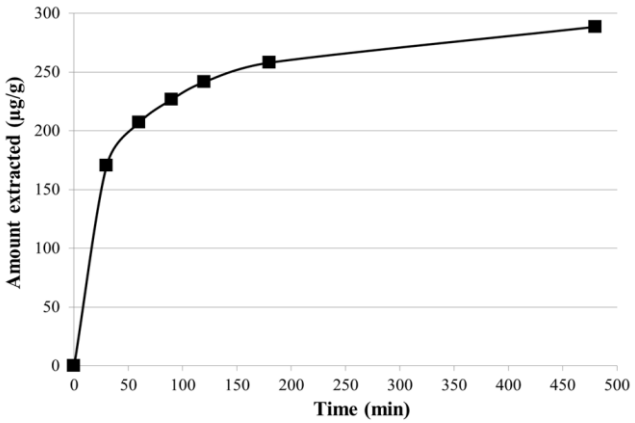

Figure 5. A plot of Cu^{2+} uptake as a function of time

However, a similar trend of the Cu^{2+} ions uptake was observed and reported earlier.[21] In the same report, it was stated that the isoelectric point of human hair is 3.67 indicating a high proton exchange above this pH value. Thus, as the pH decreases (increase in H^+ ions) due to ion exchange behaviour, less and less Cu^{2+} ions are taken up. The absence of correlation between the conductivity, Cu^{2+} uptake and pH suggests a complex ion exchange process between Cu^{2+} ions and H^+ ions.

From the appearance of the plot of [Cu^{2+}]with time (Figures 4 and 5), it seems likely that the uptake follows the first order kinetics, where the concentration at anytime t is exponentially related to time expressed mathematically as follows:

$$C_t = C_0^{-kT} \qquad (1)$$

Implying that:

$$\ln C_t = -kT + \ln C_0 \quad (2)$$

Thus a plot of ln C_t against time should yield a straight line whose slope equals the rate constant and the *y*-intercept equalling the ln C_0. However, the plot yielded a regression coefficient of 0.4455 and a regression equation:

$$y = 0.8839e^{-8E-05x} \quad (3)$$

demonstrated a deviation from a first order kinetics.

Determination ofion exchange behaviour of hair compared to Amberlite

Determining the possibility of ion exchange process being involved in the adsorption of copper ions by human hair, the suspension of Amberlite was prepared and both conductivity and pH measured and compared as in Figure 6.

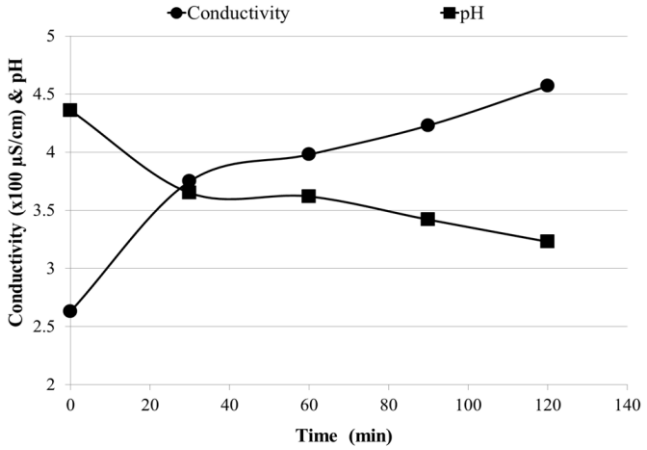

Figure 6. Conductivity- and pH-time profile of the supernatant solution suspended in Amberlite

Unlike the case of human hair, the conductivity versus pH curve yielded a sufficiently linear curve (R^2 = 0.9926) indicating the positive correlation between conductivity and the pH of the supernatant solution, hence abundance of the H^+ ions.

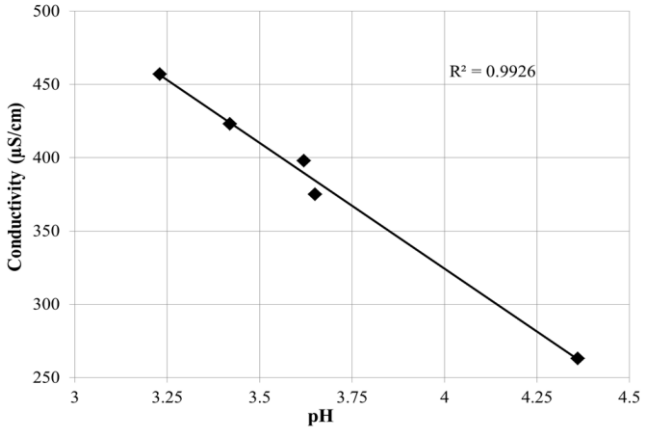

Figure 7. The correlation of measured conductivity and pH for Amberlite suspensions

Comparison of the pH and conductivities of suspensions of hair and Amberlite showed that more H^+ ions were liberated using the Amberlite than using the human hair (See Figure 8).

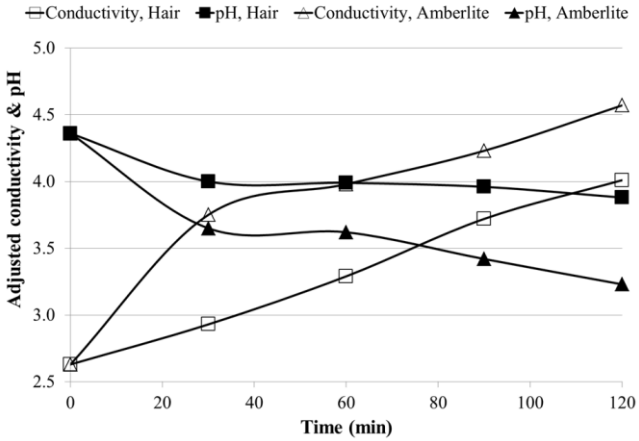

Figure 8. Comparison of conductivity and pH for Amberlite and human hair suspensions

These different behaviours suggest a complex mechanism of adsorption exist in hair than in Amberlite which is both chemisorption and ion exchange in nature.The correlation of conductivity with pH in the case of Amberlite resin (Figure 7) shows a linear relationship contrary to the case with the human hair (Figure 3). Since no quantitative analysis of Cu^{2+}ions was performed for Amberlite, no inference can be made to the concentrations of the two ions, the H^+ and the Cu^{2+} ions. However, one study revealed that Cu^{2+} could get as high as 115 mg g^{-1} when the Amberlite IR 120 is packed in a cartridge and the pH adjusted optimally.[24] However the pH of the solution could not be optimised since the activity of H^+ ions was the focus of the study. The conclusion of the ion exchange behaviour is affirmed by the report that the human hair "could be used as a cation-selective adsorbent, as it showed no capacity for removing anions".[22]

Conclusions

In conclusion, this study revealed very interesting aspects that were not envisaged that conductivity studies could reveal so much detail regarding metal uptake by sorbents. The adsorption of Cu^{2+} copper ion on human hair was found to bea combination of chemisorption and ion exchange with a maximum observed at 288 µg g^{-1} of hair. The chelation process occurs between the Cu^{2+} ions and the electron-rich nitrogen, sulphur and oxygen atoms of the hair proteins (keratin). The uptake does not follow the first order kinetics as would be expected from a simple chemisorption process, although the plot of the uptake versus equilibration time demonstrates a logarithmic increase.This ion exchange process is not an easy straightforward cation exchange as that observed with a simple classical ion exchange resin like Amberlite. Further experiments are needed to decipher the full mechanism of this process and full quantitative analysisfor all other elements that could be playing different roles in the whole process.

Acknowledgements

The authors would like to acknowledge the National University of Lesotho for the financial assistance in carrying out this project. NR acknowledges the National Manpower Secretariat of the Government of Lesotho for scholarship.

References

[1]Renge, V. C., Khedkar, S. V. and Pande, S. V., *Sci. Revs. Chem. Commun*., **2012**, *2(4)*, 580-584.

[2]Barakat, M. A., *Arabian J. Chem.,* **2011**, *4*, 361-377.

[3]Alluri, H. K., Ronda, S. R., Settalluri, V. S., Singh, J., Suryanarayana, V. and Venkateshwar, P., *Afr. J. Biotechnol*., **2007**, *6(25)*, 2924-2931.

[4]Hegazi, H. A., *Housing Build. Natl. Res. Center J.*, **2013**, *9*, 276-282.

[5]Geetha, V.V., Singh, R.K. and Sahu, V., *Int. J. Appl. Innov. Eng. Manag.,* **2013**, *2(7)*, 45-56.

[6]Wang, C., Li, J., Sun, X., Wang, L. and Sun, X., *J. Environ. Sci*., **2009**, *21*, 127-136

[7]Abraham, B. T. and Anirudhan, T. S., *Ind. J. Env. Protect.*, **1998**, *19(5)*, 363-366

[8]Vieira R. H. S. F. and Volesky B., *Int. Microbiol.,* **2000**, *3*, 17-24

[9]Valipour, A., Hamnabard, N., Woo, K.-S. and Ahn Y.-H., *J. Environ. Manag.*, **2014**, *145*, 1-8

[10]Barakat, M. A., *Arabian J. Chem.*, **2011**, *4*, 361-377.

[11]Yasemin, B. and Zeki, T. E. Z., *J. Environ. Sci.*, **2007**, *19*, 160-166.

[12]Taher, A., Mohsin, M., Farooqui, M. and Farooqui, M., *Asian J. Biochem. Pharm. Res.*, **2011**, 431-434.

[13]Nhapi, I., Banadda, N., Murenzi, R.,Sekomo, C. B. and Wali, U. G., *TOENVIEJ*, **2011**, *4*, 170-180.

[14]Ofomaja, A. E., Naidoo, E. B., and Modise, S. J., *J. Hazard Mater.*, **2009**, *168(2-3)*, 909-917.

[15]Nasiruddin Khan, M. and Farooq Wahab, M., C., *J. Hazard. Mater.*, **2007**, *141(1)*, 237-244.

[16]Volesky B. and Holan,Z. R., *Biotechnol. Prog.*, **1995**, *11*, 235-250,

[17]Schramm, K., *Chemosphere*, **2008**, *72*, 1103-1111.

[18]Li, H., Chen, F. and Xu, X., *J. Anal. Toxicol.*, **2000**, *24*, 704-707.

[19]Hinners, T. A., Terrill, W. J., Jane, J. T. and Coluccit, A. V., Hair-metal binding, *Environ. Health Perspect.*, **1974**, *8*, 191-199.

[20]Aluigi, A., Tonetti, C., Vineis, C., Tonin, C. and Mazzuchetti, G., *Eur. Polym. J.*, **2011**, *47(9)*, 1756-1764.

[21]State, A. I. and State, K., *E-J.f Chem.*, **2010**,7(4), 1296-1303.

[22]Roh, H. G., Kim, S. G. and Jung, J., *Korean J. Chem.*, **2014**, *31(2)*, 310-314.

[23]Tan, T. C., Chia, C. K. and Teo, C. K., *Water Res.* **1985**, *19*, 157-162.

[24]Jha, M. K., Nguyen, N. V., Lee, J., Jeong, J. and Yoo, J., *J. Hazard Mater*, **2009,** *164*(2-3), 948-953.

Received: 17.07.2014.
Accepted: 20.08.2014.

METABOLIC AND ANTIOXIDANT EFFECTS OF *NIGELLA SATIVA* OIL ON PREVENTION OF OBESITY DEVELOPMENT IN RATS FED HIGH-FAT DIET.

Amal Didi,[a]*, Radjaa K. Meziane[a], Fouzia Amamou[a], Amine Benhmidat[a], Daoudi Chabane Sari[a]

Keywords: Metabolic and antioxidant effect; Nigella sativa oil, obesity.

The results of this study demonstrated that *Nigella sativa* seeds oil is beneficial for attenuating complications of obesity and possibly preventing it because of its essential polyunsaturated fatty acids; linoleic and linolenic acids and other nutrients such as liposoluble vitamins like tocopherols and also minerals, essential amino acids, some polyphenols, terpenoids and quinones, particularly thymoquinone that have shown potential medicinal properties in traditional medicine.

*Corresponding Authors
Fax: +213 553 57 1929
E-Mail: didiamel13@gmail.com
[a] Laboratory of naturel products, Departement of Biology, Faculty of sciences of nature and life, sciences of earth and universe. Abou Bekr Belkaïd University-PB 119- Tlemcen-Algeria.

Introduction

Obesity is rapidly increasing worldwide. It has become a leading health problem in the 21st century loading both in developed and developing countries.[1, 2] In 2009, the World Health Organization estimates that nearly 700 million the number of obese people by 2015, with an increase of 75% in 10 years.[3,4] Obesity and overweight can lead to a high risk of health complications such as cardiovascular disease, insulin resistance and type II diabetes mellitus, hyperlipemia, hypertension and cancers .[5]

Once of their many factors that involved obesity, consumption of energy-dense foods; rich in fat and/or carbohydrates, is considered a major contributing cause to this disease. Furthermore, an increased body weight is observed in the imbalance between the energy intake and the expenditure.[1,6,7] A high fat diet intake can contribute to the development of obesity and dyslipidemia in humans and rodents by altering cholesterol and triglyceride levels in plasma and tissues.[8] Several studies have reported that diet composition in type and amount of fat favors reduced hyperlipidemia[9] and mainly diet rich in saturated fatty acids favor an acute increase in insulin resistance and adiposity.[10] Some studies also show how the effect of n-3 polyunsaturated fatty acids (n-3 PUFAs), conjugated fatty acids, phytosterols, medium-chain triglycerides and phospho lipids as important modulators, can affect obesity.[11-13]

Numerous studies have found elevated biomarkers of oxidative stress in overweight and obesity. Oxidative stress can lead to damage of biomolecules such as lipids, proteins, and DNA.[14] Oxidative stress may be the mechanism underlying the development of inflammation and diseases associated with obesity such as insulin resistance, diabetes, hypertension, and metabolic syndrome. Different factors can contribute to oxidative stress in obesity, e.g., hyperglycemia, increased muscle activity because of the need to carry excessive weight, increased tissue lipid levels, inadequate antioxidant defenses, chronic inflammation and endothelial reactive oxygen species (ROS) production.[15]

There are several treatments developed to remedy this deadly disease and its complications, including hypo caloric diets, exercise, medication and also surgery.[7] Among these treatments, dieting, exercise and behavior modification are essential to the management of obesity; even though often, long-term results are disappointing. Various anti-obesity drugs, including rimonabant, Sibutramine, fenfluramine, phentermine, phendimetrazine, and diethylpropion have been withdrawn from the market owing to an unacceptable side effects that include headaches, vomiting, and heart attacks and psychiatric problems such as anxiety and depression. The history of anti-obesity drugs development is far from glorious and only a handful of agents are currently licensed for clinical use. Orlistat is the only weight loss agent approved for long-term clinical use in Europe.[16-18]

Many researchers in the field of food science have focused on the search for functional food ingredients and/or herbal extracts that can prevent the accumulation of body fat so achieving body weight loss,[19] improving the oxidative metabolism by alleviating glycemia and lipidemia and decreasing obesity-related oxidative stress by increasing tissue antioxidant levels.[15]

Vegetable oils are a good example that depicts the actions of dietary fat on obesity and their alterations. Among the various oil seeds, black cumin (*Nigella sativa* L.), an annual *Ranunculaceae* herbaceous plant, is of particular interest because it may be used for medicinal purposes as a natural remedy for a number of illnesses. The effects of black cumin seeds have been evaluated in clinical and animal studies. These seeds have been used as diuretic, antiulcerogenic, liver tonic, immunomodulative, anti-inflammatory, antitumor and antidiabetic.[20-22] Additionally, these seeds

have been subjected to a range of pharmacological investigations in recent years.[23,24] Besides the diversity of fatty acids that contained in this seed oil, thymoquinone (TQ) is known as a pharmacologically active compound that is shown to have a protective effect mainly against hepato-toxicity induced by either chemicals or diseases.[25]

The investigations of protective effect of *N. sativa* fixed oil seeds on lipid metabolism and their corrective effect of the alterations that follow obesity in animal models are limited.[26] Consequently, in order to explore the effect of vegetable oils for preventing and eventually treating obesity, the aim of this study was carried out to examine the possible beneficial effect of *N. sativa* seeds fixed oil on body weight, lipid metabolism, pancreatic and hepatic activity and investigate their effect on the antioxidant status by quantifying the plasmatic concentrations of antioxidant vitamins (A,C and E), malondialdehyde (MDA) levels, protein carbonyls as a markers of an oxidative stress in addition of catalase (CAT) and superoxide dismutase (SOD) activities, and this was carried out in growing obese male rats fed with high fat diet (HFD) and in non-obese rats were measured.

Materials and methods

Vegetable oils

Nigella sativa L. (*Ranunculaceae*) seeds oil was extracted using the following method: Seeds obtained from Tlemcen-Algeria were grounded using a crusher (Retsch RM 100). The lipid fraction was extracted using petroleum ether (40–60 °C) in a Soxhlet apparatus for 2 hours (Natural Products Laboratory, Tlemcen, Algeria). The solvent was then evaporated and the lipid fraction residues weighed. The yield oil content on seeds was found to be 35 ± 1.8 %.

After preparation, seed oil extract was refrigerated and covred with aluminium foil, to protect from light to assure its stability.

Olive and Sunflower oils are commercial local products (Olive oil is obtained by cold extraction and sunflower oil purchased from Cevital®). All chemicals used were commercially provided with a high purity level.

Thymoquinone quantification on *N. sativa* seeds oil

TQ quantification was carried out by High Performance Liquid Chromatography (HPLC) as described by Al-saleh *et al.*,[27] with some modifications, for this; oil sample (a triplicate) was dissolved in methanol (for HPLC analysis from Sigma-Aldrich) vortexed for 1 min and centrifuged 10 min at 3000 rpm. 20 µL of supernatant was injected on reverse-phase Waters column (150×4.6mm×3.5µm particle size), using an isocratic mobile phase of water: methanol: 2-propanol (50:45:5% v/v) at a flow rate of 1 mL min^{-1}. Analyses were made at room temperature.

UV monitoring was carried out at 275 nm. Calibration curve was constructed by TQ standard at the same conditions.

Evaluation of biological activity

Animals

The experimental protocol was approved by the Animal Care and Use Committee of Tlemcen University. Fifty male Wistar rats obtained from the Pasteur Institute (Algiers, Algeria) weighing 86.7 ± 1.3 g were considered at the beginning of the experiment. One-month-old male Wistar rats were housed in clear plastic cages with natural beddings and subjected to 12 hours light-dark cycles. Food and water were available *ad libitum*. Food was replaced daily and the uneaten portions weighed. The temperature was maintained at 24 °C and humidity kept constant at 60 %.

Experimental diets

The rats were divided randomly into six diet (D1-D6) groups. Each group was fed one of six diets (**Table 1**) for eight weeks:

D 1: Control diet, rats received 4 % Sunflower oil (n=10);

D 2: Obese group received high fat diet (HFD) with 32 % Sunflower oil (n=10);

D 3: received 4 % black cumin seeds oil (n=7);

D 4: were fed 28 % Sunflower oil and 4 % black cumin seeds oil (n=8);

D 5: were fed 4 % Olive oil (n=7);

D 6: were fed 28 % of Sunflower oil and 4 % Olive oil (n=8).

Oral glucose tolerance test (OGTT)

After the two weeks period of experimentation diets and following overnight fasting, the rats were being subjected to an oral glucose tolerance test (OGTT) by intragastric feeding with a glucose solution (2 g/kg body weight). OGTT was carried out during two (02) hours. Blood samples were collected from the tail vein at 0, 30, 60, 90 and 120 min after glucose administration. Because it's stressful, only two blood samples were done from the retro-orbital sinus, and this was to determine initial (0 min) and final (120 min) insulin blood concentration.

Blood glucose was determined using a glucometer (Accu-Check Active, *Roche*, Germany). Plasma insulin concentration was measured by radio-immunoassay using Rat Ultrasensitive Insulin ELISA (ALPCO Diagnostics, NH). The homeostasis model assessment score of insulin resistance (HOMA-IR) was calculated from the fasting glucose and insulin concentration using the standard formula as described by Matthews *et al.*[28] Insulin sensitivity was determined using the quantitative oral glucose and insulin sensitivity index OGIS and calculated from a spreadsheet that can be downloaded using this link: http://webmet.pd.cnr.it/ogis/download.php, which was based on glucose oral dose and insulin levels .[29,30]

Table 1. Ingredient composition of experimental diet groups (D1-D6).

Constituent, wt. %	D1	D2	D3	D4	D5	D6
Starch	60.3	32.3	60.3	32.3	60.3	32.3
Oil	4.0	32.0	4.0	32.0	4.0	32.0
Dietary fatty acids[a]						
ΣSFA[b]	0.89+/-0.01	7.10+/-0.02[a]	0.76+/-0.01	6.98+/-0.05[b]	0.73+/-0.01	6.95+/-0.02
ΣMUFA[c]	2.40+/-0.05	19.21+/-0.08[a]	0.83+/-0.01	17.64+/-0.10[b]	2.59+/-0.08	19.40+/-0.12
ΣPUFA[d]	0.63+/-0.01	5.05+/-0.02[a]	2.22+/-0.09	6.64+/-0.07[b]	0.71+/-0.01	5.13+/-0.02
P/S[e]	0.71+/-0.01	0.71+/-0.01[a]	2.92+/-0.09	0.95+/-0.01[b]	0.85+/-0.02	0.73+/-0.01
Energy values (kcal)	371.9	517.5	371.9	517.5	371.9	517.5

In addition, the common ingredients in all diet groups were: 16 % casein, 0.3 % methionine, 5 % saccharose, 5 % cellulose, 7.37 % mineral mix* and 2 % vitamin.mix*. *Mineral mix composition (g/100 g of dry diet): Ca^{2+}, 4; K^{+}, 2.4; Na+, 1.6; Mg^{2+}, 0.4 Fe^{2+}, 0.12; trace elements: manganese, 0.032; copper, 0.05; zinc, 0.018. Vitamin mix composition (mg Kg^{-1} of dry diet): retinol, 1.8; cholicalciferol, 0.019; thiamine, 6; riboflavin, 4.5; pantothenic acid, 21; inositol, 5; ascorbic acid, 240; L-tocopherol, 51; nicotinic acid, 30; folic acid, 1.5; biotin, 0.09. Refer to text for diet groups. *a:* calculated from CG data, *b:* total saturated fatty acids, *c:* total monounsaturated fatty acids, *d:* total polyunsaturated fatty acids, *e:* polyunsaturated and Saturated fatty acids ratio. a: $p<0.05$ obese group versus controls. b: $p<0.05$ nigelle oil treated group versus obese and olive oil's treated group. c: $p<0.05$ olive oil's treated group versus obeses.

Table 2. Effect of the different diets on plasma fatty acids composition

Plasma fatty acids, wt. %	D1 (*n*=10)	D2 (*n*=10)	D3 (*n*=7)	D4 (*n*=8)	D5 (*n*=7)	D6 (*n*=8)
C14:0	nd[α]	nd	0.11+/-0.03	0.17+/-0.03[b]	nd	nd
C16:0	26.27+/-0.01	24.22+/-0.03	25.66+/-0.04	14.34+/-0.04[b]	21.29+/-0.13	15.62+/-0.03
C18:0	19.22+/-0.01	16.68+/-0.01	10.44+/-0.03	16.52+/-0.06	9.70+/-0.09	14.16+/-0.01
C18:1	29.44+/-0.04	35.55+/-0.11[a]	35.10+/-0.18	32.07+/-0.04[b]	24.08+/-0.21	25.32+/-0.01
C18:2	11.27+/-0.05	21.7+/-0.03[a]	20.85+/-0.05	29.61+/-0.1[b]	27.37+/-0.06	35.16+/-0.01
C18:3	0.67+/-0.02	Nd	0.09+/-0.01		nd	nd
C20:0	nd	Nd	0.05+/-0.00	0.88+/-0.01[b]	nd	nd
C20:1	0.58+/-0.02	Nd	nd	nd	nd	nd
C22:0	nd	Nd	nd	nd	1.4+/-0.05	nd
C20:4	6.36+/-0.03	10.59+/-0.02[a]	7.08+/-0.03	12.09+/-0.01[b]	10.2+/-0.08	8.80+/-0.02
ΣSFA[β]	45.49+/-0.01	40.9+/-0.02[a]	36.26+/-0.02	31.91+/-0.12[b]	32.39+/-0.013	29.78+/-0.12
ΣMUFA[γ]	30.02+/-0.03	35.55+/-0.05[a]	35.1+/-0.04	32.07+/-0.08[b]	24.08+/-0.35	25.32+/-0.12
ΣPUFA[δ]	18.63+/-0.03	23.29+/-0.09[a]	28.02+/-0.04	41.7+/-0.10[b]	37.57+/-0.08	43.96+/-0.22

α not detected, *β* Total saturated fatty acids, *γ* Total monounsaturated fatty acids, *δ* Total polyunsaturated fatty acids. a: $p<0.05$ obese group versus controls. b: $p<0.05$ nigelle oil treated group versus obese and olive oil's treated group. c: $p<0.05$ olive oil's treated group versus obeses.

Body weight, liver, adipose tissues weight and blood parameters

Food intake and body weight were measured on a daily basis. At the end of the eighth (8^{th}) week, the control and treated groups were sacrificed, after anesthetization with intra-peritoneal injection of chloral hydrate 10 % (3 mL Kg^{-1}). These animals were treated, manipulated and killed according to the regulations of the *Animal Care Laboratory of Tlemcen University-Algeria*.

Blood was immediately collected from the abdominal aorta in heparined tubes and the plasma obtained after centrifugation was used for the determination of biochemical markers including alanine aminotransferase EC 2.6.1.2 (ALT), aspartate aminotransferase EC 2.6.1.1 (AST), lactate deshydrogenase EC 1.1.1.27 (LDH), alkaline phosphatase EC 3.1.3.1 (ALP) using enzymatic kits (Spinreact, Girona, Spain).

Albumin, globulin, total protein, blood urea, creatinine, blood glucose (BG), triglycerides (TG) and total cholesterol (TC) using enzymatic kits (Biomérieux, Lyon, France).

HDL-cholesterol (HDL-C) was measured using also enzymatic method after precipitating HDL by sodium phosphotungstate-magnesium.[31] VLDL-cholesterol (VLDL-C) was calculated by dividing triglyceride concentration by five.[32] LDL-cholesterol (LDL-C) concentration was calculated using the Friedewald–Levy–Fredrickson formula.[33]

Liver and visceral adipose tissues (abdominal's, kidney's and testis fats) were excised and weighted.

Measurement of total plasma fatty acids

The fatty acid profile of plasma was determined by gas chromatography (CG). Fatty acids were trans-esterified into methyl esters (FAMEs) following the Bligh and Dyer procedure using 14% boron trifluoride in methanol with some modifications.[34] FAMEs were identified by CG Varian CP-3380 using a capillary column (Alltech EC-Wax) (30m×0.53mm×1.2 µm film thickness) and equipped with a flame ionization detector (FID). Helium was used as the carrier gas. The oven temperature was kept constant at

250°C and the injected volume was 1µL. The temperature was kept at 180°C for two minutes and then increased to 220°C with 6°C/min heating rate. After this period, the temperature was kept at 220°C for 10 min. FAMEs were identified using FAMEs authentic standard (Grace AOCS Mix 3A) injected in the same conditions as the plasma FAMEs (a triplicate).

Oil FAMEs composition was also analyzed as described above. The results are shown in Table 2.

Determination of anti-oxidant status

Determination of plasma levels of vitamins A, C and E

Plasma α-tocopherol (vitamin E) and retinol (vitamin A) were determined by reverse phase HPLC and detected by an UV detector at 292 nm for vitamin E and 325 nm for vitamin A.[35] Vitamin C levels were determined in plasma using the method described by of Roe *and* Kuether.[36]

Measurement of malondialdehyde (MDA):

Analysis of lipid peroxidation was estimated by measuring thio-barbituric acid reactive substances (TBARS) and was expressed in terms of malondialdehyde content, according to the method of Ohkawa *et al.*,.[37] Briefly, an aliquot of 200µl of plasma was mixed thoroughly with aqueous solution of thiobarbituric acid and heated at 95◦C for 30 min in a water bath. The suspension was then cooled to room temperature, centrifuged at 4000 rpm for 10 min, and the pink colored supernatant was taken for spectrophotometry measurement at 532 nm for MDA assay.

MDA concentration was calculated by the extinction coefficient of MDA–TBA complex $E^{M}_{532nm,1cm} = 1.56\times10^{5}$ $M^{-1}cm^{-1}$.

Measurement of protein carbonyls

Plasma carbonyl proteins (marker of protein oxidation) were assayed by the 2, 4-dinitrophenylhydrazine (DNPH) reaction.[38] Briefly, proteins were precipitated by the addition of 20% trichloroacetic acid and redissolved in DNPH and the absorbance was read at 370 nm.

Determination of antioxidant enzymes activities:

Analysis of catalase (CAT) (EC 1.11.1.6) activity was performed using the method of Aebi[39] where the enzyme-catalyzed decomposition of H_2O_2 is measured. The rate of H_2O_2 decomposition was measured at 240 nm. The activity was calculated utilizing the extinction coefficient of H_2O_2, $E^{M}_{240nm,1cm} = 0.0394\ mM^{-1}cm^{-1}$. Superoxide dismutase (SOD) (EC 1.15.1.1) activity was determinate according to the method described by Sun *et al.*[40] The principal of the method is based on the inhibition of nitroblue tetrazoium (NBT) by the xanthine oxidase system as a superoxide generator. SOD activity (1U) was defined as of the enzyme amount causing 50% inhibition in the NBT reduction rate.

Statistical analysis

The results were expressed as the mean value ± standard deviation. The comparison between the mean values of each two groups was established by Student's test "t". Significance was set at $p < 0.05$. The significance of differences between all the parameters was assessed by the one way ANOVA analysis and Tukey's post hoc test was used for the comparisons; *p-values* < 0.05 were considered statistically significant. Multiple regression analysis was used to estimate the relationship between FBW (final body weight), glycemia, insulinemia, food intake, AGPI intake, HDL-C, TG, HOMA score and OGIS index; while all confidence limits represent 95% intervals. A Pearson correlation was also made to compare all the parameters.

Results

Body weight, lipid intake and energy supply

From the first week of the experimentation (Fig. 1), body weight of rats fed by an HFD (Diet 2) started to increase significantly compared to those fed an isocaloric diet (Diet 1, 3 and 5) which suggests in at first sight the installation of obesity. Also, the weight of rats fed an HFD with 4% Nigel oil or Olive oil (Diet 4 and 6 respectively) decreased significantly from the third week compared to group 2. On the other hand, liver and abdominal adipose tissue weights (Table 3) show a significant increase in obese *versus* control rats which are positively correlated to FBW. Only for liver weight, a significant decrease in Diet 4 and 6 ($p<0.05$) compared with obese group was noted. No differences were observed between the other adipose tissues (*see* **Table 1**).

The data showed that all rats received an HFD (Diets 2, 4 and 6) presented an increase in lipid intake compared to isocaloric fed rats (Diets 1, 3 and 5). Consequently, the total energy supply (TES) was significantly higher on the HFD fed rats.

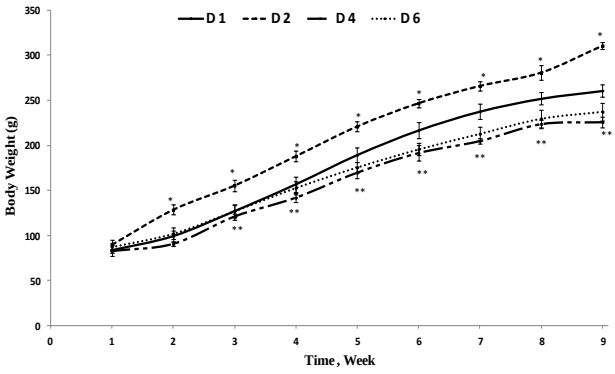

Fig 1. Changes in body weight per week of rats of different diet groups: control (D1), obese (D2), nigella (D4) and olive oil (D6) treated groups. (D3) and (D5) are not represented because of their superposition on the control curve (D1). Refer to Table 2 for diet groups. *($p < 0.05$): Significant difference between control and obese group. **($p < 0.01$): Significant difference between obese and treated groups.

Table 3. Effect of the different diets on initial and final body weight, food intake and organs weights.

	D1 (*n*=10)	D2 (*n*=10)	D3 (*n*=7)	D4 (*n*=8)	D5 (*n*=7)	D6 (*n*=8)
Initial BW, g	86.20+/-5.98	89.5+/-5.80	87.5+/-1.98	82.4+/-2.07	87.7+/-5.45	87.2+/-3.94
Final BW, g	202.0+/-7.05	310.5+/-4.13[a]	228.0+/-22.63	225.7+/-6.26[b]	237.0+/-2.54	237.2+/-9.64[c]
Food intake, g d^{-1} 100 g BW^{-1}	11.90+/-0.66	12.8+/-066	13.1+/-0.86	13.4+/-0.99	11.2+/-0.22	9.80+/-1.27[c]
Lipid intake, g d^{-1} 100 g BW^{-1}	0.48+/-0.03	5.10+/-0.27[a]	0.53+/-0.03	5.30+/-0.39	0.45+/-0.01	3.90+/-0.51[c]
TES, kcal d^{-1} 100g BW^{-1}	43.34+/-1.82	63.48+/-7.16[a]	47.52+/-1.66	57.78+/-10.32	40.56+/-1.67	49.85+/-10.40[c]
Liver weight, rel. %	3.37+/-0.12	3.82+/-0.20[a]	3.6+/-0.08	2.96+/-0.32[b]	3.31+/-0.10	3.26+/-0.11
Abdominal fat, rel. %	0.91+/-0.02	1.54+/-0.09[a]	1.20+/-0.06	1.35+/-0.02[b]	1.28+/-0.01	1.11+/-0.05[c]
Peri-testis fat, rel. %	1.46+/-0.10	1.48+/-0.02[a]	1.40+/-0.03	1.34+/-0.09[b]	1.48+/-0.15	1.46+/-0.13
Peri-renal fat, rel. %	0.24+/-0.10	0.31+/-0.02[a]	0.27+/-0.05	0.24+/-0.03[b]	0.22+/-0.07	0.20+/-0.02[c]

BW: Body weight, TES: Total energy supply; d: day; W: watt; rel: relative weights; a: $p<0.05$ obese group versus controls; b: $p<0.05$ nigelle oil treated group versus obese and olive oil's treated group; c: $p<0.05$ olive oil's treated group versus obeses rats.

Table 4. Effect of the different diets on the biochemical parameters.

	D1 (*n*=10)	D2 (*n*=10)	D3 (*n*=7)	D4 (*n*=8)	D5 (*n*=7)	D6 (*n*=8)
Glycemia, mmol L^{-1}	4.30+/-0.01	8.10+/-0.03[a]	4.70+/-0.07	4.20+/-0.04[b]	4.60+/-0.05	4.50+/-0.04[c]
Total cholesterol, g L^{-1}	0.45+/-0.02	0.73+/-0.25[a]	0.57+/-0.07	0.53+/-0.08[b]	0.49+/-0.02	0.53+/-0.03[c]
Triglycerids, g L^{-1}	0.40+/-0.03	0.47+/-0.01[a]	0.73+/-0.16	0.29+/-0.06[b]	0.33+/-0.06	0.37+/-0.01[c]
HDL-C, g L^{-1}	0.34+/-0.03	0.28+/-0.01[a]	0.34+/-0.02	0.34+/-0.05[b]	0.37+/-0.05	0.36+/-0.02[c]
LDL-C, g L^{-1}	0.03+/-0.01	0.36+/-0.07[a]	0.08+/-0.05	0.13+/-0.07[b]	0.05+/-.01	0.10+/-0.03[c]
VLDL-C, g L^{-1}	0.08+/-0.00	0.09+/-0.01	0.15+/-0.03	0.06+/-0.01	0.07+/-0.01	0.07+/-0.00
Total proteins, g dL^{-1}	5.66+/-1.15	5.62+/-1.73	5.60+/-0.02	6.70+/-0.87	5.25+/-3.20	5.26+/-0.58
Albumin, g dL^{-1}	2.65+/-0.21	2.70+/-0.08	2.80+/-0.16	3.60+/-0.12	2.95+/-1.08	2.75+/-0.05
Globulin, g dL^{-1}	2.98+/-0.23	2.88+/-0.09	2.74+/-0.06	3.06+/-0.19[b]	2.28+/-0.09	2.51+/-0.19
A/G ratio	0.88+/-0.12	1.43+/-0.13[a]	1.02+/-0.11	1.17+/-0.21[b]	1.29+/-0.12	1.09+/-0.15[c]
TGO, UI L^{-1}	112.7+/-1.87	94.1+/-5.50[a]	77.5+/-2.37	115.0+/-1.68[b]	106.2+/-7.10	87.5+/-3.15
TGP, UI L^{-1}	42.03+/-30.11	52.2+/-11.30[a]	38.8+/-6.55	45.5+/-6.54[b]	44.8+/-1.34	60.2+/-6.70
TGO/TGP ratio	2.34+/-0.20	3.20+/-0.7[a]	2.50+/-0.60	2.08+/-0.14[b]	2.30+/-0.22	2.30+/-0.19
LDH, UI L^{-1}	3421.4+/-132.34	3093.9+/-320.39[a]	3320.2+/-264.13	3181.5+/-710.43[b]	3171.32+/-530.04	3223.8+/-567.65
ALP, UI L^{-1}	412.5+/-23.33	305.2+/-11.67	396.2+/-0.18	448.8+/-14.0[b]	405.7+/-19.45	367.9+/-53.7[c]
Creatinine, mg L^{-1}	9.10+/-0.43	6.80+/-0.035[a]	6.70+/-0.18	7.05+/-1.06	7.10+/-0.24	7.40+/-0.10
Urea, g L^{-1}	0.66+/-0.02	0.50+/-0.01[a]	.38+/-0.01	0.40+/-0.01	0.34+/-0.01	0.41+/-0.01

a: $p<0.05$ obese group versus controls; b: $p<0.05$ nigelle oil treated group versus obese and olive oil's treated group; c: $p<0.05$ olive oil's treated group versus obeses rats. Data represents means+/-SD.

Table 5. Effect of *Nigella sativa* and olive oils oxidative stress biomarkers.

	D1 (*n*=10)	D2 (*n*=10)	D3 (*n*=7)	D4 (*n*=8)	D5 (*n*=7)	D6 (*n*=8)
Vitamin C, µg mL^{-1}	15.40+/-2.3	11.08 +/-1.9[a]	16.16 +/-1.2 b	16.27 +/-1.8[b]	15.80+/-1.06[c]	16.12 +/-1.07[c]
Vitamin E, µmol mL^{-1}	7.65+/-0.6	6.87 +/-0.7[a]	8.22 +/-0.65[b]	8.58 +/-0.8[b]	7.98 +/-0.54	8.08 +/-0.63[c]
Vitamin A, µmol mL^{-1}	16.09+/-3.12	10.03 +/-2.18[a]	14.08 +/-2.04[b]	14.55 +/-2.09[b]	14.15+/-2.02[c]	14.20 +/-1.78[c]
MDA, nmol mL^{-1}	2.14 +/-2.3	4.47+/-4.0[a]	2.13+/-5.0	2.40 +/-4.1 b	2.24+/-2.8[c]	2.50+/-2.4[c]
Protein carbonyls, mmol mL^{-1}	1.94 +/-0.3	2.63 +/-0.5[a]	1.24 +/-0.1[b]	1.42+/-0.1[b]	1.34 +/-0.2[c]	1.07 +/-0.6[c]
SOD, U mL^{-1}	10.02 +/-1.91	11.89+/-1.85[a]	09.74+/-2. 21[b]	10.11+/-0.96[b]	08.60+/-0.85[c]	09.25+/-0.99[c]
Cat activity, U mL^{-1}	18,43+/-2.6	21,93 +/- 4.2[a]	20,27+/-10.8[b]	19,83 +/-10.9[b]	20,93+/-13.9[c]	20,61+/-11.2[c]

Data represents means+/-SD. a: $p<0.05$ obese group versus controls; b: $p<0.05$ nigelle oil treated group versus obese and olive oil's treated group; c: $p<0.05$ olive oil's treated group versus obeses rats. Refer to Table 1 for diet groups.

Final body weight an Biochemical parameters

Concerning the investigated biochemical parameters presented in Table 4, the HFD group (D 2) points out a significant increase in alanin aminotransferase (ALT) and aspartate aminotransferase (AST) compared to the control group (D 1). In opposite, ALT and AST concentrations decreased ($p<0.05$) significantly when comparing the HFD group with obese treated groups (Diets 4 and 6). A statistical difference is also observed between the two treated groups D 4 and D 6 which present a difference in their fatty acid composition (*see* Table 1). Also ALP levels increased significantly after dietary treatment with NS and olive oil. In contrast, no statistical difference was noted in LDH levels.

Total proteins, albumin and globulin levels decreased significantly in the HFD group compared to the control group. In opposite, after 08 weeks of daily treatment with NS oil, these parameters raised up, although the A/G ratio decreased in the same treated group when compared with obese rats reflecting the production of albumin by the hepatic cells which are the site of albumin synthesis and that the liver gets back their functional status. Also, there was a significant decrease in urea and creatinine levels in the obese rats (D 2) group *vs.* the control group (D1) an there was no statistical difference observed between the other groups.

BG, insulin, TG and TC were significantly higher in the HFD group compared to the control group, but decreased significantly ($p < 0.05$) for rats that received NS and olive oils compared to the HFD group. The HDL-C concentrations tended to increase in the treated groups (D4 and D6) while LDL-C was decreased significantly.

Blood glucose, plasma insulin and insulin resistance

The results of OGTT are shown in Figure 2. HOMA and OGIS results are summarized in Figure 3. For the duration of 120 min of the test, the animals were manipulated carefully to avoid stress. During the OGTT (Figure 2), the blood glucose levels in the control (D1) and treated group rats (D4 and D6) remained higher and reached the fasting levels at 2 hours and no significant difference was noted between these two groups. In contrast, in a HFD group (D2) glucose levels were significantly higher than in Diet 4 ($p<0.01$) even at 2 hours of test. HOMA-IR score is correlated to insulin sensibility OGIS has found to give a very similar results compare to hyper-insulinemic-euglycemic clamp.

Based on a multiple regression model, we can predict at 80.1% of the final weight from the amount of lipid intake, the insulin and glucose levels taken during an oral glucose tolerance test.

Oxidative stress biomarkers

Results of vitamins (A, C and E), MDA and protein carbonyls contents, CAT and SOD activities are shown in Table 5.

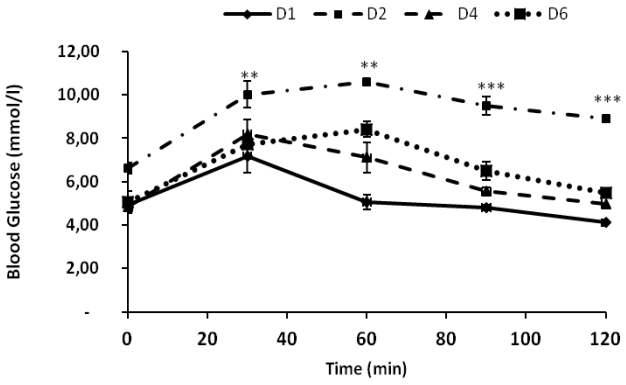

Fig 2. Evolution of blood glucose during *OGTT*. Results are expressed as means+/-SD. **($p<0.05$) ; ***($p<0.01$): significant difference between obese and control and treated obese groups.

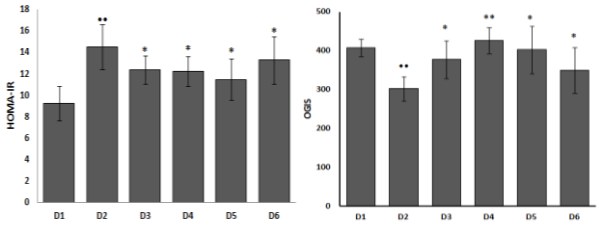

Fig 3. HOMA-IR score and OGIS values. • : Significant difference between between obese group and control ($p<0.05$); •• ($p<0.01$); ***:**Significant difference between obese and treated groups (*Nigella* or olive oil) ($p<0.05$); ****** ($p<0.01$).

We have noted a significant reduction on vitamins concentrations in obese rats compared to control group and treated groups with NS fixed oil and olive oil. A significant increase was observed in the levels of plasma MDA and protein oxidation in HFD group (D2) compared to control group (D1) and supplemented groups with nigelle and olive oils (D4 and D6). The SOD and CAT activities were significantly higher ($p<0.05$) in rats feeding with HFD. The treatment with NS oil induced a significant correction in SOD and CAT activities in both control (D3) and obese treated rats (D4).

Discussion

The aim of this study was to verify whether the supplementation with vegetable oils (*Nigella sativa* and olive oils) if it can prevent obesity. In fact, HFD induced obesity in growing rats during the 08 weeks of experimentation 32.02 % of weight gain was noted in the HFD group compared with the control group. It has been reported that HFD consumption may predispose individuals to obesity, and it can be explained that a high fat intake can contribute to excess of energy and consequently promote or support obesity.[41] It can also be explained that excessive weight gain may result from high energy intake resulting from the high caloric density of fat-enriched food or a failure in the ability to oxidize fat in obese rats.[42] These results can also be explained by the fact that high fat diets

are rich in SFAs which are considered as enhancing compounds in the development of adipose tissues.[43] On the other hand, it was shown the beneficial effects of PUFAs, due to the presence of double bonds ending up with low energy following their oxidation.[44] The oxidation rate of oleic acid is faster than that of linoleic acid and the increase in PUFAs induces a decrease in adipose tissue mass and prevents obesity development compared with MUFAs and SFAs .[45]

Moreover, the results obtained showed a significant body weight decrease which can also be explained by the high *P/S* ratio that is equal to 2.92, 0.85 and 0.71 in *N. sativa* oil, olive oil and sunflower oil, respectively. Actually, a high *P/S* ratio constitutes an important determinant for preventing HFD induced obesity. Liao and collaborators[45] reported similar results to ours in hamsters fed a low *P/S* ratio diet, which increased body weight gain and supported fat accumulation, whereas a high *P/S* ratio diet appeared to be beneficial in preventing white adipose tissue accumulation by increasing hepatic lipolytic enzyme activities involved in *β*-oxidation.

In fact, our results showed a significant decrease in the development of hyperglycemia and hyperlipidemia (total serum cholesterol and triglyceride levels) in groups treated with *N. sativa* and olive oils compared to the HFD group. The correction of lipid profile and glycemia comes to confirm that *N. sativa* fixed oil possesses favorable metabolic effects. Therefore in the study led by Houcher *et al.*,[46] the authors mentioned that an oil seed extract of *N. sativa* cause an important decrease in glycemia. This hypoglycemiant effect can be explained by either inhibition of intestinal absorption, the stimulation of insulin secretion or sensibility of tissues to insulin action which is confirmed by the HOMA-IR score and OGIS index, or by the inhibition of gluconeogenesis enzymes which must be verified. At the same time, the presence of thymoquinone on *N. sativa* as detected by the HPLC at the concentration of 6.01 ± 0.54 mg g^{-1} of oil can be another explanation to the corrective effect on the glycemia level; this is which Fararh *et al.*,[47] proved in their study. We find out that the proportion S/M/P of NS seed oil is about 1:1.1:2.6 close enough to the proportion cited in a recent study where the authors[48] mentioned that the proportion of different fatty acids in diets played an important role in metabolism and specifically, the proportion of S/M/P at 1:1:2 improved glucose and lipids metabolism, and increase insulin sensitivity.

Grundy[41] imputed the increased cholesterol and triglyceride levels to high intakes of SFAs when compared with UFAs, which can be explained by the fact that the effect of SFAs on the intestinal absorption of dietary cholesterol is greater than UFAs action.[49] Similar results were obtained by El-Dakhakhny *et al.*,[50] who found that *N. sativa* oil administrated to rats decreased significantly the serum levels of total cholesterol, TG, LDL-C and increased HDL-C. Also, Zaoui *et al.*,[51] indicated that oral treatment with *N. sativa* oil, reduced serum cholesterol and TG and glycemia levels compared with normal rats. Moreover, Meddah *et al.*,[52] showed that chronic *N. sativa* treatment improved glucose tolerance as efficiently as metformin and reduced body weight without any toxic effect.

Many studies correlate the level of serum triglycerides have been associated with insulin resistance.[29,53] In a recent study, Yang *et al.*,[54] showed that the proportion of different fatty acids in diets plays an important role in improving lipid and glucose metabolism and increasing insulin sensitivity. In fact, one of the destinies of PUFAs in cells is incorporated into membrane phospholipids. When in membranes, PUFAs contribute to their fluidity that is an important factor in the correct hormone-receptor binding. In fact, increasing in membrane fluidity might result in an enhanced number of insulin receptors that can explain by the opposite the insulin resistance, which might be associated with a rigid membrane, which limits the number of insulin receptors and decreased affinity of insulin to its receptors .[55]

On the other hand, the difference noted between the two fat supplemented diets (diets 4 and 6) can be explained by the difference in fatty acid composition of both oils. *N. sativa* oil is rich in ω6-PUFAs, which are present in low amount in olive oil. ω6-FAs have shown a cholesterol-lowering effect. They reduce insulin-resistance as well as the risk of type 2 diabetes. The main FA in olive oil is the monounsaturated oleic acid, which has a controversial action.[56] A recent study made on Spanish adult's shows that the risk of obesity increased with olive oil consumption when not controlled for total energy intake. The authors explain this result by the failure of energy compensation for olive oil consumption but at the isocaloric level, olive oil consumption did not affect obesity risk in plausible energy intake reporters.[57]

The effect of *N. sativa* on albumin synthesis was long recognized to be used as a liver disease cure. Several studies reported that treatment with *N. sativa* seeds increased the total proteins and especially the serum albumin levels in rats.[58,59] Also, in a recent study similar results were found by Tousson *et al.*,[26] where *N. sativa* supplemented diet increased plasma total protein, albumin, ALT and AST levels in rabbits and decreased total lipid serum concentrations. The change in albumin level reflects the change in the liver function and the presence of fatty acids may have an effect on the muscle protein synthesis through a prostaglandin-dependent mechanism. It is also possible as a hypothesis that the high albumin level in NS treated group may be due to an induction of their synthesis by the detected TQ and it is important to note a proof that TQ have a specific binding site on human albumin,[60] which remains to be confirmed in rodents. Moreover, Nagi *et al.*,[61] treated with an oral supplementation of TQ in acetaminophen-induced hepato-toxicity in mice and confirmed a corrected effect of ALT in a dose-dependent manner which is therefore protecting the liver.

In a recent study, the authors find for the first time that n-3 PUFA causes alterations in several novel functional proteins involved in regulating lipid, carbohydrate and protein metabolisms, and suggesting integrated regulation of metabolic pathways. These novel proteins are potential targets to develop therapeutic strategies against metabolic disorders such as obesity.[62]

Furthermore, in order to investigate the anti-oxidant effect of NS fixed oil, we analyzed plasmatic MDA and protein carbonyl contents, plasmatic vitamins levels and CAT and SOD activities in HFD rats and supplemented rats by this oil compared to olive oil supplementation. Lower vitamins

concentrations and a higher plasmatic MDA and protein carbonyls contents were found in obese rats compared with the control group, that reflect the amount of oxidative stress that rats have been exposed to during the time of experimentation. These results confirm the fact that obesity is associated with the oxidant stress increase. Possible mechanisms contributing to the obesity-associated oxidant stress include increased oxygen consumption *via* mitochondrial respiratory chain, increased fat deposition and cell injury causing increased rates of radicals and reactive oxygen species (ROS) formation such as H_2O_2.[63] Lee H.I. *et al.*,[64] reported that increased fat deposition results mainly from consumption of a hyperlipidemic diet, and is vulnerable to oxygen metabolism that can cause lipid peroxydation and consequently malondihaldehyde (MDA-TBARS) formation. The low plasma levels of vitamins could reflect their high utilization rate, suggesting that these vitamins may be used to reduce oxidative stress in obese rats. In addition and unexpectedly, an increase in SOD and CAT activities were observed in obese rats. These results suggest an up regulation of these antioxidants enzymes in our growing young obese rats. It's could be interpreted as a positive feedback mechanism reflecting a favorable response of the organism to oxidative stress if compared to old obese rats in other studies.[65,66]

Elevated levels of oxidant markers in obese rats could result from their insulin resistance state, hypercholesterolemia and abnormal metabolism. Actuality, recent studies, have proposed that ROS such as H_2O_2 are produced transiently in response to insulin stimulation and also act as a second messenger for insulin signaling in adipocytes. In fact, a brief increase of intracellular ROS is important for the insulin signaling pathway, while excessive and long-term exposure to ROS reduces insulin sensitivity and impairs glucose and lipid metabolism. These results suggest that increased ROS production caused by fat accumulation may prevent further lipid storage, but may simultaneously cause insulin resistance.[14]

In our study, a NS and olive oils supplementation in obese rats show a corrective effect in the antioxidant defense system. These results show the potential antitoxic effect of NS seeds oil mediated by their antioxidant properties. Many studies have reported that dietary supplementation by the small molecular-weight antioxidants and the free radical scavengers such as vitamins, minerals, polyphenols, quinones and PUFAs prevent or at least attenuate the damages due to ROS in the case of an oxidative stress.[19,67] In a recent study,[68] the authors found that the protective effect of NS against petrochemical-induced oxidative stress may be due to TQ which is the most potent in terms of antioxidant capacity. In addition, Mansour M.A. *et al.*,[69] suggested that TQ may act as an antioxidant agent and prevent the membrane lipid peroxidation and antioxidant enzymes in hepatocytes and that may well sustain our results.

Conclusion

The results of this study demonstrated that *Nigella sativa* seeds oil is beneficial for attenuating complications of obesity and possibly preventing it because of its essential polyunsaturated fatty acids; linoleic and linolenic acids and other nutrients such as liposoluble vitamins like tocopherols and also minerals, essential amino acids, some polyphenols, terpenoïds and quinones, particularly thymoquinone that have shown potential medicinal properties in traditional medicine.

Thus, *N. sativa* seeds oil supplement has shown a beneficial impact by ameliorating glucose tolerance, liver enzymes activities, pancreatic function in obese rats and metabolic rate as well. So, further investigations are encouraged in this way in order to unveil the molecular mechanisms of this oil on body cells and then show its importance for human use as a supplementary source of lipids and nutraceutical rich source to correct obesity and theirs consequences or to prevent their installation also in a favorable environment like a consumption of high caloric diet.

Acknowledgements

Special thanks for Pr Villemin Didier (LCMT-ENSICaen-UMR6507) and Pr. Cardinal Pascal (IRCOF-Sciences et Méthodes Séparatives, Rouen University) and his team for the HPLC an CG analyses, respectively.

References

[1]Hong, J. and Friedman, M. I., *Metabolism*, **2007**, *56*, 1124.

[2]McCrory, M. A., Fuss, P. J., McCallum, E. J., Yao, M., Vinken, A. G., Hays, P. N., Roberts, S. B., *Am. J. Clin. Nutr.*, **1999,** *69*, 440.

[3]WHO: *World Health Organisation, Obesity and overweight*. Fact sheet N° 311, **2013**.

[4]Shahzya, S. H., Lauren, E. B., Naveed, S., *Semin. Fetal. Neonatal Med.*, **2010,** *15*, 70.

[5]Kim, S. O., Yun, S. J., Jung, B., Lee, E. H., Hahm, D. H., Shim, I., Lee, H. J., *Life Sci.*, **2004**, *75*, 1391.

[6]Kim, J., Li, Y., Watkins, B. A., *Prostaglandins Other Lipid Mediators*, **2013**, *32, 104.*

[7]Kretschmer, B. D., Schelling, P., Beier, N., Liebscher, C., Treutel, S., Kroger, N., Scholz, H. P., Haus A., *Life Sci.,* **2005**,*76*, 1553.

[8]Lee, J. S., Lee, M. K., Ha, T. Y., Bok, S. H., Park, H. M., Jeong, K. S., Woo, M. N., Do, G.-M., Yeo, J. Y., Choi M. S., *Food Chem. Toxicol.*, **2006**, *44*, 1875.

[9]Platat, C., *Rech. cliniq., Santé Publ.*, **2005**, *15*, 34.

[10]McAuley, K., Mann, J., *J. Lipid Res.*, **2006**, *47*, 1668.

[11]During, A., Combe, N., Mazette, S., Entressangles, B., *J. Am. Coll. Nutr.*, **2000**, *19*, 458.

[12]Ramadan, M. F., Kroh , L. W., Mörsel, J. T., *J. Agric. Food Chem.*, **2003**, *51*, 6961-6969.

[13]Koji, N., Teruyoshi, Y., *Prog. Lipid Res.*, **2007**, *47*, 127.

[14]Furukawa, S., Fujita, T., Shimabukuro, M., Iwaki, M., Yamada, Y., Nakajima, Y., Nakayama, O., Makishima, M., Matsuda, M., Shimomura, I., *J. Clin. Invest.*, **2004**, *114*, 1752.

[15]Castrillejo, V. M., Romero, M. M., Esteve, M., Ardevol, A., Blay, M., Blade, C., Arola, L., Salvado.M. J., *Nutrition*, **2011**, *27*, 1172.

[16]Mathus-Vliegen, E. M. H., Basdevant, A., Finer, N., Hainer, V., Hauner, H., Micic, D., Maislos, M., Roman, G., Schutz, Y., Tsigos, C., Toplak, H., Yumuk, V., Zahorska-Markiewicz, B., *Obes. Facts*, **2012,** *5*, 460.

[17]Rodgers, A. J., Tschöp, M. H. and Wilding, J. P. H., *Dis. Models & Mech.*, **2012**, *5*, 621.

[18]You, J. S., Lee, Y. J., Kim, K. S., Kim, S. H., Chang, K. J., *Nutr. Res.* **2014**, doi: 10.1016/j.nutres.2014.01.003.

[19]Yun, J. K., Keun-Young, K., Min, S. K., *Genes Nutr.*, **2008**, *2*, 353.

[20]Kanter M., Coskun O., Kalayci, M., Buyukbas, S., Cagavi, F., *Hum. Exp. Toxicol.*, **2006**, *25*, 127.

[21]Bhupendra, K. M., Uma, S., Sumit, A., Vikas, P., Nidhi, J., Meenal, G., *Med. Chem. Res.*, **2008**, *17*, 462.

[22]Salih, B. T., Sipahi, E., Oybak, D., *J. Ethnopharmacol.*, **2009**, *124*, 416.

[23]Kökdil, G., Tamer, L., Ecran, B., Ilcim, A., Aras, N., Atik, U., *J. Ethnopharmacol.*, **2005**, *99*, 131.

[24]Gargari, P. B., Ebrahimzadeh-Attary, V., Rafraf, M., Gorbani, A., *J. Med. Plants Res.*, **2009,** *3*, 815.

[25]Ilhan, A., Gurel, A., Armutcu, F., Kamisli, S., Iraz, M., *Neuropharmacology*, **2005,** *49*, 456.

[26]Tousson, E., El-Moghazy, M. and El-Atrsh, E., *Toxicol. Ind. Health*, **2011**, *27*, 107.

[27]Al-Saleh, I. A., Billedo, G., El-Doush, I. I., *J. Food Comps. Anal.*, **2006,** *19*, 167.

[28]Matthews, D. R., Hosker, J. R, Rudenski, A. S., Naylor, B. A., Treacher, D. F., Turner, R. C., *Diabetologia*, **1985**, *28*, 412.

[29]Thien, T. T., Neehar, G., Tracy, G., Dinaz N., Marie C. C., Niloofar K., Shruti M., Gail M-E., Garcia A., and Bruce, W. R., *Cancer Epidemiol., Biomarkers Prev.*, **2003**, *12*, 47.

[30]Papandreou, D., Rousso, I., Malindretos, P., Makedou, A., Moudiou, T., Pidoni, I., Pantoleon, A., Economou, I., Mavromichalis, L., *Clin. Nutr.*, **2008,** *27*, 233.

[31]Grove, T. H., *Clin. Chem.*, **1979**, *25*, 560.

[32]Wilson, P. W., Abbot, R. D., Garrison, R. J., Castelli, W. P., *Clin. Chem.*, **1981**, *27*, 2008.

[33]Friedewald, W. T., Levy, R. I., Fredrickson, D. S., *Clin. Chem.*, **1972**, *18*, 499.

[34]Liu, J. W., DeMichele, S. J., Palombo, J., Chuang, L. T., Hastilow, C., Bobik, E. and Huang, Y. S., *J. Agr. Food Chem.*, **2004**, *52*, 3960.

[35]Zaman, Z., Fielden, P., Frost, P. G., *Clin. Chem.*, **1993,** *39*, 2229.

[36]Roe, J. H., Kuether. C. A., *J. Biol. Chem*, **1943,** *147*, 399.

[37]Ohkawa, H., Ohishi, N., Yagi, K., *Anal. Biochem.*, **1979,** *95*, 351.

[38]Levine. R. L., Garland. D., Oliver. C. N., Amici. A., Climent. I., Lenz. A. G., Ahn,. B. W., Shaltiel, S., Stadtman, E. R., *Methods Enzymol.*, **1990,** *186*, 464.

[39]Aebi, H.,*Methods Enzymol.*, **1984**, *105*, 121.

[40]Sun, Y., Oberley, L. W., Li, Y., *Clin. Chem.*, **1988,** *34*, 497.

[41]Grundy, M. S., *Ann. Rev. Nutr.*, **1999,** *19*, 325.

[42]Lichtenstein, A. H., Kennedy, E., Barrier, P., Dandford, D., Nancy, D., Grundy, M. S., Leveille, G. A., Van Horn, L., Williams, C. L., Booth, S. L., *Nutr. Rev.*, **1998,** *56*, S3.

[43]Pérez-Matute, P., Pérez-Echarri, N., Martinez, J. A., Marti, A., Moreno-Aliaga, M. J., *Brit. J. Nutr.*, **2007,** *97*, 389.

[44]Garton, L., *Le rôle des aliments à base de plantes dans la lutte contre l'obésité. Congrès européen sur l'obésité. ALPRO Foundation*. Amsterdam, **2009.**

[45]Liao, Fang-Hsuean, M. S., Liou, Tsan-Hon, M. D., Shieh, M-J., Chien, Y-W., *Nutrition*, **2010,** *26*, 811.

[46]Houcher, Z., Boudiaf, K., Benboubetra, M., Houcher, B., *Pteridines*, **2007**, *18*, 8.

[47]Fararh, K. M., Shimizu, Y., Shiina, T., Nikami, H., Ghanem, M. M., Takewaki, T., *Res. Vet. Sci.*, **2005**, 79, 219.

[48]Xuefeng, Y., Yi, Z., Jieyi, L., Anfang, P., Chenjiang,Y., Wenhong, C., Limei, M., *Nutr. Res.*, **2012**, *32*, 285.

[49]Strange, E. F., Alavi, M., Schneider, A., Ditschuneit, H., Poley, J. R., *J. Lipid Res.*, **1981**, *22*, 47.

[50]El-Dakhakhny, M., Mady, N. I., Halim, M. A., *Arzneim. Forsch.*, **2000**, *50*, 832.

[51]Zaoui, A., Cherrah, Y., Mahassini, N., Alaoui, K., Amarouch, H., Hassar, M., *Phytomedicine*, **2002**, *9*, 69.

[52]Meddah, B., Ducrocb, R., Moulay El Abbes, F., Etoc, B., Mahraoui, L., Benhaddou-Andaloussi, A., Martineaud, L. C., Cherraha, Y., Haddadd, P. S., *J. Ethnopharmacol.*, **2009**, 121, 419.

[53]Yang, P., Baochang, C., Kelin, W., Sumin, W., Shuyuan, Z., Xiaochun, Y., Bin, X., Long, C., *J. Ethnopharmacol.*, **2009**, *124*, 98.

[54]Yang, X., Zhang, Y., Lin, J., Pen, A., Ying, C., Cao, W., Mao, L., *Nutr. Res.*, **2012**, *32*, 285.

[55]Russo, G. L., *Biochem. Pharm.*, **2009**, *77*, 937.

[56]Jacomelli, M., Pitozzi, V., Zaida, M., Larrosa, M., Tonini, G., Martini, A., Urbani, S., Taticchi, A., Servili, M., Dolara, P., Giovannelli, L., *J. Nutr. Biochem.*, **2010**, *21*, 290.

[57]Benítez-Arciniega, A. D., Gómez-Ulloa, D., Vila, A., Giralt, L., Colprim, D., Rovira Martori, M. A., Schröder, H., *Obes. Facts*, **2012**, *5*, 52.

[58]Al-Gaby, A. M., *Die Nahrung*, **1998**, *42*, 290.

[59]Al-Jishi, S.A., Abou Hozaifa, B., *J. Ethnopharmacol.*, **2003**, *85*, 7.

[60]Lupidi, G., Scireb, A., Camaionic, E., Khalifea, K. H., De Sanctisa, G., Tanfanib, F., Damiani, E., *Phytomedicine*, **2010**, *17*, 714.

[61]Nagi, M. N., Almakki, H. A., Sayed-Ahmed, M. M., Al-Bekairi, A. M., *Food Chem. Toxicol.*, **2010**, *48*, 2361.

[62]Ahmed, A. A., Balogun, K. A., Bykova, N. V. and Cheema, S. K., *Nutr. Metabol.*, **2014,** *11*, 6.

[63]Begriche, K., Massart, J., Robin, M. A., Borgne-Sanchez, A., Fromenty, B., *J. Hepatol.*, **2011,** *54*, 773.

[64]Lee, H. I., Kim, M. S., Lee, K. M., Park, S. K., Seo, K. I., Kim, H. J., Kim M. J., Choi M. S., Lee, M. K., *Food Chem. Toxicol*,, **2011,** *49*, 2370.

[65]Finkel, T., Holbrook, N. J., *Nature*, **2000**, *408*, 239.

[66]Kregel, K. C., Zhang, H. J., *Am. J. Physiol. Regulat., Integrat. Comp. Physiol.*, **2007,** *292*,18.

[67]Salem, M. L., *Int. Immunopharmacol.*, **2005**, *5*, 1749.

[68]Ashraf, S. S., Rao, M. V., Kaneez, F. S., Qadri, S., Al-Marzouqi, A., Chandranath, I. S., and Adem, A., *J. Chromatogr. Sci.*, **2011,** *49*, 321

[69]Mansour, M. A., Nagi, M. N., El-khatib, A. S., Al-Bekairi, A. M. *Cell Biochem. Funct.*, **2002,** *20*, 143.

Received: 20.07.2014.
Accepted: 25.08.2014.

PYRIDAZINE AND ITS RELATED COMPOUNDS, PART 39. SYNTHESIS AND ANTIMICROBIAL EVALUATION OF SOME THIENOPYRIDAZINE BASED HETERCYCLE

A. Deeb,*[a], F. El-Mariah, [b] K. El-Badry, [b] and H. K. Abd El-Mawgoud [b]

Keywords: Thienopyridazines; pyrrolothienopyridazines; pyrimidothienopyridazines, pyrazolothienopyridazines; pyridazinothieno-quinolines; synthesis; antimicrobial activity.

The starting material, 5-amino-3,4-diphenylthieno[2,3-c]pyridazine-6-carbonitrile was subjected to subsequent reactions with aromatic and heteroaromatic aldehydes, benzylchloride, cyclohexanone, phenyl isothiocyanate, hydroxylamine hydrochloride and hydrazine hydrate to afford new polycyclic compounds. The new synthesized compounds were confirmed by their infrared, mass spectrum, ^{1}H-NMR, and elemental analyses, and further screened for antimicrobial activity.

* Corresponding Authors
E-Mail: dralideeb@hotmail.com
[a] Department of Chemistry, Faculty of Science, Zagazig University, Zagazig, Egypt.
[b] Department of Chemistry, College of Women For Arts, Science, and Education, Ain Shams University, Cairo, Egypt.

INTRODUCTION

Pyridazine derivatives and heterocyclic-annulated pyridazines continue to attract interest due to a wide spectrum of biological and therapeutic effects. They are used as analgesic,[1] antibacterial,[2] anti-inflammatory,[3] antihypertensive,[4] antihistaminic,[5] anti-nociceptive agents,[6] as well as platelet aggregation inhibitors.[7] Thieno-pyridazines[8] have been reported to possess considerable antiasthmatic[9] and fibrinolytic activities.[10] Also, the enami-nonitrile serves as a good synthon for construction of a many condensed heterocyclic systems.[11] Based on these considerations, our interest was focused on synthesizing new heterocyclic compounds including thienopyridazine moiety with suitable substituents, these structures all on different derivatives related to compounds of biological and pharmacological interest to be obtained. The biological activity of some of the synthesized compounds has been screened.

RESULTS AND DISCUSSION

The starting material, 5-amino-3,4-diphenylthieno[2,3-*c*]pyridazine-6-carbonitrile **1** was synthesized following the literature procedure by refluxing a solution of 4-cyano-5,6-diphenylpyridazine-3(2*H*)-thione with chloroacetonitrile in dry acetone in presence of potassium carbonate.[12,13]

The reaction of 5-amino-3,4-diphenylthieno[2,3-*c*]pyridazine-6-carbonitrile **1** with an equimolecular quantity of aromatic and / or heteroaromatic aldehydes in benzene gave 5-arylidene- and 5-heteroarylideneaminothieno-pyridazine derivatives **2$_{a-h}$** (**Scheme 1**).

A mixture of compound **1** and benzyl chloride was heated in ethanol under reflux afforded 5-benzylamino derivative **3**, which undergoes cyclization upon heating under reflux in presence of sodium ethoxide in ethanol gave 7-amino-3,4,6-triphenyl-5H-pyrrolo[2`,3`:4,5]thieno-[2,3-*c*]pyridazine **4**. Alternatively, compound **4** was obtained directly upon refluxing a solution of compound **1** in ethanol with benzyl chloride in presence of sodium hydroxide. Reaction of compound **4** with nitrous acid followed the normal course of diazotization yielding clear diazonium salt solution **5**, which underwent coupling with 2-naphthol in ethanolic solution in presence of sodium acetate trihydrate as buffered solution to give the corresponding azo derivative **6** (**Scheme 1**).

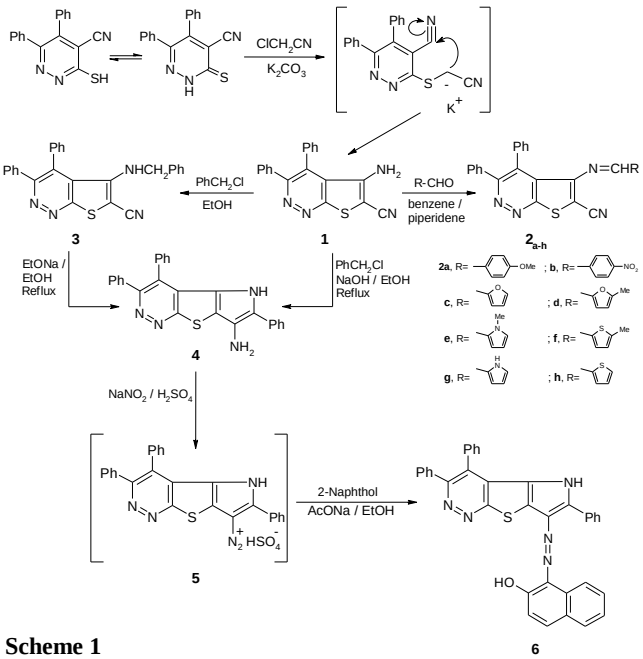

Scheme 1

Treatment of compound **1** with cyclohexanone in presence of one molar equivalent of anhydrous zinc chloride led to the separation of 1:1 complex of the expected amino derivative with zinc chloride **7**. 10-Amino-3,4-diphenyl-

6,7,8,9-tetrahydropyridazino[4`,3`:4,5]thieno[3,2-*b*]quinoline **8** was liberated by treatment of the resulting complex with alkali and extracted with benzene[14,15] (**Scheme 2**).

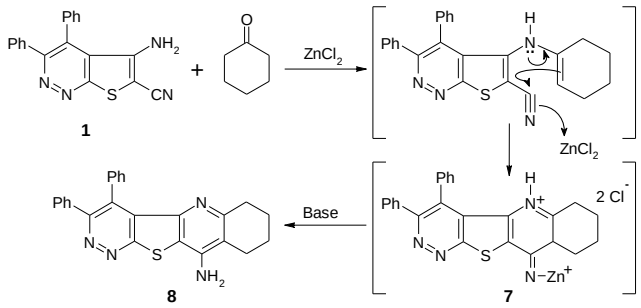

Scheme 2

Treatment of compound **1** with phenyl isothiocyanate in dimethylformamide as solvent in the presence of triethylamine at room temperature for 18 h led to the corresponding N,N`-di-substituted thiourea **9**, which was transformed into 7-amino-6-anilino-8-imino-3,4-diphenylpyrimido[4`,5`:4,5]thieno[2,3-*c*]pyridazine **10** by the reaction with hydrazine hydrate (98 %) in boiling ethanol. Treatment of compound **10** with acetic anhydride yielded the 7-acetyl-amino derivative **11** (**Scheme 3**).

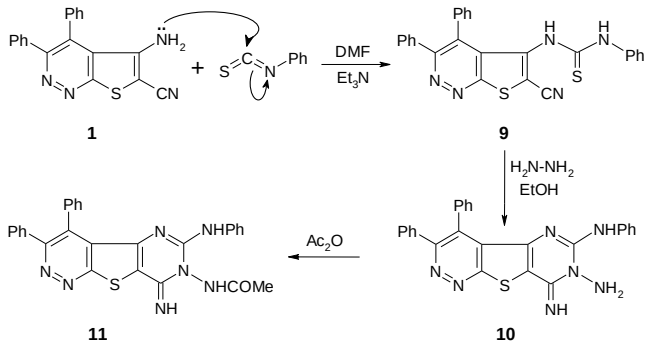

Scheme 3

The reaction of 5-amino-3,4-diphenylthieno[2,3-*c*]pyridazine-6-carbonitrile **1** with hydroxylamine hydrochloride was carried out in methanol containing ammonium hydroxide at room temperature to give the corresponding 6-carboxamidoxime derivative **12**. Further attempted reaction in boiling pyridine for 5 h afforded 3-amino-7,8-diphenyl-1*H*-pyrazolo[3`,4`:4,5]thieno[2,3-*c*]-pyridazine hydrochloride **13**, *via* the initial formation of **12** followed by intermediate intramolecular nucleophilic attack of amino group at position 5 to the oxime nitrogen atom with elimination of one molecule of water. Diazotization reaction of compound **13** with nitrous acid followed the normal course yielding clear diazonium salt solution **14**, which underwent coupling with 2-naphthol in ethanol in presence of sodium acetate trihydrate as buffered solution to give the corresponding azo derivative **15**. The latter compound underwent readily cyclization upon heating in glacial acetic acid at reflux temperature to give **16**, which was formed by elimination of one molecule of water (**Scheme 4**).

Compound **1** was reacted with hydrazine hydrate (98 %) in refluxing ethanol for 2 h to give 5-amino-3,4-diphenylthieno[2,3-*c*]pyridazine-6-carboximidohydrazide **17**, while reflux-ing for 6 h gave 3-amino-7,8-diphenyl-1H-pyrazolo[3`,4`:4,5]thieno[2,3-*c*]pyridazine **18**. Also, compound **18** was afforded by heating the imido derivative **17** in ethanol under reflux for 5 h. Additional evidences for the structure of pyrazolothienopyridazine derivative **18** was proved by its reaction with acetic anhydride to give the corresponding 3-acetylamino derivative **19**, and with $NaNO_2$ / H_2SO_4 to give the diazotized aminopyrazolothieno-pyridazine, which upon coupling with 2-naphthol in presence of sodium acetate trihydrate as buffered solution in ethanol (50 %) gives **15** (**Scheme 4**).

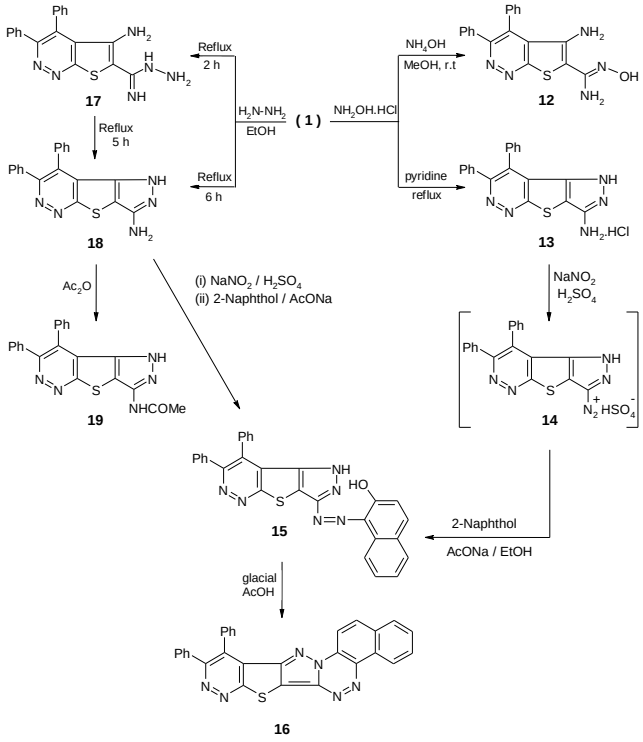

Scheme 4

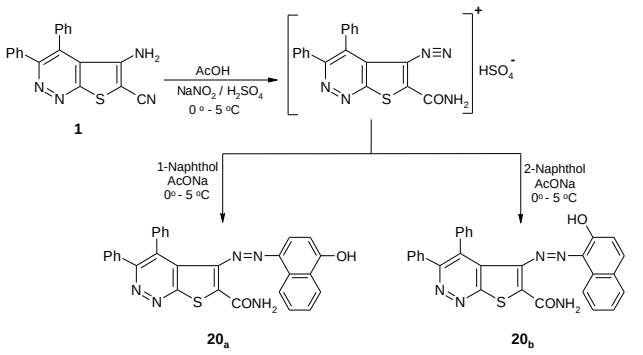

Scheme 5

 DOI: 10.17628/ecb.2014.3.897-903

Table 1. Antimicrobial activity of the synthesized compounds

Compd. No.	Zone of inhibition					
	Staphylococcus Aurous	***Bacillus subtitles***	***Escherichia coli***	***Pseudomonas aeruginosa***	***Candida albicans***	***Aspergillums Niger***
2_a	++	++	++	-	++	+++
2_b	++	++	-	-	+++	++
2_c	-	-	++	-	+++	++++
2_d	+	++	++	-	++++	++
2_e	-	++	++	-	++++	++++
2_f	-	+	++	+	+++	+++
2_g	++	++	++	-	+++	-
2_h	+	++	++	-	+++	-
9	+	++	+	++	++	++++
12	++	+	+	+	+++	++
17	++	++	-	-	++	++
19	++	++	-	-	+	++
20_b	++	++	-	+	+++	-
Ciprofloxacin	++++	++++	++++	++++	-	-
Nystin	-	-	-	-	++++	++++

The concentration of the all synthesised compounds and the two references was 0.30 mg 0.10 mL^{-1} of dimethylformamide. Zone of inhibition: + = < 15 mm; ++ = 15-24 mm; +++ = 25-34 mm; ++++ = 35-44 mm; - = no inhibition.

Diazotization of the 5-amino-3,4-diphenylthieno[2,3-*c*]pyridazine-6-carbonitrile **1** was carried out, followed by coupling with 1- and 2-naphthol to give the azo derivatives **20_a** and **20_b**, respectively (**Scheme 5**). The structure of the prepared compounds was confirmed on the basis of spectroscopic data (IR, mass, ^{1}H-NMR spectra) and elemental analysis as described in the experimental part.

Screening for antimicrobial activities

Applying the agar plate diffusion technique,[16] the newly synthesised compounds were screened in vitro for antimicrobial activity against Gram positive bacteria (*Staphylococcus aureus* and *Bacillus subtilis*), Gram negative bacteria (*Escherichia coli* and *Pseudomonas aeruginosa*), yeast (*Candida albicans*), and fungi (*Aspergillus niger*).

In this method,a standard 5 mm sterilised filter paper disk impregnated with the compound (0.3 mg / 0.1 ml of dimethylformamide) was placed on agar plate seeded with the tested organism. The plates were incubated for 24 h at 37 °C for bacteria and 28 °C for fungi. The inhibition zone of bacteria and fungi growth around the disk were determined. The screening results are given in (**Table I**).

The results indicated that seven synthesized compounds **2_a**, **2_b**, **2_g**, **12, 17, 19** and **20_b** showed moderate antimicrobial activity against the examined Gram positive bacteria *Staphylococcus aureus*. On the other hand, ten synthesized compounds **2_a**, **2_b**, **2_d**, **2_e**, **2_g**, **2_h**, **9**, **17**, **19** and **20_b** showed moderate antimicrobial activity against the examined Gram positive bacteria *Bacillus subtilis*. Only the six synthesised compounds **2_a**, **2_b**, **2_g**, **17**, **19** and **20_b** showed moderate antimicrobial activity against the both examined Gram positive bacteria *Staphylococcus aureus* and *Bacillus subtilis*.

On the other hand, seven compounds **2_a**, **2_c**, **2_d**, **2_e**, **2_f**, **2_g** and **2_h** and one compound **9** showed moderate antimicrobial activity against the examined Gram negative bacteria *Escherichia coli* and *Pseudomonas aeruginosa*, respectively.

In addition, two compounds **2_d** and **2_e** and three compounds **2_c**, **2_e** and **9** showed very high antifungal activity against the examined fungi *Candida albicans* (yeast) and *Aspergillus niger*, respectively. Only one compound **2_e** showed very high antifungal activity against the both examined fungi *Candida albicans* and *Aspergillus niger*. The results revealed also that seven synthesised compounds **2_b**, **2_c**, **2_f**, **2_g**, **2_h**, **12** and **20_b** and two synthesised compounds **2_a** and **2_f** showed high antifungal activity against the examined fungi *Candida albicans* and *Aspergillus niger*, respectively. Only one synthesised compound **2_f** showed high antifungal activity against the both examined fungi *Candida albicans* and *Aspergillus niger*.

In conclusion, results of antimicrobial activity revealed that the synthesised compounds showed moderate and / or very high antimicrobial activity against bacteria and fungi, respectively. It could be concluded from these results that the biologically active synthesised compounds are nearly as active as the standard antibacteria Ciprofloxacin against the both tested Gram positive bacteria (*Staphylococcus aureus* and *Bacillus subtilis*) and Gram negative bacteria (*Escherichia coli* and *Pseudomonas aeruginosa*). On the other hand, the biologically active synthesised compounds are active as the standard Fungicid Nystin against the both tested fungi *Candida albicans* and *Aspergillus niger*.

EXPERIMENTAL

Melting points were determined in open glass capillaries and are uncorrected. Elemental analysis (CHN) were carried out using a Perkin-Elmer 240 C Microanalyzer the Microanalytical Laboratory-Cairo University.

The IR spectra of compounds were recorded on a Perkin-Elmer spectrophotometer model 1430 as potassium bromide pellets and frequencies are reported in cm^{-1}. The ^{1}H-NMR spectra were recorded on a Perkin-Elmer R12B spectrometer 200 MHz and chemical shifts δ are in ppm relative to internal TMS, and mass spectra were recorded on a mass spectrometer HP model MS 5988 El 70 ev. Reactions were routinely followed by thin layer chromatography (TLC) on silica gel; F_{254} aluminum sheets (Merck). The spots were detected by UV irradiation at 254–365 nm.

General procedure for the synthesis of 5-arylidene- and 5-heteroarylideneamino-3,4-diphenylthieno[2,3-*c*]pyridazine-6-carbonitriles, 2_{a-h}.

A mixture of compound **1** (0.5 g, 1.52 mmol) and the appropriate aromatic and heteroaromatic aldehydes (1.52 mmol) in benzene (10 mL) was heated under reflux for 3 h in presence of piperidine (0.5 mL). The solvent was then evaporated under reduced pressure, and the solid product was recrystallised from ethanol to give **2_{a-h}**.

5-[[(4-Methoxyphenyl)methylidene]amino]-3,4-diphenylthieno-[2,3-*c*]pyridazine-6-carbonitrile, 2_a.

Yield: (0.51 g, 75 %); m.p. 154°-156 °C; IR: 2246 (C≡N), 1678 (C=N), 2926, 1448 (–OCH_3); MS (*m/z* %): 446 (M^+, 2.72 %), 329 (M^+ - C_8H_8O, 100 %); Anal Calcd. For $C_{27}H_{18}N_4OS$: C, 72.62; H, 4.06; N, 12.55; Found: C, 72.30; H, 4.13; N, 12.27 %.

5-[[(4-Nitrophenyl)methylidene]amino]-3,4-diphenylthieno[2,3-*c*]-pyridazine-6- carbonitrile, 2_b.

Yield: (0.52 g, 74 %); m.p. 128° - 129 °C; IR: 2248 (C≡N), 1675 (C=N), 1516 (NO_2, asym.), 1341 (NO_2, sym.); MS (*m/z* %): 461 (M^+, 1.81 %), 329 (M^+ - $C_7H_5NO_2$, 100 %); Anal Calcd. For $C_{26}H_{15}N_5O_2S$: C, 67.66; H, 3.28; N, 15.18; Found: C, 67.96; H, 3.22; N, 15.42 %.

5-[[(Furan-2-yl)methylidene]amino]-3,4-diphenylthieno[2,3-*c*]-pyridazine-6-carbonitrile, 2_c.

Yield: (0.49 g, 79 %); m.p. 212° - 214 °C; IR: 2245 (C≡N), 1665 (C=N); MS (*m/z* %): 407 (M^+ +1, 6.89 %), 103 (M^+ - $C_{17}H_9N_3OS$, 100 %), 77 (64.59 %); Anal. Calcd. For $C_{24}H_{14}N_4OS$: C, 70.92; H, 3.47; N, 13.79; Found: C, 70.58; H, 3.55; N, 13.51 %.

5-[[(5-Methylfuran-2-yl)methylidene]amino]-3,4-diphenylthieno-[2,3-*c*]pyridazine-6-carbonitrile, 2_d.

Yield: (0.54 g, 84 %); m.p. 196° - 198 °C; IR: 2973 (–CH_3), 2245 (C≡N), 1666 (C=N); MS (*m/z* %): 420 (M^+, 0.64 %), 329 (M^+ - C_6H_6O, 100 %); Anal Calcd. For $C_{25}H_{16}N_4OS$: C, 71.41; H, 3.84; N, 13.33; Found: C, 71.76; H, 3.90; N, 13.07 %.

5-[[(1-Methyl-1*H*-pyrrol-2-yl)methylidene]amino]-3,4-diphenylthieno[2,3- *c*]-pyridazine-6-carbonitrile, 2_e.

Yield: (0.52 g, 82 %); m.p. 209° - 210 °C; IR: 2976 (–CH_3), 2241 (C≡N), 1665 (C=N); MS (*m/z* %): 419 (M^+, 0.23 %), 329 (M^+ - C_6H_7N, 100); Anal Calcd. For $C_{25}H_{17}N_5S$: C, 71.57; H, 4.09; N, 16.70; Found: C, 71.23; H, 4.18; N, 16.41 %.

5-[[(5-Methylthiophene-2-yl)methylidene]amino]-3,4-diphenylthieno[2,3-*c*]pyridazine-6-carbonitrile, 2_f.

Yield: (0.53 g, 80 %); m.p. > 300 °C; IR: 2965 (–CH_3), 2246 (C≡N), 1664 (C=N); MS (*m/z* %): 436 (M^+, 0.13 %), 329 (M^+ - C_6H_6S, 100 %); Anal Calcd. For $C_{25}H_{16}N_4S_2$: C, 68.78; H, 3.70; N, 12.84; Found: C, 69.10; H, 3.62; N, 12.58 %.

3,4-Diphenyl-5-[[(1*H*-pyrrol-2-yl)methylidene]amino]thieno-[2,3-*c*]pyridazine-6-carbonitrile, 2_g.

Yield: (0.48 g, 78.5 %); m.p. 208° - 210 °C; IR: 3281 (–NH), 2243 (C≡N), 1664 (C=N); MS (*m/z* %): 405 (M^+, 4.80 %), 57 (M^+ - $C_{14}H_{10}N_2$, - $C_8H_5N_3$, 100 %); Anal Calcd. For $C_{24}H_{15}N_5S$: C, 71.09; H, 3.73; N, 17.27; Found: C, 70.76; H, 3.65; N, 17.51 %.

3,4-Diphenyl-5-[[(thiophene-2-yl)methylidene]amino]thieno-[2,3-*c*]pyridazine-6-carbonitrile, 2_h.

Yield: (0.49 g, 76 %); m.p. 140° - 142 °C; IR: 2247 (C≡N), 1673 (C=N); MS (*m/z* %): 422 (M^+, 0.44 %), 329 (M^+ - C_5H_4S, 100 %); Anal Calcd. For $C_{24}H_{14}N_4S_2$: C, 68.22; H, 3.34; N, 13.26; Found: C, 68.59; H, 3.29; N, 13.55 %.

5-Benzylamino-3,4-diphenylthieno[2,3-*c*]pyridazine-6-carbonitrile, 3.

A solution of equimolar mixture of compound **1** (0.5 g, 1.52 mmol) and benzyl-chloride (0.2 g, 1.52 mmol) in absolute ethanol (10 mL) was heated under reflux for 3 h. The solvent was evaporated, and the residue was treated with petroleum ether 40° - 60°C. The solid precipitate was filtered off, dried, and recrystallised from ethanol to give **3**. Yield: (0.44 g, 69.5 %); m.p. 192° - 194 °C; IR: 3284 (–NH), 2922 (–CH_2–), 2197 (C≡N); MS (*m/z* %): 419 (M^+ +1, 46.2 %), 149 (M^+ - C_6H_5, - $C_{14}H_{10}N$, 100 %); Anal Calcd. For $C_{26}H_{18}N_4S$: C, 74.62; H, 4.33; N, 13.39; Found: C, 74.95; H, 4.25; N, 13.13 %.

7-Amino-3,4,6-triphenyl-5*H*-pyrrolo[2`,3`:4,5]thieno[2,3-*c*]pyridazine 4.

Method A

To a solution of equimolar mixture of compound **1** (0.5 g, 1.52 mmol) and benzyl-chloride (0.2 g, 1.52 mmol) in absolute ethanol (10 mL), NaOH (0.5 g) was added.

The reaction mixture was heated under reflux for 6 h, cool to room temperature, poured into ice water, and neutralised with HCl. The precipitate was filtered off, washed with water, dried, and recrystallised from ethanol to give **4**. Yield: (0.29 g, 45.5 %); m.p. 155°-156 °C; IR: 3442, 3319, 3177 (–NH_2, –NH); MS (*m/z* %): 418 (M^+, 30.8 %), 149 (M^+ - C_6H_5, - $C_{14}H_{10}N$, 100 %); Anal Calcd. For $C_{26}H_{18}N_4S$: C, 74.62; H, 4.33; N, 13.39; Found: C, 74.99; H, 4.24; N, 13.11 %.

Method B

To a solution of sodium ethoxide [(0.1 g) of Na in (10 mL) absolute ethanol], compound **3** (0.5 g, 1.19 mmol) was added. The reaction mixture was refluxed for 5 h, cool to room temperature, poured into ice water, and neutralized with HCl. The precipitate was filtered off, washed with water, dried, and recrystallised from ethanol to give **4**. It was identical with the compound prepared by method A (m.p and mixed m.p). Yield: (0.34 g, 68 %).

7-[(2-Hydroxynaphthalen-1-yl)diazenyl]-3,4,6-triphenyl-5*H*-pyrrolo[2`,3`:4,5]thieno[2,3-*c*]pyridazine, 6.

Compound **4** (0.5 g, 1.19 mmol) was dissolved in concentrated H_2SO_4 (5 mL), cooled to 0° - 5°C in an ice bath, then a solution of $NaNO_2$ (0.16 g, 2.39 mmol) in H_2O (5 mL) was added with stirring, keeping the temperature at 0° - 5°C. The above mixture was added drop by drop to a solution of 2-naphthol (0.17 g, 1.19 mmol) and sodium acetate (1.0 g) in ethanol (50 %, 10 mL) with stirring for 1.5 h. The precipitate was filtered off, washed with water, dried, and recrystallised from ethanol to give **6**. Yield: (0.36 g, 52.7 %); m.p. 104° - 105°C; IR: broad band around 3198 (–OH, –NH), 1599 (N=N), 1242 (C–O, phenolic); MS (*m/z* %): 573 (M^+, 0.17 %), 63 (M^+ - $C_{32}H_{22}N_4OS$, 100 %); Anal Calcd. For $C_{36}H_{23}N_5OS$: C, 75.37; H, 4.04; N, 12.21; Found: C, 75.75; H, 4.12; N, 12.50 %.

10-Amino-3,4-diphenyl-6,7,8,9-tetrahydropyridazino[4`,3`:4,5]-thieno[3,2- *b*]quinoline, 8.

To a solution of compound **1** (0.5 g, 1.52 mmol) in cyclohexanone (10 mL), anhydrous zinc chloride (0.04 g, 1.52 mmol) was added, and the reaction mixture was heated under reflux for 30 minute. Evaporate the solvent under reduced pressure, and dissolve the residue in NaOH (10 mL, 40 %), then extract with benzene. The benzene layer was dried over anhydrous $MgSO_4$, and evaporated to give **8**. Yield: (0.35 g, 57 %); m.p. 189° - 190 °C; IR: 3500, 3358 (–NH_2), 2929 (CH, aliphatic), 1657 (C=N); MS (*m/z* %): 408 (M^+, 3.78 %), 77 (M^+ - $C_{19}H_{15}N_4S$, 100 %); Anal Calcd. For $C_{25}H_{20}N_4S$: C, 73.50; H, 4.94; N, 13.72; Found: C, 73.82; H, 4.85; N, 13.45 %.

***N*-(6-Cyano-3,4-diphenylthieno[2,3-*c*]pyridazin-5-yl)-*N*`-phenylthiourea, 9.**

Method A

To a solution of compound **1** (0.5 g, 1.52 mmol) in dimethylformamide (10 mL), phenyl isothiocyanate (0.21 g, 1.52 mmol) and triethylamine (0.5 mL) were added, the reaction mixture was stirred at room temperature for 18 h. The reaction mixture was poured into water, then the solid product was filtered off, washed with water, dried, and recrystallised from ethanol to give **9**. Yield: (0.51 g, 73 %); m.p. 218° - 219 °C; IR: 3451, 3333 (two –NH), 2243 (C≡N), 1240 (C=S); MS (*m/z* %): 463 (M^+, 0.02 %), 329 (M^+ - C_7H_6NS, 100 %); ^{1}H-NMR (DMSO-d_6): 8.09 (s, 1H, NH), 7.90 (s, 1H,–NHPh), 7.17-7.39 (m, 15H, 3Ph); Anal Calcd. For $C_{26}H_{17}N_5S_2$: C, 67.36; H, 3.70; N, 15.11; Found: C, 67.01; H, 3.62; N, 15.40 %.

Method B

To a solution of compound **1** (0.5 g, 1.52 mmol) in pyridine (10 mL), phenyl isothio-cyanate (0.21 g, 1.52 mmol) was added. The reaction mixture was heated under reflux for 6 h. After cooling, the reaction mixture was poured into ice water, then the solid product was filtered off, dried, and recrystallised from ethanol to give **9**, which identical with that prepared by method A (m.p and mixed m.p). Yield: (0.5 g, 71 %).

7-Amino-6-anilino-8-imino-3,4-diphenylpyrimido[4`,5`:4,5]thieno[2,3-*c*]pyridazine, 10.

To a solution of compound **9** (0.5 g, 1.08 mmol) in ethanol (10 mL), hydrazine hydrate (98 %, 1.08 mmol) was added. The reaction mixture was refluxed for 3 h. The solvent was evaporated under reduced pressure, and the residue was treated with water. The solid product was filtered off, dried, and recrystallised from ethanol to give **10**. Yield: (0.36 g, 72.5 %); m.p. 190° - 191 °C; IR: broad bands around 3318, 3185 (–NH_2, =NH, –NH), 1664 (C=N); MS (*m/z* %): 463 (M^+ +2, 0.27 %), 371 (M^+ - C_6H_6N, 100 %); Anal Calcd. For $C_{26}H_{19}N_7S$: C, 67.66; H, 4.15; N, 21.24; Found: C, 67.31; H, 4.22; N, 21.51 %.

7-Acetylamino-6-anilino-8-imino-3,4- diphenylpyrimido-[4`,5`:4,5]thieno[2,3-*c*]-pyridazine, 11.

A solution of compound **10** (0.5 g, 1.08 mmol) in acetic anhydride (10 mL) was refluxed for 5 h. The solvent was evaporated under reduced pressure, and the solid product was recrystallised from acetic acid to give **11**. Yield: (0.45 g, 83 %); m.p. 204° - 205 °C; IR : broad band around 3444 (=NH, –NH, –NH amide), 2919 (–CH_3), 1734 (C=O amide), 1668 (C=N); MS (*m/z* %): 503 (M^+, 0.29 %), 63 (M^+ - $C_{24}H_{20}N_6OS$, 100%); Anal Calcd. For $C_{28}H_{21}N_7OS$: C, 66.78; H, 4.20; N, 19.47; Found: C, 67.15; H, 4.11; N, 19.76 %.

5-Amino-3,4-diphenylthieno[2,3-*c*]pyridazine-6-carboxamid-oxime, 12.

To a solution of compound **1** (0.5 g, 1.52 mmol) in methanol (10 mL), hydroxylamine hydrochloride (0.11 g, 1.52 mmol) and ammonium hydroxide (0.5 mL) were added. The reaction mixture was stirred at room temperature for 24 h. The solid product was filtered off, dried, and recrystallised from ethanol to give **12**. Yield: (0.29 g, 54 %); m.p. 212° - 213°C; IR: 3459 (–OH), 3380, 3292, 3229, 3158 (two –NH_2), 1661 (C=N); MS (*m/z* %): 362 (M^+ +1, 12.2 %), 51 (M^+ - $C_{15}H_{12}N_5OS$, 100 %); ^{1}H-NMR (DMSO-

d_6) : 9.27 (s, 1H, OH), 7.14-7.39 (m, 10H, 2Ph), 5.74 (s, 2H, 6-NH_2), 4.09 (s, 2H, 5-NH_2); Anal Calcd. For $C_{19}H_{15}N_5OS$: C, 63.14; H, 4.18; N, 19.38; Found: C, 63.52; H, 4.24; N, 19.09 %.

3-Amino-7,8-diphenyl-1*H*-pyrazolo[3`,4`:4,5]thieno[2,3-*c*]pyridazine hydrochloride, **13.**

To a solution of compound **1** (0.5 g, 1.52 mmol) in pyridine (10 mL), hydroxylamine hydrochloride (0.11 g, 1.52 mmol) was added. The reaction mixture was heated under reflux for 5 h. The solvent was evaporated under reduced pressure, and the residue was treated with water. The solid product was filtered off, dried, and recrystallised from ethanol to give **13**. Yield: (0.41 g, 71 %); m.p. > 300 °C; IR: 3296, 3155 (–NH_2, –NH), 1673 (C=N); MS (*m/z* %): 380 (M^+, 0.03 %), 382 (M^+ +2, 0.10 %), 304 (M^+ - CH_3ClN_2, 100 %); Anal Calcd. For $C_{19}H_{14}ClN_5S$: C, 60.07; H, 3.71; N, 18.44; Found: C, 60.40; H, 3.79; N, 18.19 %.

3-[(2-Hydroxynaphthalen-1-yl)diazenyl]-7,8-diphenyl-1*H*-pyrazolo[3`,4`:4,5]thieno-[2,3-*c*]pyridazine, **15.**

Method A

Compound **13** (0.5 g, 1.32 mmol) was dissolved in concentrated H_2SO_4 (5 mL), cooled to 0° - 5°C in an ice bath, then a solution of $NaNO_2$ (0.18 g, 2.63 mmol) in H_2O (5 mL) was added with stirring, keeping the temperature at 0° - 5°C. The above mixture was added drop by drop to a solution of 2-naphthol (0.19 g, 1.32 mmol) and sodium acetate (1.0 g) in ethanol (50 %, 10 mL) with stirring for 1.5 h. The precipitate was filtered off, washed with water, dried, and recrystallised from ethanol to give **15**. Yield: (0.49 g, 76 %); m.p. 201° - 202 °C; IR: broad band around 3181(–OH, –NH), 1670 (C=N), 1623 (N=N), 1243 (C–O, phenolic); MS (*m/z* %): 499 (M^+ +1, 1.03 %), 77 (M^+ - $C_{23}H_{13}N_6OS$, 100 %); Anal Calcd. For $C_{29}H_{18}N_6OS$: C, 69.86; H, 3.64; N, 16.86; Found: C, 69.55; H, 3.69; N, 16.58 %.

Method B

Compound **18** (0.5 g, 1.45 mmol) was dissolved in concentrated H_2SO_4 (5 mL), cooled to 0° - 5°C in an ice bath, then a solution of $NaNO_2$ (0.2 g, 2.91 mmol) in H_2O (5 mL) was added with stirring, keeping the temperature at 0° - 5°C. The above mixture was added drop by drop to a solution of 2-naphthol (0.21 g, 1.45 mmol) and sodium acetate (1.0 g) in ethanol (50 %, 10 mL) with stirring for 1.5 h. The precipitate was filtered off, washed with water, dried, and recrystallised from ethanol to give **15**, which identical to the compound prepared by method A (m.p and mixed m.p). Yield (0.51 g, 70.5 %).

3,4-Diphenylnaphtho[2,1- *e*]pyridazino[4``,3``:4`,5`]thieno[2`,3`:4,5]pyrazolo[3,2-*c*][1,2,4]triazine, 16.

A solution of compound **15** (0.5 g, 1.0 mmol) in glacial acetic acid (10 mL) was heated under reflux for 3 h. The solvent was then evaporated under reduced pressure, and the solid product was recrystallised from ethanol to give **16**. Yield: (0.2 g, 41.5 %); m.p. 211° - 212°C; IR: 1644 (C=N), 1558 (N=N), and there is no bands in the –OH and –NH regions; MS (*m/z* %): 480 (M^+, 0.35 %), 371 (M^+ - C_6H_5, - N_2, -2 H_2, 100 %); Anal Calcd. For $C_{29}H_{16}N_6S$: C, 72.48; H, 3.36; N, 17.49; Found: C, 72.80; H, 3.45; N, 17.76 %.

5-Amino-3,4-diphenylthieno[2,3-*c*]pyridazine-6-carboximidohydrazide, 17.

To a solution of compound **1** (0.5 g, 1.52 mmol) in ethanol (10 mL), hydrazine hydrate (98 %, 1.52 mmol) was added, and the reaction mixture was heated under reflux for 2 h. The solvent was then evaporated under reduced pressure, and the residue was treated with water. The solid product was filtered off, dried, and recrystallised from ethanol to give **17**. Yield: (0.38 g, 69 %); m.p. 179° - 180 °C; IR: broad bands around 3350, 3158 (two –NH_2, =NH, –NH), 1670 (C=N); MS (*m/z* %): 360 (M^+, 10.36 %), 287 (M^+ - NH_2, - CH_4N_3, 100 %); ^{1}H-NMR (DMSO-*d_6*): 8.16 (s, 1H, –NH), 8.05 (s, 2H, –NH_2), 7.05-7.83 (m, 10H, 2Ph), 5.38 (s, 1H, =NH), 4.16 (s, 2H, 5-NH_2); Anal Calcd. For $C_{19}H_{16}N_6S$: C, 63.31; H, 4.48; N, 23.32; Found: C, 63.01; H, 4.55; N, 23.05 %.

3-Amino-7,8-diphenyl-1*H*-pyrazolo[3`,4`:4,5]thieno[2,3-*c*]pyridazine, **18.**

Method A

To a solution of compound **1** (0.5 g, 1.52 mmol) in absolute ethanol (10 mL), hydrazine hydrate (98 %, 1.52 mmol) was added, and the reaction mixture was heated under reflux for 6 h. The solvent was then evaporated under reduced pressure, and the residue was treated with water. The solid product was filtered off, dried, and recrystallised from ethanol to give **18**. Yield: (0.37 g, 70 %); m.p. 250° - 251°C; IR: 3356, 3295, 3206 (–NH_2, –NH), 1658 (C=N); MS (*m/z* %): 343 (M^+, 22.6 %), 51 (M^+ - $C_{15}H_{10}N_5S$, 100 %); Anal Calcd. For $C_{19}H_{13}N_5S$: C, 66.45; H, 3.81; N, 20.40; Found: C, 66.80; H, 3.75; N, 20.65 %.

Method B

A solution of compound **17** (0.5 g, 1.39 mmol) in absolute ethanol (10 mL) was heated under reflux for 5 h. The solvent was concentrated, and the solid product was filtered off, and dried to give **18**. It was identical with that prepared by method A (m.p and mixed m.p). Yield: (0.36 g, 75.2 %).

3-Acetylamino-7,8-diphenyl-1*H*-pyrazolo[3`,4`:4,5]thieno-[2,3-*c*]pyridazine, 19.

A solution of compound **18** (0.5 g, 1.45 mmol) in acetic anhydride (10 mL) was refluxed for 5 h. The solvent was then evaporated under reduced pressure, and the solid product was recrystallised from acetic acid to give **19**. Yield: (0.46 g, 82 %); m.p. 170° - 171 °C; IR: 3413, 3168 (–NH pyrazolo, –NH amide), 2923 (–CH_3), 1749 (C=O amide), 1675 (C=N); MS (*m/z* %): 385 (M^+, 100 %); ^{1}H-NMR (DMSO-*d_6*): 11.94 (s, 1H, NH-pyrazolo), 9.71 (s, 1H, –NHCO), 7.24-7.47 (m, 10H, 2Ph), 2.02 (s, 3H, CH_3); Anal Calcd. For $C_{21}H_{15}N_5OS$: C, 65.44; H, 3.92; N, 18.17; Found: C, 65.10; H, 3.85; N, 17.90 %.

General Procedure for the synthesis of 5-[(hydroxynaphthalen-1-yl)diazenyl]-3,4-diphenylthieno[2,3-*c*]pyridazine-6-carboxamide, $20_{a,b}$.

Compound **1** (0.5 g, 1.52 mmol) was dissolved in acetic acid (90 %, 5 mL), cooled to 0° - 5°C in an ice bath, then a solution of $NaNO_2$ (0.21 g, 3.04 mmol) in concentrated sulphuric acid (5 mL) was added with stirring, keeping the temperature at 0° - 5°C. The above mixture was added drop by drop to a solution of 1- and/or 2-naphthol (0.22 g, 1.52 mmol) and sodium acetate (1.0 g) in ethanol (50 %, 20 mL) with stirring for 1.5 h. The precipitate was filtered off, washed with water, dried, and recrystallised from ethanol to give $\mathbf{20_{a,b}}$.

5-[(4-Hydroxynaphthalen-1-yl)diazenyl]-3,4-diphenylthieno-[2,3-*c*]pyridazine-6-carboxamide, 20_a.

Yield: (0.46 g, 61 %); m.p. 249°- 250 °C; IR: 3390 (–OH), 3300, 3168 (–NH_2, amide), 1674 (C=O, amide), 1594 (N=N), 1201 (C–O, phenolic), there is no absorption bands referred to C≡N group; MS (*m/z* %): 504 (M^+ +3, 0.09 %), 78 (M^+ - $C_{23}H_{13}N_5O_2S$, 100 %); Anal Calcd. For $C_{29}H_{19}N_5O_2S$: C, 69.44; H, 3.82; N, 13.96; Found: C, 69.75; H, 3.89; N, 13.68 %.

5-[(2-Hydroxynaphthalen-1-yl)diazenyl]-3,4-diphenylthieno-[2,3-*c*]pyridazine-6-carboxamide, 20_b.

Yield: (0.49 g, 64 %); m.p. > 300 °C; IR: 3381 (–OH), 3307, 3168 (–NH_2, amide), 1682 (C=O, amide), 1604 (N=N), 1245 (C–O, phenolic), there is no absorption bands referred to C≡N group; MS (*m/z* %): 499 (M^+ -2, 0.26 %), 394 (M^+ - C_7H_5N, - H_2, 100 %); Anal Calcd. For $C_{29}H_{19}N_5O_2S$: C, 69.44; H, 3.82; N, 13.96; Found: C, 69.78; H, 3.91; N, 14.22 %.

REFERENCES

[1]Rohet, F., Rubat, C., Coudert, P. and Couquelet, J., *Bioorg. Med. Chem.*, **1997**, *5*, 655.

[2]Tucker, J. A., Allwine, D. A., Grega, K. C., Barbachyn, M. R., Klock. J. L., Adamski, J. L., Brickner, S. J., Hutchinson, D. K., Ford, C. W., Zurenko, G. E., Conradi, R. A., Burton, P. S., and Jensen, R. M.; *J. Med. Chem.*, **1998,** *41*, 3727.

[3]Tamayo, N., Liao, L., Goldberg, M., Powers, D., Tudor, Y. Y., Yu, V., Wong, L. M., Henkle, B., Middleton, S., Syed, R., Harvey, T., Jang, G., Hungate, R., and Dominguez, C.; *Bioorg. Med. Chem.*, **2005**, *15*, 2409.

[4]Benson, S. C., Palabrica, C. A. and Snyder, J. K.; *J. Org. Chem.*, **1987,** 52, 4610.

[5]Gyoten, M., Nagaya, H., Fukuda, S., Ashida, Y. and Kawano, Y.; *Chem. Pharm. Bull.*, **2003**, *51*, 122.

[6]Piaz, V. D., Vergelli, C., Giovannoni, M. P., Scheideler, A. M. A., Petrone, G. and Zaratin, P.; *ll Farmaco*, **2003**, *58*, 1063.

[7]Crespo, A., Meyers, C., Coelho, A., Sotelo, E., Fraiz, N., Sotelo, E., Yanez, M., Maes, B. U. W., Laguna, R., Cano, E., Lemiere, G. L. F. and Ravina, E., *Bioorg. Med. Chem. Lett.*, **2006**, *16*, 1080.

[8]Kamal El-Dean, A. M., Gaber, A. M., El-Gaby, M. S. A., Eyada, H. A. and Al-Kamali, A. S. N., *Phosphorus, Sulfur and Silicon*, **2004**, *179*, 321.

[9]Yamaguchi, M., Maruyama, N., Koga, T., Kamei, K., Akima, M., Kuroki, T., Hamana, M. and Ohi, N., *Chem. Pharm. Bull.*, **1995**, *43 (2),* 236.

[10]Vartanyan, R. S., Kazaryan, Z., Sheiranyan, M. A., Agaronyan, A. S. and Stepanyan, N. O., *Khim. Farm. Zh.*,**1996**, *30*, 29.

[11]Vieweg, H., Leistner, S., Wagner, G., Boehm, N., Krasset, U., Grupe, R., Lohmann, D. and Loban, G., *German Patent*, **1988**, D257, 830. Chem. Abst., **1989**, *110*, 995262p.

[12]Deeb, A., Said, S. A., Hamed, M. M. and Yasin, F., *J. Chin. Chem. Soc.*, **1990**, *37*, 287.

[13]Quintela, J. M., Veiga, M. C., Conde, S. and Peinador, C., *Monatsh. Chem.*, **1996**, *127*, 739.

[14]Moore, J. A. and Kornreich, L. D., *Tetrahedron Lett.*, **1963**, *4 (20)*, 1277.

[15]Deeb, A., Essawy, A., Yassine, F., Fikry, R., *Z., Naturforsch.* **1991**, *46b*, 845-847.

[16]Bauer, A. W., Mkriby, W. W., Sherris, J. C. and Turck, M.; *Am. J. Clin. Pathol*., **1966,** *45*, 493.

Received: 20.07.2014.
Accepted: 26.08.2014.

NOVEL TECHNOLOGIES FOR ENHANCED PRODUCTION OF ETHANOL: IMPACT OF HIGH PRODUCTIVITY ON PROCESS ECONOMICS

M. M. Azam,[a], T. C. Ezeji[b] and N. Qureshi[c]*

Keywords: Ethanol; calcium carbonate and calcium chloride additives; productivity; ethanol yield; cell recycle, process economics

In these studies *Saccharomyces cerevisiae* NRRL Y-566 was used to produce ethanol from a concentrated glucose (250-300 g L^{-1}) solution. When fermentation media were supplemented with $CaCO_3$ and $CaCl_2$, ethanol concentrations, yield, and productivities were improved significantly. In control batch fermentation, the culture was able to produce 20.87 g L^{-1} ethanol with a productivity of 0.25 g L^{-1} h^{-1} when using 100 g L^{-1} sugar solution in feed. When supplemented with a solution of 0.40 g L^{-1} $CaCl_2$, ethanol concentration, yield, and productivity were improved to 90.0 g L^{-1}, 0.48, and 1.25 g L^{-1} h^{-1} (500 % increase), respectively. The effect of $CaCO_3$ supplementation was not as pronounced as that of $CaCl_2$. Using these parameters, the process economics for production of ethanol was performed and it was projected that supplementation with 0.40 gL^{-1} $CaCl_2$ would result in the production of ethanol for \$0.91 kg^{-1}. It was also projected that improving productivity to 37.5 g L^{-1} h^{-1} using cell recycle and supplementation with $CaCl_2$ would result in the production of ethanol for \$0.70 kg^{-1} employing *S. cerevisiae* NRRL Y-566. Using *Z. mobilis* in membrane cell recycle reactors and application of $CaCl_2$ can result in achieving high productivities (500-600 g L^{-1} h^{-1}) and reduction in ethanol production price to \$0.59 kg^{-1}.

***Corresponding Author: Nasib Qureshi
Tel: +1 (309) 681-6318
Fax: +1 (309) 681-6427
E-Mail: Nasib.Qureshi@ars.usda.gov
[a] Plant Breeding Division, Crop Improvement Section, Directorate of RiceResearch (DRR), Rajendra Nagar, Hyderabad, AP 500 030, INDIA
[b] The Ohio State University (OSU), Department of Animal Sciences and Ohio State Agricultural Research and Development Center (OARDC), 305 Gerlaugh Hall, 1680 Madison Avenue, Wooster, OH 44691, USA
[c] United States Department of Agriculture (USDA)**, Agricultural Research Service (ARS), National Center for Agricultural Utilization Research (NCAUR), Bioenergy Research Unit, 1815 N University Street, Peoria, IL 61604, USA

Introduction

Depletion of fossil fuel reserves, increased fuel demand due to world's population increase, and uncertainty in its availability have rekindled an interest in alternative biofuels that are renewable and sustainable in nature. Ethanol/or ethyl alcohol fermentation offers promising alternative as it can be produced from various renewable resources such as corn, molasses and agricultural residues and significant research on the production of ethanol from these resources has occurred over the last 3-4 decades.[1-6] However, the basic hurdle to the economical production of ethanol is its high cost of production. The major factors that affect the cost of ethanol production include:

- low reactor productivity,

- requirement of high energy for distillative recovery due to low product concentration in the broth, and often,

- low product yield.

All these factors can be addressed through the application of cutting edge science and technology as outlined below. Additionally, development of superior microbial cultures would be beneficial for this fermentation, however, this is beyond the scope of this article.

Improvement in the reactor productivity can be achieved by the application of suitable reactor designs such as high productivity biofilm reactors or cell recycle membrane reactors, effective nutrient management for efficient cell growth and fermentation, productivity or product enhancers, and process optimization .[3,4,6-12] It has also been shown that several compounds like unsaturated fatty acids and sterols, proteins, amino acids, vitamins, and metal ions can lead to improvements in alcohol fermentation productivity.[13-14] Reduction in energy requirement for distillative recovery can be reduced by increasing product concentration in the fermentation broth as this would reduce size of the distillation column and hence lower process and capital costs. Product yield can also be increased by reducing cell growth by recycling carbon to fermentation product. Some success has been achieved in the development of superior cultures that can improve both yield and product concentration in particular when using lignocellulosic sugars.[15]

Among various ethanol producing micro-organisms *Saccharomyces cerevisiae* has been used most commonly.[16] Objectives of the present studies were to improve and quantify reactor productivity, ethanol yield, and product concentration using *Saccharomyces cerevisiae* NRRL Y-566 on medium supplementation with product enhancers such as $CaCO_3$ and $CaCl_2$. Furthermore, process economics of the developed processes using *S. cerevisiae* NRRL Y-566 and *Zymomonas mobilis* were compared.

Materials and Methods

Organism and maintenance

Lyophilized *Saccharomyces cerevisiae* (NRRL Y-566) was obtained from the culture collection of National Center for Agricultural Utilization Research [formerly Northern Regional Research Laboratory (NRRL), United States Department of Agriculture], Agricultural Research Service, Peoria, IL. For rehydration, sterile water (0.3 mL) was added to the lyophilized yeast and entire content was transferred to a test tube containing 5 mL water and allowed to hydrate overnight. The culture was maintained on YEPD (yeast extract, peptone, and dextrose) medium consisting yeast extract 10 g L^{-1}; peptone, 20 g L^{-1}; glucose, 20 g L^{-1}; and agar, 15 g L^{-1}. The pH of the medium was adjusted to 5.0. Before inoculation, the medium was sterilized in an autoclave for 15 min at 121 ^oC followed by cooling to 25 ^oC.

Preparation of inoculum and medium

The liquid inoculum development medium contained: yeast extract, 10.0 gL^{-1}; magnesium chloride, 1.00 gL^{-1}; ammonium sulfate, 1.00 gL^{-1}; potassium dihydrogen phosphate, 1.00 gL^{-1}; glucose, 50.00 gL^{-1}; $MnSO_4.7H_2O$, 0.01 gL^{-1}, and; $FeCl_3.2H_2O$, 0.01 gL^{-1}. The pH of the solution was adjusted with dilute sulphuric acid solution to pH 5.5 and then sterilized in an autoclave for 15 minutes at 121 ^oC. After the medium (100 mL contained in 250 mL screw capped glass bottle) was cooled to room temperature, a colony of *S. cerevisiae* NRRL Y-566 was transferred to it. Then the culture was kept for growth in an incubator at 30 ^oC at an agitation speed of 150 rpm.

Effect of glucose, $CaCO_3$, and $CaCl_2$ concentrations on the batch fermentation process

To evaluate the fermentation performance of the microbial culture and the effects of medium components, batch fermentations were performed in 250 mL Pyrex^{TM} screw capped bottles. The bottles containing 100 mL fermentation medium (glucose 100-300 gL^{-1}) were autoclaved at 121 ^oC followed by cooling to 30 ^oC. Autoclaved and cooled fermentation media were supplemented with different concentrations of calcium carbonate ($CaCO_3$; 0.0, 0.5, 1.0, 2.0, and 3.0 g L^{-1}; in 250 g L^{-1} glucose solution) and calcium chloride ($CaCl_2$; 0.0, 0.2, 0.4, 0.8, and 1.2 g L^{-1}; in 250 g L^{-1} glucose solution) solutions separately ($CaCO_3$ was autoclaved separately and $CaCl_2$ solutions were sterilized by filtration through 0.22 µm filter) and then inoculated with 24 h old 6 % (v/v) pre-culture/inoculum developed above. All fermentations were conducted in triplicate at 30 ^oC and the agitation was maintained at 150 rpm. Two mL samples were taken at regular intervals to measure glucose and ethanol concentrations.

Material balance, energy balance and economic analysis

To estimate ethanol prices, SuperPro Designer Software (version 9.0, built 8, special built 2012, Intelligen, Inc., Scotch Plains, NJ, USA) was used for material balance, energy balance and economic analysis. The equipment and chemical prices reported are for 2014 (SuperPro Designer). The ethanol prices reported are factory gate selling prices (FGSP) and do not include transportation costs. Various parameters that were used to estimate ethanol prices are presented in **Table 1**. The plant capacity was assumed to be 100,000 metric tons of ethanol production per year. In this fermentation there were two by-products (CO_2 and cell mass) and both were sold for credit. The plant was a grass rooted/green field plant with annual operation for 350 days per year. The capital would be borrowed at 7.0 % interest rate until it is paid off.

Analytical procedures

Ethanol concentration was measured using 7890A Agilent Technologies gas chromatograph (Agilent Technologies Inc., Palo Alto, CA, USA) equipped with a flame ionization detector (FID) and 30 m (length) x 320 µm (internal diameter) x 0.5 µm (HP-Innowax film) J x W 19091 N-213 capillary column. The operating conditions were: column temperature 150 ^oC (isothermal); program run time: 5.5 min; ethanol retention time: 2.3 min; carrier gas: nitrogen; injector temperature: 175 ^oC; detector temperature: 250 ^oC; N_2 flow rate: 40 $mL{\cdot}min^{-1}$; H_2 flow rate: 60 $mL{\cdot}min^{-1}$; sample quantity: 1 µL with split ratio of 10:1. The supernatant was filtered through 0.22 µm cellulose acetate filter for GC analysis.

Sugar concentrations in samples were analyzed using an Agilent 1100 HPLC system (Agilent Technologies Inc., Palo Alto, CA, USA) equipped with a refractive index detector at 45 ^oC. Separation was achieved using a ICSep COREGEL-87H3 column (Transgenomic Inc., Omaha, NE, USA) maintained at 65 ^oC with 4 mM H_2SO_4 as the eluent at a flow rate of 0.8 $mL{\cdot}min^{-1}$. Each fermentation sample was filtered through a 0.22 µm filter and diluted appropriately using deionized water.

Ethanol productivity was calculated as maximum ethanol concentration (g L^{-1}) during fermentation divided by fermentation time (h) and is expressed as g L^{-1} h^{-1}. Fermentation time was considered as time period between inoculation and time at which maximum ethanol concentration was produced. Ethanol yield was estimated as the amount of ethanol produced (g L^{-1}) divided by the amount of glucose utilized (g L^{-1}).

Results and Discussion

Effect of $CaCO_3$ and $CaCl_2$ on fermentation

Batch fermentation experiments were conducted with various initial glucose levels with an aim to obtain high ethanol concentration in the broth. The initial glucose concentrations in the batch experiments were 100, 150, 200, 250, and 300 gL^{-1}. The results of this experiment are presented in **Fig. 1A**. The figure indicates that the ethanol concentrations increased with increase in initial glucose concentrations and fermentation completed in 72 to 84 h. Maximum ethanol production of 34.3 gL^{-1} was obtained when glucose concentration was 250 gL^{-1}. However, when a higher concentration of glucose (300 gL^{-1}) was used, ethanol concentration decreased to 27.4 gL^{-1}.

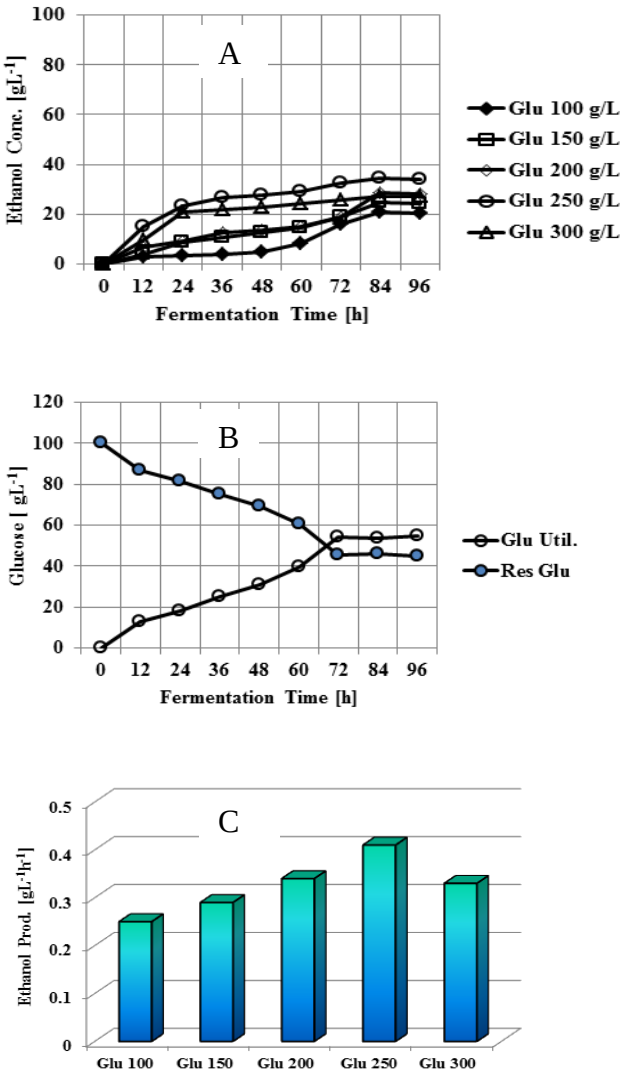

Figure 1. Production of ethanol from glucose using *S. cerevisiae* Y-566 in batch process. A: Ethanol concentration at various time periods and at different glucose concentrations; B: Glucose utilization and residual glucose at 100 gL^{-1} initial glucose; C: Ethanol productivity at different initial glucose levels.

In these fermentations ethanol yield of 0.39 ± 0.03 was obtained. Sugar utilization was also incomplete. In fermentation experiment with 100 gL^{-1} initial glucose, about 55.0 gL^{-1} glucose was utilized leaving behind 45.0 gL^{-1} as residual sugar. The concentrations of utilized and residual glucose are shown in **Fig. 1B**.

In these five experiments run at various sugar concentrations (100-250 gL^{-1} glucose), ethanol productivities ranged from 0.25 to 0.41 $gL^{-1}h^{-1}$ (**Fig. 1C**) which showed an upward ethanol production trend in relation to initial glucose concentration. Since, 250 gL^{-1} glucose was found to produce more ethanol with improved productivity, it was used for further studies. The concentration of ethanol in 100 gL^{-1} glucose fermentation should have been more than that in 250 gL^{-1} fermentation due to the fact that high sugar concentrations are inhibitory to the cell. It is plausible that the initial osmotic pressure exerted on *S. cerevisiae* NRRL Y-566 at high sugar concentration may have induced ethanol production.

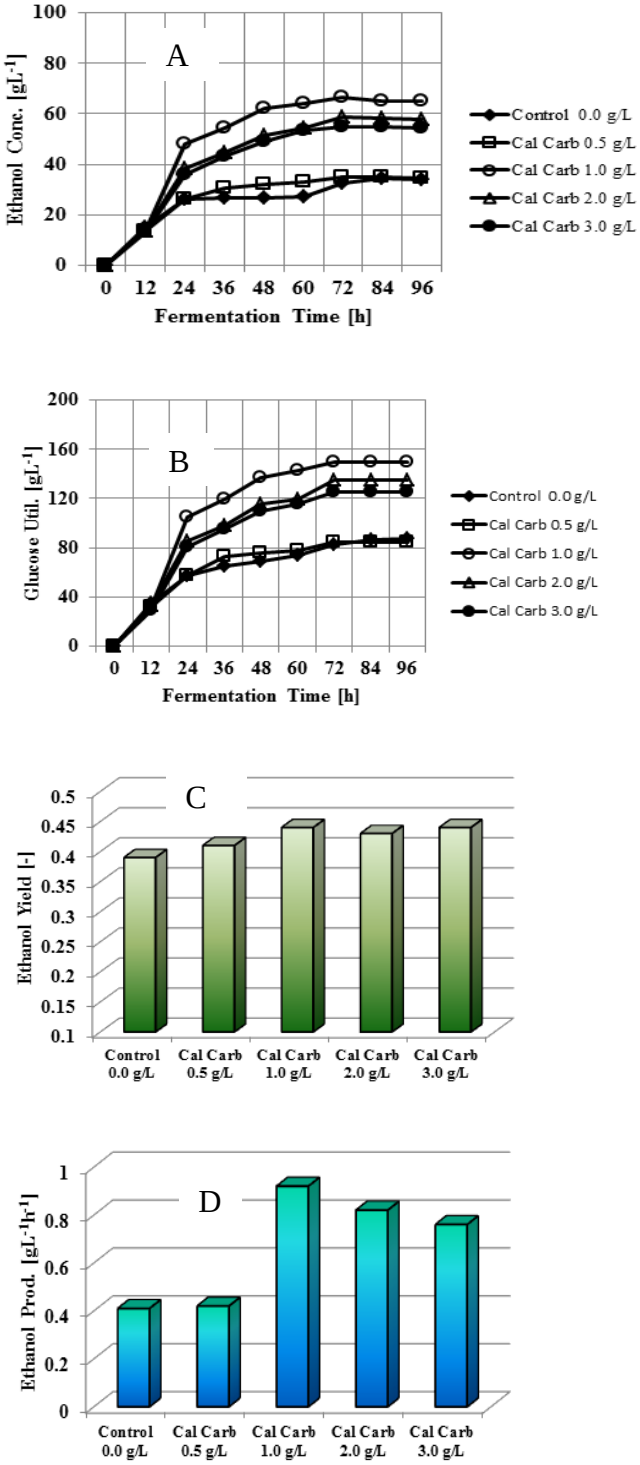

Figure 2. Effect of $CaCO_3$ on ethanol production and productivity from glucose (250 g L^{-1}) in batch process. A: Ethanol at various levels of $CaCO_3$; B: Glucose utilization; C: Ethanol Yield; and D: Ethanol productivity.

Subsequently, experiments were performed where 0.0 to 3.0 gL^{-1} $CaCO_3$ (**Fig. 2A**) was supplemented to the medium. Fermentation medium containing 0.0 g L^{-1} calcium carbonate was considered as the control. The results confirmed that supplementation with calcium carbonate improved ethanol production. At a $CaCO_3$ concentration of 1.0 g L^{-1}, 66.63 g L^{-1} ethanol was produced. This is an increase of 94.1 %.

 DOI: 10.17628/ecb.2014.3.904-910

Further increase in $CaCO_3$ concentration did not improve ethanol production. At $CaCO_3$ concentrations of 2.0 and 3.0 gL^{-1}, ethanol concentrations of 59.0 and 55.0 gL^{-1} were obtained, respectively. Utilization of glucose was the highest (150.0 gL^{-1}) at 1.0 gL^{-1} $CaCO_3$ concentration (**Fig. 2B**). As compared to the control experiment, ethanol yield improved slightly (**Fig. 2C**) to 0.44. It should be noted that productivity improved due to increased production of ethanol and faster fermentation. At a $CaCO_3$ concentration of 1.0 gL^{-1} fermentation was complete in approximately 72 h as opposed to 84 h for the control fermentation. In this run a productivity of 0.92 $gL^{-1}h^{-1}$ was obtained (**Fig. 2D**) which is 224% of that achieved in the control run.

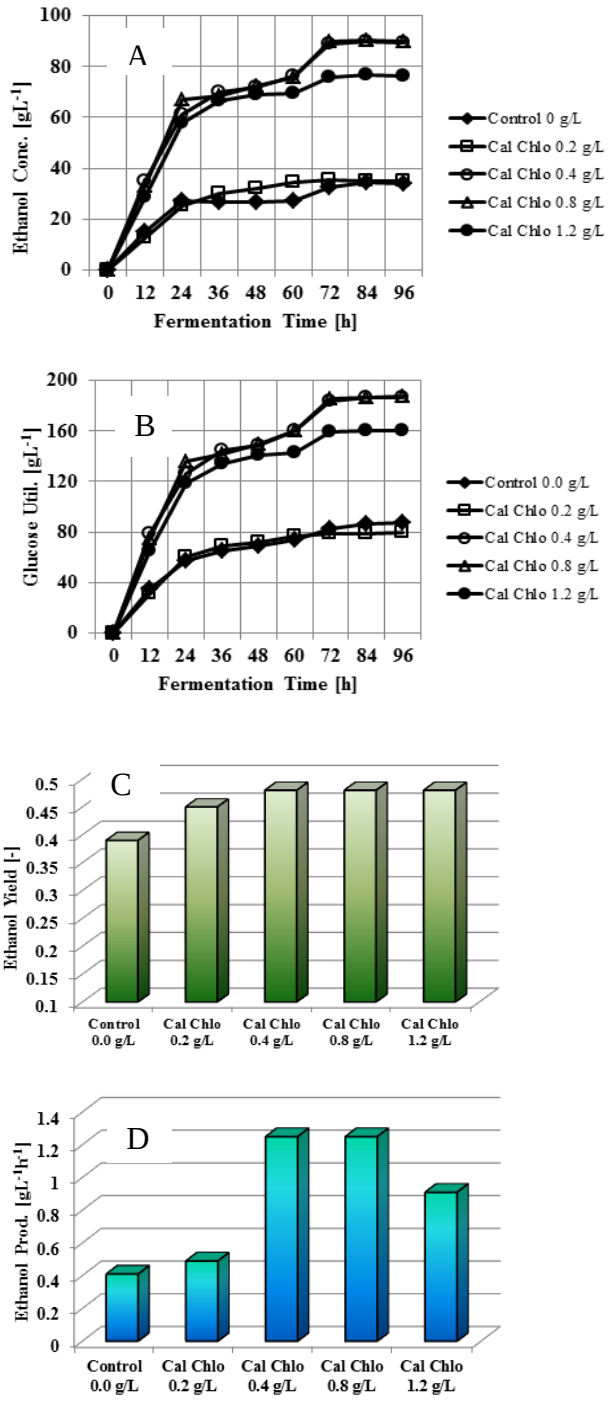

Figure 3. Effect of $CaCl_2$ on ethanol production and productivity from glucose (250 gL^{-1}) in batch process. A: Ethanol; B: Glucose utilization; C: Yield, and; D. Productivity.

Next, experiments with calcium chloride ($CaCl_2$) supplementation were performed where $CaCl_2$ ranging from 0.0 to 1.20 gL^{-1} was added to the medium. At $CaCl_2$ concentrations of 0.40 to 1.20 gL^{-1} fermentation improved dramatically. At a $CaCl_2$ concentration of 0.40 gL^{-1} maximum ethanol production (89.8 gL^{-1}) was achieved (**Fig. 3A**). This ethanol concentration is 262% of that achieved in the control experiment. Although, there was marked increase in ethanol production, the fermentation broth still contained residual sugars. Glucose consumption increased from 86.4 gL^{-1} to 186.5 gL^{-1} when 0.40 gL^{-1} calcium chloride was added to the medium. The utilization of sugars is shown in **Fig. 3B**. In these fermentations, ethanol yield also increased with a maximum of 0.48 at $CaCl_2$ concentrations ranging from 0.40-1.20 gL^{-1} (**Fig. 3C**). The highest ethanol productivity of 1.25 $gL^{-1}h^{-1}$ was achieved at a $CaCl_2$ concentration of 0.40 gL^{-1} (**Fig. 3D**).

An early study on effect of $CaCl_2$ on ethanol fermentation was performed by Bajpai and Margaritis using a bacterial strain of *Zymomonas mobilis*.[17] In these studies they indicated that there was no appreciable change in rates of cell mass production and ethanol formation in the medium containing up to 2.0 gL^{-1} $CaCl_2$. Further increases in $CaCl_2$ concentrations, resulted in decreased cell growth and ethanol production rates. These studies were followed by Sreekumar and Basappa [18] who demonstrated that supplementation of $CaCl_2$ and $CaCO_3$ to the fermentation medium enhanced ethanol production. The only difference between studies performed by these two groups was that Bajpai and Margaritis[17] used 100 gL^{-1} glucose solution while Sreekumar and Basappa[18] used 200-400 gL^{-1} glucose in their medium. Hence, it was concluded that calcium salts enhance ethanol concentration and yield in presence of high sugar concentration. It should be noted that there was no mention of increase in ethanol productivity and the microorganism used was a bacterium and not yeast.

Similar studies were performed by Nabais et al. for the production of ethanol using yeasts.[19] The cultures that were used included *S. bayanus* IST 154, *S. cerevisiae* IGC 3507 III and *Kluyveromyces marxianus*. It was observed that supplementation of fermentation medium with $CaCl_2$ resulted in the rapid production of higher concentrations of ethanol from high glucose concentration (320 gL^{-1}). It was also reported that calcium in optimal concentrations somehow protects the culture from toxic effects of ethanol, [19-20] and hence, results in the accumulation of higher concentration of ethanol in the broth which is economically beneficial for the product recovery. Similar studies were also performed for a commercial substrate (corn semolina) with similar observations.[21] In these studies it was reported that mineral salts take part in yeast metabolism as the activators of enzymes or are part of the enzyme in their active center. However, none of these authors investigated the effect of calcium carbonate on *S. cerevisiae* fermentation and on ethanol productivity.

Although supplementation of concentrated glucose medium with calcium salts results in enhanced production of ethanol, from process engineering point of view, use of concentrated sugar solution is preferred [4, 8, 22, 23] as it would reduce capital and process operational costs thus benefitting the economics of the process. Additionally, application of concentrated sugar solution would result in more concentrated product[9] in the broth which would further

reduce energy requirement for product separation by distillation. In these studies we were able to use 250 gL^{-1} sugar solution and accumulated approximately 90.0 gL^{-1} ethanol. In our process, use of calcium salts in combination with concentrated sugar solution resulted not only in enhanced ethanol concentration, they also enhanced yield, and productivity. The productivity was improved by 500% which would dramatically impact the economics of the process that is presented below.

Process Economics

Based on the data generated above, process economics of ethanol production was evaluated. For this purpose a plant with annual capacity of 100,000 tons of ethanol per year was considered with 350 working days per year. The process economic details of the plant are presented in **Table 1** while a process flow diagram is shown in **Fig. 4**.

Table 1. Parameters that were used to evaluate the process economics of ethanol production.

Plant Capacity:	100,000 metric tons ethanol $year^{-1}$
Ethanol yield:	0.48
Glucose price:	\$0.20 kg^{-}
Plant operation:	350 days·$year^{-1}$; continuous process
Plant life:	15 years
Glucose conc. in feed:	186 g·L^{-1}
Ethanol conc in effluent:	89-90 g·L^{-1}
Plant:	Grass rooted or green field
Plant & capital details:	Depreciation 10 % straight line, depreciation period 10 years, tax 40 % on profit
Product recovery:	Distillation
Year of analysis:	2014, construction period 30 months, construction start 2014 & start up period 4 months

The total direct fixed capital (TDFC), working capital (WC), and start costs (SC) were projected to be \$192.5 x 10^6, \$4.7 x 10^6, and \$9.6 x 10^6, respectively (**Table 2**). Ethanol, cell mass, and carbon dioxide were considered as revenue streams with cell mass and CO_2 selling prices of \$0.05 kg^{-1} each. Using these parameters ethanol production cost was projected to be \$0.91 kg^{-1} (\$2.83.US gal^{-1}). The operating cost of the plant was projected to be \$91.32 x 10^6. $year^{-1}$. For these calculations ethanol productivity of 1.25 $gL^{-1}h^{-1}$ was considered as obtained in the above studies using $CaCl_2$ as productivity enhancer.

In numerous publications, it has been presented that the productivity of ethanol, and acetone-butanol-ethanol (ABE) can be increased by a factor of 30-45 by application of cell recycle technology.[7, 24-26] The reason behind this productivity increase is the high cell concentration that can be achieved in the cell recycle bioreactor.

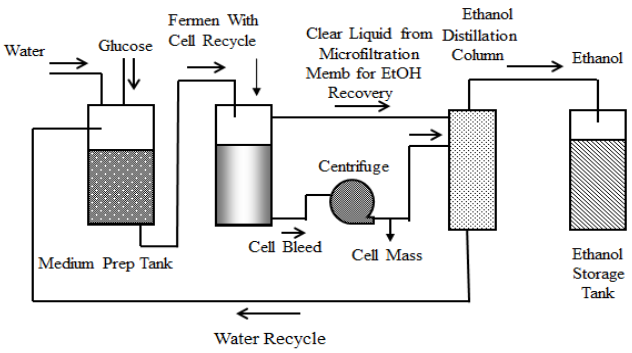

Figure 4. A schematic diagram of ethanol production from glucose by *S. cerevisiae* Y-566 or *Z. mobilis* in cell recycle continuous process employing $CaCl_2$ to enhance ethanol productivity.

In these cell recycle bioreactors cell concentration in excess of 80-100 g·L^{-1} can be achieved as compared to cell concentration in free cell batch reactors which is usually of the order of 3-5 g L^{-1}. Considering this increase in productivity, we assumed that the productivity can be increased by a factor of at least 30. Use of 0.40 g L^{-1} $CaCl_2$ resulted in an increase in productivity by a factor of 5. A combination of application of $CaCl_2$ and cell recycle technology is expected to result in a productivity of 37.5 g L^{-1} h^{-1} (1.25 x 30). Using this productivity we calculated price of ethanol production to be \$0.70·kg^{-1} (\$2.18·US gal^{-1}). The various economic details for this process are presented in **Table 2**.

The productivity of ethanol production by *Z. mobilis* in batch reactors is reported to be 4-6 g·L^{-1} h^{-1} [25, 27] which was improved to 120 g·L^{-1} h^{-1}. Further improvement in this productivity by application of $CaCl_2$ is possible. If use of $CaCl_2$ can increase this productivity by a factor of 5, the cell recycle experiment would result in a productivity of 600 g·L^{-1} h^{-1}. We considered a productivity of 500 g·L^{-1} h^{-1} and performed a cost estimation. For this plant total capital investment was estimated to be \$20.0 x 10^6 and it was projected that by using this technology ethanol can be produced for \$0.59 kg^{-1}.

In conclusion it has been shown that *S. cerevisiae* NRRL Y-566 was able to grow and produce ethanol in concentrated sugar solutions (250-300 g L^{-1}). With the use of $CaCO_3$ and $CaCl_2$ both ethanol concentrations and productivities were improved significantly. In a control batch fermentation the culture produced less than 20.87 g L^{-1} ethanol when using 100 g L^{-1} sugar solution with a productivity of 0.25 g L^{-1} h^{-1}. When using 0.40 g L^{-1} $CaCl_2$ solution, both ethanol concentration and productivity were improved to 90.0 g L^{-1} and 1.25 g L^{-1} h^{-1}, respectively. Also ethanol yield was improved to 0.48 which is 94 % of theoretical value and is close to commercial yield. Using these parameters, ethanol's process economics was performed and it was projected that supplementation with 0.40 g L^{-1} $CaCl_2$ would result in the production of ethanol for \$0.91 kg^{-1}. It was also projected that improving productivity to 37.5 g L^{-1} h^{-1} would result in the production of ethanol for \$0.70 kg^{-1}. It is possible to achieve this productivity with the combination of $CaCl_2$ supplementation and the use of cell recycle technology when employing *S. cerevisiae* NRRL Y-566.

 DOI: 10.17628/ecb.2014.3.904-910

Table 2. Process economics of ethanol production from corn derived glucose using *Saccharomyces cerevisiae* Y-566 and *Zymomobilis mobilis*.

Parameters	*S. cerevisiae* Y-566		*Z. mobilis*
	Prod. 1.25 g L^{-1} h^{-1}	**Prod. 37.5 g L^{-1} h^{-1}**	**Prod. 500 g L^{-1} h^{-1}**
A Direct fixed capital [$]	192,525,000	79,547,000	20,010,000
B Working capital [$]	4,674,000	4,674,000	4,674,000
C Startup cost [$]	9,626,000	3,977,000	1,000,000
D Total investment (A+B+C) [$]	206,825,000	88,198,000	25,684,000
E Investment charged to project [$]	206,825,000	88,198,000	25,684,000
F **Production Rates**			
CO_2 [kg·$year^{-1}$]	104,168,400	104,168,400	104,168,400
Cell mass [kg·$year^{-1}$]	49,749,840	49,749,840	49,749,840
Ethanol [kg·$year^{-1}$]	100,000,000	100,000,000	100,000,000
G **Revenue Price**			
CO_2 [$·$kg^{-1}$]	0.05	0.05	0.05
Cell mass [$·$kg^{-1}$]	0.05	0.05	0.05
H **Revenues/savings**			
CO_2 [$·$year^{-1}$]	5,208,420	5,208,420	5,208,420
Cell mass [$·$year^{-1}$]	2,487,492	2,487,492	2,487,492
Ethanol [$·$year^{-1}$]	91,000,000	70,000,000	59,000,000
Total revenues [$·$year^{-1}$]	**98,695,912**	**77,695,912**	66,695,912
I **Annual Operating Cost (AOC)**			
Actual AOC [$.$year^{-1}$]	91,318,000	70,021,000	58,799,000
J **Unit Production Cost/Revenue [$.$kg^{-1}$]**	**0.91**	**0.70**	**0.59**
K Gross Profit (H-I) [$.$year^{-1}$]	7,377,912	7,385,000	18,608,000
L Taxes (40%) [$.$year^{-1}$]	2,951,165	2,954,000	7,443,000
M Depreciation [$.$year^{-1}$]	18,289,000	7,557,000	1,901,000
N Net profit (K-L+M) [$.$year^{-1}$]	22,715,747	11,988,000	24,231,000

Prod. - Productivity

Table 3. A summary of production of ethanol from glucose using *S. cerevisiae* NRRL Y-566 supplemented with $CaCO_3$ and $CaCl_2$.

Process	Initial sugar [g L^{-1}]	Max. ethanol concn. [g L^{-1}]	Yield [-]	Productivity [g L^{-1} h^{-1}]
Control	100	20.83	0.39	0.25
$CaCO_3$ (1.0 g L^{-1})	250	65.63	0.44	0.92
$CaCl_2$ (0.40 g L^{-1})	250	90.00	0.48	1.25

Using *Z. mobilis* in membrane cell recycle reactors and application of $CaCl_2$ could result in achieving high productivity (500-600 g L^{-1} h^{-1}) and reduction of ethanol production price to \$0.59 kg^{-1}. The results obtained in these studies have been summarized in **Table 3**.

In brief the objectives mentioned in the introduction section of this article have been achieved. Three most important factors (ethanol concentration, yield, and productivity) for ethanol production from corn or corn derived glucose have been improved.

Acknowledgements

MM Azam would like to thank US-INDIA Education Foundation, New Delhi, India and Fulbright Commission Washington DC, USA for the Fulbright Fellowship and financial support. NQ would like to thank Michael A. Cotta (United States Department of Agriculture, Agricultural Research Service, National Center for Agricultural Utilization Research, Peoria, IL, USA) for reading this article and providing constructive comments which improved quality of the paper.

TCE would like to acknowledge SEED grant financial support from Ohio Agricultural Research and Development Center (OARDC).

**Mention of trade names or commercial products in this article is solely for the purpose of providing scientific information and does not imply recommendation or endorsement by the United States Department of Agriculture. USDA is an equal opportunity provider and employer.

References

[1]Vega, J. L., Clausen, E. C., Gaddy, J. L., *Biotechnol. Bioeng.*, **1987**, *29*, 429-435.

[2]Ryu, D. D., Kim, Y. J., Kim, J. H., *Biotechnol. Bioeng.*, **1984**, *26*, 12-16.

[3]Mancilha, I. M. D., Pearson, A. M., Waller, G. J., Hogaboam, B. B., *Biotechnol. Bioeng.*, **1984**, *24*, 632-634.

[4]Converti, A. P., Lodi, P. A., Parisi, F., Borghi, M. D., *Biotechnol. Bioeng.*, **1985**, 27, 1108-1114.

[5]Qureshi, N., Dien, B. S., Liu, S., Saha, B. C., Cotta, M. A., Hughes, S., Hector, R., *Biotechnol. Prog.*, **2012**, *28*, 1179-1185.

[6]Qureshi, N., Dien, B. S., Liu, S., Saha, B.C., Hector, R., Cotta, M. A., Hughes, S., *Biotechnol. Prog.*, **2012**, *28*, 1167-1178.

[7]Cheryan, M., Mehaia, M.A., *Process Biochem.*, **1984**, *19*, 204-208.

[8]Gregory, P. C., Carol, A. M., Ingledew, W. M., *Appl. Environ. Microbiol.*, **1984**, *48*, 639-646.

[9]Yu, S., Wayman, M., Parekh, S. K., *Biotechnol. Bioeng*., **1987**, *29*, 1144-1150.

[10]Favela-Torres, E., Allais, J. J., Baratti, J., *Biotechnol. Bioeng.*, **1986**, *28*, 850-856.

[11]Tobias, J. B., Menezes, D., Das Santo, C. L. M., Azzini, A., *Biotechnol. Bioeng*., **1983**, *25*, 1071-1082.

[12]Sitton, O. C., Gaddy, J. L., *Biotechnol. Bioeng.* **1980**, *22*, 1735-1748.

[13]Casey, G. P., Ingledew, M., *Crit. Rev. Microbiol*. **1986**, *13*, 219-290.

[14]Hayashida, S., Feng, D. D., Ohta, K., Chaitiumvong, S., Hongo, M., *Agric. Biol. Chem*., **1976**, *40*, 73-78.

[15]Dien, B. S., Nichols, N. N., O'Bryan, P. J., Bothast, R. J., *Appl. Biochem. Biotechnol.*, **2000**, *84*, 181-196.

[16]Knauf, M., Kraus, K., Specific yeasts developed for modern ethanol production. *Sugar Ind.*, **2006**, *131*, 753-758.

[17]Bajpai, P. K., Margaritis, A., *Biotechnol. Lett.* **1984**, *6*, 673-676.

[18]Sreekumar, O., Basappa, S. C., *Biotechnol. Lett.*, **1992**, *14*, 511-514.

[19]Nabais, R. C., Sá-Correia, I., Viegas, C. A., Novais, J. M., *Appl. Environ. Microbiol.*, **1988**, *54*, 2439-2446.

[20]Ciesarova, Z., Smogrovicova, D., Domeny. Z., *Folia Microbiol.* **1996**, *41*, 485-488.

[21]Nikolic, S., Mojovic, L., Pejin, D., Rakin, M., Vucurovic, V., *Food Technol. Biotechnol*., **2009**, *47*, 83-89.

[22]Maddox, I. S., Qureshi, N., Roberts-Thomson, K., *Process Biochem.*, **1995**, *30*, 209-215.

[23]Qureshi, N., Dien, B., Nichols, N. N., Saha, B. C., Cotta, M. A., *Trans. IChemE, Part C (Food Bioprod. Process)*, **2006**, *84*, 114-122.

[24]Afschar, A. S., Biebl, H., Schaller, K., Schugerl, K., *Appl. Microbiol. Biotechnol.*, **1985**, *22*, 394-398.

[25]Rogers, P. L., Lee, K. J., Skotnicki, M. L., Tribe, D. E., *Adv. Biochem. Eng*., [Fiechter, A. (ed)], **1982**, *23*, 37-84.

[26]Lee, J. M., Pollard, J. F., Coulman, G. A., *Biotechnol. Bioeng.*, **1983**, *22*, 497-511.

[27]Qureshi, N., Manderson, G. J., *Energy. Sources*, **1995**, *17*, 241-265.

Received: 08.08.2014.
Accepted: 27.08.2014.

THE MECHANISMS OF REORGANIZATION OF BLOOD VESSELS OF MYOCARDIAL RIGHT ATRIA AT HEMODYNAMIC CHANGES

Kukurtchyan, N. S.[a] and Karapetyan, G. R.[a]

Keywords: Transmission electron microscopy, light optical microscopy, right heart atria, angiogenesis, arteriogenesis, pulmonary arterial valve stenosis.

It was shown that pulmonary arterial valve stenosis moderate changes in hemodynamic parameters of patients lead to a change in the structure of cardiomyocyte and blood vessel. Strengthening of plastic processes, lead to hypertrophy and proliferation of endothelial cells as well as to increase of blood vessels' lumen diameter. Quite interesting is the fact that new capillaries formed mostly by intuscusseptive angiogenesis. In the same way new arteries are formed. Hemodynamic changes of heart right compartment accompanied by structural vascular and cardiomyocyte remodeling. In the later stages of disease vascular remodeling goes by the mechanism of intussusceptions forming vessels of different caliber.

* Corresponding Authors: Karapetyan, G. R.
Fax: +374 -10-28 19 51
E-Mail: sapootraa_a@yahoo.com
[a] H. Buniatian Institute of Biochemistry, of National Academy of Sciences of Republic Armenia, Paruir Sevag str. 5/1, 0014, Yerevan, Republic of Armenia.

INTRODUCTION

In vertebrates the cardiovascular system is the first to function for the same purpose throughout the entire lifespan of the individual. It generates pressure for the displacement of blood within it and of metabolites through its walls. It has long been recognized that in fluid transport systems in which only on pressure source the heart provides the driving force for transport through billions of minuscule capillaries one optimizing feature is a system of hierarchical bifurcations.[1] Cardiac hypertrophy is formed as an adaptive response to increased work load to maintain cardiac function.[2] An increase in heart tissue must be matched by a corresponding expansion of the coronary vasculature to maintain.[3] Myocardial hypertrophy, secondary to increased hemodynamic demands, required to provide adequate oxygen and nutrients to the increasing cardiac mass.[4] When deregulated the formation of new blood vessels contributes to numerous malignant ischemic inflammatory infections and immune disorders.

There are two forms of vascular remodeling associated with physiological and pathological processes: angiogenesis and arteriogenesis. Angiogenesis is a potent physiological process that underlies the natural manner in which our bodies respond to a diminution of blood supply to vital organs namely the production of new collateral vessels. However under pathological conditions angiogenesis can be found as a part of pathological process such as in diabetic retinopathy, tumor growth and wound healing. Increased capillaring also can be found in the heart with coronary artery occlusion in young adult animals.[5] Angiogenesis is a process of growing of new capillaries from the existing capillaries trough capillary sprouting or intussusceptions.[6,7] Variant of angiogenesis different from sprouting is intussusceptive angiogenesis. Intussusceptive microvascular growth is fast process that can take place within hours or even minutes, because it does not need proliferation of endothelial cells and with a little amount of energy.[8,9,10] The physiological mechanisms that underlie the coordination of angiogenesis and cardiomyocyte growth are unknown.[3]

Prolonged cardiac hypertrophy causes heart failure, and its mechanisms are largely unknown.[11] Right ventricular failure is an important clinical problem with no available therapies, largely because its molecular mechanism is unknown. Lack of coordination between the myocytes – driven hypertrophic response and the production of angiogenic growth factors hallmarks the transition to heart failure.[4] Inhibition and suppressed angiogenesis and the resultant ischemia may contribute to the rapid deterioration of right ventricular function upon entrance to a decompensation phase.[11]

We have previously shown the relationship of structural changes of cardiomyocytes and blood capillaries in the development of hypertrophy of the right compartment of heart.[12,13,14,15]

The aim of this study is to investigate the reorganization of the blood vessels of myocardium at hemodynamic changes.

MATERIALS AND METHODS

Reagents

Crystalloid cardioplegic solution (Na-147 meq L^{-1}, K-19 meq L^{-1}, Ca-4 meq L^{-1}, Cl-155 meq L^{-1}, HCO_3- 25 meq L^{-1}, Glucose-0,2% , pH-7,4, Mg –2 meq L^{-1}); powdered paraformaldehyde; OsO_4; Sodium cacodylate trihydrate; 96º ethyl alcohol, acetone, Epon 812, Epon Hardener MNA, Epon Hardener DDSA, Epon accelerator DNP-30, uranyl acetate, citrate Na, nitrate Pb, photoplates.

All reagent used were of analytical grade and purchased from Sigma Chemical Co. (USA).

Human Subject

All procedures involved human subject were approved by institutional review board/bioethical committee (Erevan State Medical University, RA) conformed to the Legal Aspects of Research Ethics and Science in European Community directive (2001/20/EC), (IRB Approval YSMU Bioethical committee N7 by 26.04.2011).

In this study the myocardium of right atria of 10 patients with pulmonary arterial valve stenosis (PAVS) was investigated. The patients were divided into 3 groups depend on the systolic pressure of right ventricular: I group - mercury column pressure was up to 60mm (2 patients); II group - mercury column pressure was from 60 to 100mm (3 patients); III group - mercury column pressure was more than 120mm (5 patients).

Collecting biopsy material during cardiosurgical procedure of patients was performed during canulation.

Treatment of material

The bioptates taken during canulation (small pieces of the right atrii) have immediately put in cold 4 ºC mix of paraformaldehyde in a sodium cacodylate buffer and glutaraldehyde for 12 hours with following post fixation in 1% OsO_4 solution during 2 hours; dehydration in ascending series of spirits; saturation in a mixture of acetone and Epon resins of different proportions and pouring in gelatinous capsules into epon.

Obtaining of ultrathin slices and its treatment

The ultrathin slices (up to 500 Å) were made using ultracut LKB (Swedish) and Reichert (Austria). Ultrathin slices were double contrasted with uranyl acetate and citrate Na and nitrate Pb solutions.

Observation under TEM

Obtained ultrathin slices were observed under the transmission electron microscope (Phillips CM 10) with resolution X 20.000.

Observation under light microscope

Obtained semithin epoxy sections stained with Azur 2 and observed under the light microscope with resolution X 1.000.[16]

RESULTS

It was shown that pulmonary arterial valve stenosis (PAVS) moderate changes in hemodynamic parameters of patients lead to a change in the structure of cardiomyocyte and blood vessel.

In the first group patients with right ventricular blood pressure up to 60mm of mercury column the process of enhancing of the plastically processes in cardiomyocytes as well as in blood vessels without cardiomyocytes organelles hyperplasia and hypertrophy takes place. Changes in the endothelial lining go in two directions. In one case, it is a relatively thin and uniform thickness, the other marked irregularity of its thickening. Strengthening of plastic processes, the presence of many ribosome, rough reticulum hypertrophy lead to hypertrophy and proliferation of endothelial cells (Fig. 1) as well as to increase of blood vessels' lumen diameter.

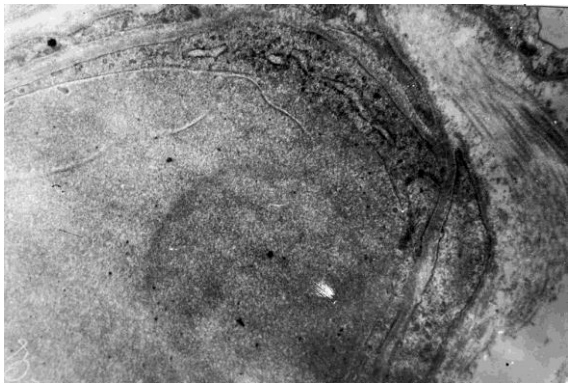

Figure 1. Plastic processes in endothelial cells. X 20.000

In the second group of patients with blood pressure in the right ventricular up to 60 -100mm of mercury column the processes of myofibrils hypertrophy and Mch hyperplasia take place. The plastically processes are enhanced lead to reorganization of cardiomyocytes and blood capillaries as well. Blood vessels are presented in significant number. The studies performed by TEM showed proliferation of cellular elements in the walls of small arteries of patients with PAVS. Endothelial cells were increased not only in quantity but also in size (hypertrophic).

Proliferation of smooth muscle cells lead to its unevenly localization. Proliferation of contractile fibers inside of these cells are expressed (Fig. 2).

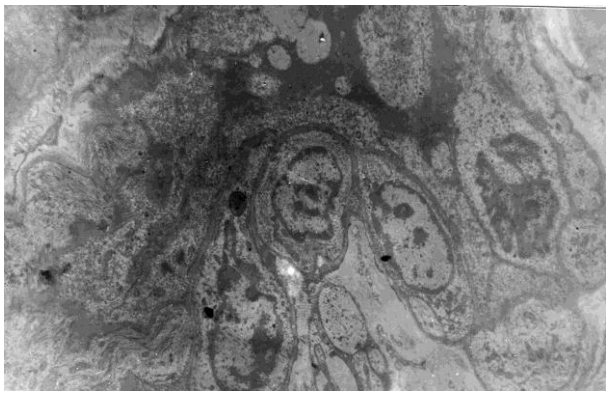

Figure 2. Proliferation of cellular elements in the walls of small arteries. X 20.000

When blood pressure in right ventricular is more than 120mm myofibrils are not hypertrophied. The process of hyperplasia of Mch takes place. The plastically processes are enhanced in cardiomyocytes and blood vessels. Endothelial lining has different thickness, took place the process of proliferation of endotheliocytes as well as sharp expansion of the capillaries lumen. It must be noted that some patients of this group have interruption of myocardial blood flow, lead to ultrastructural destruction of cardiomyocytes and blood vessels.

By the method of light microscopy used semithin epoxy sections of patients with PAVS were found formation of new blood vessels from preexisted (Fig. 3, 4).

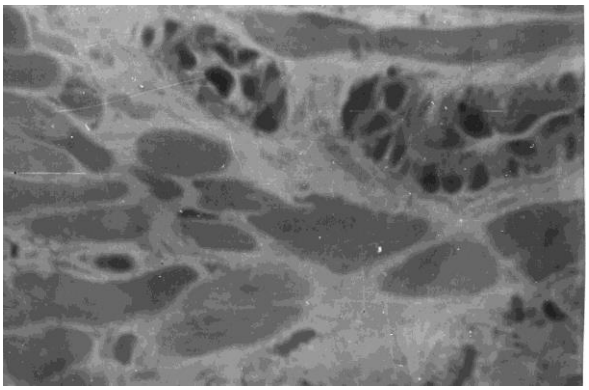

Figure. 3. Intussusceptive angiogenesis of small arteria. X 1000

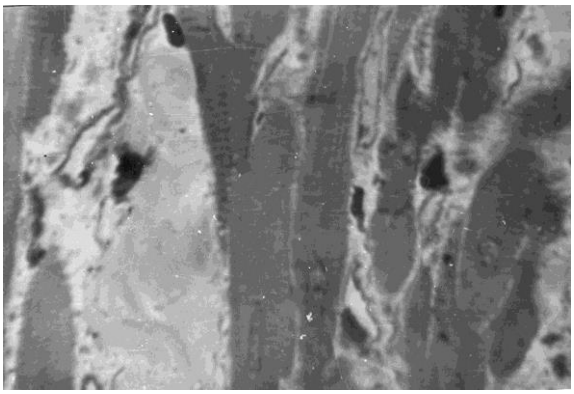

Figure 4. Intussusceptive angiogenesis of capillaries. X 1000

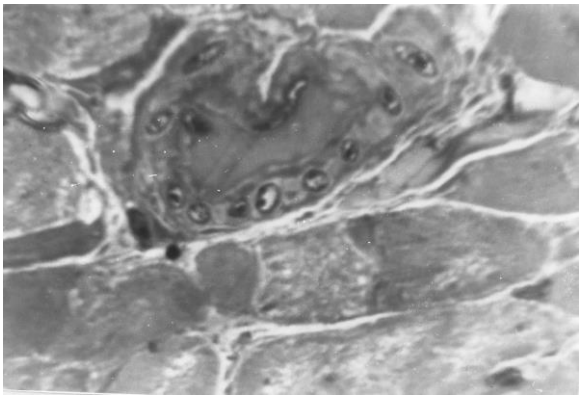

Figure 5. Pillar formation in small arteria. X 1000

In some capillaries transluminal bridges dividing the lumen of the capillary are observed. In most cases took place the invagination of the opposing capillary walls on both sides into the lumen forming pillar.

The cytoskeleton itself is actively involved in this process. Quite interesting is the fact that new capillaries formed in this way have visually identical profiles. In the same way new arteries are formed. This process is different from capillaries by involving only one side of artery wall in the process of invagination and pillar formation (Fig. 5). It should be noted that these new vessels are different by sizes and their lumen diameter varies from very small to larger. The hyperplasia of the cellular elements of the wall is observed.

Increasing number of transluminal bridges in blood vessels and pillars, as well as in the same capillary 2 or more invaginations of the opposing walls of the capillary take place. This process indicates that the new formed vessels will be of different caliber.

DISCUSSION

Progressing changes of hemodynamic parameters at PAVS accompanied by the inclusion of growth stimuli, increase plastic processes which lead to remodeling of blood capillaries in the direction of increasing of their caliber.

One of the conditions for the success of remodeling process is proliferation of endothelial and smooth muscle cells.[17] However, the proliferation and hypertrophy of endothelial cell, proliferation of smooth muscle cells and the randomness of their location in the wall of collateral vessels at the changes in the severity of hemodynamic parameters of patients with PAVS leads to the formation of blood vessels look like giant structures with a wide lumen.

The accepted point of view is that arteriogenesis and angiogenesis have been through to be distinct processes mediated by different mechanisms.[18,19,20,21] Our study indicate that strengthening of the growth stimulus leads to an increase of cell elements in the wall of collateral blood vessels and capillaries, as well as to most expressed change in their caliber in the later stages of the disease.

Studies of angiogenesis induced by adeno Vpf have shown that angiogenic response in skin was much more intense than that with developed in either skeletal or heart muscle.[22] The kinetics of new blood vessel formation and the structure and functional capacities of the newly formed vessels induced by VPF/ VEGF or other cytokines in ischemic tissues have not been carefully investigated. At adeno Vpf many mother vessels divided into smaller "daughter vessels" by sprouting, or by projection of EC cytoplasmic processes into and across mother vessel lumens, forming translumenal EC 'bridges'. These bridges divided blood flow into smaller sized channels. The course of several days separated from each other to form smaller caliber daughter vessels.[22]

Mother vessels in ear skin evolved along yet another pathway, that of intussusceptions a process distinct from translumenal bridging. Intussusception occurs in embryogenesis when 'pillars' of connective imprignge from without on hollow tubular structures causing focal invagination.[23] Although the mechanism of intussusceptions is not fully understood, there are several keypalyers that cold influence pillar formation.[24] Alteration in blood flow dynamics in arterial branches could stimulate this process.[25] Pillar formation and remodeling is not observed in capillary plexuses, but also within smaller arteries and veins.[26]

Intossusception is a relatively new mechanism of angiogenesis in biology. It should be noted that there are conflicting views regarding the mechanism. Some studies combined the process of intussusceptions with forming transluminal endothelial bridges.[27] However, other researchers believe that transluminal endothelial bridges formation and intussusceptions are different processes. Intussusception causes to pillar formation and then to separation and formation of new blood vessel.

At the expressed alteration of hemodynamic parameters of myocardium formation of new blood vessel take place on the basis of preexisting capillaries increased in size. In the myocardium of right atrium at PAVS the presence of intussusception process with transition to pillar formation in the capillaries, as well as formation of transluminal bridges in small arteries are observed. The type of blood vessel formation was closely dependent on the pathology.

It could be mentioned that because of the fact that intussusception is a faster process and compared with the formation of transluminal bridges is more preferably in the compartments of heart with hypertrophy.

However, it should be noted that for myocardium these processes are not positive, because there is an uneven caliber in formed blood vessels, especially concerning the small collateral vessels, as there are risks of failure to ensure some regions of the myocardium with oxygen and nutrients that may lead to postoperative complications. Such structural reorganization of the blood vessels in parallel with changes in cardiomyocytes themselves can be the cause of chronic heart failure.

CONCLUSION

The alterations of SS structures as well as in mitochondria of cells could be one of the main reasons leading to postsurgical damages of cardiomyocytes.

ACKNOWLEDGEMENT

Current work was performed by support of H. Buniatian Institute of Biochemistry Natl. Acad. Sci. of RA.

REFERENCES

[1]Kurz, H., *J. Neurooncol.*, **2000**, *50*, 1-19.

[2]Masanori, S., Tohru, M., Yunzeng, Z., Haruhizo, T., Mutsuo, H., Issei, K., *J. Mol. Med.*, **2013,** *3*, 2401.

[3]Jaba, I. M., Shuang, Z., Li, N., Jiang, Y., Mantiu, K. A., Sinusas, A. J., Papadematris, X., Simons, M., Sessa, W. C., Young, L. H., Tirziu, D., *J. Clinic. Invest.*, **2013,** *123 (4)*, 1718-1731.

[4]Tirziu, D., Giordano, F. J., Simons, M., *Circulation*, **2010,** *122(9)*, 928-937.

[5]Xie, Z., Cao, M., Batra, S., Kojama, T., *Cardiovasc. Res.*, **1997,** *33*, 671-5.

[6]Hudlicka, O., Brown, M., Egginton, S., *Physiol. Res.*, **1992**, *72*, 369-417.

[7]Simons, M., *Circulation*, **2005,** *111*, 1556-66.

[8]Caduff, J. H., Fischer, L. C., Burri, P. K., *Anat. Record*, **1986,** *216*, 154-164.

[9]Burri, P. H., Tarek, M. R., *Anat. Record*, **1990,** *228*, 35-45.

[10]Burri, P. H., Hlushchuk, R., Djonov, V., *Dev. Dynam.*, **2004,** *231*, 474-488.

[11]Sutendra, G., Dromparis, P., Paulin, R., Zervopoulos, S., Haromy, A., Nagendran, J., Michelakis E. D., *J. Mol. Med.*, **2013,** *91(11)*, 1315–27.10.1007/s00109-013-1059-4.

[12]Kukurtchyan, N., Aglintsyan, T., Popov, A., *4th All-Union Sci. Conf.*, Yerevan, Armenia, **1989,** 369-370.

[13]Kukurtchyan, N. S., Aglintsyan, T., *11th Congr. Anatomists, Histologists and Embryologist*, Russia, Smolensk, **1992,** 73**.**

[14]Kukurtchyan, N., Aglintsyan, T., *J. Bull. Surgery*, **1993**, *2*, 76-79.

[15]Kukurtchyan, N., Sultanyan, T., Gasparyan, V., *Electron Microscopy Conf. Mater., Yerevan, Armenia,* **1997**, 65.

[16]Kukurtchyan, N. S., Karapetyan, G. R., Patent N2844A, Republic of Armenia, **2014**

[17]Heil, M., Schaper, W., *J. Circulation Res.*, **2004**, *95*, 449-458.

[18]Buschmann, I., Schaper, W., *News Physiol Sci.***, 1999,** *14*, 121-125.

[19]Cohen, M. V., *Coronary Collaterals: Clinical and Experimental Observations*, **1985,** 1-91.

[20]Cohen, M., Rentrop, K. P., *Circulation*, **1986,** *74*, 469-476.

[21]Skalak, T., Price, R., Zeller, P., *Microcirculation*, **1998**, *5*, 91-94.

[22]Petterson, A., Nagy, G. A., Brown, L. F., Sundberg, C., Morgan, E., Gunglet, S., Carter, R., Krieger, G. E., Manseau, E. J., Harvey, V. S., Eckelhoefer, I. A., Feng, D., Dvorak, A. M., Mulligan R. C., Dvorak, H. F., *J. Lab. Invest.*, **2000**, *80*, 99-115.

[23]Patan, S., Haenni, B., Burri, P. H., *Anat. Embryol.*, **1993**, *187*, 121-130.

[24]Augustin, HG., *Circulation Res.*, **2001,** *89*, 645-647.

[25]Hillen, F., Griffioen, A. W., *Cancer Met. Rev*, **2007**, *25*, 489-502.

[26]Clauss, M., Breier, G., *17 Gen. Springer*, **2006.**

[27]Djonow, V. G., Kurz, A., Burri, P. H., *Dev. Dynam.*, **2002**, *224*, 351-402.

Received: 03.08.2014.
Accepted: 29.08.2014.

SYNTHESIS AND SPECTRAL STUDIES OF METAL COMPLEXES WITH 3,4,6,7-O,O,O,O-TETRAKIS-(CARBOXY(CHLORO)METHYL)-L-ASCORBIC ACID (H_4L)

Salah Mohammed Fizea[a]*, Falih Hassan Musa[a], Huda Ahmed Fidhel[a]

Keywords: synthesis, 3,4,6,7-O,O,O,O-tetrakis(carboxy(chloro)methyl)-L-ascorbic acid, metal complexes; analysis.

The reaction of L-ascorbic acid with the dichloroacetic acid in the presence of potassium hydroxide gave new product 3,4,6,7-O,O,O,O-tetrakis(carboxy(chloro)methyl)-L-ascorbic acid (H_4L), which was isolated and characterized by ^1H,^{13}C-NMR, elemental analysis (CHN), thermogravimetric analysis (TGA), UV-visible and Fourier Transform infrared (FTIR) methods. The complexes of the ligand (H_4L) with metal ions, M^{+2}= (Cu, Co, Ni, Cd and Hg) were synthesized and characterized by FTIR, UV-Visible, molar conductance, atomic absorption, magnetic susceptibility, thermogravimetric analysis (TGA) and molar ratio methods. The analysis showed the evidence of binding of the metal ions with (H_4L) through the bidendate carboxylato group manner resulting in six-coordinated metal ion. The TLC for (H_4L) and complexes showed one spot for each indicating the purity of these compounds.

* Corresponding Authors
E-Mail: Salahmohammadiraq@gmail.com
[a] Department of Chemistry, College of Education for Pure Science, Ibn Al-Haitham, University of Baghdad

Introduction

L-Ascorbic acid (vitamin C) is an important molecule in both chemistry and biology, and its complexes with metals are of particular interest in both of these areas.[1-3] This vitamin is present in various foods, particularly of plant origin, that are several orders of magnitude higher than those of other vitamins.[4] Structurally, ascorbic acid (H_2A) is a sugar acid, a γ-lactone and an ene-diol. As a weak dibasic acid (pK_{a1} = 4.25 and pK_{a2} = 11.79), the monoanion (HA) forms at pH 4–5 with deprotonation of O(3)–H and the dianion (A) forms at pH 11–12 with deprotonation of the O(2)–H.[5] The mono-anionic form is more stable due to the delocalization of the negative charge between the oxygen atoms at the 1- and 3-positions.[6] Musa et al.[7-9] synthesized derivatives of L-ascorbic acid such as 5,6-O-isopropylidene-2,3-(2-X,1-carboxyl)deoxy-L-ascorbic acid, where X = H, Cl, 1,2-dihydroxyethyl-1-(2-mercaptophenyl)-5-(2-mercaptophenyl)-2,5-dihydro-1H-pyrrol-3,4-diol.

In the present work we show the result on synthesis of a new ligand, 3,4,6,7-O,O,O,O-tetrakis(carboxy (chloro) methyl)-L-ascorbic acid (H_4L) and its complexes with various divalent metal ions such as Cu, Co, Ni, Cd and Hg. The properties and characterization of these new metal complexes are also presented.

Experimental part

Instruments, materials and methods

All chemicals were purchased from BDH, and used without further purifications. FTIR spectra were recorded in KBr on Shimadzu- spectrophotometer in the range of 4000-400 cm^{-1}. Electronic spectra in distilled water were recorded using the UV-visible spectrophotometer type Shimadzu in the range of 200-1100 nm with quartz cell of (1 cm) path leangth. Melting points where measured with an electrothermal Stuart apparatus, model SMP30. Electrical conductivity measurements of the complexes were recorded at (25 °C) for 10^{-3} mol L^{-1} solution of the samples in distilled water using Ltd 4071 digital conductivity meter. ^1H NMR and ^{13}C NMR spectra were recorded on a Bruker 300-MHz spectrometer in DMSO-d_6. Chemical shifts in ppm relative to internal Me_4Si was performed. Elemental microanalyses of the ligand were carried out by using Euro Vectro-3000A.

Metal content of the complexes were measured using atomic absorption technique by Perkin-Elmer 5000, while Hg metal is determined using Biotech Eng. Management Co. Ltd. (UK), Thermogravimetric analysis (TGA) was carried out using a Perkin-Elmer TGA 4000. The measurement was conducted under helium as inert gas at a heating rate 20 °C min^{-1}. Magnetic susceptibility values were obtained at room temperature using the Gouy method, Johnson Mattey, model M_5B-MKs, were performed. Thin layer chromatography (TLC) was performed on aluminum plates coated with silica gel (Fluka), and detection was performed with using iodine.

Table 1. Physical properties and analytical data for the synthesized ligand (H_4L) and its complexes

Empirical formula	Color	Mp., °C	Yield, %	Found(Calc.)(%)			R_f
				C	H	M(II)	
Ligand $C_{14}H_{12}O_{14}Cl_4$	White	191	79.3	31.68 (30.7)	2.05 (2.22)	—	0.6
$[Cu_2(C_{14}H_8O_{14}Cl_4)(H_2O)_4].5H_2O$	Green	233	72	—	—	15.21 (15.30)	0.46
$[Co_2(C_{14}H_8O_{14}Cl_4)(H_2O)_4].4H_2O$	Red	257	76	—	—	14.02 (13.13)	0.50
$[Ni_2(C_{14}H_8O_{14}Cl_4)(H_2O)_4].7H_2O$	Deep green	228	70	—	—	13.71 (14.08)	0.42
$[Cd_2(C_{14}H_8O_{14}Cl_4)(H_2O)_4].2H_2O$	White	212	67	—	—	25.13 (24.27)	0.32
$[Hg_2(C_{14}H_8O_{14}Cl_4)(H_2O)_4].4H_2O$	White	249	55	—	—	36.24 (35.77)	0.20

Synthesis of ligand (H_4L)

L-ascorbic acid (0.18 g, 1 mmol) was dissolved in a mixture of 15 ml ethanol+5ml water. Potassium hydroxide (0.23 g, 4 mmol) in ethanol (10 ml) was added. The solution was stirred for 30 minutes. Dichloroacetic acid (0.52 g, 4 mmol) was added dropwise and stirring was continued for one hour. A pale yellow solution was formed, this solution was left to stand at room temperature for a few days when a yellowish white crystalline mass was crystallized out. The resulted mass was recrystallized from ethanol when a white crystalline material was formed , melting point was found to be 191°C, the yield was 79.3%.

Synthesis of complexes (M^{II} = Cu, Co, Ni, Cd, Hg)

To a solution of the (H_4L) (0.55 g, 1 mmol) in (20 ml ethanol) a solution of 2 mmol of metal chloride in 20 ml ethanol 0,34 g $CuCl_2.2H_2O$, 0.48 g $NiCl_2.6H_2O$, 0.48 g $CoCl_2.6H_2O$, 0.46 g $CdCl_2.H_2O$, 0.54 g $HgCl_2$ was added. The solutions were stirred for one hour and were left to evaporate slowly to bring down the complexes. The complexes were recrystallized from ethanol. The isolated complexes are colored solids, stable in air and insoluble in common organic solvents but completely soluble in water, ethanol, DMSO and DMF. Some physical properties for all synthesized ligand (H_4L) and its complexes are shown in Table 1.

Results and discussion

The 3,4,6,7-O,O,O,O-tetrakis(carboxy(chloro)methyl)-L-ascorbic acid (H_4L), was synthesized in a good yield by the reaction of L-ascorbic acid with dichloroacetic acid in the ratio (1:4) in presence of four mole of potassium hydroxide Scheme 1.

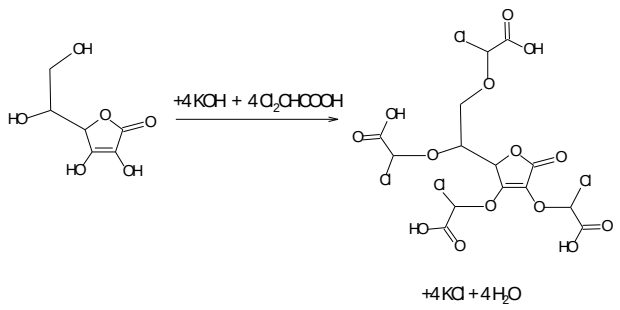

Scheme 1. The reaction of L-ascorbic acid with dichloroacetic acid in base media

FT-IR spectral analysis

The IR spectrum of L-ascorbic acid as starting material is compared with the new ligand (H_4L) spectrum, the results are summarized in Table 2. L-ascorbic acid exhibits bands at 3525, 3410, 3313 and 3213 cm^{-1} caused by υ(OH) positions (C-5,6,2,3) respectively, these are disappeared in the spectrum of the new ligand accompanied by the appearance of three bands in the 3429 (broad), 1595 (asym.), 1435 (sym.) are due to carboxyl group. (C-1=O) stretching vibration appeared at 1716 cm^{-1}. The bands at 1678, and 1647 cm^{-1} in the starting L-ascorbic acid are due to the υ(C=C), υ(C=O) are shifted and appeared as a broad band centre at 1631 cm^{-1} in the new ligand. The bands located at 1595 and 1435 cm^{-1} which were assigned to υ(C=O) stretching vibration for (COOH) in free ligand (H_4L), were shifted to lower frequency and appeared at 1404 and 1332 cm^{-1} in the Cu-complex, at 1450 and 1396 cm^{-1} in the Co-complex, at 1445 and 1384 cm^{-1} in the Ni-complex, at 1404 and 1320 cm^{-1} in the Cd-complex, and at 1404 and 1330 cm^{-1} in the Hg-complex. Components of the bands were assignable to the asymmetric and the symmetric stretching frequencies of the carboxylate ion with average separation $\Delta\upsilon_{COO^-}$= 72, 54, 61, 84, 74 cm^{-1}, respectively indicating the deprotonation of the carboxylic proton and suggests that coordination occurs through the carboxylate ion as a bidentates bonding nature.[10,11] New bands appeared in the range 418-459 cm^{-1} in the all complexes assignable to υ(M-O) vibrations.[12,13] A band due to υ(C=O) of the lacton ring appeared as a shoulder within the range of 1720-1740 cm^{-1} in all complexes. A strong broad absorption band appeared around 3552-3410 cm^{-1} associated with water molecules in these metal complexes. Coordinated H_2O appeared at range 823-827 cm^{-1} in all complexes.[14,15]

NMR spectra for the ligand (H_4L)

^{1}H-NMR spectrum of the ligand (H_4L) Figure 1 in DMSO-d_6 exhibited several signal at 3.61 ppm is attributed to CH_2-6, CH-5 while CH-4 of lactone ring is appeared at 4.64 ppm. The CH-7, CH-8, CH-9 and CH-10 proton signals are appeared at 5.86 ppm, the weak signal at 6.31 ppm can be assigned to CH-9 and CH-10.

^{13}C-NMR spectrum Figure 2 showed weak signal at 172 ppm which belongs to carboxylic acid, while the C=O carbon signal is appeared at 164 ppm. The two peaks at 123 and 144 ppm are attributed to C-2 and C-3 carbons, respectively. This may be due to the conjugated double bond from C-1 to C-3 causing upfield shift of C-3 carbon signal. The C-Cl carbon signal is appeared at 80 ppm, the signals at 71, 67 and 62 ppm are assigned to C-4, C-5 and C-6 carbon atoms, respectively.

 DOI: 10.17628/ecb.2014.3.915-919

Table 2. Assignments of the IR spectral bands of L-ascorbic acid, ligand(H_4L) and its complexes(cm^{-1})

Empirical formula	υ_{OH}, υ_{COOH}	$\upsilon_{C=O}$	$\upsilon_{C=C}$ $\upsilon_{C=O}$	$\upsilon_{as(COO)-}$	$\upsilon_{s(COO)-}$	Coordinated H_2O	υ_{M-O}
L-ascorbic acid	3525,s; 3410,s;	1720	1678	—	—	—	—
$C_6H_8O_6$	3313,s 3213,s		1647				
Ligand $C_{14}H_{12}O_{14}Cl_4$	3429, br	1716	1631,br	1595	1435	—	—
$[Cu_2(C_{14}H_8O_{14}Cl_4)(H_2O)_4].5H_2O$	3342, m	1730	1662,m	1404	1332	823,m	443
$[Co_2(C_{14}H_8O_{14}Cl_4)(H_2O)_4].4H_2O$	3448, br	1735	1640,m	1450	1396	827,s	440
$[Ni_2(C_{14}H_8O_{14}Cl_4)(H_2O)_4].7H_2O$	3377, br	1740	1655,m	1445	1384	825,m	459
$[Cd_2(C_{14}H_8O_{14}Cl_4)(H_2O)_4].2H_2O$	3473, br	1720	1627	1404	1320	825,s	426
$[Hg_2(C_{14}H_8O_{14}Cl_4)(H_2O)_4].4H_2O$	3520, m	1734	1635	1404	1330	823,s	418

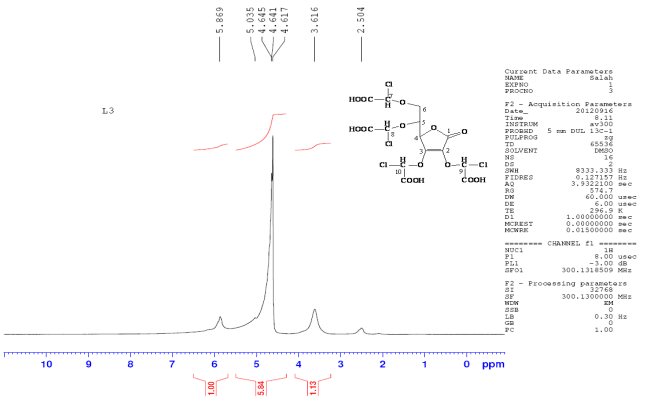

Figure 1. ^{1}H-NMR spectrum of the ligand

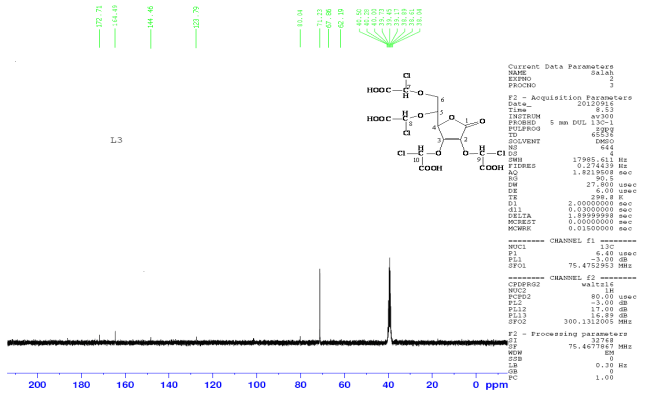

Figure 2. ^{13}C-NMR spectrum of the ligand

Spectral studies

The electronic absorption bands as well as the magnetic moment values are summarized in Table 3. The UV-Visible spectrum of the ligand (H_4L) showed one absorption at (41152cm^{-1}) is due to $\pi-\pi^*$ transition.[16]

The electronic spectrum of Co-complex in water solution exhibited two bands appeared at (15797 cm^{-1}) and (19646 cm^{-1}) were assigned to the $^4T_1g\rightarrow{}^4A_2g$ (υ_2) and $^4T_1g\rightarrow{}^4T_1g(p)$ (υ_3) transitions respectively of octahedral geometry[17]. From the ratio of (υ_3)/(υ_2) (1.24) the value of *Dq*/*B* (0.95) was obtained. The value of *B*' (890.93) as well as the position of υ_1(10*Dq*) (8463 cm^{-1}) were calculated by using Tanaba-Sugano diagram for d^7 configuration of the octahedral configuration geometry.[18] The value of β (0.91) indicates some covalent character. The conductivity measurement indicates that the Co-complex is non-ionic.

Spectrum of Ni(II) complex showed three bands in the visible region at (25773 cm^{-1}) $^3A_2g\rightarrow{}^3T_1g_{(P)}$ (υ_3), (14556 cm^{-1}) $^3A_2g\rightarrow{}^3T_1g_{(F)}$ (υ_2) and the last one is at (9174 cm^{-1}) $^3A_2g\rightarrow{}^3T_2g$, ($\upsilon_1$). The ratio of υ_2/υ_1, (1.59) was applied on Tanaba-Sugano diagram for d^8 octahedral complexes,[19,20] $B_{complex}$ and β, 10*Dq*(υ_1) were calculated theoretically. The conductivity showed that the Ni(II)-complex was non-electrolyte. The spectrum of Cu(II) complex showed broad band at (12422 cm^{-1}) assigned to $^2Eg\rightarrow{}^2T_2g$ transition which refers to Jahn-Teller distortion of octahedral geometry.[21] The conductivity measurement of the complex indicates that the complex is non-electrolyte.

The spectra of Cd(II), Hg(II) complexes gave no bands in the visible region, only bands assigned to charge transfer transitions (40983 cm^{-1}) Cd(II), (35211 cm^{-1}) Hg(II) complexes were observed, compared with free ligand showed one band at (41152 cm^{-1}) confirms the complex formation.[22] The conductivity measurements of the two complexes indicate that the complexes are non-electrolyte.

Magnetic studies

The magnetic moment values at (294 K) of the $[M_2LCl_4].XH_2O$ M^{2+} = Cu, Co, Ni Table 3 show values 0.80, 2.76 and 1.62 B.M., respectively which are lower than the total spin-only values indicating a high spin octahedral geometry around metal ion. The lowering of these magnetic moments indicates a dominate antiferromagnetic interaction in all complexes. This may due to the fact that the syn-syn carboxylate provide a small metal-metal distance and results in a good overlap of the magnetic orbitals, an antiferromagnetic coupling is always induced.[23-24]

Molar ratio

The complexes of the ligand (H_4L) with metal ions [Co(II), Ni(II), Cu(II), Cd(II), Hg(II)] were studied in solution using water as solvent, in order to determine (M:L) ratio in the prepared complexes, following molar ratio method.[25] A series of solutions were prepared having a constant concentration (*c*) 10^{-3} M of the hydrated metal salts and the ligand (H_4L). the (M:L) ratio was determined from the relationship between the absorption of the observed light and mole ratio (M:L) found to be 2:1.

 DOI: 10.17628/ecb.2014.3.915-919

Table 3. Magnetic moments and electronic spectral bands (cm^{-1}) of the complexes.

Complex	μ_{eff}, B.M.	Band position, cm^{-1}	Assignments	$B_{complex}$	β	$10Dq$ (υ_1) theoretical, cm^{-1}	Λ_m $\Omega^{-1} cm^2 mol^{-1}$
L-Co(II)	2.76	19646 υ_3	$^4T_1g \rightarrow {}^4T_1g(p)$	890.93	0.91	8463	10.73
		15797 υ_2	$^4T_1g \rightarrow {}^4A_2g$				
		25773 υ_3	$^3A_2g \rightarrow {}^3T_1g_{(P)}$				12.35
L-Ni(II)	1.62	14556 υ_2	$^3A_2g \rightarrow {}^3T_1g_{(F)}$	773.38	0.75	13920	
		9174 υ_1	$^3A_2g \rightarrow {}^3T_2g$				
L-Cu(II)	0.80	12422	$^2Eg \rightarrow {}^2T_2g$	—	—	—	7.19
L-Cd(II)	—	40983	ILCT	—	—	—	13.68
L-Hg(II)	—	35211	ILCT	—	—	—	11.47

Table 4. Molar ratio data for H_4L-complexes

V, ml	L-Cu (λ=805)	L-Co (λ=509)	L-Ni (λ=710)	L-Cd (λ=290)	L-Hg (λ=284)
(1) 0.5	1.90	1.95	0.78	2.14	1.48
(2) 1	2.64	2.75	1.44	2.68	1.97
(3) 1.5	2.87	2.97	1.38	3.52	2.14
(4) 2	3.42	3.49	1.89	3.72	2.64
(5) 2.5	3.58	3.68	1.95	3.92	2.81
(6) 3	3.78	4.12	2.26	4.12	2.97
(7) 3.5	3.89	4.35	2.47	4.19	3.29
(8) 4	4.11	4.76	2.59	4.34	3.57
(9) 4.5	4.24	4.78	2.74	4.41	3.66
(10) 5	4.27	4.79	2.79	4.57	3.78

The results of complexes formation in solution are shown in Table 4, these data are compatible with the results obtained by atomic absorption for determination metal analysis in the complexes Table 1.

Thermal decomposition measurement

The TGA thermal analysis curve for $C_{14}H_{12}O_{14}Cl_4$ ligand is shown in Figure 3. The sample decomposes into two decomposition processes with peaks detected over in the 213-440 °C range. About half weight of the complex decompose at the first step occurs at 213 °C with weight loss of 4.5743 mg, 50.0969 % (calc.=4.6825 mg, 51.2820 %) is related to the loss of chlorine containing fragments.

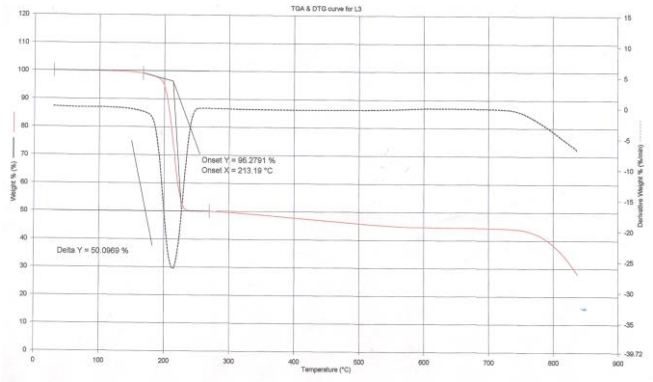

Figure 3. TGA, DTG thermograms of the ligand (H_4L)

The second step from 440 °C corresponding to the loss of (CO) molecule, showed a weight loss 0.4656 mg, 5.0991 % (calc.=0.4682 mg, 5.1282 %). The final weight of the residue is 4.0911 mg, 44.8045 %

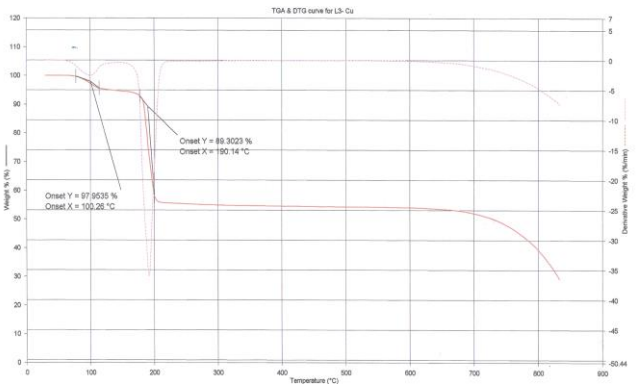

Figure 4. TGA, DTG thermograms of Cu(II) complex

The TGA curve for $[Cu_2(C_{14}H_8O_{14}Cl_4)(H_2O)_4].5H_2O$ is shown in Figure 4. The sample found to be stable up to 74 °C as shown by the TG curve. The complex decomposes in two steps over the temperature range 100-190 °C. The first decomposition shows weight loss of 2.0994 mg, 5.4229 % (calc.=2.5188 mg, 6.5060 %) which is due to the loss of three H_2O molecules. The second step with weight loss of 15.5811 mg, 40.2458 % shows a peak in the DTG at 190 °C which is related to the loss of residual water and organic fragments.

 DOI: 10.17628/ecb.2014.3.915-919

Thin layer chromatography (TLC)

The solution of ligand (H_4L) and its complexes in water as solvent appeared in one spot, this is confidence that all these compounds are pure and have one isomer. Table 1 shows the R_f for complexes and ligand (H_4L).

Conclusion

The ligand (H_4L) acts as a tetra-dentate dianion with two metal ions coordinate with each carboxylate group in an octahedral geometry. Figure 5

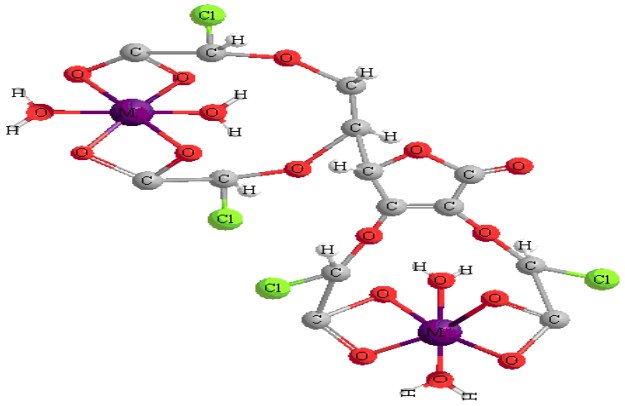

Figure 5. The proposed molecular structure of complexes, M^{II}= Cu, Co, Ni, Cd, Hg

Acknowledgment

I wish to express my deepest and sincerest appreciation to Prof. Dr. Falih H. Musa for his positive guidance, enlightened mentoring and encouragement. Sincere thanks are also to the staff members of the Department of the Chemistry.

References

[1]Martell, A. E., Seib, P. A. and Tolbert, B. M., *ACS Adv. Chem. Ser*., **1982**, *200*, 153−178, Eds., American Chemical Society, Washington,

[2]Hughes, D. L., *J. Chem. Soc., Dalton Trans*. **1973**, *21*, 2209−2215.

[3]Hollis, L. S., Amundsen, A. R. and Stern, E. W., *J. Am. Chem. Soc*., **1985**, *107*, 274−276.

[4]Padayatty, S. J., Katz, A., Wang, Y., Eck, P., Kwon, O., Lee, J. H., Chen, S., Corpe, C., Dutta, A., Dutta, S. K. and Levine, M., *J. Am. Coll. Nutr*., **2003**, *22*, 18-35.

[5]Jernov, J., Blount J., Oliveto, E., Perrotta, A., Rosen, P. and Toome. V., *Tetrahedron*, **1979**, *35*, 1483.

[6]Andrews, G. C., Crawford, T., Seib, P. A. and Tolbert, B. M., Ascorbic Acid: Chemistry, Metabolism and Uses, Advances in Chemistry Series 200, *American Chemical Society*, Washington, DC, **1989** pp. 59–79.

[7]Musa, F. H., Mukhlus, A. A. and Sultan, J. S., *J. Ibn-Al-Haitham Pure Appl. Sci.*, **2011**, *24*, 2.

[8]Musa, F. H., Mukhlus, A. A. and Sultan, J. S., *J. Ibn-Al-Haitham Pure Appl. Sci.*, **2012**, *25*, 1.

[9]Fizea, S. M., Musa, F. H. and AL-Bayti, H. A. F., Accepted in *J. Ibn-Al-Haitham Pure Appl. Sci.*, **2013,**

[10]Nakamoto, K., *Infrared and Raman Spectra of Inorganic Coordination Compounds*, 5th Editioin, John Wiley & Sons, **1997**.

[11]Abu-Melha, K. S. and El-Metwaly, N. M., *Transit. Met. Chem*., **2007**, *32*, 828-834.

[12]Huang, J., Quj, Q., Wang, L. F., Liu, Y. Q., Wang, Y. Y., Song, Y. M., Zhang, C. J., Zhau, R., *Chem. Papers*, **2005**, *59*: 267-270.

[13]Pansuriva, P. B. and Patel, M. N., *J. Enzym. Inhib. Med. Chem*., **2008**, *23* (1), 108-19.

[14]Jabs, W. and Gaube, W., *Z. Anorg. Allerg. Chem.*, **1984**, *514*, 179-184.

[15]Wimalasena, K. and Mahindrate, M. P. D., *J. Org. Chem.*, **1994**, *59*, 3427-3432.

[16]Olabisi, O., Mahindrate, M. P. D. and Wimalasena, K., *J. Org. Chem*., **2005**, *70*, 6782-6789.

[17]Yadav, P. N., Demertzis, M. A., Demertzi, D., Skoulika, S. and West, D. X., *Inorg. Chem. Acta.*, **2003**, *349*, 30-36.

[18]Chohan, H. Z., *Synth. React. Inorg. Met. Org. Chem.*, **2001**, *31*, 1.

[19]Jabs, W. and Gaube, W., *Z. anorg. All. Chem.*, **1986**, *538*, 166-176.

[20]Lever, A. B. P., *J. Chem. Ed*., **1968**, *45*, 711.

[21]Lever, A. B. P. *Inorganic Electronic Spectroscopy*, 2nd Edition, Elsevier, Amsterdam, **1984**.

[22]Mohamed, G. G. and Abd El-Wahab, Z. H., *Spectrochem. Acta*, **2005**, A*61*: 1059-1068.

[23]Cotton, F. A. and Willinson, G. *Advanced Inorganic Chemistry*, 4th Edition, John Wiley and Sons, **1980**.

[24]Himanshu, A., Francesc, L. and Rabindranath, M., *Eur. J. Inorg. Chem.*, **2009**, *22*, 3317-3325.

[25]Tohyama, T., Saito, T., Mizumaki, M., Agui, A. and Shimakawa, Y., *Inorg. Chem.*, **2010**, *49*, 2492-2495.

Received: 04.06.2014.
Accepted: 30.08.2014.

LONG TERM STUDY OF FULLERENE $C_{60}^{+\bullet}$ RADICAL CATION BY ELECTRON SPIN RESONANCE (ESR)

Franco Cataldo*[a,b] and Susana Iglesias-Groth[c]

Keywords: electron spin resonance, radical cation, fullerene C_{60}, oleum, near infrared spectroscopy, kinetics

The dissolution of fullerene C_{60} in oleum (fuming sulphuric acid 20 % free SO_3) was followed simultaneously with ESR (Electron Spin Resonance) and NIR (Near Infrared Spectroscopy). It is shown that the intensity of the ESR signal associated to the formation of C_{60} radical cation ($C_{60}^{+\bullet}$) follows the same kinetics as the NIR absoption band at about 938 nm. Thus, the band at about 938 nm represents the optical counterpart of the ESR signal of $C_{60}^{+\bullet}$. After the formation of $C_{60}^{+\bullet}$, the evolution of the ESR spectrum and its optical counterpart in the NIR suggest the formation of other fullerene oxidation products as well. These products were recovered from the oleum solution and analyzed with FTIR and found to be fullerol (hydroxylated derivative of fullerene). The work-up of the oleum solution led to the desulfonation of the substrate. The ESR signal of $C_{60}^{+\bullet}$ in oleum was followed for two weeks. Even after so long time, the ESR signal appeared strong and clear although under slow decay. Thus, the oxidation species of $C_{60}^{+\bullet}$ (polycations, dimers and oligomers of C_{60}, sultonated and sulfated derivatives) are persistent radicals in oleum.

* Corresponding Author
E-Mail: franco.cataldo@fastwebnet.it
[a] Actinium Chemical Research srl, Via Casilina 1626A, 00133 Rome, Italy
[b] INAF – Osservatorio Astrofisico di Catania, Via S. Sofia 78, 95123 Catania, Italy
[c] Instituto de Astrofisica de Canarias, Via Lactea snc, Tenerife, Canary Islands, Spain

Introduction

Fullerene C_{60} is widespread in the Universe[1] as demonstrated by recent discoveries essentially based on the detection of infrared emission bands of this molecule.[2-4] The detection of fullerene in young planetary nebulae and in other astrophysical environments as well as the quantification of its relative abundance in space was made possible thanks to the laboratory studies made on the infrared spectrum of C_{60}, on its derivatives and on the determination of the molar extinction coefficients and integrated molar absorptivities.[6-13]

Although C_{60} has been detected in the infrared in space, its detection in the ultraviolet and in the visible part of the spectrum has not yet been achieved for a number of reasons, including the fact that, especially in the ultraviolet, there are a number of different "carriers" emitting in that spectral region, covering the possible "spectral signature" of C_{60}. On the other hand, it is known that C_{60} in the interstellar medium should be ionized into its radical cation form: $C_{60}^{+\bullet}$.[1,14] The ionization mechanism involves the extraction of one electron from the C_{60} molecule by the action of cosmic rays and it is favored by the relatively low first ionization potential of C_{60} (E_i=7.61 eV). The electronic absorption (and emission) spectrum of $C_{60}^{+\bullet}$ is characterized by the presence of electronic transitions in the near infrared, a spectral region relatively less crowded by the interference of other molecules than in the ultraviolet. In a previous work, we have determined the molar extinction coefficient of the $C_{60}^{+\bullet}$.[15] The radical cation bands are characterized by a molar extinction coefficient ε_{823} = 7500 L cm^{-1} mol^{-1} and ε_{943} = 4570 L cm^{-1} mol^{-1}.[15]

The most typical approach for the synthesis of $C_{60}^{+\bullet}$ involves the high energy irradiation of neutral C_{60} trapped in frozen matrix of helium or neon.[16-19] The advantage of this technique regards the minimization of the so-called "matrix effect" which involves a band shift due to the interaction of the guest molecule with the host matrix. Helium and neon are completely inert matrices and the interaction with the guest radical cation is considered negligible. On the other hand, another approach used to generate radical cations in laboratory involves the use of a superacid medium.[20] The most popular superacid is fuming sulfuric acid (oleum) as solvent and oxidizing medium.[21-30] Alternatively triflic acid and an oxidant[22] or other sophisticated superacids were used successfully.[31,32]

Although the use of superacids as medium for the generation of the radical cations is more practical, there is the problem that the strong interaction of the radical cation with the superacid medium may cause important band shift of the radical cation band transitions in the near infrared and also a limited lifetime of the in situ generated radical cation specie.[15,22,23,31] However, as discussed by us in a earlier paper[15] and as summarized in a review,[31] at least for the $C_{60}^{+\bullet}$ the band shift in the optical spectra by passing from He or Ne matrix to a superacid medium is really small and could be considered as negligible.

The optimal approach for the study of the radical cation species is always the combination of the optical spectroscopy with the electronic paramagnetic resonance (EPR) or electron spin resonance (ESR) spectroscopy. The confirmation of the formation of the radical cation derives exclusively from the ESR signal to which it is associated the optical counterpart in the visible or in the near infrared. Indeed, the first work on $C_{60}^{+\bullet}$ in oleum was made with ESR spectroscopy.[21] Only later, the $C_{60}^{+\bullet}$ in oleum was analyzed by optical spectroscopy.[22] However, also in recent works quite rarely the ESR spectroscopy was applied to $C_{60}^{+\bullet}$ simultaneously with the near infrared (NIR) spectroscopy.[15,23,30]

The present paper is dedicated to the simultaneous investigation of $C_{60}^{+\bullet}$ in oleum both with ESR and NIR. The investigation is not limited to the early minutes of interaction of C_{60} with oleum but it was prolonged for several days after the fullerene dissolution and oxidation with the purpose to verify the stability of $C_{60}^{+\bullet}$ in oleum and eventually to detect its dimerization reaction[25-29] as well as further reactions with the host matrix which involve sultonation and sulfation reactions.

Experimental

Materials and Equipment

C_{60} was obtained from Aldrich (USA) and was 99.5% pure. Oleum (fuming sulphuric acid) 20 % free SO_3 and was obtained from Sigma-Aldrich (Germany).

The near infrared spectra were recorded on Nicolet 6700 FT-NIR spectrometer from Thermo Scientific using a CaF_2 beam splitter. The oleum solution of C_{60} was analyzed in a conventional quartz cuvette having 5 mm path length and sealed with a Teflon stopper.

The mid-FT-IR spectra were recorded on KBr pellets Nicolet 6700 FT-IR spectrometer from Thermo Scientific using a KBr beamsplitter.

The ESR spectra were obtained on a X-band spectrometer from Active Spectrum model Micro-ESR using 2 mm internal diameter quartz capillaries. Each spectrum recorded was the average of 20 scans.

Preparation of the C_{60} solution in oleum

Fullerene C_{60} (8.8 mg) was quickly shaken with oleum (7 g) in a flask with stopcock. After 1 min shaking the heterogeneous solution was pipetted into the ESR capillary tube and the first spectra recorded immediately after the necessary tuning operations of the spectrometer. Simultaneously, the same C_{60} solution in oleum was also studied with the FT-IR spectrometer in the near infrared spectral region.

Recovery of C_{60} oxidation products from oleum

After 15 days of preparation, the above mentioned solution of C_{60} in oleum was poured into 100 ml of distilled water, stirred and left to settle. A brown-orange precipitate was deposited at the bottom of the flask. The water was decanted and new distilled water was added, the mixture was stirred and decanted until neutrality was reached as measured with the pH test paper. Water was decanted again and the residual water was evaporated in a water bath at 80 °C until dryness. About 10 mg of brown-orange product was recovered and studied with FT-IR spectroscopy.

Results and Discussion

Near Infrared (NIR) spectra of $C_{60}^{+\bullet}$

The NIR spectra of $C_{60}^{+\bullet}$ were already shown and discussed in earlier works.[15,22,23] Fig. 1 and 2 show the NIR spectra of $C_{60}^{+\bullet}$ as recorded with the FT-NIR. The spectra are substantially analogous to those recorded in a conventional spectrophotometer. The novelty in the present case is the spectral range covered from 800 to 2000 nm while in the previous works the spectral range analyzed was from 190 to 1100 nm.[15,22,23] However, no additional features were detected above 1100 nm attributable to $C_{60}^{+\bullet}$.

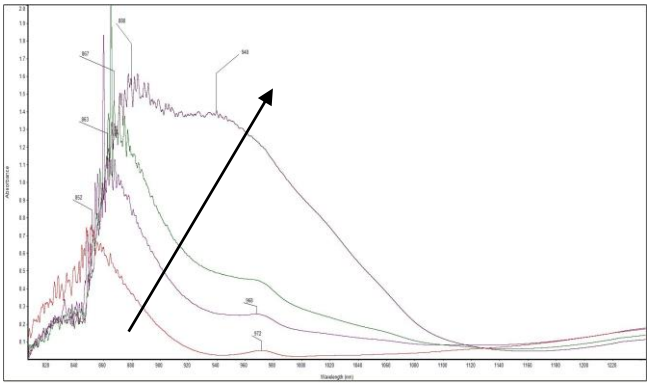

Figure 1. FT-NIR spectrum of $C_{60}^{+\bullet}$ in oleum. The spectra were recorded in the first hour after mixing and are characterized by a steady growth in intensity as shown by the arrow pointing upward.

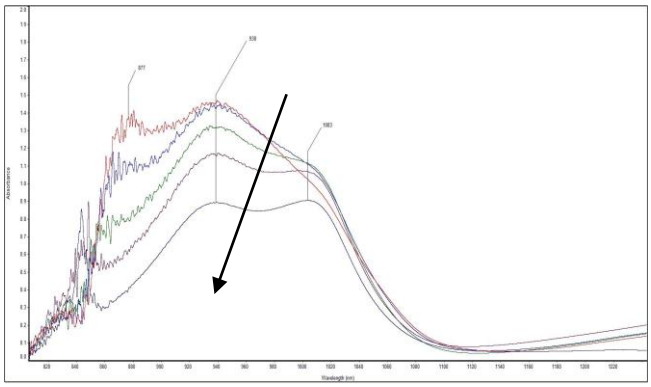

Figure 2. FT-NIR spectrum of $C_{60}^{+\bullet}$ in oleum. The spectral evolution till 5 h after mixing show now a steady decrease in intensity as indicated by the arrow pointing downward. However, after 5 h the two bands at 938 nm and 1003 nm result stable for very long time.

Fig.1 reports a series of spectra recorded in the first hour of mixing. It shows a steady growth in intensity of the absorption bands. There is the steady growth of the absorption band at 852 nm which is shifted at 867 nm and then 880 nm with time. Another weak feature can be observed at about 970 nm. The mixture is not showing a stable spectral pattern. In fact, between the first and the fifth hour after mixing there are further changes as shown in Fig.2. This time the initially fast growing band at 880 nm is disappeared.

The broad band at 970 nm is now decreasing in intensity and can be found at about 938 nm. There is another band at about 1003 nm which is developed at later stages reaching approximately the same intensity of the band at 938 nm. The overall spectral changes are completely in line with earlier results. [15,22,23]

Electron Spin Resonance (ESR) spectra of $C_{60}^{+\bullet}$

As soon as mixed with oleum C_{60} gradually dissolves into the guest matrix giving a green solution. The ESR signal of $C_{60}^{+\bullet}$ can be recorded immediately after mixing as shown in Fig. 3 and the signal grows in intensity for at least the first hour after mixing. Fig. 4 shows the kinetics of growth of the peak-to-peak amplitude of the ESR signal in comparison to the kinetics of optical counterpart recorded in the NIR at about 938 nm and at about 850 nm. In Fig. 4, it is evident that the kinetics of the absorption band at about 938 nm overlaps with the ESR signal, while the other band at about 850 nm is following another destiny. Therefore, the absorption band at about 938 nm must be necessarily assigned to the $C_{60}^{+\bullet}$ while the other band at about 850 nm is instead due to charge-transfer interactions with the solvent as it was previously supposed.[15,22,23]

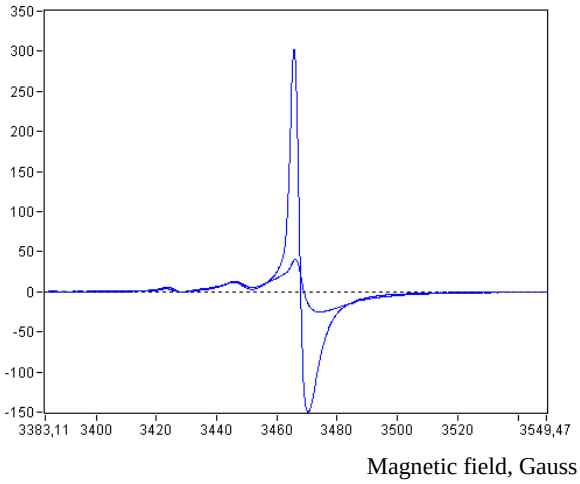

Figure 3. ESR spectra of C_{60} in oleum. The smaller signal was taken 1 min after mixing and the largest signal after 130 min

Fig. 4 provides for the first time the unambiguous assignment of the NIR band at about 938 nm to $C_{60}^{+\bullet}$ and the attribution of the other band at about 850 nm to initial charge-transfer interaction phenomena of C_{60} with the superacid at the beginning of the dissolution. With this interpretation it can be affirmed that at room temperature the C_{60} dissolution in oleum is completed in about 1h.

In Fig. 4 the optical absorption data in the NIR were plotted as $\ln[(Abs)/(Abs)_0]$ against time, where (Abs) is the absorption at a given wavelength taken at any time and $(Abs)_0$ is the absorption at the same wavelength taken at the beginning of the experiment. Similarly, in Fig. 4 the peak-to-peak amplitude of the ESR signal was plotted as $\ln[(ESR)/(ESR)_0]$ against time, where (ESR) is the peak-to-peak amplitude of the ESR signal taken at any time and $(ESR)_0$ is the peak-to-peak amplitude of the ESR signal taken at the beginning of the experiment.

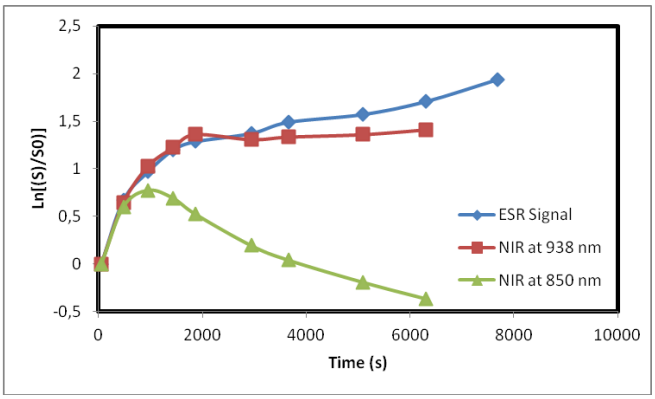

Figure 4. Kinetics of the ESR signal growth in the first two hours after mixing (blue diamonds) and the kinetics of the optical counterpart spectra measured in the NIR. It is evident that the kinetics of the band at about 938 nm (red squares) is practically the same as that of the ESR signal, while the other band at about 850 nm (green triangles) is following another destiny.

The first ESR spectrum of $C_{60}^{+\bullet}$ taken and reported in Fig. 3 shows a *g* value of 2.08632 while the latest spectrum recorded after 2 h shows a *g* value of 1.90344. The main line width of the first ESR spectrum of Fig.3 is 7.8 G and it becomes narrower 4.7 G after 2 h. The line width of the other smaller signal in the left of the main signal are respectively 5.1 and 6.0 G in the first ESR spectrum recorded. The zero-field parameters $|D|$ and $|D/2|$ as defined by Tumanskii et al.[27] were found at 45.24 and 23.37 G respectively. After 2h the $|D|$ and $|D/2|$ parameters were still found at 44.9 and 22.2 G. The ESR spectra of C_{60} in oleum were interpreted in terms of radical cation formation followed by further oxidation which leads to the trication and pentacation.[21] A series of deeper investigations has instead suggested that the radical cation of C_{60} tends dimerize and and oligomerize in oleum leading to the formation of $C_{120}O^+$ and $C_{120}O^{2+}$.[25-29] However, such dimerization/oligomerization reaction occurs when large amounts of C_{60} are dissolved in oleum. Solodovnikov showed that the line width of $C_{60}^{+\bullet}$ when generated in a mixture of toluene/sulphuric acid is about 7 G, was very close to the 7.8 G line width value found in our earlier spectrum (Fig. 3) recorded immediately after the initial dissolution of C_{60} in oleum.[25,27]

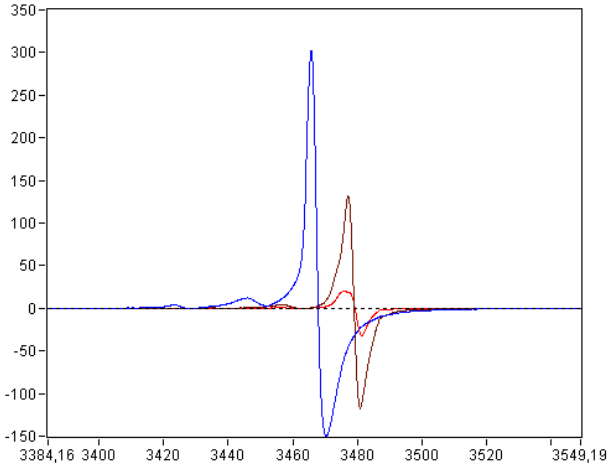

Figure 5. ESR spectra of C_{60} in oleum. The largest signal is the same as Fig. 3 taken after 130 min. The other two signals were taken respectively after 40 h and 110 h.

 DOI: 10.17628/ecb.2014.3.920-924

Till now, nobody has followed the ESR of C_{60} solution in oleum sealed in a capillary quartz tube for a long time. After the initial green-grey color, the C_{60} solution in oleum turns gradually into orange-brown. Fig. 5 shows the ESR spectra of such solution at 40 and 110 h after preparation. Surprisingly after 40 h and beyond, the ESR spectra appear shifted about -11.3 G from the original position. The g factor is now 2.09184 and the main line width is now 3.76 G, thus the signal is narrower than that of the "fresh" sample. The changes of the ESR parameters may suggest that we are dealing with other reaction products. The optical counterpart of the long term experiment of C_{60} in oleum is shown in Fig. 6. The NIR spectrum after 5 days from preparation still shows the absorption bands attributed to $C_{60}^{+\bullet}$ at 920 and 1003 nm. However two new absorption bands at 703 and 775 nm can be observed in Fig. 6 and assigned to other species than $C_{60}^{+\bullet}$.

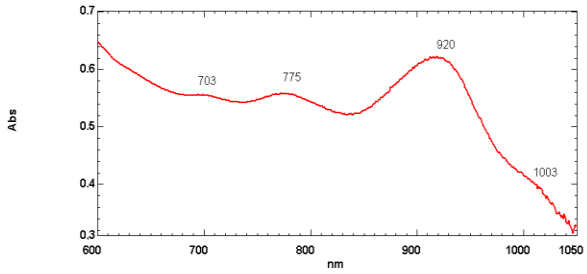

Figure 6. NIR spectrum of C_{60} in oleum after 5 days from preparation.

The long term evolution and decay of the ESR signal (peak-to-peak amplitude) can be followed in Fig. 7. Even after two weeks from the beginning of the experiment the ESR signal is still clearly detected (see also Fig. 5). Fig. 7 suggests that the ESR signal (although weak) could be detected even after 1 month after the preparation.

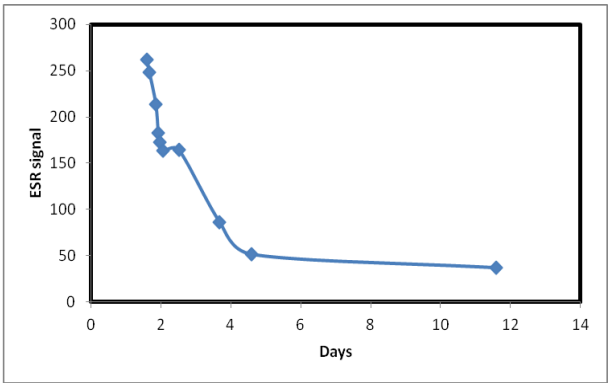

Figure 7. Long term evolution of the ESR signal of C_{60} in oleum.

FT-IR spectroscopy of the C_{60} oxidation product recovered from oleum

When the C_{60} solution in oleum is poured into an excess of water a brown-orange insoluble precipitate is obtained.[24,28,29,35] It is necessary to wash carefully with water to neutrality the precipitate to remove the contamination of residual sulfuric acid.[28,29] The resulting FT-IR spectrum of our sample is shown in Fig. 8 and it is partly similar to that shown by other authors.[28] However, the spectrum of Fig. 8 resembles that of fullerol which is characterized by three main bands at 1595, 1385 and 1085 cm^{-1}.[35] Indeed, the spectrum of Fig. 8 shows three main broad infrared bands at 1626, 1381, 1076 cm^{-1}. This implies that sultonation/sulfation of C_{60} in oleum was a minor reaction.

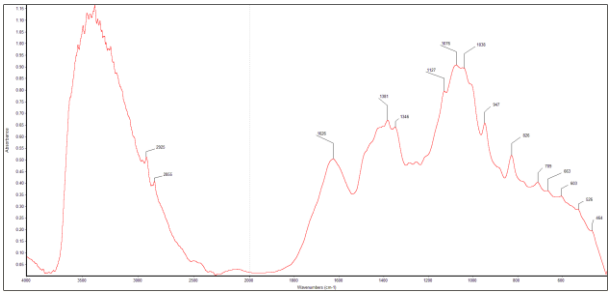

Figure 8. FTIR spectrum of C_{60} oxidation product recoverd from oleum solution

However, Taylor has proposed that the sulfonation followed by hydrolysis leads to fullerol with an almost complete removal of the SO_3H groups.[35] The presence of oxygenated sulfur functionalities in the infrared spectrum can be deduced from the S-O stretching in the asymmetric (1320-1390 cm^{-1}) and in the symmetric mode (1150-1200 cm^{-1}).[36] Fig. 8 is lacking completely the asymmetric stretching mode of S-O group ruling out any important presence of the oxygenated sulfur functionalities. Thus, the precipitate recovered from C_{60} oleum solution is indeed fullerol. The eventual dimeric/oligomeric structure of this product, as suggested by other authors,[28,29] cannot be established on the sole basis of the infrared spectra.

Conclusions

The most important result of the present work is the discovery that the peak-to-peak amplitude of the ESR signal associated to $C_{60}^{+\bullet}$ formed in oleum, grows in intensity with the same kinetic law followed by the optical NIR counterpart band at about 938 nm as shown in Fig. 4. Based on these results it is obvious to associate the 938 nm band with the radical cation of C_{60} species. The other band at about 850 nm observed in the NIR spectrum at the beginning of the dissolution of C_{60} in oleum is correctly assignable to a charge-transfer interaction of C_{60} with oleum in the early stages of its dissolution as already stated previously.[15,22,23]

The formation of $C_{60}^{+\bullet}$ in the first hours of dissolution of C_{60} in oleum is also confirmed by the line width of the ESR spectrum which corresponds to that already reported in literature for this species.[25,27]

The long term interaction (days) of $C_{60}^{+\bullet}$ with oleum causes a shift of the ESR spectrum and changes in the line widths of the spectrum. It is evident that this is due to further reactions of $C_{60}^{+\bullet}$ with oleum which can lead to the formation of polycations[21] or to the formation of oligomers of C_{60} for example of the type $C_{120}O^{+}/C_{120}O^{2+}$.[25-29] This

 DOI: 10.17628/ecb.2014.3.920-924

second hypothesis is corroborated by a quite extensive body of works but does not exclude also the first hypothesis. $C_{60}^{+\bullet}$ or its further oxidation product may undergo in the long term sultonation and sulfation reactions.[33-35] This fact is completely reasonable and expected. Less obvious is the absence of evidences of the S-O symmetric stretching band in the FT-IR spectrum of the C_{60} oxidation product recovered from the oleum solution. According to Taylor,[35] the sulfur-bearing functionalities are released by hydrolysis during the work-up leading to the formation of a fullerol as indeed is suggested by the FT-IR spectrum of Fig. 8.

Even after 2 weeks of the preparation of the C_{60} solution in oleum it is possible to detect a strong and clear ESR signal from the solution. This means that the species derived from $C_{60}^{+\bullet}$ further oxidation (polications, oligomers and sultonated/sulfated derivatives) are then quite stable in oleum. The NIR spectrum after 5 days from preparation still displays the absorption band at 920 nm associable to the $C_{60}^{+\bullet}$. This band is however accompanied by other bands which may account for the presence of other species (see Fig. 6).[1]

References

[1]Kwok, S. "*Organic Matter in the Universe*", **2012**, Wiley-VCH, Weinheim, Germany.

[2]Cami, J., Bernard-Salas, J., Peeters, E., Malek, S. E. *Science*, **2010**, *329*, 1180.

[3]García-Hernández, D. A. Iglesias-Groth, S., Acosta-Pulido, J. A. Manchado, A., García-Lario, P., Stanghellini, L., Villaver, E., Shaw, R. A. and Cataldo, F., *Astrophys. J.*, **2011**, *737*, L30.

[4]García-Hernández, D. A., Villaver, E., García-Lario, P., Manchado, A., Stanghellini, L., Shaw, R. A. and Cataldo, F., 2012, *Astrophys. J.*, **2012**, *760*, 107.

[5]Sellgren, K., Werner, M. W., Ingalls, J. G., Smith, J. D. T.,Carleton, T. M., and Joblin, C., *Astrophys. J. Lett.*, **2010**, *722*, L54.

[6]Cataldo, F., Iglesias-Groth, S. *Monthly Notices Roy. Astronom. Soc.*, **2009,** *400*, 291.

[7]Cataldo, F., Iglesias-Groth, S., "*Fulleranes: The Hydrogenated Fullerenes"*, **2010**, Springer, Dordrecht.

[8]Cataldo, F., Iglesias-Groth, S., Manchado, A., *Fullerenes Nanotubes, Carbon Nanostruct.*, **2009**, *17*, 378

[9]Cataldo, F., Iglesias-Groth, S., Manchado, A., *Fullerenes Nanotubes, Carbon Nanostruct.*, **2009**, *17*, 401.

[10]Cataldo, F., Iglesias-Groth, S., Manchado, A., *Fullerenes Nanotubes, Carbon Nanostruct.*, **2009**, *17*, 414.

[11]Cataldo, F., Iglesias-Groth, S., Manchado, A., *Fullerenes Nanotubes, Carbon Nanostruct.*, **2009**, *17*, 428.

[12]Cataldo, F., Iglesias-Groth, S., Manchado, A., *Fullerenes Nanotubes, Carbon Nanostruct.*, **2012**, *20*, 672.

[13]Cataldo, F., Iglesias-Groth, S., Manchado, A., *Fullerenes Nanotubes, Carbon Nanostruct.***2012**, *20*, 656.

[14]Foing, B. H. and Ehrenfreund, P., *Nature*, **1994**, *369*, 296.

[15] Cataldo, F., Iglesias-Groth, S., Hafez, Y. *Eur. Chem. Bull.*, **2013,** *2*, 1013.

[16]Kato, T., Kodama, T., Shida, T., Nakagawa, T., Matsui, Y., Suzuki, S., Shiromaru, H., Yamauchi, K., Achiba, Y., *Chem.Phys. Lett.*, **1991**, *180*, 446.

[17]Gasyna, Z., Andrews, L., Schatz, P. N., *J. Phys. Chem.*, **1992**, *95*, 1525

[18]Fulara, J., Jakobi, M., Maier, J. P., *Chem. Phys. Lett*., **1993**, *211*, 227.

[19]Fulara, J., Jakobi, M., Maier, J. P., *Chem. Phys. Lett*., **1993**, *206*, 208.

[20]Olah, G. A., Surya Prakash, G. K., Sommer, J., "*Superacids*", **1985**, Wiley, New York.

[21]Kukolich, S. G., Huffman, D. R., *Chem. Phys. Lett*., **1991**, *182*, 263.

[22]Cataldo, F. *Spectrochim. Acta Part A: Mol. Biomol. Spectrosc.*, **1995**, *51*, 405.

[23]Cataldo, F., Iglesias-Groth, S., Manchado, A., *Fullerenes Nanotubes. Carbon Nanostruct.*, **2012**, *20*, 656.

[24]Scharff, P., Bischof, W., Ebinal, S., Ehrhardt, C., Gerken, R., Kaiser, V., Menzel, F., Tanke, C., *Carbon*, **1994**, *32*, 709.

[25] Solodovnikov, S. P. *Russ. Chem. Bull.*, **1998**, *47*, 2302.

[26]Solodovnikov, S. P., Tumanskii, B. L., Bashilov, V. V., Sokolov, V. I., Lebedkin, S. F., Kratschmer, W., *Chem. Phys. Lett*., **1999**, *303*, 387.

[27]Tumanskii, B., Kalina, O. "Radical Reactions of Fullerenes and their Derivatives", **2001**, Kluwer Academic Publishers, Dordrecht pp 164-171.

[28]Garkusha, O.G., Solodovnikov, S. P., Lokshin, B. V., *Russ. Chem. Bull.*, **2002**, *51*, 628.

[29]Garkusha, O. G., Solodovnikov, S. P., Lokshin, B. V., *Russ. Chem. Bull.*, **2003**, *52*, 1688.

[30]Cataldo, F., Iglesias-Groth, S., Manchado, A., *Spectrochim. Acta Part A: Mol. Biomol. Spectrosc.*, **2010**, *77*, 998.

[31]Reed C. A., Bolskar, R. D., *Chem. Rev*., **2000**, *100*, 1075.

[32]Reed, C. A., Kim, K. C., Bolskar, R. D., Mueller L. J., *Science*, **2000**, *298*, 101.

[33]Miller, G. P., Buretea, M. A., Bernardo, M. M., Hsu, C. S., and Fang, H. L. *J. Chem. Soc., Chem. Commun.*, **1994**, 1549.

[34]Canteenwala, T., Patil, S., and Chiang, L. Y., *Synth. Comm.*, **2001**, *31*, 1659.

[35]Taylor, R., **1999**, "*Lecture Notes on Fullerene Chemistry. A Handbook for Chemists*", Imperial College Press, London, .117-121.

[36]Lin-Vien, D., Colthup, N. B., Fateley, W. G., Grasselli, J. G., "*Infrared and Raman Characteristic Frequencies of Organic Molecules*", Academic Press, San Diego, **1991**, 245

Received: 08.08.2014.
Accepted: 02.09.2014.

METABOLISM OF PURINE NUCLEOSIDES AND BASES IN SUSPENSION-CULTURED *ARABIDOPSIS THALIANA* CELLS

Yuling Yin[a], Riko Katahira[b] and Hiroshi Ashihara[c]*

Keywords: Purine nucleotides, Biosynthesis, Salvage, Catabolism, *Arabidopsis thaliana*.

We study the metabolism of purine nucleosides and purine bases in suspension-cultured cells of the model plant *Arabidopsis thaliana*. [8-^{14}C]Adenosine, [8-^{14}C]guanosine, [8-^{14}C]inosine, [8-^{14}C]xanthosine, [8-^{14}C]adenine, [8-^{14}C]guanine, [8-^{14}C]hypoxanthine and [8-^{14}C]xanthine were administered to cells in the cell division phase, and the uptake and metabolic fate of these compounds were monitored for 4 h. The rates of uptake of most purines were within the range 60-70 nmol gFW^{-1}. Xanthine and xanthosine were taken up more slowly. The rate of uptake was ordered as hypoxanthine > adenine > inosine > guanosine > guanine > adenosine > xanthosine > xanthine. A large amount of radioactivity from [8-^{14}C]adenosine, [8-^{14}C]guanosine, [8-^{14}C]adenine and [8-^{14}C]guanine, and a limited amount from [8-^{14}C]inosine and [8-^{14}C]hypoxanthine, was incorporated into nucleotides and RNA. The so-called purine salvage pathways of adenosine, guanosine, adenine, guanine, inosine and hypoxanthine are therefore functional in *A. thaliana*. These tracer experiments also reveal that significant amounts of these compounds were converted to xanthine, and enter the catabolic pathway via allantoin. Neither xanthosine nor xanthine is used in the synthesis of nucleotides and RNA. These compounds are entirely catabolized via allantoin and allantoic acid. Deamination of adenine and guanine rings takes place at the stage of AMP deaminase and guanosine deaminase, respectively. The pattern of purine metabolism in *A. thaliana* is similar to that in other plants. Adenine salvage activity estimated from the metabolism of [8-^{14}C]adenine, the cellular concentration of ATP, and expression of the *APT1* gene encoding adenine phosphoribosyltransferase all increased markedly at the lag phase of cell proliferation. These observations imply that the salvage pathway is important during the early stages of cell culture in *A. thaliana*.

*Corresponding Author
Fax: +81-3-5700-4225
E-Mail: ashihara.hiroshi@ocha.ac.jp
[a] Department of Biotechnology, Dalian Medical University, Dalian 116044, P.R. China
[b] Department of Lifestyle Studies, Kobe Shoin Women's University, Kobe 657-0015, Japan
[c] Department of Biological Sciences, Graduate School of Humanities and Sciences, Ochanomizu University, Tokyo, 112-8610, Japan

Introduction

The purine nucleosides adenosine, guanosine, inosine and xanthosine, and the purine bases adenine, guanine, hypoxanthine and xanthine, are produced by the degradation of purine nucleotides, AMP and GMP. Fig. 1 shows the structures of the purine nucleosides and bases used in this study. Some of these purine compounds are utilized for re-generation of nucleotide synthesis by the salvage pathways; the rest are catabolised by the purine catabolic pathways.[1-3] *Arabidopsis thaliana* is a model plant, for which the genome has been fully sequenced,[4] and it is useful in studying the metabolic function of purine compounds at the molecular level.

Only a few studies on purine nucleoside and purine base metabolism in *A. thaliana* have been carried out to date.[2,3,5-7] Many systematic studies of genomics, proteomics and metabolomics have been undertaken recently in *A. thaliana*,[8] and the present dynamic profiling of *in situ* metabolism of exogenously supplied ^{14}C-purine compounds will shed further light on the overall metabolism of purine compounds *in planta*.

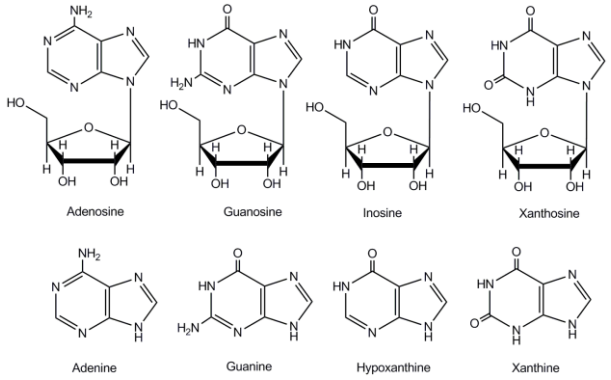

Figure 1. Structures of purine nucleosides and bases.

We have reported the *in situ* metabolism of ^{14}C-purine nucleosides and ^{14}C-purine bases in various plant materials, including cultured cells of *Catharanthus roseus*,[9] *Picea glauca*,[10] *Sonneratia alba*,[11] and *Bruguiera sexangula*,[12] and in tissue segments of *Phaseolus mungo* (=*Phaseolus aureus*),[13] *Solanum tuberosum*,[14] *Coffea arabica*,[15] *Theobroma cacao*[16] and *Camellia sinensis*.[17] Riegler *et al*.[6] recently reported their findings of *in situ* metabolism of [8-^{14}C]inosine and [8-^{14}C]xanthosine in roots of intact *A. thaliana* seedlings, as part of their study on nucleosidases. They argued that *A. thaliana* plants are able to salvage xanthosine for nucleic acid synthesis.[6] This novel finding differs from our previous observations in various plant species. As a result, it is important to determine whether purine metabolism is different in *A. thaliana* and in other plant species, especially because *A. thaliana* is a common model plant.

In the present study, the metabolism of labelled purine compounds was investigated using the culture system of *A. thaliana* which is suitable for our metabolic studies.[18,19] The metabolic fate of four purine ribonucleosides, [8-^{14}C]adenosine, [8-^{14}C]guanosine, [8-^{14}C]inosine and [8-^{14}C]xanthosine and four purine bases, [8-^{14}C]adenine, [8-^{14}C]guanine, [8-^{14}C]hypoxanthine and [8-^{14}C]xanthine, was investigated in the exponential growth phase of cells of *A. thaliana*.

Fluctuations in the *in situ* metabolism of [8-^{14}C]adenine and [8-^{14}C]inosine and the intracellular purine nucleotide level during culture growth were also examined. Finally, the expression of genes that encode enzymes involved in adenine and adenosine salvage was investigated. Our results indicate that the metabolism of purine nucleosides and bases in *A. thaliana* is essentially the same as in other non-purine alkaloid forming plant spices, such as *C. roseus* and *S. tuberosum*.

Materials and Methods

Plant material

Suspension cell-cultures of *A. thaliana*, accession Columbia (Strain T87), were obtained from the Experimental Plant Division of the RIKEN Bioresource Center, Tsukuba, Japan. The cell cultures used in this study are the same as in our previous study on phosphoribosylpyrophosphate synthetase.[18] In the growth experiments, the cells were sub-cultured at 10-day intervals in 25 ml of JPL medium, as in the work of Axelos et al.,[20] which contained 1 mM naphthaleneacetic acid and 1.5 % sucrose, in 100-ml Erlenmeyer flasks. The culture flasks were held on a horizontal rotary shaker (120 strokes min^{-1}, amplitude 80 mm) in a dedicated plant growth room at 22 ºC with a 16 h : 8 h light : dark cycle. Chlorophyll content was determined according to the method of Bruinsma.[21]

Radiochemicals and biochemicals

We obtained [8-^{14}C]adenosine (specific activity 2.0 GBq mmol^{-1}), [8-^{14}C]guanosine (specific activity 1.85 GBq mmol^{-1}), [8-^{14}C]inosine (specific activity 1.92 GBq mmol^{-1}), [8-^{14}C]xanthosine (specific activity 2.07 GBq mmol^{-1}), [8-^{14}C]adenine (specific activity 1.85 GBq mmol^{-1}), [8-^{14}C]guanine (specific activity 1.96 GBq mmol^{-1}), [8-^{14}C]hypoxanthine (specific activity 1.85 GBq mmol^{-1}) and [8-^{14}C]xanthine (specific activity 1.85 GBq mmol^{-1}) from Moravek Biochemicals Inc. (Brea, CA, USA). Standard nucleotides, nucleosides and nucleobases, and biochemicals were purchased from Sigma-Aldrich, St. Louis, Mo, USA.

Administration of ^{14}C-labelled purine nucleosides and bases

Our experimental methods were essentially the same as Ashihara *et al.*[10] Incorporation of radioactivity into purine residues of nucleic acids was examined by the methods of Schmidt and Thannhauser[22] or Schneider,[23] with a slight modification as follows.[14] Suspension-cultured cells (~100 mg fresh weight) and 2 ml culture medium in which the cells had been grown were placed in the main compartment of a 30 ml Erlenmeyer flask. The flask was fitted with a glass tube containing a piece of filter paper impregnated with 0.1 ml of 20 % aq. KOH in a centre well, to collect $^{14}CO_2$. Each reaction was started by adding 10 µl (37 kBq) of [8-^{14}C]purine nucleoside or [8-^{14}C]purine base solution to the main compartment of the flask. The flasks were incubated in an oscillating water bath at 22 ºC.

Extraction of ^{14}C-labelled metabolites

After incubation, the glass tube was removed from the centre well and placed in a 50 ml-Erlenmeyer flask containing distilled water (10 ml). At the same time the cells were harvested by filtration over Miracloth (Calbiochem, La Jolla, CA, USA), washed with distilled water, and frozen with liquid N_2. They were then stored at -80 ºC. $KHCO_3$ that had been absorbed by the filter paper was allowed to diffuse into distilled water overnight, and aliquots of the resulting solution (usually 0.5 ml) were used for the determination of radioactivity.

The frozen cells were extracted with cold 6 % perchloric acid (PCA), using a glass homogenizer. After extraction, the homogenate was centrifuged at 12,000 *g* for 7 min. The resulting supernatant was collected and the precipitate was re-suspended with the same extraction reagent, and the supernatant was collected by centrifuging.

The first and second PCA-soluble fractions were combined and neutralized with 20 % aq. KOH. After brief centrifuging to remove potassium perchlorate, the samples were lyophilized overnight. For analysis of nucleic acids, the PCA-insoluble materials were extracted successively with a mixture of ethanol and diethylether (1:1, v/v) at 50 °C for 15 min. The ethanol and diethylether mixture insoluble fraction was hydrolysed with 0.3 M aq. KOH at 37 °C for 18 h, and adjusted to pH 2 with 6 M HCl. After centrifuging of the mixture at 10,000 *g* for 5 min, we collected the supernatant (RNA hydrolysates). DNA in the precipitate was hydrolysed with 6 % PCA at 100 °C for 20 min. Because the incorporation of radioactivity into the DNA fraction was negligible during the short incubation period (4 h), then, in order to simplify the methods, RNA and DNA were simultaneously hydrolysed with 6 % PCA at 100 °C for 20 min in some experiments.[23]

Analysis of ^{14}C-labelled metabolites

The PCA-soluble metabolites and hydrolysates of nucleic acids were neutralised, concentrated and loaded on microcrystalline cellulose TLC plates (Merck, Darmstadt, Germany) suitable for TLC analysis of ^{14}C-metabolites. The solvent systems used were (I) *n*-butanol–acetic acid–water (4:1:2, v/v/v) and (II) distilled water.[24,25]

The radioactivity of liquid samples was determined using a multi-purpose scintillation counter (Type LS 6500; Beckman, Fullerton, Calif., USA) with a liquid scintillation fluid ACS-II (GE Healthcare, Tokyo, Japan). Distribution of the radioactive spots of ^{14}C-metabolites on the TLC plate was determined using a Bio-Imaging Analyzer (FLA-2000, Fuji Photo Film Co. Ltd., Tokyo, Japan). Incorporation of radioactivity into individual metabolites was calculated from the total radioactivity of the liquid samples measured by the scintillation counter, and the % distribution of radioactivity on the plate obtained from the bio-imaging analyzer.

Determination of ATP and GTP

Nucleotides were extracted from *A. thaliana* cells (~500 mg fresh weight) and were analysed using an anion exchange column, Shim-pack WAX-1 (Shimadzu Corporation, Kyoto, Japan), as detailed in Ashihara et al.[26], with slight modifications. The freshly harvested cells were homogenized in chilled 6 % PCA with a glass homogeniser. The homogenates were centrifuged at 20,000 *g* for 20 min at 2 ºC, and the supernatant was collected and neutralized with 20 % aq. KOH. After brief centrifuging to remove potassium perchlorate, the samples were lyophilised. The dried samples were dissolved in the solvent for HPLC and filtered using disposable syringe filter units. Aliquots of 10–50 µl were taken for HPLC using a LC 10A HPLC system (Shimadzu Corporation, Kyoto, Japan). The absorbance at 260 nm was monitored using a Shimadzu Diode Array Detector, type SPD-M10A. Experiments to assess recovery were performed in parallel with all assays. To do this, known quantities of standard were added to the extraction medium in one member of each pair of duplicate samples prior to homogenisation. Recovery of standards usually exceeded 90 %. Some loss of ATP and GTP was observed when the cells were frozen with liquid nitrogen and stored in a deep-freezer at -80 ºC for a month. As a result, all assays were performed using freshly harvested cells and were completed on the same day.

Semi-quantitative RT-PCR

Total RNA was extracted from cells of *A. thaliana* at various stages of growth, as in our previous paper.[19] DNA-free total RNA was used for first strand cDNA synthesis. The reaction mixture (50 µl) contained 62.5 U of MuLv reverse transcriptase (Applied Biosystems, Foster City, CA, USA) and 1 mM oligo-d(T)16. The PCR reaction mixture (25 µl) contained 40 ng cDNA and 12.5 µl GoTaq Green mastermix (Invitrogen, Carlsbad, CA, USA). PCR amplification was performed according to the following program: 94 °C for 5 min, followed by 30 cycles at 94 °C for 30 s, 55 °C for 30 s, 72 °C for 30 s and final extension at 72 °C for 7 min. The reaction product was visualised under UV light on 1 % agarose gels stained with SYBR Green I (Takara Bio Company, Tokyo, Japan), using a luminescent image analyzer (LAS-3000, Fuji Film, Tokyo, Japan). The primers for *APT* and *ADK* were designed using the Primer 3 program (http://frodo.wi.mit.edu/cgi-bin/primer3/primer3 www.cgi).The primers used in this study were as follows:

APT1 (GenBank accession no. At1g27450):
5′-ACCGTTCAACCACCTCACTC-3′ and
5′-AAAGGCCTCAGTGTCGAGAA-3′;

APT2 (At1g80050):
5′-GGGAGACCCGAGATTAAAGG-3′ and
5′-AACGAACTTGGCACCTATGG-3′;

APT3 (At4g22570):
5′-GATCCGTGTCGTTCCAGATT-3′ and
5′-ACGAGCCTCTATTCCTGCAA-3′;

APT4 (At4g12440):
5′-TCGTTCCAGATTTTCCCAAG-3′ and
5′-CCGGCAATTTCTTTGGTTTA-3′;

APT5 (At5g11160):
5′-TGTCGTTGCTGGAGTTGAAG-3′ and
5′-CAATGATAATGACGCGTTCG-3′;

ADK1 (At3g09820):
5′-GCCTGCCGTACATGGACTAT-3′ and
5′- AGCTTCTCTTTGGGGAGAGG-3′;

ADK2 (At5g03300):
5′-AAAACTGGGCATTGGTTGAG-3′ and
5′-GGCAAGAACTTCTCCTGCAC-3′;

Actin-2 (At3g18780):
5′-TGCCAATCTACGAGGGTTTC-3′ and
5′-TTCTCGATGGAAGAGCTGGT-3′.

Results

Profile of the proliferation of *A. thaliana* cells in suspension-culture

Growth of a suspension culture of *A. thaliana*, together with the concentration of chlorophyll during culture, is shown in Fig. 2. In general, following inoculation of suspension-cultured starved plant cells into the fresh culture medium, the cells undergo synchronous growth, as well as synchronous uptake and utilisation of the constituents of the medium.[1,27,28] The changing growth pattern of *A. thaliana* cells is essentially the same as that observed in culture cells of *Catharanthus roseus* (=*Vinca rosea*),[28] *Acer pseudoplatanus*,[29] *Datura innoxia*[30] and *Lotus japonicus*.[31]

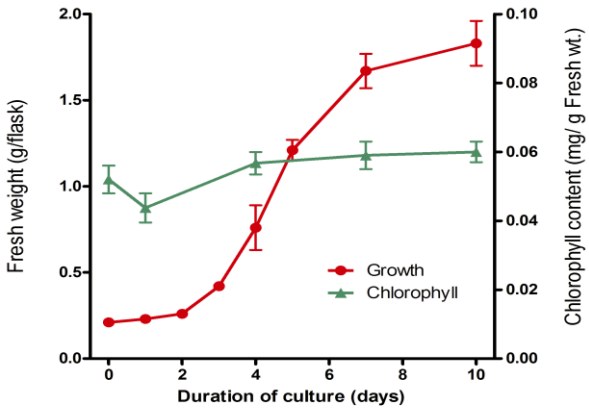

Figure 2. Fluctuations of fresh weight and chlorophyll content during growth of suspension-cultured *A. thaliana* cells. Fresh weight (g) is shown per culture, and the concentration of chlorophyll (mg) is expressed per g FW. Mean values and *SD* are shown.

When 10-day-old *A. thaliana* cells were transferred into the fresh culture medium, their fresh weight began to increase after a 2-day lag. Exponential growth began at day 3 and continued to day 7. After day 7, growth had reached the stationary phase. The chlorophyll concentration remained almost constant during culture, although a slight decrease was observed in the early lag phase of cell growth (Fig. 2).

In the present study, comparison of the metabolism of eight purine compounds was made using cells in the early-exponential phase (day 4). To determine whether the profile of the purine metabolism is changed during culture, we compared the metabolism of [8-^{14}C]adenine and [8-^{14}C]inosine in cells collected at days 0, 1, 4, 7, and 10. These cells are correspond to the initial-phase, the lag-phase, the cell division-phase, the cell expansion-phase and the stationary phase cells reported in the suspension culture of *C. roseus*.[28]

Uptake of [8-^{14}C]purine nucleosides and [8-^{14}C]purine bases by *A. thaliana* cells

Total uptake of precursors by the cells was calculated by adding the radioactivity found in PCA-soluble and PCA-insoluble fractions and CO_2. The purine nucleosides and bases were taken up by *A. thaliana* cells at differing rates during 4 h incubation time (Fig. 3).

Hypoxanthine was taken up fastest by the cells (84.0 nmol gFW^{-1}). Adenosine, guanosine, inosine, adenine and guanine were taken up at between 59 and 68 nmol gFW^{-1}. A relatively slow rate of uptake was found in xanthine (34 nmol gFW^{-1}) and xanthosine (41 nmol gFW^{-1}). The uptake rate was in the order hypoxanthine > adenine > inosine > guanosine > guanine > adenosine > xanthosine> xanthine (Fig. 3).

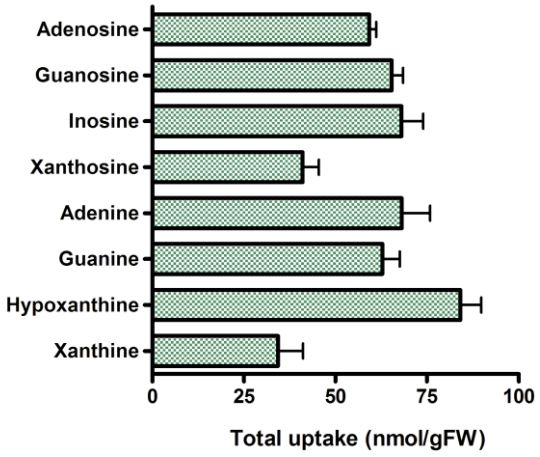

Figure 3. Uptake of [8-^{14}C]purine nucleosides and bases by 4-day-old cultured cells of *A. thaliana*. Incubation with labelled compounds took place for 4 h. The total uptake was calculated by summation of the radioactivity found in all cellular metabolites and CO_2. Uptake of purine compounds is expressed as nmol per g FW cells. Mean values and *SD* are shown.

***In situ* metabolism of [8-^{14}C]purine nucleosides**

To study the metabolic pathways of purine nucleosides in *A. thaliana*, the metabolic fate of [8-^{14}C]adenosine, [8-^{14}C]guanosine, [8-^{14}C]inosine and [8-^{14}C]xanthosine was investigated using 4-day-old *A. thaliana* cells (Fig. 4). After 4-h incubation the radioactivity from [8-^{14}C]nucleoside was found in salvage products (purine nucleotides and RNA), purine bases and/or catabolites (allantoin, allantoic acid, other unidentified catabolites and CO_2). Less than 20 % of the radioactivity was retained in unmetabolized ^{14}C-precursors.

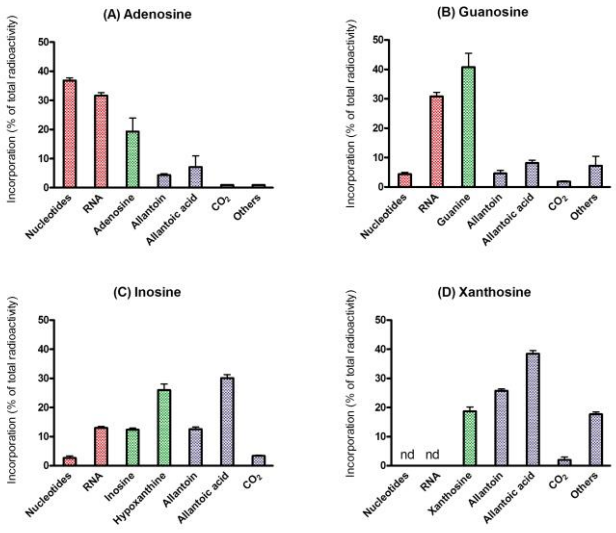

Figure 4. Metabolic fate of [8-^{14}C]adenosine (A), [8-^{14}C]guanosine (B), [8-^{14}C]inosine (C) and [8-^{14}C]xanthosine (D) in 4-day-old cultured cells of *A. thaliana*. The incubation time was 4 h. All detectable ^{14}C-metabolites are shown. The others are a few unidentified metabolites, possibly catabolites. The distributions of radioactivity are expressed as a percentage of the total radioactivity taken up by the samples ± *SD*. Red, green and blue bars respectively indicate salvage products, nucleoside and bases, and catabolites.

A. thaliana cells have different ability to form purine nucleotides from the four purine nucleosides. Radioactivity from [8-^{14}C]adenosine, [8-^{14}C]guanosine and [8-^{14}C]inosine was incorporated into the salvage compounds (nucleotides and RNA), but no incorporation from [8-^{14}C]xanthosine was observed (Fig. 4). Much of the radioactivity from [8-^{14}C]adenosine was incorporated into nucleotides (37 %) and RNA (32 %) (Fig. 4A). In RNA, the most radioactivity from [8-^{14}C]adenosine was recovered in adenine residues of RNA (74 %), and the rest was in guanine residues (26 %). These results suggest that adenosine is converted to AMP. A portion of AMP is converted to ATP or to GTP and then incorporated into RNA. Although 35 % of radioactivity from [8-^{14}C]guanosine was found in the salvage products, only 4 % was detected in nucleotides, and the rest (31 %) was found in guanine residues of RNA. This implies that guanosine is converted to GMP, and then GTP is formed via GDP. The smaller pool size of guanine nucleotides probably corresponds to weak distribution of ^{14}C in nucleotides. Conversion of GMP to adenine nucleotides appears to be negligible.

Only limited salvage ability of [8-^{14}C]inosine was observed. The radioactivity was found in nucleotides (3 %) and RNA (13 %) (Fig. 4C). In RNA, the radioactivity was distributed mainly in guanine residues (82 %), and the rest (18 %) was in adenine residues. In contrast to the three other purine nucleosides, neither nucleotides nor RNA were labelled when [8-^{14}C]xanthosine was administered to *A. thaliana* cells (Fig. 4D). This implies that the cells have no xanthosine salvage capability.

Considerable amounts of ^{14}C-labelled purine nucleosides and bases were found when cells were incubated with [^{14}C]nucleosides for 4 h (Fig. 4 A-D). In the case of [^{14}C]adenosine and [^{14}C]xanthosine, these nucleosides remained unaltered (Fig. 4A and 4D). [^{14}C]Guanosine was completely converted to guanine, (Fig. 4B) and some [^{14}C]inosine (Fig. 4C) was converted to hypoxanthine. This indicates high hydrolytic activity of guanosine and inosine in *A. thaliana* cells.

Radioactivity from the four [8-^{14}C]nucleosides was incorporated into allantoin, allantoic acid and CO_2. Small amounts of the radioactivity were also detected into other unidentified metabolites, possibly catabolites of allantoic acid (Fig. 4). For [8-^{14}C]adenosine and [8-^{14}C]guanosine, only limited amounts of radioactivity were recovered in these catabolites (Figs. 4A and 4B). In contrast, more than half of the total radioactivity from [8-^{14}C]inosine was found in hypoxanthine (26 %) and its catabolites, allantoin (13 %), allantoic acid (30 %) and CO_2 (3 %) (Fig. 4C). All radioactivity from [8-^{14}C]xanthosine metabolized by the cells was observed in catabolites. Nearly 65 % of the radioactivity was incorporated into ureides, specifically allantoin and allantoic acid (Fig. 4D). During the 4 h of the experiment, release of $^{14}CO_2$ from [8-^{14}C]purine nucleosides was only 1-3 % of the total radioactivity taken up by the cells.

In situ metabolism of [8-^{14}C]purine bases

We examined the metabolic fate of the four purine bases, [8-^{14}C]adenine, [8-^{14}C]guanine, [8-^{14}C]hypoxanthine and [8-^{14}C]xanthine in *A. thaliana* cells (Fig. 5). The metabolic profiles of these four purine bases are similar to those of the corresponding nucleosides (Fig. 4). Radioactivity from [8-^{14}C]adenine (58 %), [8-^{14}C]guanine (36 %) and [8-^{14}C]hypoxanthine (17 %) was incorporated into the salvage products (nucleotides and RNA), but no radioactivity was detected from [8-^{14}C]xanthine in the salvage products.

In RNA, the radioactivity from [8-^{14}C]adenine was mainly distributed in adenine residues (72 %), and the rest (28 %) was distributed in guanine residues, whereas radioactivity from [8-^{14}C]guanine and [8-^{14}C]hypoxanthine was extensively incorporated into guanine residues. This observation suggests that adenine is converted mainly to AMP, whereas guanine and hypoxanthine are used for the synthesis of GMP and IMP, respectively. As stated above, some AMP and GMP are converted to nucleoside triphosphate and are incorporated into RNA. No radioactivity from [8-^{14}C]hypoxanthine was recovered in the adenine residues of RNA. This implies that IMP derived from hypoxanthine is utilized preferentially in GMP synthesis, and conversion to AMP is very limited.

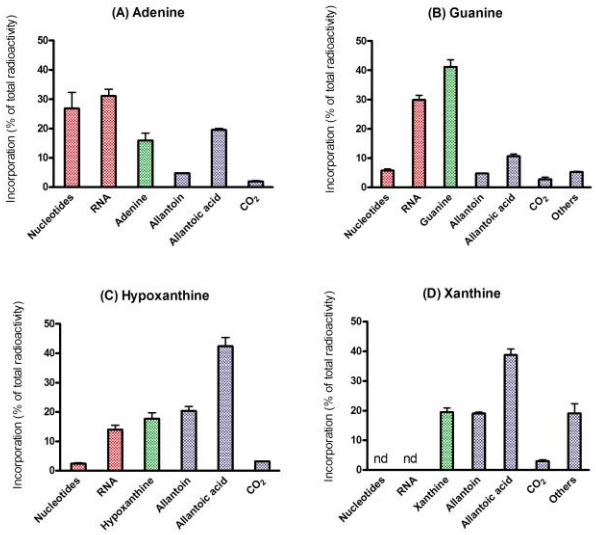

Figure 5. Metabolic fate of [8-^{14}C]adenine (A), [8-^{14}C]guanine (B), [8-^{14}C]hypoxanthine (C) and [8-^{14}C]xanthine (D) in 4-day-old cultured cells of *A. thaliana*. The incubation time was 4 h. All detectable ^{14}C-metabolites are shown. The others are a few unidentified metabolites, possibly catabolites. The distributions of radioactivity are expressed as a percentage of the total radioactivity taken up by the samples ± *SD*. Red, green and blue bars respectively indicate salvage products, nucleoside and bases, and catabolites.

All four purine bases were catabolised, and radioactivity was observed, in allantoin and allantoic acid, and in some cases in other catabolites (Fig. 5). Catabolic activity of hypoxanthine and xanthine was greater than that of adenine and guanine. Radioactivity was always higher in allantoic acid than in allantoin. The rate of $^{14}CO_2$ released from [^{14}C]purine bases during 4 h incubation corresponds to only 2-3 % of the total radioactivity.

Patterns in the metabolic fate of [8-^{14}C]adenine and [8-^{14}C]inosine during growth

[8-^{14}C]Adenine and [8-^{14}C]inosine have been used in several studies to determine the function of purine metabolism accompanied by growth and development of plant cells. They are suited to these studies because adenine metabolism is closely related to the status of the cellular energy metabolism and to the requirement of nucleic acid synthesis, and inosine metabolism is an indicator of the potential for catabolic activity of purine compounds.[32-35]

To study the profile of purine salvage and degradation during growth of *A. thaliana* cells, we monitored the metabolic fate of [8-^{14}C]adenine and [8-^{14}C]inosine 4 h after the labelled precursors had been administered to cells at different growth stages (Fig. 6). The greatest incorporation of radioactivity from [8-^{14}C]adenine into RNA was observed in cells in the lag phase (day 1), after which the rate of incorporation gradually decreased. The adenine residues of RNA are always heavily labelled (63-73 % of radioactivity recovered in RNA), more so than guanine residues (Fig. 7). In contrast, incorporation into nucleotides was high during the first 4 h after transfer of the stationary phase cells. Radioactivity in nucleotides decreased rapidly on day 1, and then increased gradually. The patterns of incorporation into

RNA and nucleotides were mirror images of each other. Incorporation of [8-^{14}C]adenine into ureides took place during the entire culture period, and radioactivity in allantoic acid (9.4–21.5 %) was always higher than in allantoin (2.3–6.7 %) (Fig. 6A).

RNA synthesis from [8-^{14}C]inosine is also observed. The highest incorporation was found in the cells at day 1 (Fig. 6B)**,** and 80-89 % of radioactivity in RNA was recovered in the guanine residues at every stage of growth (Fig. 7). Incorporation of radioactivity from [8-^{14}C]inosine into the nucleotides was extremely low (1.0-5.2 %), in contrast to [8-^{14}C]adenine. The highest rate of catabolism was observed in the first 4 h of inoculation, in which nearly 70 % of total radioactivity was recovered as catabolites.

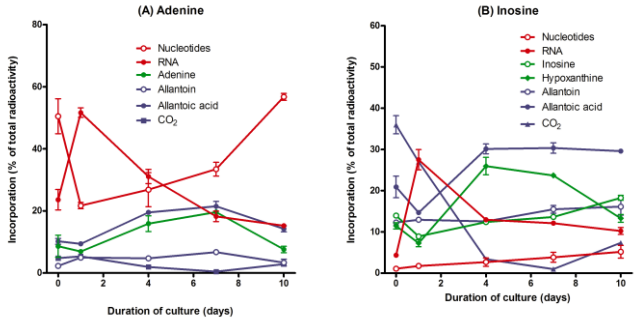

Figure 6. Metabolic fate of [8-^{14}C]adenine (A) and [8-^{14}C]inosine (B) in suspension cultured *A. thaliana* cells at distinct growth phases. Labelled compounds were administered to the 0, 1, 4, 7 and 10-day-old cells and incubated for 4 h. The distribution of radioactivity is expressed as % of total radioactivity taken up by the cells. All detectable ^{14}C-metabolites are shown. Mean values and *SD* are stated. Red, green and blue lines respectively indicate salvage products, nucleoside and bases, and catabolites.

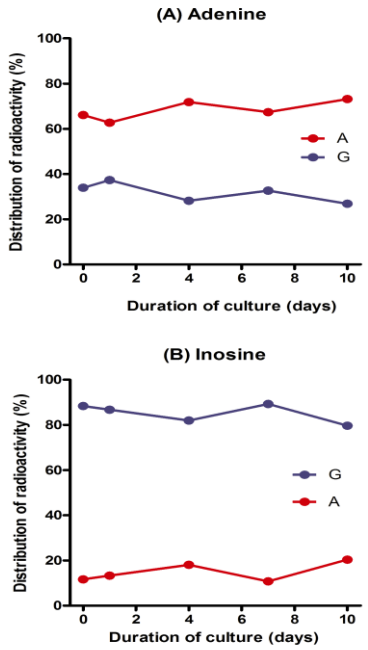

Figure 7. Incorporation of radioactivity from [8-^{14}C]adenine (A) and [8-^{14}C]inosine into the adenine and guanine residues of RNA in suspension-cultured *A. thaliana* cells at different growth phases. The distribution of radioactivity is expressed as % of radioactivity of RNA. Mean values and *SD* are shown.

Large amounts of $^{14}CO_2$ were released in the first two stages of culture, but this activity decreased rapidly 4 days after culture, coinciding with high radioactivity of allantoic acid (Fig. 6B).

Changes in ATP and GTP content during growth

The ATP and GTP content per culture flask increased at first 1 day after culture. A more prominent increase took place during days 4 to 7 (Fig. 8). The concentration of ATP and GTP expressed per g fresh weight increased markedly on the first day after transfer of the cells to the fresh medium (38.4 to 91.4 nmol gFW^{-1} for ATP and 9.3 to 22.1 nmol gFW^{-1} for GTP).

It decreased and remained almost constant (35.2-38.4 nmol gFW^{-1} for ATP and 7.3-11.4 nmol gFW^{-1} for GTP) until the end of the experiment (Fig. 8). The pool size of ATP was always 3-5 times larger than that of GTP. Since no visible increase in fresh weight was found on the first day of culture, there must be a net increase in ATP and GTP per cell. In *C. roseus* the highest concentration of ATP and GTP was also observed in the lag phase of cells.[36,37]

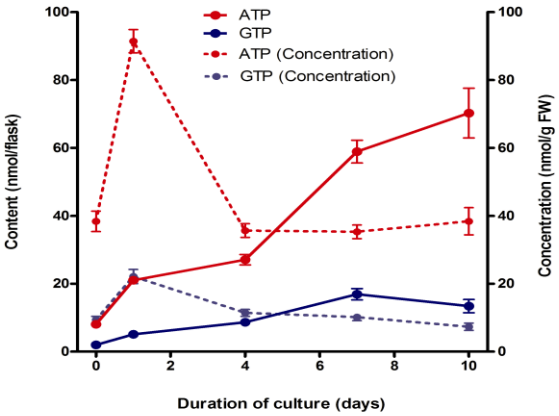

Figure 8. Fluctuation of the intracellular ATP and GTP during growth of *A. thaliana* cells in suspension culture. The nucleotide contents and concentrations are expressed as nmol flask^{-1} and nmol gFW^{-1}. Mean values and *SD* are shown.

Changes in levels of *APT* and *ADK* transcripts

The genome of *A. thaliana* contains five sequences specified as encoding adenine phosphoribosyltransferase, *APT1-APT5*. Adenine phosphoribosyltransferase catalyzes the conversion of adenine to AMP. This enzyme also catalyzes the formation of cytokinin riboside from cytokinin and PRPP. Allen *et al.*[38] have cloned *APT1*, *APT2* and *APT3*, and utilized over-expression in *E. coli* so as to compare kinetic properties for adenine and three cytokinin substrates (zeatin, isopentenyladenine, benzyladenine). The results suggest that *APT1* is involved in the conversion of adenine to AMP, while *APT2* and *APT3* are likely to participate in cytokinin interconversion. There is evidence for the expression of *APT1-APT*3, but no ESTs specific for *APT4* or *APT5* have been identified. Expression of *APT1* increased after cells were transferred to new medium, and the maximum expression was observed in the early-exponential phase (day 4), after which it decreased, whereas *APT 2* and *APT 3* were constitutive (Fig. 9).

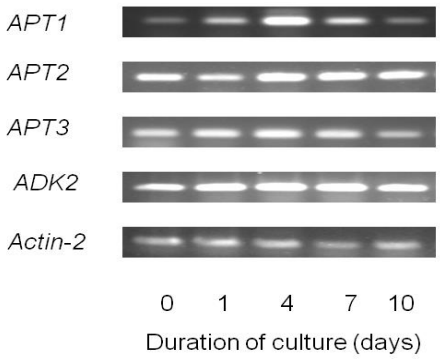

Figure 9. Expression of genes encoding adenine phosphoribosyltransferase (*APT1*, *APT2* and *APT3*) and adenosine kinase (*ADK2*) in suspension cultured *A. thaliana* cells, at different growth stages. Transcripts of *Actin-2* are also shown as standards.

The genes *ADK1* and *ADK2*, encoding two isoforms of adenosine kinase, have been isolated from *A. thaliana*.[39] In intact plants, *ADK1* expression was high in flowers, stems and roots, and *ADK2* expression was greatest in leaves.[39] In the present study using cultured cells, clear constitutive expression was observed only for *ADK2* (Fig. 9). For *ADK1* an ambiguous expression profile was detected (data not shown).

Discussion

Transport of purine nucleosides and bases

We have found that uptake of xanthosine and xanthine was slower than for other purine nucleosides and purine bases in several plant materials, including leaf disks of cacao,[16] slices of potato tubers,[14] and leaf and root segments of tea seedlings.[17] Although we have not carried out detailed kinetic studies of the uptake of these purine compounds here, our results from rather short-duration experiments clearly indicate the presence of substrate-specific transporters for certain nucleosides and bases in plants. Two types of nucleoside transporter, equilibrative and concentrative, have been postulated, but only equilibrative nucleoside transporters have been identified in *A. thaliana*.[40] Recently, Riegler *et al.*[6] reported that roots of *A. thaliana* seedlings took up [8-^{14}C]inosine and [8-^{14}C]xanthosine at almost the same rate (~57 nmol gFW^{-1}) after 48 h-incubation. It is possible that the discrepancy between Riegler's results and our own is due to the incubation time. Our results were obtained using the shorter incubation time during which uptake was linear throughout.

Possible salvage of purine nucleosides and bases in *A. thaliana*

From the *in situ* ^{14}C-tracer experiments (Figs. 4 and 5) and the information obtained from our previous enzymatic studies of potato tubers[14] and tea leaves,[17] pathways of purine salvage in *A. thaliana* can be proposed. Possible metabolic pathways are shown in Fig. 10. Adenosine is exclusively salvaged to AMP by adenosine kinase (EC 2.7.1.20, step 1), and guanosine and inosine are respectively converted to GMP and IMP by inosine/guanosine kinase (EC 2.7.1.73, step 2). Non-specific nucleoside phosphotransferase (EC 2.7.1.77, step 14) may also be involved in these reactions in plant cells.[14]

In situ inosine salvage activity was less than for guanosine salvage (Fig. 4B, 4C), although the step is catalyzed by the same enzyme, inosine/guanosine kinase (EC 2.7.1.73, step 2). Since this enzyme catalyzes the formation of nucleotides from inosine and guanosine at a similar rate,[14] the lesser inosine salvage may be due to the high catabolic activity of inosine.

Unlike the other purine nucleosides, xanthosine salvage is not evident in our ^{14}C-tracer experiments (Fig. 4). No xanthosine kinase has been detected in plants, and plant (non-specific) nucleoside phosphotransferase (EC 2.7.1.77) cannot use xanthosine as a substrate.[14] Riegler *et al.*[6] reported active xanthosine salvage for RNA synthesis in intact seedlings of *A. thaliana*, however, in which 14 % of the total radioactivity from [8-^{14}C]xanthosine was recovered in the RNA fraction. The results of Riegler *et al.*[6] also differed from our previous results using disks of potato tubers[14] and leaf disks of cacao[16] and tea.[17] Riegler *et al.*[6] suggested that the discrepancy between our results and theirs arose from the difference in experimental conditions; they used intact seedlings which more closely resembled natural situations, whereas we used artificial excised tissues. To see whether our previous results using excised tissues reflect purine metabolism *in planta*, we therefore studied (in an earlier paper[41]) the metabolism of [8-^{14}C]xanthosine in intact mungbean seedlings. We found no significant salvage of xanthosine to RNA, even in intact plants. We therefore supposed that low xanthosine salvage in plants is probably due to the different plant species used, and almost certainly not due to the excision of the tissues. The present results indicate that xanthosine salvage does not occur in *A. thaliana* cells, however. Presumably the discrepancy is due to differences in experimental procedure. As described elsewhere,[41] the RNA used by Riegler *et al.* may include some contaminants; they did not confirm the radioactivity in the purine residues of RNA.[6] Slow salvage and rapid catabolism of xanthosine appear to be inherent properties of many plant species.

Of the purine bases, adenine, guanine and hypoxanthine are salvaged by adenine phosphoribosyltransferase (EC 2.4.2.7, step 3), and by hypoxanthine/guanine phosphoribosyltransferase (EC 2.4.2.8, step 4). These purine bases are usually not salvaged by purine nucleoside phosphorylase (EC 2.4.2.1, step 18), as this enzyme was not detected in many other plant materials.[1,14] In the present study, we detected no xanthine salvage in *A. thaliana* cells (Fig. 5D). No activity of xanthine phosphoribosyltransferase is detectable in potato tuber extracts,[14] but low levels of activity have recently been found in tea leaf extracts.[17] Activity of guanine/xanthine phosphoribosyltransferase and hypoxanthine/guanine/xanthine phosphoribosyltransferase has also been reported in *Escherichia coli* [42] and in some parasites.[43,44] Theoretically, therefore, xanthine salvage may be possible. However, ^{14}C-tracer experiments strongly suggest that xanthine is catabolised predominantly by the oxidative purine ring catabolic pathway, and that virtually no xanthine salvage for XMP synthesis occurs in *A. thaliana*.

Possible catabolic pathways of purines

Our tracer experiments suggest that an oxidative purine degradation pathway is active in *A. thaliana* cells **(**Figs. 4 and 5**)**. As Fig. 10 shows, the first distinct step in purine

catabolism is the xanthine dehydrogenase reaction (EC 1.1.1.204, step 20). There are several routes for producing xanthine from other purine compounds in plants. Exogenously supplied adenosine and adenine are not directly deaminated to inosine and hypoxanthine, because plant cells contain neither adenosine deaminase (step 16) nor adenine deaminase (step 19).[1] Consequently adenosine and adenine are first salvaged to AMP and then converted to xanthine via IMP (steps 12, 13, 15 and 20) or via XMP (steps 12, 10, 13, 15). Deamination of the adenine structure is performed by AMP deaminase (EC 3.5.4.6, step 12). In contrast, inosine and xanthosine are hydrolyzed to their respective purine bases by inosine/guanosine nucleosidase (EC 3.2.2.2, step 15). Guanosine is deaminated to xanthosine by guanosine deaminase (EC 3.5.4.15, step 17), and xanthosine is hydrolyzed to xanthine (15). Guanine deaminase (EC 3.5.4.3, step 21) has been found in tea leaves,[45] but was not detected in potato tubers.[14] Recent molecular biological studies indicate that guanosine deaminase is required for the generation of xanthosine in *A. thaliana*.[46] At least in *A. thaliana*, catabolism of guanine is therefore performed after guanine has been salvaged to GMP (step 4). A pathway GMP → guanosine → xanthosine → xanthine (steps, 13, 17, 15) is the major path for guanine nucleotide catabolism in *A. thaliana*.[46]

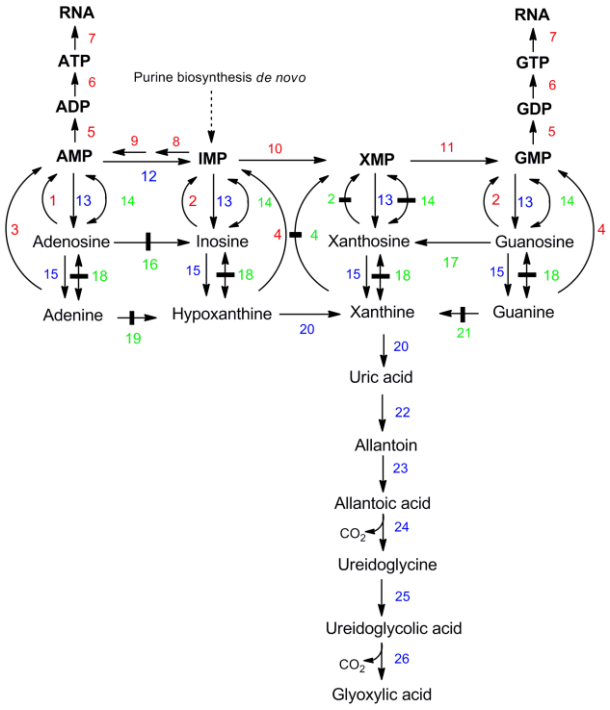

Figure 10. Metabolic pathways of purine compounds in *A. thaliana* cells estimated from the fate of exogenously supplied [8-^{14}C]purine nucleosides and [8-^{14}C]purine bases. The numbers show the enzymes participating in individual reactions. Arrows broken with a vertical bar represent reactions which are not present in *A. thaliana*. Enzymes: 1, adenosine kinase; 2, inosine/guanosine kinase; 3, adenine phosphoribosyltransferase; 4, hypoxanthine/guanine phosphoribosyltransferase; 5, nucleoside monophosphate kinase; 6, nucleoside diphosphate kinase; 7, RNA polymerase; 8, adenylosuccinate synthetase; 9, adenylosuccinate lyase; 10, IMP dehydrogenase;11, GMP synthetase; 12, AMP deaminase; 13, 5'-nucleotidase; 14, nucleoside phosphotransferase; 15, adenosine nucleosidase and/or inosine-guanosine nucleosidase; 16, adenosine deaminase; 17, guanosine deaminase; 18, purine nucleoside phosphorylase; 19, adenine deaminase; 20, xanthine dehydrogenase; 21, guanine deaminase; 22, allantoin synthase; 23, allantoin amidohydrolase; 24, allantoate amidohydrolase; 25, ureidoglycine aminohydrolase; 26, ureidoglycolate amidohydrolase.

In contrast to adenine and guanine, hypoxanthine and xanthine are intermediates of the purine catabolic pathway, and these compounds are therefore more readily catabolized (Fig. 5). These results indicate that release of the amino group in the purine ring at the AMP deaminase or guanosine deaminase steps is important in determining whether purine molecules are salvaged or catabolized.

Catabolism of the purine ring

In the present study, radioactivity from [8-^{14}C]purine nucleosides and purine bases was found to be incorporated into allantoin, allantoic acid and CO_2. The highest radioactivity was found in allantoic acid. Our results suggest that the purine ring is easily catabolised to allantoic acid via allantoin (steps 20 and 22). Details of ureide catabolism have recently been determined.[47-49] In *A. thaliana*, the pathways catalysed by allantoinase (EC 3.5.2.5, step 23), allantoate amidohydrolase (EC 3.5.3.9, step 24), ureidoglycine aminohydrolase (EC 3.5.3.26, step 25) and ureidoglycolate amidohydrolase (EC 3.5.1.116, step 26), have been proposed as active in the complete hydrolysis of allantoin. We did not find the details of the catabolic pathway, because we did not detect radioactivity in intermediates of the pathway. If this pathway is operative, the 8 position carbon of the purine ring is released as CO_2 at the final stage (step 26) of purine catabolism.

Purine metabolism during proliferation of *A. thaliana*

Using *A. thaliana* cells in the early-exponential phase (day 4), we examined the metabolic fate of purine nucleosides and bases. To determine whether the patterns of metabolism are similar in cells in other stages, we compared the pattern of metabolism of selected purine compounds. Salvage of adenine is active in every stage of culture. In cells in the initial phase (0-4 h), nucleotides were more heavily labelled than in the following lag phase (day 1) in which radioactivity shifting into RNA was maximum. This suggests that ATP accumulation is preceded by RNA synthesis. Accumulation of ATP by the salvage pathway, as well as conversion of AMP and ADP to ATP, may begin immediately after cell transfer to the fresh medium, and accumulation of ATP may act as a trigger of nucleic acid and protein synthesis, as observed in other cultured system.[50] A similar pattern was also found in RNA synthesis from [8-^{14}C]inosine. This suggests that purine salvage contributes to the initial RNA synthesis which begins immediately after the cells are transferred to the fresh medium; this may initiate the following cell division.

Catabolic activity of inosine is higher than that of adenine during every culture phases. Marked release of $^{14}CO_2$ from [8-^{14}C]inosine was observed in the initial and lag culture phases. This suggests that degradation of allantoic acid is extremely active in the early stages of cell proliferation. In the allantoin degradation, glyoxylic acid and ammonia are produced as end products, together with CO_2. The *A. thaliana* cells are able to recycle these end products to synthesize new organic molecules for use in proliferation.[48] The degradation of allantoin in the early phase of proliferation may be for this purpose.

 DOI: 10.17628/ecb.2014.3.925-934

The metabolic fate of exogenously supplied [^{14}C]precursors in various stages of the growth of *A. thaliana* cells shows the ability of purine salvage and purine catabolism in the cells of corresponding proliferation stages. The results are influenced by the concentration of endogenous precursors and intermediates. Furthermore, *in planta* purine metabolism is dependent upon the endogenous supply of precursors. The net increase of purine nucleotides accompanying cell proliferation requires the *de novo* purine biosynthesis, because the supply of purine nucleosides and bases for salvage pathways is limited. We confirmed the activity of the *de novo* purine biosynthesis using [^{14}C]formate and [2-^{14}C]glycine in *A. thaliana* (data not shown). Estimation of the relative activity of the *de novo* pathway during cell proliferation is difficult, because [^{14}C]formate and [2-^{14}C]glycine are utilised not only for nucleotide biosynthesis but also in many other metabolic pathways.

Menges *et al.*[51] reported genome-wide gene expression in suspension cultured cells of *A. thaliana*. They presented an integrated genome-wide view of the transcriptional profile of a plant suspension culture, and identified a refined set of 1082 cell cycle regulated genes. Neither *APT* nor *ADK* genes appeared in their lists, however. Our results suggest that *APT1* and *ADK2*, which encode the enzymes for AMP synthesis from adenine and from adenosine, are expressed differently.

Adenine phosphoribosyltransferase requires 5-phosphoribosyl-1-pyrophosphate (PRPP) for reaction. Our previous paper reported the expression of the *PRS* genes encoding phosphoribosylpyrophosphate synthetase.[18] As well as the generally distributed phosphate-dependent PRPP synthetase (class I), phosphate-independent PRPP synthetase (class II) is also present in plants. The transcript levels of *PRS1* and *PRS2* encoding class I enzymes and *PRS3* encoding class II enzymes increased rapidly after the cells were transferred to the fresh medium, and then remained almost constant during the early exponential growth phase. Constitutive expression of *PRS4* encoding cytosolic class II enzyme was observed during culture. The changing profile of transcript levels of *APT1* is similar to *PRS1-3*, and it follows that the adenine salvage system may be induced in the early phase of cell proliferation. The adenosine salvage system, in contrast, is somewhat constitutive.

The endogenous pool size of nucleosides and free nucleobases is usually small in plant cells. In *C. roseus* cells, for example, the pool of adenosine varied from 2 to 9 nmol gFW^{-1} during culture, and free adenine was practically undetectable.[52] This fact suggests that the salvage activity of adenine and adenosine is very high, and that nucleosides and bases generated by the degradation of nucleotides are immediately salvaged to nucleotides *in planta*.

Conclusion

Using ^{14}C-labelled purine nucleosides and bases, the present study found very clearly that adenosine, guanosine, adenine and guanine are salvaged to nucleotides and utilized for RNA synthesis. Inosine and hypoxanthine are also salvaged to nucleotides, mainly guanine nucleotides. These compounds are intermediates of the purine nucleotide catabolism, and so significant amounts are converted to xanthine and enter the catabolic pathway via allantoin. Neither xanthosine nor xanthine is used for the synthesis of nucleotides and RNA. These compounds are catabolized via allantoin and allantoic acid. The results indicate that release of the amino group in the purine ring is a crucial step in determining whether purine molecules are salvaged or catabolized. Deamination of adenine and guanine rings proceeds at the stage of AMP and guanosine, respectively. The pattern of purine metabolism in *A. thaliana* is similar to that in other plants.

References

[1]Stasolla, C., Katahira. R., Thorpe, T. A. and Ashihara H., *J. Plant Physiol.*, **2003**, *160*, 1271-1295.

[2]Zrenner, R. and Ashihara, H., *Plant Metab. Biotechnol.*, John Wiley & Sons, **2011**, 135-162.

[3]Moffatt, B. A. and Ashihara, H., *The Arabidopsis Book*, **2002,** 1-20.

[4]Arabidopsis-Genome-Initiative, *Nature*, **2000**, *408*, 796-815.

[5]Zrenner, R., Stitt, M., Sonnewald, U. and Boldt, R., *Ann. Rev. Plant Biol.*, **2006**, *57*, 805-836.

[6]Riegler, H., Geserick, C. and Zrenner, R. *New Phytol.*, **2011**, *191*, 349-359.

[7]Dahncke, K. and Witte, C. P., *Plant Cell*, **2013**, *25*, 4101-4109.

[8]Okazaki, Y., Oikawa, A., Kusano, M., Matsuda, F. and Saito, K., *Plant Metab. Biotechnol.*, John Wiley & Sons, 373-388, **2011**.

[9]Hirose, F. and Ashihara, H., *Z. Naturforsch.*, **1983**, *38c*, 375-381.

[10]Ashihara, H., Stasolla, C., Loukanina, N. and Thorpe, T.A., *Physiol. Plant.*, **2000**, *108*, 25-33.

[11]Akatsu, M., Hosoi, Y., Sasamoto, H. and Ashihara, H., *J. Plant Physiol.*, **1996**, *149*, 133-137.

[12]Suzuki-Yamamoto, M., Mimura, T. and Ashihara, H., *Physiol. Plant.*, **2006**, *128*, 405-414.

[13]Ashihara, H., *Z. Pflanzenphysiol.*, **1983**, *113*, 47-60.

[14]Katahira, R. and Ashihara, H., *Planta*, **2006**, *225*, 115-126.

[15]Ashihara, H., Monteiro, A.M., Gillies, F.M. and Crozier, A., *Plant Physiol.*, **1996**, *111*, 747-753.

[16]Koyama, Y., Tomoda, Y., Kato, M. and Ashihara, H., *Plant Physiol. Biochem.*, **2003**, *41*, 977-984.

[17]Deng, W. W. and Ashihara, H., *Plant Cell Physiol.*, **2010**, *51*, 2105-2118.

[18]Yin, Y. and Ashihara, H., *Phytochem. Lett.*, **2009**, *2*, 126-129.

[19]Yin, Y. and Ashihara, H., *Z. Naturforsch.*, **2008**, *63c*, 713-720.

[20]Axelos, M., Curie, C., Mazzolini, L., Bardet, C. and Lescure, B., *Plant Physiol. Biochem.*, **1992**, *30*, 123-128.

[21]Bruinsma, J., *J. Phtochem. Photobiol.*, **1963**, *2*, 241-249.

[22]Schmidt, G. and Thannhauser, S. J., *J. Biol. Chem.*, **1945**, *161*, 83-89.

[23]Schneider, W. C., *J. Biol. Chem.*, **1946**, *164*, 747-751.

[24]Matsui, A., Yin, Y., Yamanaka, K., Iwasaki, M. and Ashihara, H., *Physiol. Plant.*, **2007**, *131*, 191-200.

[25]Katahira, R. and Ashihara, H., *Planta*, **2002**, *215*, 821-828.

[26]Ashihara, H., Mitsui, K. and Ukaji, T., *Z. Naturforsch.* **1987**, *42c*, 297-290.

[27]Wylegalla, C., Meyer, R. and Wagner, K. G., *Planta*, **1985**, *166*, 446-451.

[28]Kanamori, I., Ashihara, H. and Komamine, A., *Z. Pflanzenphysiol.*, **1979**, *93*, 437-448.

[29]Brown, E. G. and Short, K. C., *Phytochemistry*, **1969**, *8*, 1365-1372.

[30]Meyer, R. and Wagner, K. G., *Planta*, (**1985**) *166*, 439-445.

[31]Yin, Y., Matsui, A., Sakuta, M. and Ashihara, H., *Phytochemistry*, **2008**, *69*, 2891-2898.

[32]Ashihara, H., Luit, B., Belmonte, M. and Stasolla, C., *Plant Physiol. Biochem.*, **2008**, *46*, 752-759.

[33]Stasolla, C., Loukanina, N., Ashihara, H., Yeung, E. C. and Thorpe, T. A., *Plant Sci.*, **2006**, *171*, 345-354.

[34]Stasolla, C., Loukanina, N., Yeung, E. C. and Thorpe, T. A., *Physiol. Plant.*, **2005**, *123*, 254-261.

[35]Ashihara, H., Stasolla, C., Loukanina, N. and Thorpe, T. A., *Plant Sci.*, **2001**, *160*, 647-657.

[36]Ashihara, H., Li, X. N. and Ukaji, T., *Ann. Bot.*, **1988**, *61*, 225-232.

[37]Shimazaki, A., Hirose, F. and Ashihara, H., *Z. Pflanzenphysiol.*, **1982**, *106*, 191-198.

[38]Allen, M., Qin, W., Moreau, F. and Moffatt, B., *Physiol. Plant.*, **2002**, *115*, 56-68.

[39]Moffatt, B. A., Wang, L., Allen, M. S., Stevens, Y. Y., Qin, W., Snider, J. and von Schwartzenberg, K., *Plant Physiol.*, **2000**, *124*, 1775-1785.

[40]Li, G., Liu, K., Baldwin, S. A. and Wang, D., *J. Biol. Chem.*, **2003**, *278*, 35732-35742.

[41]Ashihara, H., *Phytochem. Lett.*, **2012,** *5*, 100-103.

[42]Liu, S. W. and Milman, G., *J. Biol. Chem.*, **1983**, *258*, 7469-7475.

[43]Keough, D. T., Ng, A. L., Winzor, D. J., Emmerson, B. T. and de Jersey, J., *Mol. Biochem. Parasitol.*, **1999**, *98*, 29-41.

[44]Wang, C. C. and Simashkevich, P. M., *Proc. Nat. Acad. Sci. USA*, **1981**, *78*, 6618-6622.

[45]Negishi, O., Ozawa, T. and Imagawa, H., *Biosci. Biotech. Biochem.*, **1994**, *58*, 1277-1281.

[46]Dahncke, K. and Witte, C. P., *Plant Cell*, **2013**, *25*, 4101-4109.

[47]Werner, A. K., Romeis, T. and Witte, C. P., *Nat Chem Biol*, **2010**, *6*, 19-21.

[48]Werner, A. K. and Witte, C. P., *Trend. Plant Sci.*, **2011**, *16*, 381-387.

[49]Werner, A. K., Medina-Escobar, N., Zulawski, M., Sparkes, I. A., Cao, F. Q. and Witte, C. P., *Plant Physiol.*, **2013**, *163*, 672-681.

[50]Yin, Y., Shimano, F. and Ashihara, H., *J. Exp. Bot.*, **2007**, *58*, 1025-1033.

[51]Menges, M., Hennig, L., Gruissem, W. and Murray, J. H., *Plant Mol. Biol.*, **2003**, *53*, 423-442.

[52]Yabuki, N. and Ashihara, H., *Biochim. Biophys. Acta*, **1991**, *1073*, 474-480.

Received: 20.08.2014.
Accepted: 03.09.2014.

SELF-ASSEMBLY OF COPPER(II) MACROTRICYCLIC CHELATE COMPLEX WITH 2,8-DITHIO-3,5,7-TRIAZANONANDITHIOAMIDE-1,9 WITH BIOPOLYMER-POLYPEPTIDE MATRIX

O. V. Mikhailov[a]

Keywords: self-assembly, metalheterocycle**,** macrotricyclic ligand, molecular structure, DFT calculation

A template synthesis of copper(II) chelate coordination compound with 2,8-dithio-3,5,7-triazanonandithioamide-1,9 ligand has been achieved under soft conditions at room temperature. Reaction of $Cu_2[Fe(CN)_6]$ biopolymer-polypeptide matrix with aqueous-alkaline solutions containing dithiooxamide, formaldehyde and ammonia yielded the aforesaid chelate. It has been noted that the chelate is formed only under the given conditions and not in solution or solid phase. The molecular structure of the complex has been calculated using DFT B3LYP technique.

*Corresponding Author
E-Mail: olegmkhlv@gmail.com
[a] Analytical Chemistry Department, Kazan National Research Technological University, K. Marx Street 68, 420015 Kazan, Russia

Introduction

It is known that the template synthesis of metalheterocyclic compounds of *d*-elements occurs from simpler fragments (the so-called ligsons) in solutions and solid phase mostly under rather drastic conditions. However, it is possible, that under special conditions like complexing in 3*d*-metal-containing biopolymer-polypeptide (gelatin) immobilized matrix (BPIM), for example in some metal(II)hexacyanoferrate(II),[1-4] at least certain template processes to occur under soft conditions, primarily at room temperature. Indeed, such processes have been observed to take place[5,6] with triple systems like the M(II)-dithiooxamide ($H_2N–C(S)–C(S)–NH_2$)-formaldehyde complexes where M = Co, Ni or Cu and with the M(II)-dithiooxamide-propanone, where M = Ni or Cu, in the corresponding $M_2[Fe(CN)_6]$-BPIM matrix. One more possible ligand synthon for template synthesis in the M(II)-dithiooxamide- formaldehyde system, is ammonia. We report in this communication that we have been able to perform such synthesis in the Cu(II)- dithiooxamide-formaldehyde- ammonia quaternary system in the $Cu_2[Fe(CN)_6]$-BPIM matrix and, as a result, to observe a formation of macrocyclic coordination compound of copper(II) with (N,N,S,S)-tetradentate ligand – 2,8-dithio-3,5,7-triazanonandithioamide-1,9.

Experimental

$Cu_2[Fe(CN)_6]$-BPIM was synthesized as described in the literature.[1-4] The synthesis of $CuC_6S_4N_5H_9$ occurs on contact of $Cu_2[Fe(CN)_6]$-BPIM with alkaline solutions (pH=11-12) containing dithiooxamide, formaldehyde and ammonia. The concentration of copper(II) hexacyanoferrate(II) in the matrix was 0.1-2.0 $mol \cdot dm^{-3}$, the concentration of dithiooxamide, formaldehyde and ammonia the solution was $(3.0 \cdot 10^{-3} - 5.0 \cdot 10^{-2})$ mol L^{-1}, $(1.5 \cdot 10^{-3} - 1.0 \cdot 10^{-1})$ mol L^{-1} and $(3.0 \cdot 10^{-3} - 5.0 \cdot 10^{-2})$ mol L^{-1}, respectively. The duration of the process was 10-12 min at 18-20 °C. The matrix obtained was treated with the solution of proteolytic enzyme, *Bacillus mesentericus*, according to already described process,[7] and as a result gelatin binding of matrix was split into soluble low molecular weight compounds whereas the synthesized coordination compound precipitated and was then isolated from the mother liquor. Finally, the coordination compound was washed with distilled water, ethanol and dried at room temperature. Found (%): Cu, 18.6; C, 21.1; S, 37.2; N, 20.5; H, 2.7; O was not found. $CuC_6S_4N_5H_9$, calc. (%): Cu, 18.53; C, 21.01; S, 37.40; N, 20.42; H, 2.64. Characteristic bands in the IR-spectra (cm^{-1}): 680 (ν(C=S)); 1640 (ν(C=N)); 2865, 2940 (ν(CH_2)); 3460 (ν(NH)). MALDI TOF mass spectrometry data: the molecular mass of the synthesized compound is 343.0.

Electron absorption spectra of the BPIM were recorded using Specord UV-VIS (Karl Zeiss, Germany) and PU-8710 (Philips, The Netherlands) spectrophotometers in the 400-800 nm range. In order to record IR spectra, a UR-20 spectrometer (Karl Zeiss, Germany) was employed. Matrix-Assisted Laser Desorption/Ionization Time of Flight mass spectra (MALDI TOF) of substances isolated from BPIM were received using a Dynamo (Fimigan) and 4-nitroaniline matrix at 500MHz and 55.25 units of laser power.

Results and Discussion

The resulting compound colours the polymeric masses of the BPIM, which becomes red-brown. The UV-VIS-spectra of this compound contains only a shoulder due to the intense charge transfer band, whose maximum is in the UV region. It should be noted that in the absence of formaldehyde a dark-green compound with spectral characteristics similar to those of the Cu(II)-dithiooxamide complex is formed,[1,2,4] and in absence of ammonia, a brown compound having $CuC_6S_4N_4OH_8$ composition, is formed as it was shown in

our earlier work.[5] Thus there is no doubt that formaldehyde, ammonia, together with dithiooxamide and Cu(II) participate in the complexation process that occurs under these specific conditions. Decomposition of the polymeric binder of BPIM by enzymes by the known procedure[7] allowed us to isolate dark-brown compound $CuC_6S_4N_5H_9$. According to the data of MALDI TOF mass spectrometry, the molecular mass of compound synthesized is 343.0 which accords well with calculated value of 342.93.

This compound is almost insoluble in water, ethanol, acetone, chloroform, benzene and tetrachloromethane, and poorly soluble in dimethylformamide, dimethylsulfoxide and hexamethylenephosphortriamide. The DTA data indicates that it is very stable and does not undergo pyrolysis up to 600°C. The compound is found to be paramagnetic ($\mu_{eff.}$ = 1.94 μ_B); it gives ESR signals at low (77 K, liquid nitrogen) as well as at room temperatures ($g_{\|}$ = 2.23, $g_{\perp}$ = 2.06). This allows us to assume that copper in the complex is in an oxidation state of +2 with planar D_{2h}- or C_{2h}-coordination of donor centers around metal atom. The UV-VIS spectra of DMF solution of this compound are almost identical to those of their source BPIM.[8] This indicates that the immobilized compound is the same as that was isolated from BPIM.

The IR spectra of the complex have a band in the 3400-3500 cm^{-1} region, typical of NH or NH_2 groups uncoordinated to metal ion. Hence, at least a portion of the N atoms in these compounds are not bound to copper. In addition, the IR spectra of the compound under study contains ν(C=S) at 680 cm^{-1} (usually observed at 705-570 cm^{-1}) and ν(C=N) band at 1640 cm^{-1} (usually observed at 1690-1625 cm^{-1}) indicating the presence of (C=S) and (C=N) groups,[9] respectively. Unfortunately, the IR spectra obtained in the region <1000 cm^{-1}, where ν(Cu-S) and ν(Cu-N) frequencies should be observed,[9] did not allow us to reliably assign the bands they contain to the stretching vibrations indicated above. Two medium-intensity peaks belonging to ν(CH_2) at 2940 and 2865 cm^{-1} (according to the literature,[9] these bands lie within the 2945-2915 and 2870-2845 cm^{-1} ranges, respectively) was specially noted. These ν(CH_2) bands are absent in the IR spectra of dithiooxamide and in any of the coordination compounds of Cu(II) with this ligand known to date.[3] Thus, one may conclude that compound under examination contain at least one new CH_2-structural group and it is quite evident that the formation of a Cu(II) coordination compound with some novel ligand has taken place. However, a band due to the stretching vibrations of the bridging C-O-C group at 1120-1100 cm^{-1} which is observed[5] in a product of template synthesis in the Cu(II)- dithiooxamide- formaldehyde system, is absent in the IR spectra of compound studied. ^{13}C NMR spectrum of this complex showed three signals.

Since compositions of compounds formed by the complexation in the Cu(II)- dithiooxamide- formaldehyde system[5] ($CuC_6S_4N_4OH_8$) and in the Cu(II)- dithiooxamide-formaldehyde -ammonia one ($CuC_6S_4N_5H_9$) are different, it is obvious that in formation of this novel ligand, dithiooxamide and formaldehyde as well as ammonia participated. It should be noted especially in this connection that the UV-VIS absorption spectra of aqueous solutions of dithiooxamide of any concentrations in the range of 400-700 nm at pH>10 did not change even on addition of significant amounts of formaldehyde and ammonia and keeping for 2 days, and no indication of a chemical process between dithiooxamide, formaldehyde and ammonia was observed. Therefore, we have no doubt that the reaction between the reagents indicated above does not occur at all in absence of a metal ion. Such a phenomenon is possible only in template synthesis.[10,11] Moreover, it seems that dithiooxamide, formaldehyde and ammonia act as ligand synthons.

By taking into consideration the all foregoing facts, the following scheme of template synthesis proceeding by an interaction between Cu(II), dithiooxamide, formaldehyde and ammonia in the $Cu_2[Fe(CN)_6]$-BPIM matrix and leading to formation of a metal heterocyclic compound, (2,8-dithio-3,5,7-triazanonandithioamide-1,9)copper(II), may be written:

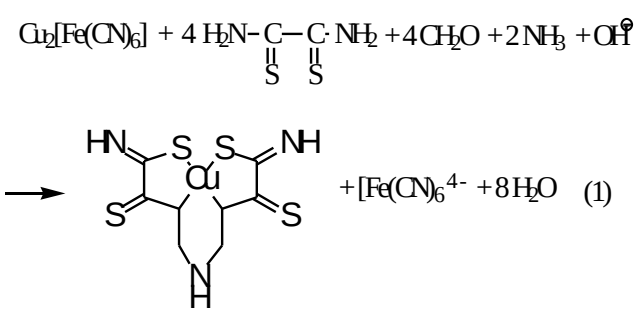

X-ray diffraction analysis of the coordination compound prepared in the $Cu_2[Fe(CN)_6]$-BPIM matrix could not be performed as the experimental procedure of its isolation yielded the compound in the form of extremely small crystals, unsuitable for diffraction analysis. For this reason, the exact space structure of the synthesized Cu(II) complex remains an open question. However, presently it is possible to assign possible structure to this complex by means of modern quantum-chemical calculations. Therefore, quantum-chemical calculation of molecular structure of macrotricyclic Cu(II) coordination compound formed in the triple system under examination, was attempted. One of most suitable and reliable methods for such calculation is hybrid method of the density functional theory DFT B3LYP. In this work, DFT B3LYP level of theory with the 6-31G(d) basis set[12,13] in Gaussian09 program[14] was used. The preliminary appraisal of the above calculation method on various chelate complexes of 3*d*-elements showed that it is possible to calculate basic geometric parameters of their structures (the Cartesian coordinates of atoms, the lengths of bonds between atoms, the angles between bonds etc.). Therefore, we have carried out a quantum-chemical calculation of the molecular structure of the macrocyclic compound under examination. Major results of the calculation are discussed below.

The molecular structure of the complex indicated has been shown in Figure 1, the important parameters of this structure, in the Table 1. As may be seen from these data, that contrary to expectations, the complex has pronounced non-coplanar configuration.

It should be noted that in this complex, quadrangle of (NSSN) donor atoms is planar (the sum of inner angles is equal to 360°). CuN_2S_2 chelate grouping may be considered as practically planar because the sum of valence angles in the given metalchelate grouping, namely ∠N2Cu1N3,

∠N3Cu1S4, ∠S4Cu1S1 and ∠S1Cu1N2, is 357.2°, and, hence, Copper atoms are only slightly raised above (NSSN) plane. However, as it may be easily noted, both 5-numbered chelate rings as well as additional 6-numbered ring, formed as a result of template stitching, are not planar because the sums of their inner angles, 522.5° and 632.0°, respectively are considerably lesser than sums of inner angles in plane pentagon and plane hexagon (540° and 720°, respectively).

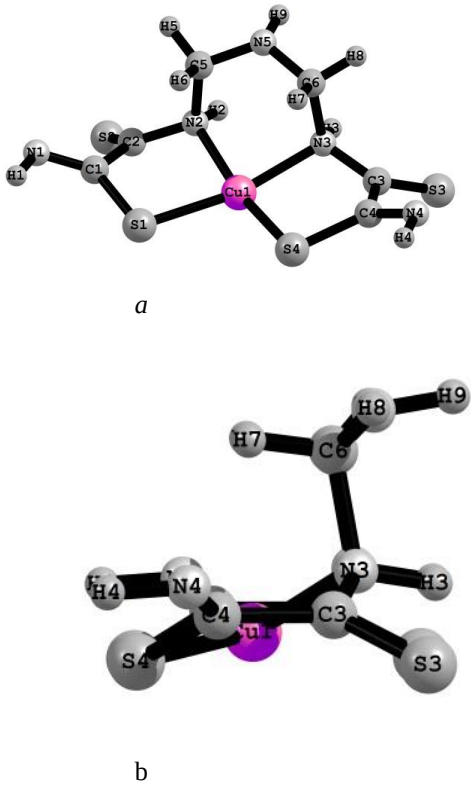

a

b

Figure 1. Molecular structure of (2,8-dithio-3,5,7-triaza-nonandithioamide-1,9)copper(II) with numbering of atoms: front view (*a*) and view from the side (*b*)

Besides, 6-numbered ring is not in one plane with metalchelate MN_2S_2 grouping but is inclined to it at 70.4°. It should be noted in this connection that the calculated Cu–N and Cu–S bond lengths (206.9 and 227.0 pm, respectively) are in the range of Cu–N and Cu–S bond lengths found experimentally in the macrocyclic complexes having MN_2S_2 chelate grouping (188–216 pm and 215–247 pm, respectively). Dipole moment of this complex is extremely high value (6.86 Debye units).

It is worth mentioning that processes of template synthesis between Cu(II), dithiooxamide, formaldehyde and ammonia occurs only in BPIM matrix**;** we failed to obtain this coordination compound in the reaction of $Cu_2[Fe(CN)_6]$ in solution or in the solid phase at room temperature. This fact indicates a specific role of gelatin-immobilized matrix system in the template synthesis in our case. It is interesting that compound under examination is not formed at interaction between NH_3 and $CuC_6S_4N_4OH_8$ synthesized by reported methods[5] either in solution or BPIM matrix.

Table 1. Selected parameters of molecular structure of (2,8-dithio-3,5,7-triazanonandithioamide-1,9)copper(II).

Bond lengths, *pm*			
Cu1–N2	206.9	Cu1–N3	206.9
Cu1–S1	227.0	Cu1–S4	227.0
N2–C2	143.4	N3–C3	143.4
C1–C2	149.8	C3–C4	149.8
C1–S1	177.8	C4–S4	177.8
C2–S2	163.1	C3–S3	163.1
C1–N1	127.7	C4–N4	127.7
N2–C5	153.2	N3–C6	153.2
N1–H1	102.5	N2–H2	102.5
C5–N5	142.9	C6–N5	142.9
Valence angles, *grad*			
Valence angles in 5-numbered cycle 1		Valence angles in 5-numbered cycle 2	
∠Cu1S4C4	98.3	∠Cu1S1C1	98.3
∠S4C4C3	113.1	∠S1C1C2	113.1
∠C4C3N3	113.2	∠C1C2N2	113.2
∠C3N3Cu1	110.6	∠C2N2Cu1	110.6
∠N3Cu1S4	87.3	∠N2Cu1S1	87.3
Angles sum (VAS[51])	522.5	Angles sum (VAS[52])	522.5
Torsion angles, *grad*			
∠N2Cu1N3C6	70.4	∠Cu1N2C2S2	131.0
∠N3Cu1N2C5	70.4	∠Cu1N3C3S3	130.9
∠N2C5C6N3	0.0	∠N2C2C1S1	45.0
∠N3C6C5N2	0.0	∠N3C3C4S4	44.9
∠S1Cu1N3C6	7.9	∠S1C1C2S2	131.1
∠S4Cu1N2C5	7.6	∠S4C4C3S3	131.0
∠Cu1S4C4N4	161.1	∠N1C1C2S2	47.0
∠Cu1S1C1N1	160.9	∠N4C4C3S3	46.9
∠Cu1N2C5N5	70.1	∠Cu1N3C6N5	70.1
∠N2C5N5C6	62.6	∠N3C6N5C5	62.6

Acknowledgement

Financial support for this research by Russian Foundation of Basic Research (RFBR), grant No. NN 09-03-97001, is acknowledged.

References

[1]Mikhailov, O. V., Budnikov, G. K., *Bull. Chem. Soc. Jpn.*, **1989**, *62*, 4016.

[2]Mikhailov, O. V., *Monatsh. Chem.*, **1990**, *122*, 595.

[3]Mikhailov, O. V., *Russ. Chem. Revs*., **1995**, *64*, 657.

[4]Mikhailov, O. V., Polovnyak, V. K., *J. Mater. Chem.*, **1997**, *7*, 337.

[5]*Comprehensive Supramolecular Chemistry* (Ed. Atwood, J. L., Davies, J. E. D., MacNicol, D. A., Vögtle, F.), Oxford: Pergamon Press, **1996**.

[6]Mikhailov, O. V., Khamitova, A. I., Morozov, V. I., *Heterocycl. Commun.*, **2000**, *6*, 137.

[7]Mikhailov, O. V., Kazymova, M. A., Shumilova, T. A., Vafina, L. R., *Heterocycl. Commun*., **2000**, *6*, 357.

[8]Mikhailov, O. V., *Indian J. Chem.*, **1991**, *30A*, 252.

[9]Nakamoto, K., *Infrared and Raman spectra of inorganic and coordination compounds*, 4th Edit., Wiley, New York, **1991.**

[10]Gerbeleu, N. V., Arion, V. B., *Template Synthesis of Macrocyclic Compounds*, Kishineu, Stiintsa, **1990** (in russ.)

[11]Kukushkin, Yu. N. *The Chemistry of Coordination Compounds*, Vysshaya Shkola, Moscow, **1985** (in russ.)

[12]Becke, A. D., *J. Chem. Phys*., **1993**, *98*, 1372.

[13]Lee, C., Yang, W., Parr, R. Q., *Phys. Revs.*, **1988**, *37B*, 785.

[14]Gaussian 09, *Revision A.01*, Frisch, M. J, Trucks, G. W., Schlegel, H. B., Scuseria, G. E., Robb, M. A., Cheeseman, J. R., Scalmani, G., Barone, V., Mennucci, B., Petersson, G. A., Nakatsuji, H., Caricato, M., Li, H., Hratchian, H. P., Izmaylov, A. F., Bloino, J., Zheng, G., Sonnenberg, J. L., Hada, M., Ehara, M., Toyota, K., Fukuda, R., Hasegawa, J., Ishida, M., Nakajima, T., Honda, Y., Kitao, O., Nakai, H., Vreven, T., Montgomery, J. A., Jr., Peralta, J. E., Ogliaro, F., Bearpark, M., Heyd, J. J., Brothers, E., Kudin, K. N., Staroverov, V. N., Kobayashi, R., Normand, J., Raghavachari, K., Rendell, A., Burant, J. C., Iyengar, S. S., Tomasi, J., Cossi, M., Rega, N., Millam, J. M., Klene, M., Knox, J. E., Cross, J. B., Bakken, V., Adamo, C., Jaramillo, J., Gomperts, R., Stratmann, R. E., Yazyev, O., Austin, A. J., Cammi, R., Pomelli, C., Ochterski, J. W., Martin, R. L., Morokuma, K., Zakrzewski, V. G., Voth, G. A., Salvador, P., Dannenberg, J. J., Dapprich, S., Daniels, A. D., Farkas, O., Foresman, J. B., Ortiz, J. V., Cioslowski, J. and Fox, D. J., **Gaussian, Inc.**, Wallingford CT, 2009.

Received: 04.08.2014.
Accepted: 13.09.2014.

GREEN SYNTHESIS OF ZnO NANOPARTICLES USING *BACILLUS SUBTILIS* AND THEIR CATALYTIC PERFORMANCE IN THE ONE-POT SYNTHESIS OF STEROIDAL THIOPHENES

Shamsuzzaman,[a]* Abad Ali,[a] Mohd Asif,[a] Ashraf Mashrai[a] and Hena Khanam[a]

Keywords: ZnO nanoparticles; *Bacillus subtilis;* steroidal thiophenes.

In the present work, we describe a low-cost, unreported and simple procedure for biosynthesis of zinc oxide nanoparticles (ZnO NPs) using *Bacillus subtilis* as eco-friendly reducing and capping agent. The synthesized ZnO NPs were characterized by UV-Vis spectroscopy, FTIR, XRD, SEM, TEM, PL and TGA techniques. The biosynthesis methods were carried out for its intrinsic advantages, as it is simple, cost-effective, environment-friendly and can be easily scaled up for large scale synthesis. The prepared nano-particles were used as catalyst for the fast and efficient synthesis of steroidal thiophenes. The one pot three-component mixture of steroidal ketones (**1**-**3**), malononitrile/ethyl cyanoacetate and elemental sulfur were converted into the corresponding steroidal thiophenes (**4**-**9**) in moderate to high yields with excellent selectivity.

Corresponding Authors
Tel: +919411003465
E-Mail: shamsuzzaman9@gmail.com
[a] Steroid Research Laboratory, Department of Chemistry, Aligarh Muslim University, Aligarh 202 002, India

Introduction

Green chemistry is an innovative research field, that reduce or eliminate the use and generation of hazardous substances[1,2] and offering a research-based approach in synthesizing chemicals such as pharmaceuticals, perfumes, flavorants, etc., with reduced needles environmental impact which benefit the environment and contribute to environmental sustainability[3] and there is no need to use high temperature, pressure, energy and hazardous chemicals. Therefore, green chemistry has advantages over chemical and physical methods.[4] Nanotechnology is emerging interdisciplinary science for synthesis of nanoparticles at the nanoscale level.[5,6] The field of nanotechnology is one of the most active areas of research in modern material science.[7] Nanoparticles can be synthesized by different physical, chemical and biological methods.[8] The biosynthesized nanoparticles have received broad attention due to their non-toxic and eco-friendly nature.[9,10] The biosynthesized nanoparticles are different in shape and size in comparison with those produced by other organism and has led to the development of new biocidal agents.[11] The biosynthesized nanoparticles have a wide variety of applications such as drug carriers for targeted delivery, cancer treatment, gene therapy and DNA analysis, antibacterial agents, biosensors, enhancing reaction rates, separation science and magnetic resonance imaging (MRI).[12] The synthesized ZnO nanoparticles possess high specific surface area, high catalytic activity and high adsorption capacity. ZnO nanoparticles has gained considerable interest due to their vast applications in various areas.[13-15] The Gewald reaction of sulfur, an active nitrile, and oxo-component provide 2-aminothiophene derivatives via a three-component one pot reaction (G-3CR). It has found diverse applications in combinatorial and medicinal chemistry. Chemistry of 2-aminothiophenes is one of the most extensive and dynamic field of present-day research. Since 1961 when first report on the Gewald reaction was published it became a universal method for synthesis of substituted 2-aminothiophenes and has gained prominence in recent times.[16] Thiophenes possess considerable attention for organic synthetic and medicinal chemists because of their unique applications in pharmaceuticals, organic semi-conductors, conducting polymers, organic light-emitting diodes (OLEDs) and lasers.[17-20] Encouraged by the above facts and in continuation of our previous work in green chemistry[21] and heterosteroids synthesis.[22] We here report a green methodology for the synthesis of highly substituted thiophenes *via* biosynthesized ZnO NPs. UV-vis spectroscopy, FTIR, XRD, SEM, TEM, PL and TGA were performed to ascertain the formation and characterization of biosynthesized ZnO NPs. The structures of newly synthesized compounds have been established on the basis of their elemental analysis and spectral data.

Experimental

All the chemicals used were purchased from Sigma Aldrich and Merck as analytical grade. The solvents were purified prior to use. The optical absorbance spectra were taken by using UV-vis double beam Perkin-Elmer LAMBDA 35 spectrophotometer at room temperature in the wavelength range of 250-800 nm. X-ray diffraction (XRD) patterns of the samples were obtained at room temperature, with a step of 0.02°, using Bruker D8 ADVANCE X-ray diffractometer with Cu K_α radiation (λ = 1.54178 Å) in the range of $0° < 2\theta < 100°$ at 40 kV. SEM images were obtained using a field emission scanning electron microscope (JSM-7600F, JEOL, Tokyo Japan) at an accelerating voltage of 15 kV and TEM images were obtained with ultra-high resolution FETEM (JEOL, JEM-

2100F) at an accelerating voltage of 200 kV. Photoluminescence (PL) spectra were measured using a Cary Eclipse EL06063917 fluorescence spectrophotometer with a xenon arc lamp as the light source. The thermal studies were carried out using TGA instrument (SHIMADZU) at a heating rate of 20 ^{o}C min^{-1}. Melting points were recorded on Riechert Thermover instrument and are uncorrected. IR spectra (KBr disks) were recorded on Perkin Elmer FT-IR Spectrometer spectrum two and its values are given in cm^{-1}. ^{1}H and ^{13}C NMR spectra in dilute $CDCl_3$ solutions at 303 K were run on a Bruker Avance II 400 NMR spectrometer equipped with a 5 mm diameter broad band inverse probehead working at 400 MHz for ^{1}H and at 100 MHz for ^{13}C, respectively. ^{1}H chemical shifts were referenced to the trace signal of $CHCl_3$ (7.26 ppm from int. TMS). Following abbreviations were used to indicate the peak multiplicity s -singlet, d -doublet, m -multiplet and values are given in parts per million (ppm) (δ) and coupling constants (J) are given in Hertz and ^{13}C chemical shifts to the center peak of the solvent signal (77.00 ppm from int. TMS). Mass spectra were recorded on a JEOL D-300 mass spectrometer.

Elemental analyses of all the new compounds were recorded on Perkin Elmer 2400 CHN Elemental Analyzer within ± 0.4 % of the theoretical values. The progress of all reactions was monitored by thin layer chromatography (TLC) plates with 0.5 mm layer of silica gel G, light petroleum ether refers to a fraction of b.p. 60-80 ^{o}C, and exposed to iodine vapors to check the purity as well as the progress of reaction. Sodium sulfate (anhydrous) was used as a drying agent.

Synthesis of ZnO nanoparticles

Bacillus subtilis cells were allowed to grow as a suspension culture in sterile distilled water containing nutrient broth media for 24 h. 25 mL of culture was taken and diluted four times by adding 75 mL of sterile distilled water containing nutrients. This diluted culture solution was again allowed to grow for 24 h. 50 mM zinc acetate dihydrate aqueous solution was injected into the bacterial suspension at a rate of 10 mL min^{-1} through a buret. After the mixture was stirred for 30 min, 200 mL of a 50 mM $NaBH_4$ aqueous solution as the reducing agent, was slowly poured into the mixture at a flow rate of 10 mL/min through the buret. Then the final mixture was robustly stirred for 24 h at room temperature. After the mixture was fully reacted, the mixture was centrifuged and subsequently the precipitate was collected.[23]

General procedure for synthesis of steroidal thiophene derivatives (4-9)

A mixture of 5α-cholestan-6-one **1-3** (1 mmol), malononitrile/ ethyl cyanoacetate (1 mmol), S_8 (1 mmol) and ZnO nanoparticles catalyst (0.003 g), in ethanol (15 mL) was refluxed for 12-18 h. The progress of the reaction was followed by TLC. After completion of the reaction, the mixture was filtered to remove the catalyst and the filtrate was taken in diethyl ether, washed with water and dried over anhydrous sodium sulfate. Removal of solvent gave the crude product which was recrystallized from methanol to obtain the pure compounds (**4-9**).

3β-Acetoxy-5α-cholest-6-eno-[6,7-d]-2´-amino-3´-cyanothiophene (4)

Brown powder, yield 70 %, m.p. 167-169 °C; IR (KBr, ν_{max}/cm^{-1}): 3344 (NH_2), 2210 (CN), 1713 ($OCOCH_3$), 1623, 1621 (C=C), 1068 (C-O), 714 (S-C); ^{1}H NMR ($CDCl_3$, δ, ppm): 6.21 (2H, brs, NH_2, exchangeable with D_2O), 4.7 (1H, m, C_3α-H, $W½$ = 14 Hz), 2.3 (dd, 1H, J = 7.55, 4.52 Hz, C_5-H), 2.05 (3H, s, $OCOCH_3$), 1.2 (3H, s, C_{13}-CH_3), 1.14 (3H, s, C_{10}-CH_3), 1.04 and 1.02 (other methyl protons); ^{13}C NMR ($CDCl_3$, δ, ppm): 172.5, 151.1, 145.2, 137.7, 120.4, 85.1, 75.5, 58.6, 50.1, 46.9, 45.2, 43.4, 40.6, 37.3, 35.3, 34.2, 33.9, 32.1, 31.0, 29.5, 27.5, 26.9, 25.2, 24.1, 23.9, 22.7, 21.2, 20.9, 19.5, 17.6, 15.3, 13.1; Anal. Calcd for $C_{32}H_{48}N_2O_2S$ %: C, 73.24, H, 9.22, N, 5.34. Found: C, 73.29, H, 9.24, N, 5.37; MS: m/z 524 [$M^{+\cdot}$].

3β-Chloro-5α-cholest-6-eno-[6,7-d]-2´-amino-3´-cyanothiophene (5)

Green brown powder, yield 72 %, m.p. 154-156 °C; IR (KBr, ν_{max}/ cm^{-1}): 3346 (NH_2), 2215 (CN), 1620, 1624 (C=C), 742 (C-Cl), 716 (S-C); ^{1}H NMR ($CDCl_3$, δ, ppm): 6.24 (2H, brs, NH_2, exchangeable with D_2O), 3.8 (1H, m, C_3α-H, $W½$ = 17 Hz), 2.2 (dd, 1H, J = 7.53, 4.56 Hz, C_5-H), 1.2 (3H, s, C_{13}-CH_3), 1.14 (3H, s, C_{10}-CH_3), 1.04 and 1.02 (other methyl protons); ^{13}C NMR ($CDCl_3$, δ, ppm): 152.7, 148.3, 137.1, 120.4, 87.4, 66.3, 59.9, 55.7, 51.7, 48.5, 45.9, 41.6, 40.2, 39.4, 38.9, 37.4, 36.2, 34.9, 32.7, 31.5, 30.7, 28.6, 27.4, 26.3, 25.4, 24.9, 23.7, 20.6, 16.8, 14.8; Anal. Calcd. for $C_{30}H_{45}ClN_2S$ %: C, 71.89, H, 9.05, N, 5.59. Found: 71.87, H, 9.09, N, 5.57; MS: m/z 500/502 [$M^{+\cdot}$].

5α-Cholest-6-eno-[6,7-d]-2´-amino-3´-cyanothiophene (6)

Brown powder, yield 71%, m.p. 149-151 °C; IR (KBr, ν_{max}/ cm^{-1}): 3343 (NH_2), 2217 (CN), 1630, 1617 (C=C), 718 (S-C); ^{1}H NMR ($CDCl_3$, δ, ppm): 6.26 (2H, brs, NH_2, exchangeable with D_2O), 2.7 (dd, 1H, J = 7.51, 4.53 Hz, C_5-H), 1.2 (3H, s, C_{13}-CH_3), 1.14 (3H, s, C_{10}-CH_3), 1.04 and 1.02 (other methyl protons); ^{13}C NMR ($CDCl_3$, δ, ppm): 150.3, 147.5, 139.1, 119.7, 85.1, 61.4, 59.7, 55.1, 49.4, 46.1, 43.5, 42.7, 41.5, 40.2, 38.7, 37.4, 35.2, 32.6, 31.5, 30.4, 29.3, 27.1, 26.3, 25.6, 24.1, 23.7, 20.5, 17.2, 14.3, 12.9; Anal. Calcd. for $C_{30}H_{46}N_2S$ %: C, 77.20, H, 9.93, N, 6.00. Found: C, 77.24, H, 9.97, N, 6.02; MS: m/z 460 [$M^{+\cdot}$].

3β-Acetoxy-5α-cholest-6-eno-[6,7-d]-2´-amino-3´-carboethoxythiophene (7)

Brown powder, yield 74 %, m.p. 175-177 °C; IR (KBr, ν_{max}/cm^{-1}): 3340 (NH_2), 1710 ($OCOCH_3$), 1669 (OCOC), 1620, 1618 (C=C), 1246, 1136 (C-O), 718 (S-C); ^{1}H NMR ($CDCl_3$, δ, ppm): 6.22 (2H, brs, NH_2, exchangeable with D_2O), 4.34 (2H, q, J = 7.02 ,CH_2),4.7 (1H, m, C_3α-H, $W½$ = 14 Hz), 2.6 (dd, 1H, J = 7.52, 4.51 Hz, C_5-H), 2.05 (3H, s, $OCOCH_3$), 1.2 (3H, s, C_{13}-CH_3), 1.14 (3H, s, C_{10}-CH_3), 1.04 and 1.02 (other methyl protons); ^{13}C NMR ($CDCl_3$, δ, ppm): 175.5, 168.3, 151.5, 142.1, 139.5, 118.7, 77.8, 65.3, 59.7, 56.9, 52.1, 45.7, 43.2, 42.1, 40.5, 39.5, 37.4, 36.2, 35.6, 33.1, 30.6, 29.9, 28.1, 26.6, 24.1, 23.9, 22.8, 21.0, 20.9, 19.9, 16.1, 15.6, 13.9, 12.4; Anal. Calcd. for $C_{34}H_{53}NO_4S$ %: C, 71.41, H, 9.34, N, 2.45. Found: C, 71.45, H, 9.38, N, 2.49; MS: m/z 571 [$M^{+\cdot}$].

3β-Chloro-5α-cholest-6-eno-[6,7-d]-2´-amino-3´-carboethoxy-thiophene (8)

Green brown powder, yield 72 %, m.p. 176-178 °C; IR (KBr, ν_{max}/cm^{-1}): 3339 (NH_2), 1665 (OCOC), 1623, 1615 (C=C), 1140 (C-O), 740 (C-Cl), 720 (S-C); ^{1}H NMR ($CDCl_3$, δ, ppm): 6.27 (2H, brs, NH_2, exchangeable with D_2O), 4.35 (2H, q, J = 7.01, CH_2), 3.8 (1H, m, C_3α-H, $W½$ = 16 Hz), 2.7 (dd, 1H, J = 7.55, 4.53 Hz,C_5-H), 1.2 (3H, s, C_{13}-CH_3), 1.14 (3H, s, C_{10}-CH_3), 1.04 and 1.02 (other methyl protons); ^{13}C NMR ($CDCl_3$, δ, ppm): 169.5, 152.2, 143.6, 140.1, 114.6, 67.1, 64.2, 59.9, 56.1, 53.7, 49.4, 45.4, 41.5, 40.2, 39.1, 38.3, 37.2, 36.5, 34.7, 32.9, 30.5, 29.3, 28.9, 26.3, 25.2, 24.5, 23.9, 21.7, 20.6, 17.2, 15.7, 13.1; Anal. Calcd. for $C_{32}H_{50}ClNO_2S$ %: C, 70.10, H, 9.19, N, 2.55. Found: C, 70.13, H, 9.16, N, 2.52; MS: m/z 547/549 [$M^{+\cdot}$].

5α-Cholest-6-eno-[6,7-d]-2´-amino-3´-carboethoxythiophene (9)

Brown powder, yield 71 %, m.p. 175-177 °C; IR (KBr, ν_{max}/cm^{-1}): 3335 (NH_2), 1668 (OCOC), 1623, 1621 (C=C), 1138 (C-O), 716 (S-C); ^{1}H NMR ($CDCl_3$, δ, ppm): 6.25 (2H, brs, NH_2, exchangeable with D_2O), 4.32 (2H, q, J = 7.02, CH_2), 2.7 (dd, 1H, J = 7.53, 4.54 Hz, C_5-H), 1.2 (3H, s, C_{13}-CH_3), 1.14 (3H, s, C_{10}-CH_3), 1.04 and 1.02 (other methyl protons); ^{13}C NMR ($CDCl_3$, δ, ppm): 171.4, 152.3, 145.7, 138.2, 118.1, 65.7, 59.6, 57.7, 53.1, 46.2, 44.5, 43.2, 42.9, 41.7, 40.5, 39.7, 37.3, 35.1, 32.1, 31.7, 29.1, 28.3, 27.2, 25.9, 24.1, 23.4, 22.9, 21.5, 20.9, 17.3, 15.6, 13.9; Anal. Calcd. for $C_{32}H_{51}NO_2S$ %: C, 74.80, H, 10.00, N, 2.73. Found: C, 74.83, H, 10.02, N, 2.70; MS: m/z 513 [$M^{+\cdot}$].

Result and discussion

Characterization of ZnO nanoparticles

UV spectrophotometry study

The UV-vis absorption spectrum findings demonstrate a novel technique for the preparation of ZnO nanoparticles (**Figure 1**), by dispersing ZnO nanoparticles in distilled water and using distilled water as the reference. An absorption peak focused at 375 nm. The electronic band gap (E_g) of ZnO nanoparticles was determined by employing the following relationship:

$$E_g = \frac{hc}{\lambda}$$

whereas

h is Planck's constant,

c is speed of light and

λ is the cut off wavelength value of ZnO nanoparticles.

The E_g value was determined to be 3.31 eV which is in good agreement with the previous work.[24]

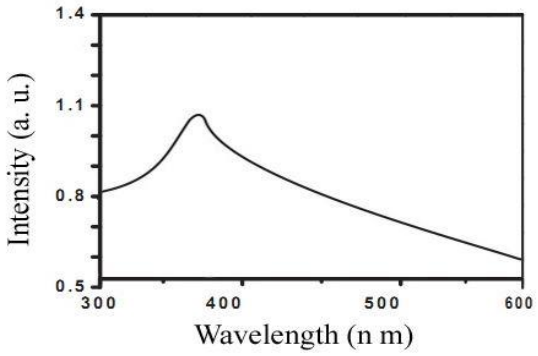

Figure 1. UV-vis spectrum of ZnO nanoparticles.

Fourier transform infrared spectroscopy

The synthesized zinc oxide nanoparticles have peaks at 3414.57 cm^{-1} for NH_2 stretching in adenine, cytosine, quinine and H-bonded OH groups while 2934.14 cm^{-1} for C-H stretching in aliphatics of cell walls (fatty acids, carbohydrates). 1625.64 cm^{-1} for NH_2 bending, C=O, C=N stretching (amide I band). The peak at 1385.69 cm^{-1} for amide III band and 1052.22 cm^{-1} for C-O-C asymmetric stretching in aliphatic esters.[25] Zn-O-Zn stretching modes at 609.33 cm^{-1} were well supported by available literature.[26] These peaks are the combined characteristics of zinc oxide and bacterial strain

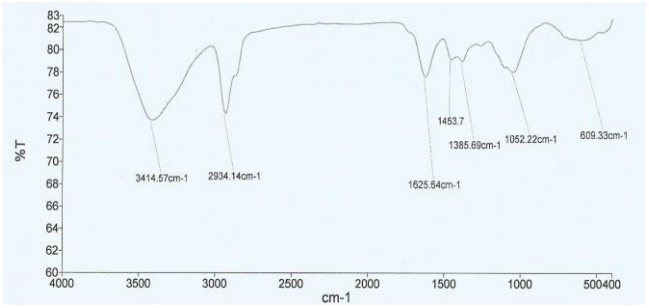

Figure 2. FTIR spectrum of ZnO nanoparticles.

XRD analysis

X-ray diffraction is taken in order to further confirm ZnO phase of the nanoparticles. The XRD patterns of the obtained ZnO nanoparticles are shown in **Figure 3**. Powder XRD of the product was carried out with Cu K_α radiation (λ = 1.54056 Å), employing a scanning rate of 0.02° s^{-1} and 2θ ranges from 20^o to 80^o for ZnO. The observed peaks correspond to the Bragg angle for the (100), (002), (101), (102), (110) and (200) planes of the crystalline ZnO, which are consistent with standard JCPDS No. 89-7102 and no indication of a secondary phase. All the peaks of XRD are very well matched with the hexagonal phase (wurtzite structure). The strong and narrow diffraction peaks indicate that the product has good crystalline structure. The crystallite size of the nanoparticles was calculated using Debye Scherrer formula

$$D=K\frac{\lambda}{\beta\cos\theta}$$

where,

K is constant,

λ is the wavelength of employed X-rays (1.54056 Å),

β is corrected full width at half maximum and

θ is Bragg's angle.

The 2θ value from the equation comes out to be at 35.81 and therefore the calculated crystallite size of the powder particles is about 24 nm.

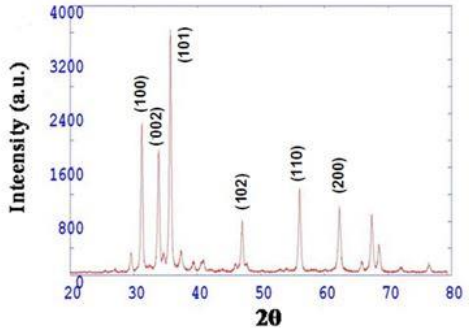

Figure 3. XRD analysis of ZnO nanoparticles.

SEM and TEM analysis

The conformation of the nanostructure morphology of ZnO particles comes from the analysis of SEM and TEM micrographs. SEM micrograph (**Figure 4**) showed the average size of nanoparticles between 20 and 30 nm.

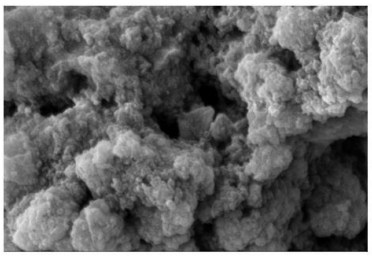

Figure 4. SEM image of the ZnO nanoparticles

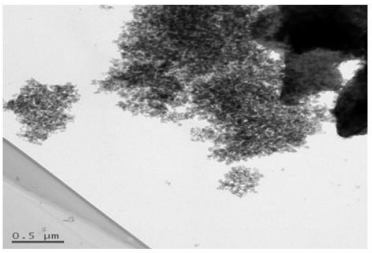

Figure 5. TEM image of the ZnO nanoparticles.

The size and morphology of ZnO particles analyzed by TEM is represented in **Figure 5**. This image reveals that most of the ZnO nanoparticles are quasi-spherical and their diameter is about ~25 nm. This result is in agreement with the value calculated from the X-ray diffraction.

Photoluminescence analysis

The Photoluminescence spectrum of ZnO nanoparticles consists of two emission peaks (**Figure 6**). A weak deep-level emission at 2.25 eV in the visible range is caused by a structural defect.[27] The other peak in the UV range at 3.1 eV which can be explained by the direct combination of excitons through an exciton-exciton collision process and the lower energy peak in the asymmetric UV emission is associated with band-to-acceptor transitions due to the large binding energy of ZnO.[28]

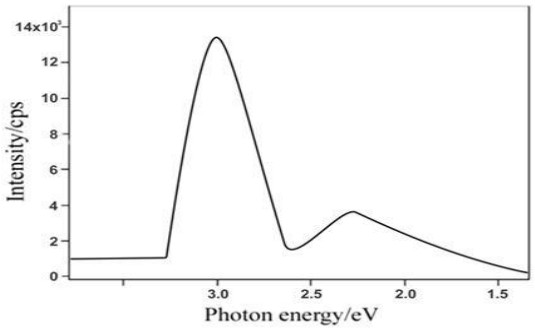

Figure 6. The Photoluminescence spectrum of ZnO nanoparticles.

Thermal stability

The thermo gravimetric analysis (TGA) has been performed on the biosynthesis of ZnO nanoparticles. TGA curve in **Figure 7** indicates that the weight loss starts at 200 ^{o}C because of the evaporation of water, the major weight loss occurs between 320 and 430 ^{o}C, which is around 40 % of the original weight due to the removal and decomposition of organic groups present during the biosynthesis. No decomposition or reaction occurs at temperatures above 500 °C.

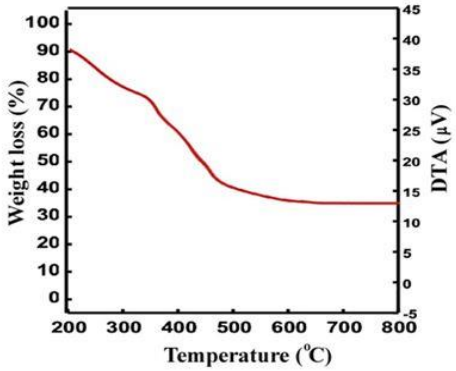

Figure 7. TGA curve of ZnO nanoparticles

The catalytic performance of ZnO in the synthesis of steroidal thiophenes

The catalytic system is influenced by various parameters, such as amount of the catalyst employed, effect of catalyst and solvent system. 3β-Acetoxy-cholestan-6-one, malononitrile and sulfur powder in DMF were selected as model substrates for carrying out the optimization studies for the synthesis of steroidal thiophenes. Initially, the model reaction was performed in the absence of ZnO nanoparticles and the reaction did not proceeded even with very long reaction time. When the model reaction was examined with ZnO nanoparticles the reaction was accelerated.

Catalytic loading

It was observed that yield was increased with enhancing catalyst concentration. The yield was increased from 38 to 70 % by enhancing the catalyst amount from 0.5 to 2.5 mol% (**Table 1**). Further increase in the catalyst concentration from 2.5 to 3.5 mol %, did not show any profound effect on the reaction rate as well as the yield this may be attributed to the coagulation of ZnO nanoparticles which decreased the effective surface area of the catalyst.[29]

Table 1. Effect of catalyst loading on the model reaction**.**

Entry	Catalysts, mol %	Time, h	Yield, %[a]
1	0.5	19	38
2	1	18	44
3	1.5	14	53
4	2.5	12	70
5	3	12	70
6	3.5	12	70

[a]Yield are related to isolated pure products

Effect of solvent

We then tried to screen the reaction in various organic solvents in order to optimize the reaction conditions using ZnO nanoparticles as catalyst (**Table 2**).

Table 2. Solvent screening for the model reaction.

Entry	Solvent	Yield, %[a]
1	DMF	70
2	Methanol	60
3	Ethanol	62
4	1,4-Dioxane	45
5	Benzen	30

[a]Yield are related to isolated pure products

The solvent screening experiments revealed that the reaction yield is dependent on the polarity and the coordinating ability of the solvents. The polar solvents afforded better yield than the nonpolar ones and the best result was obtained in ethanol in which ZnO nanoparticle catalyst worked most efficiently by phasing out of the desired product. In order to investigate the scope of this reaction, a variety of different steroidal compounds were subjected to this reaction (**Scheme 1**).

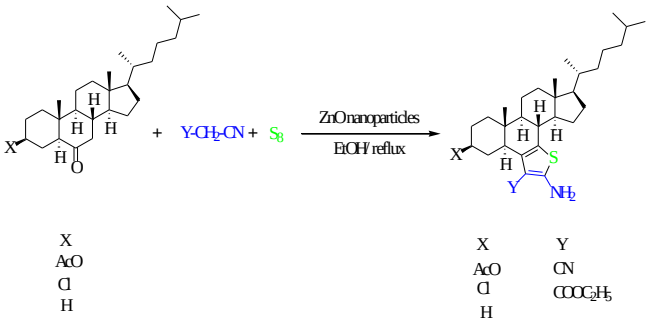

Scheme 1. Synthesis of steroidal thiophene derivatives using biosynthesized ZnO nanoparticles

All the reactions proceeded smoothly and the reaction was completed within 12 to 18 h to afford the products (**4-9**) in excellent yields (70-74 %).

Recyclability of catalyst

After completion of the model reaction in specified time, the catalyst was recovered by filtration, washed with dichloromethane and methanol and dried at 150 ºC for 4 h and used for the subsequent cycle (**Figure 8**).[30] The results revealed that the catalyst exhibited good catalytic activity up to five cycles.

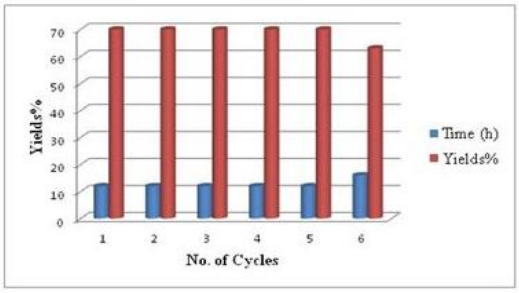

Figure 8. Recyclability of ZnO nanoparticles.

Studying the superiority of ZnO nanoparticles over some other catalyst

Various catalysts were employed to evaluate the capability and efficiency of the catalyst (**Table 3**). The model reaction was examined with imidazole, morpholine, diethyl amine and ZnO (bulk) using 2.5 mol% of each catalyst separately the reaction took longer time period for completion with lower yield of the product.

Table 3. The superiority of ZnO nanoparticles over other reagents.

Entry	Catalysts	Time, h	Yield, %[a]
1	-	-	-
2	Imidazole	22	58
3	Morpholine	20	45
4	Diethyl amine	26	52
5	ZnO (bulk)	18	53
6	ZnO	12	70

[a]Yield are related to isolated pure products

With ZnO nanoparticles the reaction was accelerated and yield of the desired product was maximum.

Proposed reaction pathway for the synthesis of steroidal thiophenes

A mechanistic route for the synthesis of steroidal thiophenes using nano-ZnO as catalyst is presented in **Scheme 2**. The mechanism involves a three-step process and nano-ZnO has dual characters of Lewis acidic (Zn^{2+}) in one hand and Lewis basic sites (O^{2-}) on the other.[31] In the first step, Lewis acid sites of ZnO (Zn^{2+}) coordinates to the oxygen of the carbonyl group, hence reactivity of carbonyl group increases. Moreover, the Lewis basic sites of nano-ZnO (O^{2-}) deprotonated the malononitrile/ cyano ethylacetate and then a nucleophilic attack to the activated carbonyl group proceeds the reaction forward. The ring closure step is the most crucial step which is performed as an intra-molecular nucleophilic attack of the sulfur anion to triple bond of the cyano group.[32]

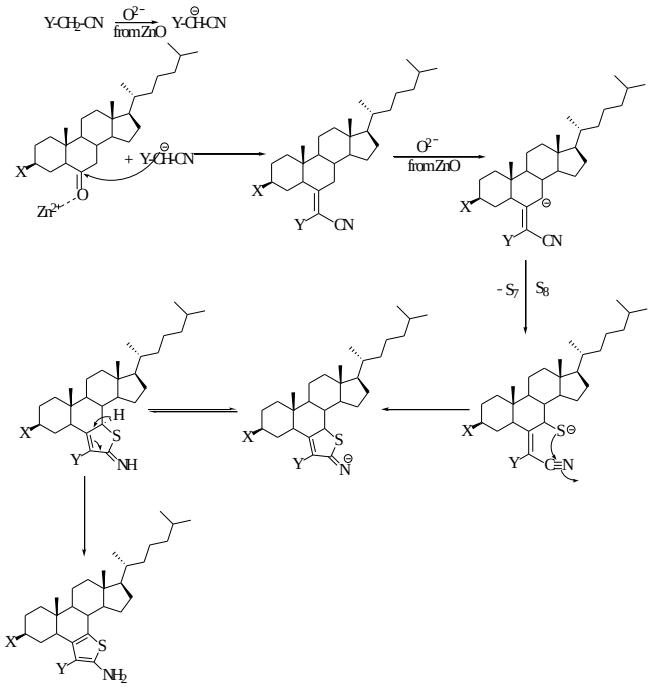

Scheme 2. Plausible reaction mechanism for the synthesis of steroidal thiophene derivatives (**4-9**).

Conclusion

In conclusion, we have synthesized zinc oxide nanoparticles (ZnO NPs) using *Bacillus subtilis* as eco-friendly reducing and capping agent. ZnO nanoparticles were used as green catalyst for one-pot three-component preparation of steroidal thiophene derivatives. The attractive features of this protocol are simple procedure, cleaner reaction and use of reusable nano catalyst. Satisfactory yields of reaction, as well as a simple experimental, isolation and purification of the products make it a useful protocol for the green synthesis.

Acknowledgments

The authors would like to thank the Chairman, Department of Chemistry, Aligarh Muslim University, Aligarh for providing necessary research facilities. Facilities provided by SAP (DRS-I) for their generous research support are also gratefully acknowledged.

References

[1]Kirchhoff, M. M., *J. Chem. Educ.*, **2001**, *78*, 1577.

[2]Anastas, P. T., *Crit. Rev. Anal. Chem*., **1999**, *29*, 167-175.

[3]Banitaba, S. H., Safari, J., Khalili, S. D., *Ultrason. Sonochem*., **2013**, *20*, 401-407.

[4]Jayaseelan, C., Ramkumar, R., Rahuman, A., Perumal, P., *Ind. Crops Prod*., **2013**, *45*, 423-429.

[5]Jr, L. A. P., *J. Chem. Educ*., **2007**, *84*, 259-264.

[6]Sadik, O. A., Zhou, A. L., Kikandi, S., Du, N., Wang, Q., Varner, K., *J. Environ. Monit*., **2009**, *11*, 1782-1800.

[7]Schmitt, S. W., Schechtel, F., Amkreutz, D., Bashouti, M., Srivastava, S. K., Hossmann, B., Dieker, C., Spiecker, E., Rech, B., Christiansen, S. H., *Nano Lett*., **2012**, *12*, 4050-4054.

[8]Mohanpuria, P., Rana, N. K., Yadav, S. K., *J. Nanopart. Res*., **2008**, *10*, 507-517.

[9]El-Rafie, H. M., El-Rafie, M. H., Zahran, M. K., *Carbohydr. Polym*., **2013**, *96*, 403-410.

[10]Shankar, S. S., Rai, A., Ahmad, A., Sastry, M., *J. Colloid Interface Sci*., **2004**, *275*, 496-502.

[11]Patel, V. K., Bhattacharya, S., *Appl. Mater. Interfaces*, **2013**, *5*, 13364-13374.

[12]Sapsford, K. E., Algar, W. R., Berti, L., Gemmill, K. B., Casey, B. J., Oh, E., Stewart, M. H., Medintz, I. L., *Chem. Rev*., **2013**, *113*, 1904-2074.

[13]Wang, Z. L., *Annu. Rev. Phys. Chem*., **2004**, *55*, 159-196.

[14]Kuo, C. L., Kuo, T. J., Huang, M. H., *J. Phys. Chem.* **2005 B**, *109*, 20115-20121.

[15]Wang, H. H., Xie, C., *J. Cryst. Growth*, **2006**, *291*, 187-195.

[16]Puterová, Z., Krutošíková, A., Végh, D., *Arkivoc* **2010 (i)** , 209-246.

[17](a)Holmes, J. M., Lee, G. C. M., Wijono, M., Weinkam, R., Wheeler, L. A., Garst, M. E., *J. Med. Chem*., **1994**, *37*, 1646-1651; (b) Luker, T. J., Beaton, H. G., Whiting, M., Mete, A., Cheshire, D. R., *Tetrahedron Lett*., **2000**, *41*, 7731-7735; (c) Pinto, I. L., Jarvest, R. L., Serafinowska, H. T., *Tetrahedron Lett*., **2000**, *41*, 1597-1600.

[18](a) Mishra, A., Ma, C. Q., Bauerle, P., *Chem. Rev*., **2009**, *109*, 1141-1276; (b) Katz, H. E., Bao, Z., Gilat, S. L., *Acc. Chem. Res*., **2001**, *34*, 359-369.

[19](a) Noda, T., Imae, I., Noma, N., Shirota, Y., *Adv. Mater*., **1997**, *9*, 239-241; (b) Noda, T., Ogawa, H., Noma, N., Shirota, Y., *J. Mater. Chem*., **1999**, *9*, 2177-2181.

[20]Pisignano, D., Anni, M., Gigli, G., Cingolani, R., Zavelani-Rossi, M., Lanzani, G., Barbarella, G., Favaretto, L., *Appl. Phys. Lett*., **2002**, *81*, 3534.

[21]Shamsuzzaman, Mashrai, A., Khanam, H., Aljawfi. R. N., *Arab. J. Chem.*, http://dx.doi.org/10.1016/j.arabjc.2013.05.004

[22](a) Shamsuzzaman, Khan, M. S., Alam, M., Tabassum, Z., Ahmad, A., Khan, A. U., *Eur. J. Med. Chem*., **2010**, *45*, 1094-1097; (b) Shamsuzzaman, Khanam, H., Mashrai, A., Sherwani, A., Owais, M., Siddiqui, N., *Steroids*, **2013**, *78*, 1263-1272.

[23]Shim, H. W., Jin, Y. H., Seo, S. D., Lee, S. H., Kim, D. W., *ACS Nano*, **2011**, *5*,443-449.

[24]Ni, Y. H., Wei, X. W., Hong, J. M., Ye, Y., *Mater. Sci. Eng. B*., **2005**, *121*, 42-47.

[25]Filip, Z., Herrmann, S., Kubat, J., *Microbiol. Res*., **2004**, *159*, 257-262.

[26]Dutta, R. K., Sharma, P. K., Pandey, A. C., *J. Nanopart. Res*., **2010**, *12*, 1211-1219.

[27]Soares, J. W., Whitten, J. E., Oblas, D. W., Steeves, D. M., *Langmuir*, **2008**, *24*,371-374.

[28]Ha, B., Ham, H., Lee, C. J., *J. Phys. Chem. Solids*, **2000**, *869*, 2453-2456.

[29]Bhattacharyya, P., Pradhan, K., Paul, S., Das, A. R., *Tetrahedron Lett*., **2012**, *53*, 4687-4691.

[30]Ghomi, J. S., Ghasemzadeh, M. A,. *Acta Chim. Slov*., **2012**, *59*, 697-702.

[31]Ghosh, P. P., Das, A. R., *J. Org. Chem*., **2013**, *78*, 6170-6181.

[32]Tayebee, R., Javadi, F., Argi, G., *J. Mol. Catal. A: Chem*., **2013**, *368/369*, 16-23.

Received: 22.08.2014.
Accepted: 25.09.2014.

THE VISCOMETRIC ANALYSIS OF BIODIESEL FROM MUSTARD AND COCONUT OILS

Olamide A. Oshodi,[a] Chikaodili E. Chukwuneke[a] and Okoro Linus[a]

Keywords: biodiesel; mustard oil; coconut oil; fuel blends; viscosity; petroleum diesel.

In this research, we report biodiesel production and viscometric analysis from mustard oil and coconut oil, by subjecting the oil to a temperature of 65 °C through base catalyzed transesterification with the use of KOH as a catalyst. The biodiesel synthesized from mustard oil was blended with petroleum diesel in the following percentage by volume 20 %, 40 %, 50 %, 70 % and 80 % corresponding to B20, B40, B50, B70 and B80, respectively. The fatty acid methyl ester of mustard oil was mixed with that of coconut oil in the ratio of 80:20, 60:40 and 50:50 respectively. Viscometric analysis was carried out and the results obtained.

* Corresponding Authors
E-Mail: linus.okoro@aun.edu.ng
[a] American University of Nigeria, Department of Petroleum Chemistry and Engineering, School of Arts and Sciences, P.M.B 2250 Yola, Adamawa State, Nigeria.

Introduction

Biodiesel is a common biofuel that is widely used in Europe and Asia. It is produced from crops such as grape, sunflower and soya and can be blended with fossil diesel in any proportion which is compatible with most diesel engines. In 2004, biodiesel production accounted for 1.2 % of total diesel fuel consumption in Europe.[1] Biodiesel has numerous benefits ranging from their low carbon emission to little or no sulfur content. This advantage eliminates the possibility of acid-rain produced as a result of sulphur oxides in the atmosphere[2]. It is a renewable, locally-produced fuel which also reduces emissions of unburned hydrocarbons, carbon monoxides, particulate matter, sulfur compounds as well as carbon dioxide.[1] Another benefit of biodiesel is its compatibility with diesel engines as opposed to other energy sources such as natural gas, having radically dissimilar ignition properties.[2] Production of biodiesel is less energy intensive than ethanol (another commonly used biofuel from corn) due to the absence of fermentation and distillation processes used in the latter. In addition, biodiesel enhances greasiness of diesel fuel, and has good lubricity properties.[3] According to Knothe, the removal of sulfur in the refining process of conventional diesel, reduces its lubricity but biodiesel is blended with it, the lubricity property is restored.[2]

Petroleum diesel and biodiesel share some similar physico-chemical properties as well as some distinct differences. Petroleum diesel has a flash point that is well below half the value for biodiesel as well as a kinematic viscosity that is less than half of the value of biodiesel. However, both forms of diesel have similar cetane number, heating values and relative densities. The energy content of biodiesel has been found to be slightly lower than petroleum diesel. However, it does not affect performance or mileage in any way when used in the same engines.[3] Generally, studies have shown that biodiesel burns more completely than conventional diesel and leaves less residue in the engine than untreated oil.[2] Biodiesel alone cannot substitute regular diesel oil; as the world's supply of vegetable oil can only replace a small proportion of the normal energy market.[2]

Biodiesel blends of B5 (signifies the ratio rating, where 5 imply that the composition is 5 % biodiesel[4]) are generally recommended in diesel engines. Studies are yet to prove the absence of performance issues with blends above B5 and on storage of biodiesel as it degrades faster than normal diesel and yields to possible biological growth.[3] Furthermore, biodiesel also has been found to emit more nitrogen oxide than petroleum diesel when burned in an engine.[2]

The transesterification process is majorly used to synthesize biodiesel. This process has been used since the mid-19th century to separate glycerin from oil and to reduce the viscosity of vegetable oil used in diesel engines.[4] In the transesterification process, a triglyceride ester is reacted with an alcohol to produce another ester and alcohol. When the triglycerides are reacted with methanol, the resulting product is a methyl ester.[5]

The mustard oil can be extracted from the yellow mustard plant, *Sinapis Alba*.[6,7] The fatty acid components in triacylglycerols of mustard oil are: 4 *wt.* % Palmitic acid (16:0), 22 *wt.*% of oleic acid (18:1), 24 *wt.* % linoleic acid (18:2), 14 *wt.%* linolenic acid (18:3), 12 *wt.* % gadoleic acid (20:1) and 20 *wt.%* erucic acid.[3]

The viscosity of a substance is referred to as the opposition to the flow of a liquid due to the frictional force that exists between layers of liquid moving over each other.[8] The higher the viscosity of a fuel, the greater is the likelihood of it causing problems in the engine. Generally, the viscosity of a particular biodiesel is far less than the oil from which it was obtained.[9] The fatty acid content of a particular biodiesel usually determines its viscosity and it is the process of transesterification that reduces this viscosity. High viscosity is the main reason why oils are not used directly in the engines as alternative fuel. It is usually due to the number of carbon atoms and usually increases with high degree of saturation.[8]

Biodiesel can be blended in any ratio or proportion with petroleum diesel. The commonly used standard for denoting biodiesel ratio is the "B" factor, where 100 % biodiesel is referred to as B100 and 2 % biodiesel is referred to as B2. Research shows that CO_2 emissions are drastically reduced by 78 % in olive and cashew nut blends compared to regular diesel.[10] The emission rate is proportional to the level of blending where B5 blends will lower emissions proportionally not as low as a B100 blend. Generally, the increase in the B-ratio indicated the level of eco-friendliness of the fuel.[10]

Materials and Methods

Potassium hydroxide (analytical grade manufactured by Acros chemicals), Methanol (analytical grade manufactured by Fluka chemicals), Petro diesel (ConOil Plc), Bomb Calorimeter (Cal2k-3), Viscometer (Rheotek TCB-7), 100 % Pure Mustard Oil , 100% Pure Coconut Oil manufactured by KTC Edibles Ltd, Wednesbury**,** West Midlands **,** United Kingdom.

Synthesis of biodiesel from mustard and coconut oil

50 ml (43.74 g) of oil was measured and poured into an Erlenmeyer flask and preheated to 65 ºC with a magnetic stirrer. Potassium hydroxide (0.788 g) was measured and mixed thoroughly with 12.5 ml of methanol in another Erlenmeyer flask until all the Potassium hydroxide dissolved to form a homogenous mixture. The homogenous mixture provides the basis for a potassium methoxide solution which is now poured into the preheated mustard oil. The stirring was maintained at 300 rpm at 65 ºC for 120 min. After refluxing, the mixture was left overnight to separate in a separating funnel to remove excess glycerol. The transesterification process was monitored by IR spectroscopy.[13] The yields from mustard oil or coconut oil were found to be 96.56 and 94.66 %, respectively.

Measurement of viscosity

15 ml of each of the biodiesel oil samples blended was measured in to a viscometer. The viscosity was measured over specified temperature range of between 30 °C and 50 °C. The viscosity test determines the kinematic viscosity of the sample by measuring the time taken for the liquid to move under the influence of gravity through a calibrated glass viscometer. Kinematic viscosity was determined using a PSL (Poulten selfe & Lee Ltd., Essex. England) glass capillary viscometer placed in a Rheotek TCB-7 Viscometer bath observed from 30-50 °C. Using a calibration constant of 3.0, the time taken was multiplied by the constant to a unit of $mm^2 s^{-1}$.

Results and discussion

The high biodiesel yields found for both type of feedstock oil (~95-96%) could be attributed to the highly pure feedstock oils and long reaction time used in the reaction. The standard time used in comparable reactions is usually 90 min but in this work, the reflux time was 120 min. Table 1 summarizes the kinematic viscosity values of mustard biodiesel, coconut biodiesel, petro-diesel and their mixtures. From the results obtained, it can be readily inferred that viscosity decreases as temperature increases.

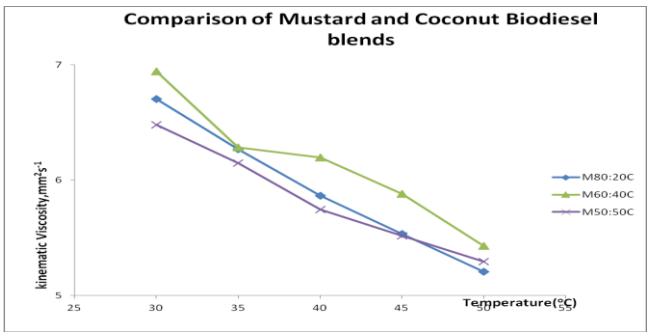

Figure 1. Viscosity of blends of mustard and coconut oil biodiesel

This is illustrated in Figure 1. The variation in viscosity between pure vegetable oil and the blends of the transesterified oil is depicted in Figure 1 and it shows that the transesterification process was effective in removing the glycerol, which is a problem in engines because of its high viscosity. In addition, blending the biodiesel of the mustard and coconut did not show any significant difference in their viscosity values (Figure 1). This implies that the biodiesel produced from the two different feedstocks have virtually the same viscosity and irrespective of the ratio of blending for both biodiesel, the viscostiy values with temperature showed no variation as depicted in figure 2. As a result of higher viscosity of biodiesel as compared to petrodiesel as shown in Figure 3, it is blended with petrodiesel in order to reduce its viscosity.

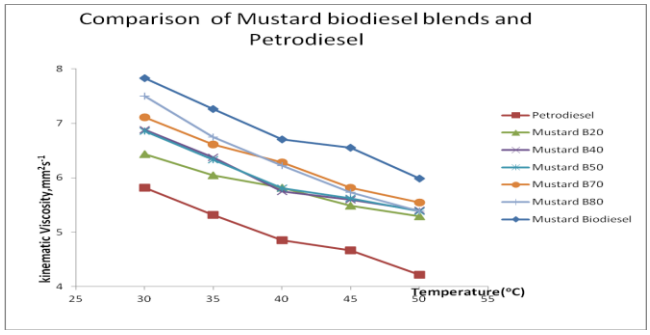

Figure 2. Viscosity of pure mustard and coconut oil compard with their biodiesel blends

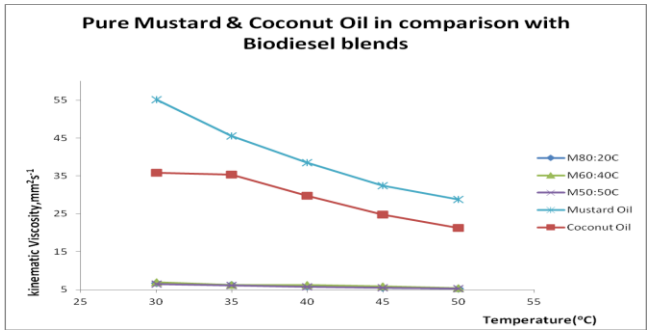

Figure 3. This shows the comparison between the viscosities of mustard biodiesel its blends and petro diesel at different temperature.

 DOI: 10.17628/ECB.2014.3.946-948

Table 1. Kinematic viscosity values in $mm^2 s^{-1}$ between 30 and 50 °C

Temp., °C	Mustard oil	Coconut oil	Mustard biodiesel	Coconut biodiesel	Petro-diesel	Mustard:coconut biodiesel		
						80:20	60:40	50:50
30	55.170	35.820	7.830	5.565	5.82	6.705	6.945	6.480
35	45.510	35.340	7.260	5.565	5.32	6.270	6.285	6.150
40	38.490	29.715	6.705	5.565	4.85	5.865	6.195	5.745
45	32.475	24.795	6.555	5.295	4.67	5.535	5.880	5.520
50	28.770	21.330	5.985	4.125	4.22	5.205	5.430	5.295

The blend ratio from B20 to B80 as shown in Figure 3, reveals that the higher the biodiesel in the blends, the higher the viscosity. By blending biodiesel and petroleum diesel in different proportions, one can monitor and regulate biodiesel production for use in a wide range of machinery. By blending as well mustard oil with lower viscous biodiesels, it is possible to achieve suitable fuel for many purposes (see Figure 3).

Conclusion

Biodiesel was synthesized from mustard and coconut oil by the process of transesterification which reduces the viscosity of oil from which the biodiesel was obtained. Petroleum diesel was blended the produced biodiesel to reduce the viscosity of pure biodiesel to acceptable standards, suitable for use in diesel engines.

References

[1]Olah, G., Goeppert, A., *Beyond Oil and Gas: The Methanol Economy Biodiesel*, Wiley-VCH: Weinheim, **2006**, 103-107.

[2]Wu, C., *Soc. Sci. Publ.*, **1998,** *154*, 364-366.

[3]Bacha, J., Freel, J., Gibbs, A., Diesel Fuels Technical Review, *Chev. Corp., California*, **2007**, 39-42.

[4]Home Made Biodiesel and History of Biodiesel, *www.home-made-biodiesel.com/history-of-biodiesel*, **2011**.

[5]Biodiesel Production Principles and Processes, *www.extension.org*, **2011**.

[6]*Mustard*. *Encyclopedia Britannica*. **2010**.

[7]Gulab, N. J., Bryan, R. M., Shailesh, N. S., Ronald, A. H., Onkar, D. D., Steven, F. V., Mark, A. B., Jill, K. W., Terry, A. I., Ray K. H., *J. Am. Oil. Chem. Soc.*, **2009,** *86*, 917-926.

[8]Knothe, G., Van Gerpen, J. Krahl, *The Biodiesel Handbook.* AOCS Press, **2005**, *89*.

[9]Okoro, L., Ekop, R., *Int. J. Res. Chem. Environ.*, **2011,** *1*, 76-82.

[10]Okoro, L. N., Sambo, F. I., Lawal, M., N., *Res. J. Chem. Sci.*, **2011,** *1(4)*, 90-97.

[11]Biofuels: The Fuel of the Future. *biofuel.org.uk/what-are-biofuels*, **2011**.

[12]Peterson, C., Thompson, J., *Biodiesel from Yellow Mustard Oil*, **2005**, *5-6*.

[13]Sherman, C., *Handbook of Instrumental Techniques for Analytical Chemistry*, Prentice hall: New Jersey, **1997**, 247-249.

Received: 21.08.2014.
Accepted: 25.09.2014.

INFLUENCE OF ALKYLATED NAPHTENİC ACID AMIDE CONTAINING BIOCIDE COMPOSİTİONS OF BAKU CRUDE OIL ON SULPHATE REDUCING BACTERIA

V. M. Abbasov,[a] A. R. Ezizbeyli,[a] R. A. Jafarova,[a] S. A. Ahmedbekova[a] and D. B. Agamalieva[a]

Keywords: corrosion; biodamage; naphthenic acids; inibitors; sulphate reducing bacteria.

Compounds formed in the reaction of napthenic acid amides of Baku crude oil with some of the alkyl halogenides are found to be multi-functional corrosion inhibitors. The structural features of compounds were studies with FT-IR spectroscopy. The efficiency of these inhibitors have also been tested against sulphate reducing bacteria (SRB) at 30 °C for and for a period of 15 days time.

Corresponding Authors
E-Mail: *ipcp@baku-az.net*
[a] Mamedaliev Institute of Petrochemical Processes, National Academy of Sciences of Azerbaijan, AZ1025 Baku, Azerbaijan

INTRODUCTION

Corrosion of metals causes significant economic losses in the oil and gas industry all over the world.[1-3] Despite the development of various methods, latest chemical technology and inhibitory protection, corrosion of metals still remains a serious and critical problem. Approximately 77-80 % of the accidents occurred in oil and gas industries were due to biocorrosion.[4-6] Bio-damage is a typical failure of metallic structures and is due to destructive effect of microorganisms and their metabolic products towards metals. The mechanisms of bio-damage basically depend on the characteristics of the metal as well as other bio-factors. Crude oil is considered to be a mixture of hydrocarbons, which is not an optimum medium for the development of microorganisms, however, water of simulated oil field enriched by sulfur compounds is favorable ecosystem for the development of sulphate reducing bacteria (SRB).[7-9]

The majority of the problems in the oil and gas industries are the result of insistent technological environment caused by hydrogen sulfide (H_2S) and carbon dioxide (CO_2). Formation of H_2S and its concentration is mainly associated with the existence of SRB's.

Corrosion problems occurr due to the presence of carbon dioxide in the oil. Inspite of various efforts and investigations on corrosion problems by carbon dioxide is still a serious problem of the oil and gas industry all over the world.[10-19] In the oil extraction and processing industries, corrosion inhibitors are considered as the front line defense against corrosion. In recent times, most of the inhibitors used in producing oil wells have been organic nitrogen compounds.

Presently, the bactericide behavior of some compounds (and their mixtures) synthesized from the reaction of amides with alkyl halogenides are investigated and reported. The results show that, the synthesized compounds are good inhibitors against SRB's activity.

EXPERIMENTAL

The compounds formed in alkylation of amides with alkylhalogenides were synthesized from the amides of naphthenic acids obtained from Baku crude oil.[20] Amides were synthesized from polyethylene polyamine and naphthenic acids from Baku crude oil and then these synthesized-amides were alkylated with the alkyl halogenides such as: $C_5H_{11}Br$; C_3H_7Br; C_6H_5Cl; C_4H_9Cl; $C_8H_{17}Br$; $C_5H_{11}Cl$ (iso); $C_6H_{13}Cl$ following the standard procedures.

The sructures of the synthesized amides and their alkylated compounds were identified by physico-chemical and spectroscopic methods (Table 1).

Infrared spectra for the synthesized compounds were obtained using a Spectogram on BX FT-IR spectrometer using KBr disks.

RESULTS AND DISCUSSION

Influence of synthesized compounds on the activity of SRB in a period of 15 days time

SRB is an obligate anaerobic bacterium which converts sulphates into H_2S. One of the most optimal cultural medium for growth of SRB is Postgate B. The compositions of this medium are recorded in Table 2. The parameters were calculated and given for 1 litre of solution. The pH was adjusted between 7.0 and 7.5.

Table 1. Physical-chemical properties of imidazoline compounds with alkyl halogenides

Compounds code name and composition		Molar ratio	Density, d_4^{20}, g cm^{-3}	Refraction coefficient, η_{20}^{D}	Freezing temperature, ^{0}C
F-1	amide and C_3H_7Br	1:1	0.9268	1.4300	-53
F-2	amide and C_3H_7Br	1:2	0.9288	1.4340	-52
F-3	amide and C_3H_7Br	1:3	0.9296	1.4310	-60
F-4	amide and $C_5H_{11}Br$	1:1	0.9124	1.4160	-60
F-5	amide and $C_5H_{11}Br$	1:2	0.9298	1.4330	-60
F-6	amide and $C_5H_{11}Br$	1:3	0.9314	1.4330	-60
F-7	amide and C_6H_5Cl	1:1	0.9664	1.4400	-40
F-8	amide and C_6H_5Cl	1:2	0.9788	1.4460	-50
F-9	amide and C_6H_5Cl	1:3	1.0381	1.4680	-58
F-10	amide and C_4H_9Cl	1:1	0.9269	1.4600	-56
F-11	amide andC_4H_9Cl	1:2	0.9500	1.4710	-56
F-12	amide and C_4H_9Cl	1:3	0.9750	1.4760	-56
F-13	amide and $C_8H_{17}Br$	1:1	0.9600	1.4550	-56
F-14	amide and $C_8H_{17}Br$	1:2	0.9700	1.4470	-56
F-15	amide and $C_8H_{17}Br$	1:3	0.9900	1.4520	-52
F-16	amide and $C_5H_{11}Cl$ (iso)	1:1	0.8650	1.4160	-56
F-17	amide and $C_5H_{11}Cl$ (iso)	1:2	0.8700	1.4110	-56
F-18	amide and $C_5H_{11}Cl$ (iso)	1:3	0.8700	1.4160	-56
F-19	amide and $C_6H_{13}Cl$	1:1	0.8480	1.4050	-56
F-20	amide and $C_6H_{13}Cl$	1:2	0.8500	1.4100	-56
F-21	amide and $C_6H_{13}Cl$	1:3	0.8800	1.4200	-56

Table 2 The composition of Postgate B cultural medium

Name of substance	Amount, g
Potassium phosphate (KH_2PO_4)	0.5
Ammonium chloride (NH_4Cl)	1.0
Calcium sulfate ($CaSO_4$)	1.0
Magnesium sulfate ($MgSO_4{\cdot}7H_2O$)	2.0
Sodium lactate	3.5
Sodium chloride	2.0

Cultural medium was optimized by the addition of special additives into the medium. Further additives used were: $FeSO_4{\cdot}7H_2O$ (5 % iron sulfate in 2% hydrochloric acid solution), sodium bicarbonate $NaHCO_3$ (5 % solution), crystalline $Na_2S.9H_2O$ (1 % sodium sulfide in 1 % sodium bicarbonate ($NaHCO_3$) solution).

SRB 1143 strain has been used in the experiments under test. Pre-sterilized test tubes (20 ml volume) were used.[21] Bactericide effects of the reagents have been tested over a 15 days period and calculated from the amount of the generated H_2S. H_2S was determined iodometrically by a standard method. Effects of compounds on the activities of SRB in concentrations of 0.025; 0.075 and 0.1 % are shown in the Table 3. It may be seen from the Table 3 that compounds synthesized from the reaction of amides with C_3H_7Br in molar ratio 1:1 (F-1) and 1:2 (F-2) showed biocide activity even at concentration of 0.025; 0.075 and 0.1 % and could stop the activity of the SRB.

The compound synthesized from amide and C_3H_7Br using 1:3 molar ratio (F-3) in concentration of 0.025 % showed a biostat effect i.e. showed a weak effect to life activities of SRB. But in concentration of 0.075 % and 0.1 % had the effect of biocide. The compound synthesized from amide and $C_5H_{11}Br$ using 1:1 molar ratio (F-4) had the effect of biocide in all concentrations, but the compound obtained using 1:2 molar ratio of amide and $C_5H_{11}Br$ (F-5) in concentration of 0.025 % and 0.075 % has biostat effect on SRB at 0.1 % concentration. The compound from the amide and $C_5H_{11}Br$ at molar ratio of 1:3 (F-6) has biocide effect. Among compounds from amide:C_6H_5Cl in molar ratio of 1:1 (F-7); 1:2 (F-8) and 1:3 (F-9), the compounds F-7 and F-8 showed biostat effects on SRB's life activity in 0.025 % concentration, and biocide effect at concentrations of 0.075 % and 0.1 %. Compound F-9 has biocide effect at all concentrations. The compounds from amide and C_4H_9Cl in 1:1 (F-10) and 1:2 (F-11) molar ratio were shown effect of biocide to life activity of SRB. But the compound synthesized from amide and C_4H_9Cl (F-12) in 1:3 molar ratio showed biostat effect in concentration of 0.025 %, but proved to be biocide at all other concentrations.

The compounds synthesized from amide and $C_8H_{17}Br$ in molar ratio 1:1 (F-13); 1:2 (F-14); 1:3 (F-15) has stopped life activity of SRB at all concentrations. The compound F-16 from 1:1 molar ratio of amide and iso-$C_5H_{11}Cl$ () was biocide in all concentrations, those from molar ratios of 1:2 (F-17) and 1:3 (F-18) showed biostat effects in concentration of 0.025 %, but showed biocide effects in 0.075 % and 0.1 % concentrations on SRB. The compounds from amide and $C_6H_{13}Cl$ in molar ratio 1:1 (F-19); 1:2 (F-20); 1:3 (F-21) stopped life activity of bacteria in all concentrations. Control 1 is a culture media without SRB, but control 2 is a culture media with SRB. As can be seen from the Table 3 that no culture grew in the control 1, butthe generated content of H_2S in the control 2 was 270 mg L^{-1} due to SRB growth.

Therefore, the compound F-4 (amide:$C_5H_{11}Br$, in molar ratio 1:1) showed the most powerful bactericidal efficiency.

Table 3. Effect of compounds on the life activities of SRB

Compounds code name and initiative matter	Molar ratio	Compound concentration, %		
		0.025	0.075	0.1
		H_2S content, mg L^{-1}		
(F-1) amide:C_3H_7Br	1:1	29	28	25
(F-2) amide:C_3H_7Br	1:2	30	26	25
(F-3) amide:C_3H_7Br	1:3	85	28	27
(F-4) amidee:$C_5H_{11}Br$	1:1	26	25	25
(F-5) amide:$C_5H_{11}Br$	1:2	85	83	28
(F-6) amide:$C_5H_{11}Br$	1:3	51	28	27
(F-7) amide:C_6H_5Cl	1:1	86	27	26
(F-8) amide:C_6H_5Cl	1:2	87	25	25
(F-9) amide:C_6H_5Cl	1:3	27	27	26
(F-10) amide:C_4H_9Cl	1:1	28	26	25
(F-11) amide:C_4H_9Cl	1:2	27	26	25
(F-12) amide:C_4H_9Cl	1:3	196	30	27
(F-13) amide:$C_8H_{17}Br$	1:1	28	27	25
(F-14) amide:$C_8H_{17}Br$	1:2	30	27	26
(F-15) amide:$C_8H_{17}Br$	1:3	27	26	25
(F-16) amide:$C_5H_{11}Cl$-i	1:1	27	26	25
(F-17) amide:$C_5H_{11}Cl$-i	1:2	187	28	26
(F-18) amide:$C_5H_{11}Cl$-i	1:3	127	26	25
(F-19) amide:$C_6H_{13}Cl$	1:1	28	26	25
(F-20) amide:$C_6H_{13}Cl$	1:2	27	26	25
(F-21) amide:$C_6H_{13}Cl$	1:3	28	26	25
Control 1 (culture media without SRB)	25			
Control 2 (culture media, with SRB)	270			

Chemical structure of the synthesized amidoalkyhalogenide compounds

The structural characteristics of purified product were confirmed by FT-IR spectroscopy in the range 4000–500 cm^{-1}, as shown in Fig. 1. IR spectrum of sample F-4 contains a series of absorption bands of varying intensity in the region 500-4000 cm^{-1}. In addition, there was a band at 729.57 cm^{-1} indicating the presence of the pendular oscillations of C-H bond in CH_2 group. The band bending at 1377.13 sm^{-1} and stretching vibrations at 2862.24, 2955.60 cm^{-1}, are characteristic for the C-H bond of the methyl (CH_3) groups. The absorption bands of strong intensity of deformation at 1377.13 cm^{-1} and stretching vibrations at 2862.24, 2955.60 cm^{-1} are characteristic for the C-H bond of the methylene (CH_2) groups. Carbonyl absorption band of N-acyl groups at 1550.00, 1643.55 and 1731.65 cm^{-1} are observed in several bands lower and upper frequency. Additionally, stretching band at 2356.97 cm^{-1} is due to NH_2 group. There are absorption bands at 814.65, 951.16, 1289.32 cm^{-1} in spectrum are characteristic for the corresponding C-H bond. Stretching band at 2335.01, 2356.97 cm^{-1} are due to NH_2 group. Stretching bands at 1047. 86, 1097.25 cm^{-1} are characteristic for the O−H bond of the OH groups. There are absorption bands of strong intensity of stretching vibrations at 505.68, 528.65, 544.00, 578.00 cm^{-1} which are characteristic of the C−Br bond.

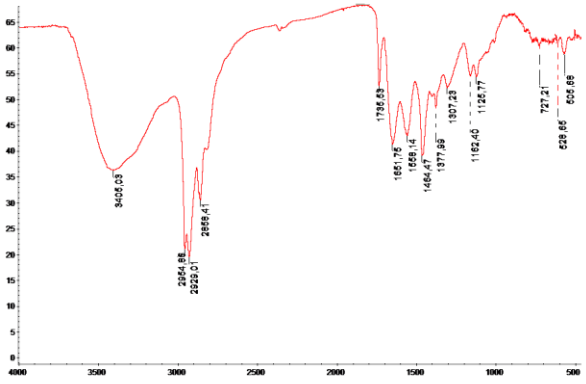

Figure 2. IR Spectrum of the **F-4** compound.

SUMMARY

The following conclusions are drawn from the present study:

SRB's 1143 strain have been used in tests to study the bactericide efficiency of friendly compounds of amidoalkylhalogenides synthesized on the bases of naphthenic acids fom Baku crude oil.

The structures of synthesized compounds were confirmed by physico-chemical and spectroscopic methods.

All synthesized compounds showed bactericidal effect as biostat and biocide.

It has been identifide that synthesized compound of amide uing $C_5H_{11}Br$ in molar ratio of 1:1 (F-4) stopped the life activities of SRB in consentrtions of 0.025; 0.075 and 0.1%. It has a stronger bactericide efficiency than could be observed in other compounds.

REFERENCES

[1]Miksic, B. Boyle, R. and Wuertz, B., *Corrosion*, **2004**, *60*, 515–522.

[2]Pao, P. S., Teng, C. R. and Gill, S. J., *Corrosion*, **2000**, *56(10)*, 1022-1031.

[3]Kolotyrkin, Ya. M., *Metals and Corrosion* (in Russian), Metallurgiya, **1985**, 88.

[4]Asfandiyarov, F. A., Kildibekov, I. G:, Nizamov, K. P., *Methods of dealing with sulfate reducing bacteria and called by them corroded steel* (in Russian), **1983**, 32.

[5]Azabou, S., Mechici, T., Sayadi, S., *Miner. Eng.*, **2007**, *20(1-2)*, 173-178.

[6]Cohen, R. R. H., *J. Cleaner Prod.*, **2006**, *14(12-13)*, 1146-1157.

[7]Moiseeva, L. S., Kondrovo, O. V., *Protec Metals (Zashch. Metallov)* (in Russian) **2005,** 417-426.

[8]Qarifullin, F. S., *Preventing the formation of complex sulfide-precipitation in the extraction water-cut oil* (in Russian) **2002,** 417-426.

[9]Qonik, A. A., *The practice of anticorrosive protection* (in Russian) **2001,** 48-57.

[10]Abd El-Lateef, H. M., Aliyeva, L. I., Abbasov, V. M., Ismayilov, T. I., Ismayilova, X. R., *Chem. J.*, **2012,** *2(2)*, 38-51.

[11]Abd El-Lateef, Hany M., Aliyeva1, L. I., Abbasov, V. M., Ismayilov, T. I., **2012,** *3(2)*, 1185-1201.

[12]Abd El-Lateef, H. M., Abbasov, V. M., Aliyeva, L. I., Ismayilov, T. I., Qasimov, E. E., Ahmadov, T. U., *Global J. Phys. Chem.*, **2012,** *3*, 14.

[13]Videm, K., Dugstad, A., *Mater. Perform.*,**1989,** *28(9)*, 63–67.

[14] Olsson, C. O. A., Landolt, D., *Electrochim. Acta*, **2003**, *48*, 1093–1104.

[15]Okafor, P. C., Nesic, S., *Chem. Eng. Com.*, **2007**, *194*, 141–157.

[16]Song F. M., Kirk D. W., Graydon, J. W., Cormack D. E., *Corrosion*, **2004**, *60*, 736.

[17]Mikhailovskii, Y. N., Marshakov, A. I., Petrov, N. A., *Prot. Met.*, **1997,** *33*, 293–295.

[18]Lopez, D. A., Schreiner, W. H., de Sanchez, S. R., Simison, S. N., *Appl. Surf. Sci.*, **2003,** *207*, 69–85.

[19]Durnie W., Kinsella B., De Marco R., Jefferson A., *Appl. Electrochem.*, **2001,** *31*, 1221–1226.

[20]Abbasov, V. M., Memedxunova, S. A., Abd El Lateef, H. M., Aliyeva, L. I., Ismayilov, T. A., Musayev, C. I., Aydamirov, O. A., Amirov, F. A., *Res. J. Appl. Sci.*, **2014**, 9(2), 66-75.

[21]Postgate, J. R., Campbell, L. L., *Bacteriol. Rev.*, **1966**. 30(4), 732- 738

Received: 17.05.2014.
Accepted: 28.09.2014.

KINETIC-SPECTROPHOTOMETRIC DETERMINATION OF TRACE AMOUNTS OF SULFIDE WITH MALACHITE GREEN IN MICELLAR MEDIUM

Nina Alizadeh[a]* and Mohammad Mahjoub[a]

Keywords: Kinetic spectrophotometry; sulfide determination; malachite green; micelle.

The determination of trace amount of sulfide based on the addition reaction of sulfide with malachite green at pH= 7.5 and 25 ºC has been investigated in micellar media. Surfactants studied include non-ionic surfactant, Trition-x-100, anionic surfactant, sodium dodecyl sulfate (SDS), cationic surfactant, cetyltrimethylammonium bromide (CTAB) and cetylpyridinium chloride (CPC). The reaction is followed spectrophotometrically by measuring the decrease in absorbance of the indicator at λ_{max}= 630 nm by the fixed time method. The reaction in the presence of Trition-x-100 is faster than in the absence of surfactant in medium. No significant change was observed with SDS, CTAB and CPC. Under the optimum experimental conditions decreases in the absorbance of malachite green is proportional to the concentration of sulfide in the range 25-1750 ng ml^{-1} with a fixed time method at the first 5, 15 and 25 seconds from initiation of the reaction. The detection limit and quantification limit of the proposed kinetic method were 0.166, 0.207and 0.281 µg ml^{-1}(Δt=5, 15 and 25 s)and 0. 555, 0.692and 0.959 µg ml^{-1}(Δt=5, 15and 25) respectively. To confirm the usefulness of the proposed method, sulfide was determined in river, spring, fish farm, and tap water wastewater samples without any purification or using masking reagents.

* Corresponding Authors
Fax: +981313233262
E-Mail: n-alizadeh@guilan.ac.ir
[a] Department of Chemistry, University of Guilan, Namjoo Street, P.B. 41335-1914, Rasht, Iran

Introduction

Determination of sulfide species concentration is important to a variety of studies including groundwater monitoring, assessment of biogeochemical processes, water and wastewater treatment,[1] environmental protections and etc. Sulfide is toxic to fish and other aquatic organisms.[2] There are limits on the total level of sulfide permitted in waste discharges.[3,4]

A number of techniques have been developed to measure sulfide species in natural systems.[5] These include colorimetric methods,[6,7] a variety of electrochemical methods using potentiometric,[8] voltammetry,[9] amperometry,[10] and polarography,[11] methods based on gas chromatography,[12,13] HPLC,[14] flow injection analysis[15,16] and spectrophotometry.[17,18] Major limit to determination of sulfide is its reactivity with O_2. For this reason, sulfide is not detected far from source areas, or long after collection, unless they are preserved. Therefore, in recently research the Methods capable of rapid measurements in the field are desirable. Spectrophotometric methods are suitable methods for in situ determination. In the literature, different spectrophotometric methods for the determination of sulfide have been reported (Table 1).

Only a few studies are found on the equation rate and kinetic parameters of spectrophotometric determination of sulfide. It is important to be able to predict the rate equation at which bleaching process occurred. Kinetic parameters help to provide valuable insights into the reaction pathways and they can useful to appropriate treatment plants. So in the presented work different kinetic parameters and rate equation was studied in the novel medium. This paper demonstrates the potential of spectrophotometric detection of the sulfide ion in micellar medium.

Experimental

Materials and methods

Reagents: All reagents used were analytical regent grade (from Merck) and their solutions made up indoubly distilled water. Standard stock sulfide solution (100 ppm) was prepared daily by dissolving 0.05 g of sodium sulfide in water and diluted to 500 ml in suitable volumetric flask. Malachite green solution(Merck, MW=927.02 g mol^{-1}) (0.1 % w/v) was prepared by dissolving 0.1 g of the reagent compound in water and solution was diluted to the mark in a 100 ml volumetric flask. Diluted Triton X-100 solution (0.1 % W/W) was used to maintain the micellar media. The other surfactants tested, namely cetyltrimethyl ammonium bromide (CTAB)), cetylpyridinium chloride (CPC) cationic micelles,, sodiumdodecyl sulphate (SDS) anionic micelles, were prepared in a similar way.

Buffer of different pH values were prepared by standard procedures (Britton-Robinson's instruction[31]).

Apparatus: Jenway 6715 UV/Vis Spectrophotometer with 1 cm matched cell was used for all measurements. CO-W06 incubator from Pars-Azma with temperature range 0-60 ºC was used to keep the temperature of all solutions at the working temperature. A Jenway 4330 digital pH-meter was used for pH measurements. C1biotech 50 µlit and 25 µlit Hamilton syringes were used to dilute and pick up the solutions.

Table 1. Number of different spectrophotometric methods reported of determination of sulfide in previous literatures.

Anal. methods	Reaction system, method	λ_{max}, nm	Medium	Dynamic range, μg mL^{-1}
Spect.[19],[a]	Solvent extraction, methylene blue	657	No micelle	0.016-0.32
Kinetic spect.[20]	Methyl green indicator	637	No micelle	0.03-1.2
Spect.[21]	Indirect extraction flotation with copper(II) ammonium sulfate-ethanol in aq. medium	510	No micelle	0.024-3.2
Spect.[22]	Ammonium (2',3'-dihydroxypyridyl-4'-azo)benzene-4-arsonate (DHP-4A)	535	No micelle	0.016-0.505
Flow injection Spect.[23]	Krap pulp mills with iron(III) in nitrilotriacetic acid	636	No micelle	20-100
Kinetic spect.[24]	Magneta	540	No micelle	0.025-2.5
Kinetic spect.[25]	A new fuchsin indicator	-	No micelle	0.05-2.5
Kinetic spect.[26]	Artificial neural networks with brilliant green indicator	605	No micelle	0.05-3.6
Kinetic spect.[27]	Partial least square (PLS) regression	617	No micelle	0.030-1.2
Kinetic spect.[28]	Methyl green indicator	628	No micelle	0.05-2.5
Flow injection spect.[29]	N,N-dimethyl-p-phenylenediamine (DMPD))	668	No micelle	0.10-1.0
Kinetic spect.[30]	Thionin indicator	600	No micelle	21.0-38.0(Δt=60 s) 10.0-20.0 (Δt=120 s)
Present work	Malachite green indicator	630	Micellar	0.025-1.5(Δt=5, 25 s), (Δt=15 s)

[a]Spect. means spectrophotometry

Procedure: 2 ml of buffer solution was transferred in to a 10 ml volumetric flask and then 0.9 ml from surfactant solution added to it. Aliquot of malachite green solution was added to the flask. The solution was diluted to 9 ml with water. Then, suitable amount of sulfide was added and solution was diluted to the mark (10 ml) with water. The solution was mixed and a portion of it was transferred to the spectrophotometric cell. After distinct lag time (3 seconds), the reaction was followed by measuring the decrease in absorbance of the solution at 630 nm for 5,15 and 25 seconds from initiation of the reaction. The same procedure was repeated without adding sulfide ions for achieving to blank signal. The difference between sample and blank absorbance was shown with $\Delta(\Delta A)$.

Results and discussion

Malachite green under goes a bleaching reaction with sulfide in neutralized media. This process was followed spectrophotometricaly by measuring the decrease in absorbance. It was found that in the presence of Triton X-100 as micellar medium, the trend of reaction was reproducible. Therefore, by measuring the decrease of absorbance versus time in the presence of selected surfactant, the concentration of sulfide can be measured. Figure 1 shows the relationship between Absorbance and reaction time.

The stoichiometry indicated by the results from mole ratio method. Concentration of malachite green was kept constant, while the concentration of sulfide varied. The absorbance of the reaction mixtures was measured after 5, 15 and 25 seconds from the initiation of the reaction.

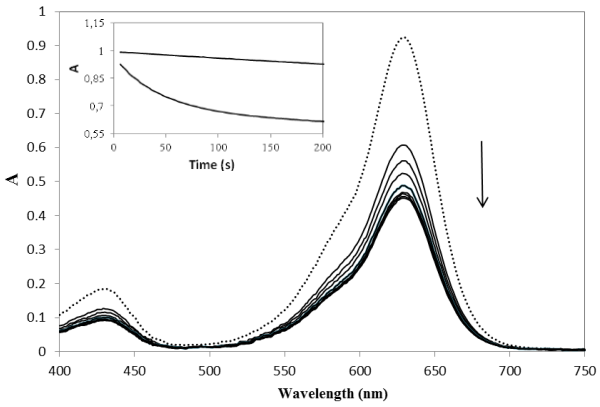

Figure 1. Absorption spectra of the malachite green-sulfide system at 25 ºC; 5.48×10^{-5} M malachite green, 5 μg ml^{-1} S^{2-}, 3.0×10^{-4} M Triton-X-100, 2 ml (K_2HPO_4-NaOH) buffer pH: 7.5; lag time: 3 seconds (absorbance measurement started 3 seconds after sulfide addition). Intercept: continues showing of decreasing in absorbance in 100 seconds (s: sample, b: blank).

Point of inflexion on the curve corresponds to reaction stoichiometry. The result from Job's method continues variation agreed with finding previously.

The 2:1 malachite green:sulfide stoichiometry indicated by results of mole ratio and Job's method continues variation in the presence of surfactant, suggests that the overall reaction can be proposed by reaction:

$$2MG^{+} + S^{2-} \rightarrow MG_2S$$

After inflexion point, when the absorbance values have been constant, the molar absorptivity calculated 1.99±0.016 $\times10^4$ M^{-1} cm^{-1}.

 DOI: 10.17628/ecb.2014.3.953-960

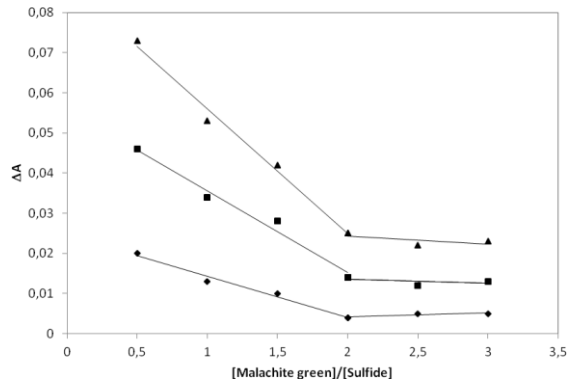

Figure 2. Plot of absorbance versus mole ratio for the reaction of malachite green with sulfide. Experimental conditions: malachite green: 6.85×10^{-5} M, sulfide (2.74×10^{-4}-2.28×10^{-5} M), 2 ml (K_2HPO_4-NaOH) buffer pH: 7.5; lag time: 3 seconds; *T*: 25 ºC, (—◆—Δ*t*: 5 s), (—■—Δ*t*: 15 s) and (—▲—Δ*t*: 25 s).Intercept: Job's method of continues variations of malachite green-sulfide systems; concentration of malachite green and sulfide solutions: 5.52×10^{-4} M.

Effect of pH: the effect of pH on the rate of reaction was investigated in pH range 5.5 – 8.5. Δ(ΔA) in three selected fixed times measured and plotted versus pH. It was observed that the color of malachite green bleaches in neutralized pH. Therefore study was carried out in pH: 8.

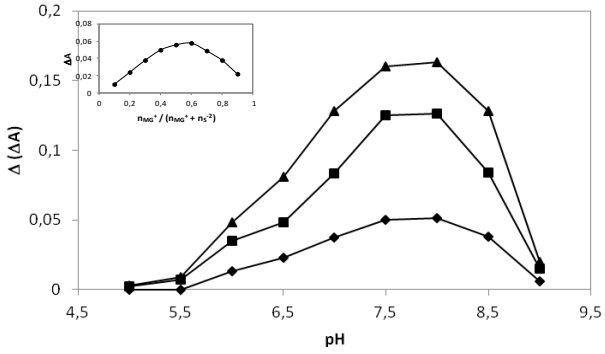

Figure 3. Effect of pH on the rate of reaction. Experimental conditions: 5.48×10^{-5} M malachite green, 5 µg ml^{-1} S^{2-} (blank was without sulfide), 2 ml (K_2HPO_4-NaOH) buffer pH: 7.5; lag time: 3 seconds; fixed time method: (—◆—Δt: 5 s), (—■—Δt: 15 s) and (—▲—Δt: 25 s).

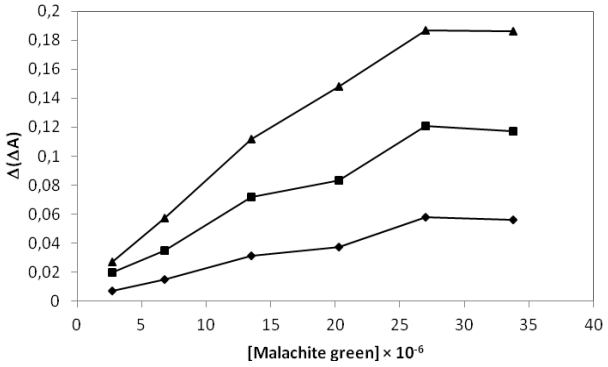

Figure 4. Effect of malachite green concentration on the rate of reaction. Experimental conditions: 1.37×10^{-5}–1.096×10^{-4} M malachite green, 5 µg $ml^{-1}$of S^{2-} (blank was without sulfide), 2ml (K_2HPO_4-NaOH) buffer pH: 7.5; lag time: 3 seconds; fixed time method: (—◆—Δ*t*: 5 s), (—■—Δ*t*: 15 s) and (—▲—Δ*t*: 25 s).

Effect of reagent's concentration: Fig. 4 shows the effects of concentration of malachite green. It was observed that the difference in the absorbance ($\Delta(\Delta A)=\Delta A_S-\Delta A_b$) increases with increasing malachite green concentration up to 6.85×10^{-5} M and reached to constant value at higher concentration. This phenomenon was due to the fact that in high concentration of indicator the blank effect increased and caused to decrease the net reaction rate.

Effect of temperature: the effect of solution temperature on the malachite green- sulfide system was studied at various temperatures and the results obtained were shown in Figure 5. Temperature influence on the reaction rate was investigated in the range of 15 to 30 ºC at optimum conditions. The rate of reaction was increased with increasing temperature. The blank absorbance had affected up to 25 ºC more than sample. So the difference between blank and sample Absorbance (Δ(Δ*A*)) beginning to decrease or has same value after 25 ºC. Thus, 25 ºC was selected as optimum temperature.

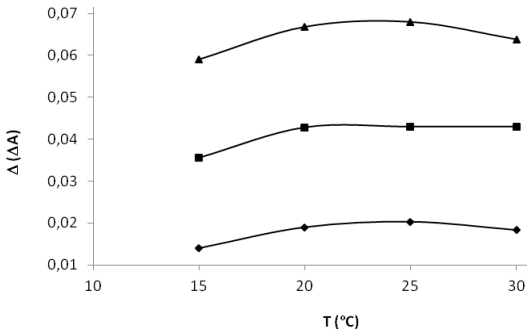

Figure 5. Effect of temperature on the reaction rate. Experimental conditions: 6.85×10^{-5}M malachite green, 3µg/ml^{-1} S^{2-} (blank was without sulfide), 2ml (K_2HPO_4-NaOH) buffer pH: 7.5; lag time: 3seconds;T: 5-45 ºC. Fixed time method: (—◆—Δt: 5 s), (—■—Δt: 15 s) and (—▲—Δt: 25 s).

Order of addition of reagents. Different order of addition of reactants was discussed in figure 6. It was found that the order of addition can affected the rate of reaction. The sequence (3) with buffer-surfactant-indicator-water-sulfide order, gave the maximum rate of reaction.

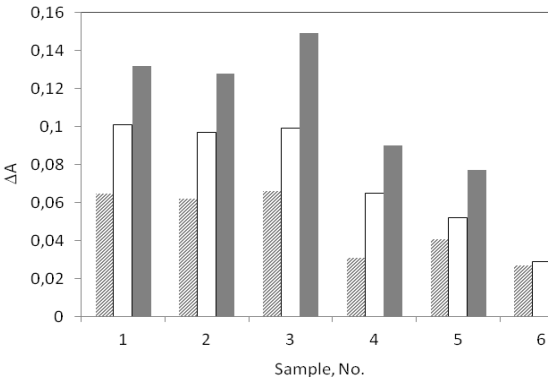

Fig. 6. Reaction rate variation with reactants addition order. (1) surfactant (Su.) + malachite green (M.G.) + buffer(Buf.) + water (W) + Sulfide ion (S) (2) Buf+M.G+Su+W+S (3) Buf+Su+M.G+W+S (4) Buf+Su+M.G+S+W (5) Su+M.G+S+Buf+W (6) M.G+S+Su+Buf+W. Experimental conditions: 6.85×10^{-5}M malachite green, 5µg.ml^{-1} S^{2-} , 2ml (K_2HPO_4-NaOH) buffer pH: 7.5; lag time: 3 seconds; T: 25ºC. Black columns: Δ*t*=25, white columns: Δ*t*=15 and dashed columns: Δ*t*=5.

 DOI: 10.17628/ecb.2014.3.953-960

Concentration of surfactant: Under the optimum conditions, surfactants can promote the reaction rate.[33-36] The influence of micellar medium on the reaction rate was examined. The surfactants solutions were used at concentration above the critical micelle concentration (CMC).

Table 4. Surfactant effects tasted on the rate of malachite green-sulfide reaction.

Surfactant	Type	CMC (M)	Micellar effect
Triton X-100	Nonionic	3.0×10^{-4}	Positive
SDS[a]	Anionic	8.1×10^{-3}	Negative
CTAB[b]	Cationic	1.3×10^{-3}	Inert
CPC[c]	Cationic	1.2×10^{-4}	Inert

[a]Sodium dodecyl sulfate. [b]Cetyltrimethyl ammonium bromide. [c]Cetylpyridinium chloride

It seems that both ionic micelles, cationic and anionic surfactant, are not suitable surfactant for malachite green-sulfide system. In the presence of Triton X-100, positive effect on reaction rate occurred. To see the role of nonanionic surfactant Triton X-100 on the raction rate, a series of kinetic runs were carried out with varied concentrations of surfactant from 0 M to 0.025 M (Figure 7). The reaction was found to be accelerated by Triton X-100 with the rate constant increasing as Triton X-100 concentration increased reaching a plateau at higher concentration.

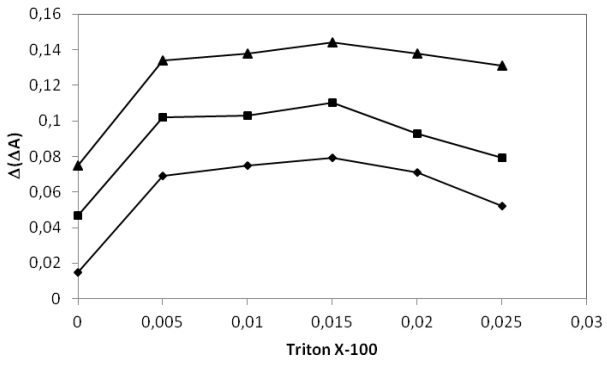

Figure 7. Effect of Triton X-100 concentration on the reaction rate. Experimental conditions: 0–0.025 M Triton X-100, 6.85×10^{-5} M malachite green, 3 µg mL^{-1} S^{2-} (blank was without sulfide), 2 ml (K_2HPO_4-NaOH) buffer pH: 7.5; lag time: 3 seconds; T: 25ºC. Fixed time method: (—◆— Δ*t*: 5 s), (—■— Δ*t*: 15 s) and (—▲— Δ*t*: 25 s).

The presence of Triton X-100 molecules on the interfacial region provides possible an additional attractive interaction for the malachite green molecules. This is likely thr role Triton X-100 is playing towards the observed catalysis. The surfactant thus, helps in bringing the reactants together into a small volume, which orients in a manner suitable for the reaction to take place followed by rearrangement of Triton X-100 molecules.

Analytical characteristics

Three calibration graphs were obtained by plotting Δ*A vs.* sulfide concentration, with applying the fixed time method at 5, 15 and 25 seconds from the initiation of the reaction. These interval times selected due to the good correlation obtained between Δ*A* and concentration of sulfide. The linearity was obtained under the already mentioned optimum experimental conditions.The maximum linearity range was achieved 25-1750 ng.mL^{-1} for 15 seconds fixed time method.The statistical parameters such as different standard deviation andtheoretical and experimental limit of detection and limit of quantificationcalculated and reported in Table 2.

Table 2. Statistical and regression parameters from calibration curves.

Time interval (s)	Δ*t*=5	Δ*t*=15	Δ*t*=25
Linear range, ng mL^{-1}	25 - 1500	25 - 1750	25 - 1500
Slope	3.6×10^{-2}	7.95×10^{-2}	11.47×10^{-2}
Intercept	5×10^{-3}	1.06×10^{-2}	2.23×10^{-2}
Correlation coefficient	0.9986	0.9978	0.9981
$SD_{(y/x)}$	2.86×10^{-3}	4.08×10^{-3}	1.09×10^{-2}
SD of slop	1.52×10^{-3}	2.16×10^{-3}	5.78×10^{-3}
SD of intercept	2.01×10^{-3}	2.87×10^{-3}	7.68×10^{-3}
Number of replicate	5	5	5
Theoretical LOD (µg.ml^{-1})	0.238	0.153	0.285
Theoretical LOQ (µg.ml^{-1})	0.794	0.513	0.959
Experimental LOD (µg.ml^{-1})	0.166	0.207	0.287
Experimental LOQ (µg.ml^{-1})	0.555	0.692	0.959

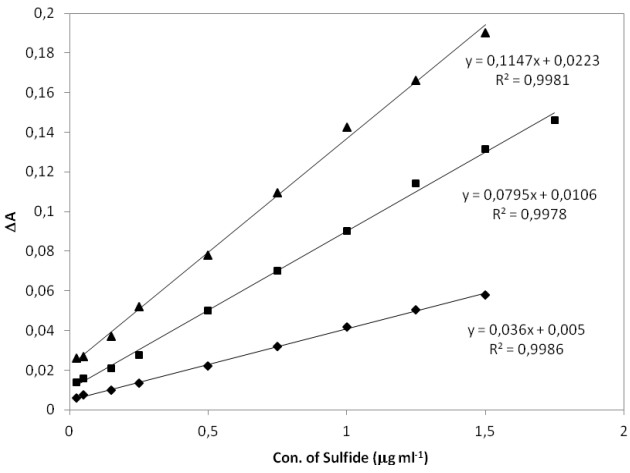

Figure 8. Calibration graph. Experimental conditions: 6.85×10^{-5} M malachite green, 25-1750 ppb of S^{2-}, 2 ml (K_2HPO_4-NaOH) buffer pH: 7.5; lag time: 3 seconds; *T*: 25 ºC. Fixed time method: (—◆— Δ*t:* 5 s), (—■— Δ*t:* 15 s) and (—▲— Δ*t*: 25 s).

 DOI: 10.17628/ecb.2014.3.953-960

A Ringbom plot is established standard method to give the effective range of concentration for a system that obeys Beer's law. The plot of Ringbom was drawn between 1-*T* and log *C*, where *T* is transmittance and *C* is sample concentrations. The plot is not a straight line in different Δ*t*. The effective range of concentration for accurate determination from Ringbom's plot obtained and reported in Table 3.

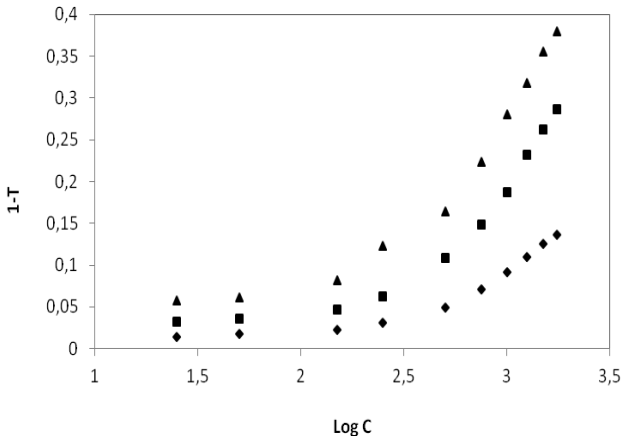

Figure 9. Ringbom plot. Experimental conditions: 6.85×10^{-5} M malachite green, 25-1750 ppb of S^{2-}, 2 ml (K_2HPO_4-NaOH) buffer pH: 7.5; lag time: 3 seconds; *T*: 25 ºC. Fixed time method: (—◆—Δ*t*: 5 s), (—■—Δ*t*: 15 s) and (—▲—Δ*t*: 25 s).

From Figure 9 the slop of the linear range of Ringbom's plot found. Based on this value, the ratio between the relative error in concentration and photometric error are calculated. For a photometric error, Δ*P*=0.01, the relative error in concentration is determined and tabulated in Table 3.

Table 3. Parameters achieved from Ringbom's plot.

Δ*T*, s	Effective conc. range, μg.ml^{-1}	Slop	$RE^{a}_{conc.}/(\Delta P^{b})$	$RE_{conc.}$
5	250-1500	0.064	35.54	0.35
15	250-1750	0.136	16.93	0.17
25	250-1500	0.160	14.39	0.14

[a]Relative error in concentration. [b]Photometric error

Table 4. Determination of standard solution of sulfide (*n*=8).

Fixed time, s	Taken amount, ng.ml^{-1}	Found[a] amount ng.ml^{-1}	Confidence limit[b] ng.ml^{-1}	Recovery (%)	SD (%)
Δ*t* =5	1500	1472	±3.26	98.13	3.9
	700	698	±2.51	99.71	3.0
	50	48	±1.17	96	1.4
Δ*t* =15	1500	1571	±1.25	104.73	1.5
	700	716	±1.50	102.28	1.8
	50	48	±0.58	96	0.7
Δ*t* =25	1500	1530	±3.43	102	4.1
	700	694	±2.59	99.14	3.1
	50	47	±0.67	94	0.8

[a]Average of 8 determination, [b]*t* for p: 0.05 is 2.365, respectively.[32]

In order to estimate the accuracy and precision of the suggested method, three standard solutions of sulfide were used. For this purpose, eight replicate determination of each concentration were done and finding results were reported in Table 4.

Effect of foreign ions

The interference of different foreign ions was discussed in the determination of 0.5 μg ml^{-1} of sulfide. The tolerance limit was defined as a concentration of added ion causing less than a ±5 % relatively error. Aliquot amount of foreign ions with 50, 100, 500 and 1000 ppm were used. The results are summarized in Table 5.

Table 5. Influence of foreign ion on the determination of sulfide

Foreign ion	Tolerance limit (ppm)
Ba^{2+}, Na^{+}, K^{+}, NO_3^{-}, Cl^{-}, I^{-}	1000[a]
Mg^{2+}, PO_4^{3-}, ClO_4^{-}, SO_4^{-}	500
Fe^{2+}, Ca^{2+}, Ni^{2+}, CO_3^{2-}	100
Ag^{+}, Pb^{2+}, Hg^{2+}	Interfered

[a] Maximum concentration studied.

Most common ions in water such as Na^{+}, K^{+}, NO_3^{-}, Cl^{-}, I^{-} did not interfere, even when present on maximum concentration (1000 ppm). Some ions such as Ag^{+} and $Pb^{2+}$and Hg^{2+} in the first concentration test at 50 ppm were shown interfered effect. In some literatures, the interfering of ions effects were considerably removed by suitable methods like that addition of EDTA or use from ion exchanger.[26,28] In the presented work, the effect of diverse ions tabulated without using any masking or modified external reagents.

Determination of kinetic parameters

A primary goal of chemical kinetics experiments is to measure the rate law for a chemical reaction. One of the many ways to do this is the method of pseudo-first order conditions. All the kinetic measurements were carried out at the concentration of malachite green at least 10 folds greater than of the sulfide concentration. The total equation of reaction rate to be of the form:

$$r = k\left[MG^{+}\right]^{n}\left[S^{2-}\right]^{m} \quad (1)$$

$$r = k\left[MG^{+}\right]_{0}^{n}\left[S^{2-}\right]^{m} = k_{obs}\left[S^{2-}\right]^{m} \quad (2)$$

$$r = -\frac{\Delta A}{\Delta t} = k\left[S^{2-}\right] \quad (3)$$

By taking a natural log of the rate equation, the pseudo-first order plots of the $\log(A_t - A_\infty)$ versus time were made (Fig. 10) (A_∞ and A_t are the absorbance of reaction at the end and selected time t at the reaction).

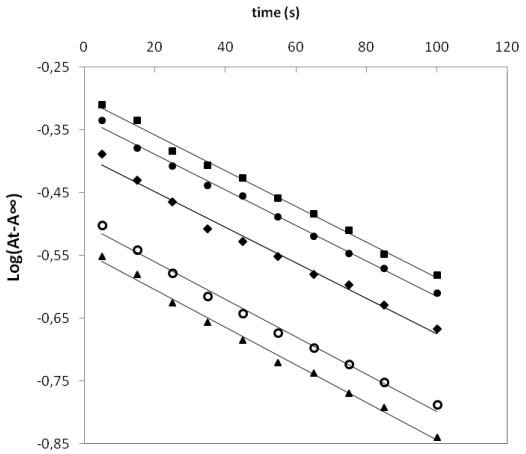

Figure 10. Pseudo-first order diagram for the reaction between malachite green and sulfide. Reaction conditions: $[S^{2-}] = 3.2\times10^{-6}$, $[MG^{+}] = 4.7\text{-}3.61\times10^{-5}$, λ_{max}=630 nm, pH=8 and T=25ºC.

The pseudo-first order plots were linear. This suggest that the reaction is the first order in sulfide ion (m=1). The observed pseudo-first order rate constant (k_{obs}) obtained from the slopes of the above plots. The actual rate constant (k_{act}) was obtained from $k_{obs}/[MG^{+}]$. k_{obs} and k_{act} reported in Table 6. The values of actual rate constant were fairly constant. It is suggesting that the reaction is also first order in malachite green (n=1) and that the reaction is second order overall. It is verified with plotting log (A_t-A_∞) versus time (Fig. 11) while the concentration of sulfide at least 10 folds greater than of the malachite green concentration. The new pseudo-first order plots were linear, too. This suggests that there is no product inhibition.

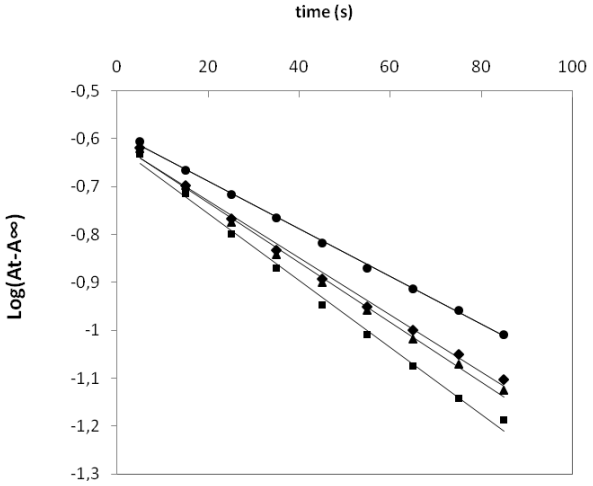

Figure 11. Pseudo-first order diagram for the reaction between malachite green and sulfide. Reaction conditions: $[S^{2-}] = 3.2\times10^{-5}$, $[MG^{+}] = 4.7\text{-}3.61\times10^{-6}$, λ_{max}=630 nm, pH=8 and T=25ºC.

The overall rate equation as function of concentration of malachite green and sulfide ions can now be written as:

$$rate = k_{act}\left[MG^{+}\right]\left[S^{2-}\right] \quad (4)$$

where $k_{act}$and k_{obs} are 1.40±0.12 M^{-1} min^{-1} and 5.76±0.16 min^{-1}.

Table 6. Observed and actual rate constant for the reaction of malachite green with sulfide. $[S^{2-}] = 3.2\times10^{-6}$ M, pH = 8, λ_{max}= 630 nm and T = 25 ºC.

[Malachite green] M	k_{obs} min^{-1}	k_{act} $M^{-1}min^{-1}$
4.70×10^{-5}	5.84	1.24
4.52×10^{-5}	5.89	1.30
4.11×10^{-5}	5.89	1.43
3.75×10^{-5}	5.59	1.49
3.61×10^{-5}	5.57	1.54

In order to evaluate the activation energy, Arrhenius equation was applied using the relationship below:

$$K = Ae^{-\Delta E^{\#}/RT} \quad (5)$$

$$\ln K = \ln A - \frac{\Delta E^{\#}}{RT} \quad (6)$$

$$\ln\frac{\Delta A}{\Delta t} = \ln A - \frac{\Delta E^{\#}}{R}\frac{1}{T} \quad (7)$$

where $\Delta E^{\#}$ is the Arrhenius activation energy, A is the Arrhenius constant and R is the global gas constant. When $\ln(\Delta A/\Delta t)$ was plotted against $(1/T)$, a straight line with slop $-\Delta E^{\#}/R$ and intercept $\ln A$ was obtained. The founded value of $\Delta E^{\#}$ presented in Table 6.

The enthalpy of reaction ($\Delta H^{\neq}$) was obtained from equation (8) and the entropy of activation achieved from equation:

$$\Delta E^{\#} = \Delta H^{\#} + RT \quad (8)$$

$$A = \frac{kT}{h}e^{\left(R+\Delta S^{\#}/R\right)} \quad (9)$$

where k and h are rate constant and Plank's factor, respectively, and A achieved from Equation 7. Finally, free energy of activation calculated according to equation:

$$\Delta G^{\#} = \Delta H^{\#} - T\Delta S \quad (10)$$

The obtained results are shown in Table 7.

The $\Delta G\#$ values were negative which reflects the spontaneous nature of the bleaching of malachite green dye in the presence of sulfide at the range of temperatures studied. The positive $\Delta H^{\#}$ indicates that the bleaching process was endothermic.

Determination of sulfide in real samples

The analytical potential of the method was tested by applying it to the determination of spiked amounts of sulfide in real water samples from river, spring, drinking water and fish farms without any purification or using from masking agents. These results indicate that common constituents in real water samples did not interfere in the proposed method. The results are given in Table 8.

 DOI: 10.17628/ecb.2014.3.953-960

Table 7. Determination of kinetic parameters ($\Delta H^{\#}$, $\Delta S^{\#}$ and $\Delta G^{\#}$ calculated in 25 ºC)

Δt (s)	$\Delta E\#$ (J mol^{-1})	$\Delta H^{\#}$ (J mol^{-1})	$\Delta S^{\#}$ (J mol^{-1} K^{-1})	$-\Delta G^{\#}$ (kJ mol^{-1})
5	26607.29	24171.29±41.57	583.25±1.78	146.72±3.45
15	13733.89	11297.89±41.56	649.80±0.84	179.09±3.52
25	10182.60	7745.99±41.58	666.06±0.77	187.41±3.58

$\Delta H^{\#}$, $\Delta S^{\#}$ and $\Delta G^{\#}$ are the average of three calculations in three temperatures (15, 20 and 25 ºC).

Table 8. Simultaneous determination of sulfide in natural waters.

Sample	*EC*(µS)/pH	Added, ng.ml^{-1}	Found, ng ml^{-1}					
			Δt=5(s)	*RE*, %	Δt=15(s)	*RE*, %	Δt=25(s)	*RE*, %
Fish farm	263/7.7	500	533	6.6	528	5.3	531	6.2
		1000	1036	3.6	1035	3.5	1059	5.9
Drinking water	732/7.1	500	479	4.2	483	3.4	473	5.4
		1000	980	2.0	992	0.80	971	2.9
Nahran (River)	452/8.1	500	503	0.60	491	1.8	487	3.8
		1000	985	1.5	981	1.9	1011	1.1
Barajin (River)	688/7.9	500	469	6.2	478	4.4	473	5.4
		1000	973	2.7	980	2.0	978	2.2
Shamdasht (Spring)	345/7.4	500	485	3.0	490	2.0	477	4.6
		1000	983	1.7	979	2.1	974	2.6

Conclusion

The malachite green- sulfide system in micellar medium, proposed in this paper, could be used successfully for the determination of trace amount of sulfide in different water samples. Using this method, it is possible to determine sulfide at levels as low as 1ng/ml without the need for any preconcentration steps. Therefore, the method could be proposed for environmental analyses. Suggested method has added advantages over other reported spectrophotometric methods (table 1) like sensitivity, time of analytical signal, simple instrument for operator and cheaper chemical reagents.

Acknowledgements

Financial support from the research affairs of University of Guilan and Qazvin water Board Company is acknowledged.

References

[1]Guenther, E. A., Jonson, K. S., Coale, K. H., *Anal. Chem*., **2001**, *73*, 3481-3787.

[2]Eaton, A. D., Clesceri, L. S., Greenberg, A. E., *Standard methods for the Examination of Water and Wastewater*; 19 th Ed. American Public Health Association; Washington, **1995**.

[3]Kirk, R. E., Othemer, D. F., *Encyclopedia of Chemical Technology*; 3rd Ed.; Wiley: New York, **1981**; Vol. 17.

[4]Ebdon, L., Hill, S. J., Jameel, M., Corns, W. T., Stochwell, P. B., *Analyst*, **1997,** *122*, 689.

[5]Kuhl, M., Steuckart, C., In: *In Situ Monitoring of Aquatic Systems: Chemical Analysis and Speciation*; Buffle, J., Horvai, G., Eds.; Wiley: Chichester, U.K., **2000**; p. 121.

[6]Cline, J. D., *Limnol. Oceanogr*., **1969**, *14*, 454-58.

[7]Sakamoto-Arnold, C. M., Johnson, K. S., Beehler, C. L., *Limnol. Oceanogr*., **1986,** *31*, 894-900.

[8]Berner, R. A., *Geochim. Cosmochim. Acta*, **1963**, *27*, 563-75.

9Brendel, P. J., Luther, G. W. III., *Environ. Sci. Technol*., **1995**, *29*, 751.

[10]Jeroschewski, P., Steuckart, C., Kuhl, M., *Anal. Chem*., **1996,** 68, 4351.

[11]Canterford, D. R., *Anal. Chem*., **1975**, *47*, 88.

[12]Cutter, G. A., Oatts, T. J., *Anal. Chem*., **1987**, *59*, 717.

[13]Radford-Knoery, J., Cutter, G. A., *Anal. Chem*., **1993**, *65*, 976.

[14]Tang, D., Santschi, P. D., *J. Chromatogr. A*, **2000**, *883*, 305.

[15]Lambert, J. L., Manzo, D. T., *Anal. Chim. Acta*, **1969**, *48*, 185.

[16]Roman Ceba, M., Vinagre Java, F., Munoz Leyva, J. A., *Analyst*, **1982**, *107*, 781.

[17]Wood, C. F., Marr, I. L., *Analyst*, **1988,** *113*, 1635.

[18]Koh, T., Miura, Y., Yamamuro, N., Takaki, T., *Analyst*, **1990**, **115**, 1133.

[19]Koh, T., Takashi, N., Yamamuro, N., Miura, Y., *Anal. Sci.*, **1993,** *9*, 487-492.

[20]Barzegar, M., Jabbari, A., Esmaeili, M., *Bull. Korean Chem. Soc.* **2003,** *24*, 1261-1264.

[21]Zheng, H., Li, Q., Bai, H., Liu, G., J. Chinese Chem. Soc., **2005** *52*, 269-272.

[22]Varma, Y. S., Singh, I., Garg, B. S., Singh, R. P., Microchemical, **1984,** *30*, 20-26.

[23]Kester, M. D., Shiundu, M., P., Wade, A. P., *Talanta*, **1992,** *39*, 299-312.

[24]Safavi, A., Ramezani, Z., *Talanta*, **1997,** *44*, 1225-1230.

[25]Ghasemi, J., Mohammadi, D. E., *Microchem. J.*, **2002,** *71*, 1-8.

[26]Safavi, A., Moradlou, O., Maesum, S., *Talanta*, **2004**, *62*, 51-56.

27Afkhami, A., Srlak, N., Zarei, A., Madrakian, T., *Bull. Korean Chem. Soc.*, **2006,** *27*, 863-868.

[28]Jabbari, A., Shamsipur, M., Microchem. J., **1993,** *48*, 349-355.

[29]Silva, R. C., Barros, A. F. V., Basso, L. C., Zagetto, A. G., *Talanta*, **2011,** *85*, 1703-1785.

[30]Emami, M., Mousavi, M. F., Barzegar, M., *J. Chin. Chem. Soc.*, **2004,** *51*, 517-521.

[31]Thomas, H., Britton, S., Robinson, R. A., *J. Chem. Soc*., **1931,** 1456-1462.

[32]Ensafi, A. A., Keyvanfard, M., Anal. Lett., **2000,** *35*, 423-433.

[33]Keyvanfard, M., Sharifian, A., *Anal. Chem*., **2006,** *61*, 646-650.

[34]Ensafi, A. A., Keyvanfard, M., *Anal. Chem*., **2002,** *8*3, 397-404.

[35]Shemirani, F., Asghari, A., Hajimoosa, M., *Talanta*, **1999,** 48, 879-883.

[36]Abbasi, S., Khani, H., Gholivand, M. B., Naghipour, A., Farmany, A., Abbasi, F., *Spectrochim. Acta*, **2009,** *72*, 327 – 331.

[37]Miller J. N. Miller, J. C., *Statistical and Chemometrics for Analytical Chemistry*., Fifth ed., Person education, London, **2005**.

Received: 03.07.2014.

Accepted: 28.09.2014.

KINETIC STUDIES ON EOSINOPHIL PEROXIDASE ENZYME ISOLATED FROM HEMOLYSATED BLOOD CELLS OF INDUCED ATHEROSCLEROTIC MICE AND ITS INHIBITION WITH SOME ISOFLAVONE COMPOUNDS

Nahida Saieed Al- Chalabi[a] and Eman Saieed Al-Choka[a]

Keywords: Atherosclerosis, inhibitors, eosinophil peroxidase enzyme, isoflavone compounds

This study includes an isolation, partial purification and study of the kinetic properties of Eosinophil peroxidase (EPO) enzyme from hemolysate blood cells in induced atherosclerosis and normal mice, then comparison between them. Isolation of two protein peaks I and II were carried out using ion exchange chromatography (DEAE cellulose), specific activity for these two peaks I and II for EPO enzyme for normal and induced atherosclerosis were (0.018, 0.02) and (0.126, 0.031). unit mg $^{-1}$ of protein respectively, peak I has a high specific activity for EPO enzyme which was isolated from induced atherosclerosis mice. The optimum condition of EPO for the peak I separated from hemolysate blood cells in induced atherosclerosis mice showed an optimum reaction incubation time at 21 minutes, pH of sodium acetate buffer 6, temperature at 30 °C, volume of enzyme 500 µL and the substrate concentration was about, 200 µM. When we used Line Weaver-Burk plot, the maximum velocity (Vmax) and Michale's - Menten constant (Km) were found to be 0.045 unit ml^{-1} and 400 µM L^{-1} respectively, all cationic metal ions such as Mg^{+2}, Na^{+}, Ca^{+2}, K^{+}, Mn^{+2}, Hg^{+2} (10 mM) shows a catalytic effect on the activity of EPO enzyme but maximum that for Hg^{+2} ions. Also at this study shows an inhibition effect of some isoflavone compounds such as genistein, daidzein, biochanin A and formononetin on the activity of this enzyme. The results indicate different relative inhibition in enzyme activity, for these compounds, according to Line Weaver- Burk plot genistein compound shows a competitive inhibition whereas daidzein, biochanin A and formononetin shows non competitive inhibition for EPO enzyme..

* Corresponding Authors
E-Mail: nahida_alchalabi@yahoo.com
[a] Department. of chemistry, College of Education, University of Mosul, Mosul, Iraq

Introduction

Atherosclerosis disease is one of cardiovascular diseases word wise in the world, which is characterized by a thicking wall of large, medium and small volumes of arteries. Mechanism appearance of the lesion of atherosclerosis represented by oxidation of low density lipoprotein (LDL-C), swallowing the oxidized LDL-C particles by phagocytic cells and formation of foam cells with adherence and penetration of monocyte cells for the wall of the blood vessel then the formation of cytokines of vascular smooth muscle cells .[1]

Atherosclerosis consider to be a disease mediated inflammation which is occur by a complex interactions with leukocytes, plates and vascular wall of the cells, this inflammatory interaction reinforced by liberation of atherosclerosis plaques, [2] because of EPO enzyme present plenty in Eosinophil leukocyte , [3] Which is a smaller constituent present in phagocytic leukocyte circles in blood under normal conditions, which where can be much larger in blood for different disorders of inflammation.[4] Thus the level of EPO enzyme was increased at different disorders of inflammation, one of them is vascular inflammation . The substrates for EPO to be (Br^{-}, Cl^{-}, I^{-}) in addition pseudo SCN^{-} which is substitute for halides as a substrate in the reaction of EPO using hydrogen peroxide.[5]

In addition to halides there is another substrate which was done is ortho methoxy phenol (guaiacol) in the reaction which is dependent on hydrogen peroxide.[6] It is found that bromide and thiocyanate which are a main substrates of EPO in vivo among another halides [7].

The aim of present study was to purified EPO enzyme from the Hemolysate blood cells in mice induced atherosclerosis and study the inhibition of it by some isoflavone compounds

Materials and methods

Animals used

Female albino mice were used for this study which was provided from the two Colleges of Education and Medicine for the University of Mosul , with approximate weight about 30 - 35 g , placed in a special cage provided for this purpose and provided with water and special animal feed continuously.

Induction of Atherosclerosis

The animal was divided to two groups each containing 20 mouse. Control group leaved takes animal feed and water *ad Libitum* for 60 days. Groups exposed to atherosclerosis which gives hydrogen peroxide 1 % with a drinking water for 60 days.

After the end of 60 days, these animals anesthesized with diethylether for some seconds then blood was pulled from the sinus puncture using special capillary tubes, put the blood in a clean, dry and sterilized plan tube. Serum of blood was isolated after clotting and centrifugation at 1008*g* for 10 minutes, then the sample of serum was conserved in a freeze at (-18 °C). The preparation of hemolysate cells of the blood takes place according to the method,[8] which was prepared by taking the isolated blood cells after serum was isolated, washed three times with a solution 0.9% NaCl with using a refrigerated centrifuge at 4 °C with 1008*g* for 5 minutes.

The precipitate wase taken which included blood cells after washing and hydrolyzed it with the addition twice their volume with distilled water. The tubes which contains hemolysate cells of the blood were put in a freeze at (-18 °C), then separation of the filterate of hemolysate cells was carried out blood after centrifugation using cold centrifuge at 4 °C with a velocity 1008xg for 30 minutes. After centrifugation the solution of hemolysate cells of the blood were taken for using the following experiments directly in order to isolate EPO enzyme from it.

Protein estimation was carried out for blood cells hemolysate (BCH) according to modified Lawry method ,[9] using a standard curve for bovine serum albumin for the determination of protein.

The animals after finishing the pull of their bloods, sacrified and explanation of it and then aortic artery was taken, placed in neutral formarline 10 % as a fixer for 72 hours.

Surely atherosclerosis was occurred, histological sections were carried for the aorta and then staining it by a dye hematoxylin and Eiosene [10] and the method of AL–Haj [11] was followed for colouring of these tissues sections.

Estimation the activity of EPO activity in hemolysate blood cells

Estimation of EPO activity was carried out according to Desser *et al*., method, [12] this method depends on following of an increasing for concentration of products at a wave length 470 nm.

The following equation demonstrate the action of EPO enzyme.

$$4\text{guaiacol} + \xrightarrow{EPO} \text{Tetraguaiacol} + 4H_2O_2$$

Reagents and procedures

Reagents used were the following: 1. Buffer solution of sodium phosphate (100 mM , pH 7). 2. Guaiacol solution (100 μM). 3. Hydrogen peroxide solution (100 μM).

Table 1. explains all substances added in each tube (sample and blank).

	Sample	Blank
Hemolysate of blood cells	250 μL	
Distilled water		250 μL
Phosphate buffer	250 μL	250 μL
Guaiacol	250 μL	250 μL
Hydrogen peroxide	250 μL	250 μL

Calculations

The EPO activity (φ) was expressed as:

$$\varphi = \frac{1000 \Delta A V_t}{E_0 V_s d}$$

where

ΔA= the difference in absorbance at on minute .

V_t= Total volume

E_0= molar extinction coefficient (26600 L mol^{-1})

d= path length (1 cm).

V_s= sample volume

Partial purification of EPO enzyme from hemolysate cells of the blood

Partial purification of EPO enzyme of hemolysate cells of the blood for both induced atherosclerosis and normal mice were carried out after estimated of the activity of this enzyme using the following steps:

Dialysis

10 ml of hemolysate cells of the blood was dialyzed overnight at 4 °C using sodium phosphate buffer (100 mM , pH 7). The final volume was measured , the protein concentration was estimated then EPO activity was also determined.

Ion- exchange chromatography

DEAE - cellulose was used as anion exchanger for partial purification of enzyme. (9 ml) of the sample was applied to a column (2.5 × 40 cm) containing DEAE - cellulose to (37 cm)height. Elution was carried out at a flow rate 1.2 ml min^{-1} (72 ml h^{-1}) using sodium phosphate (100 mM, pH 7) at 4 °C as eluent. The volume of fractions produced were collected manually then the concentration of protein in each tubes were applied according to modified Lawry method. After plotting a diagram for absorbance against fractions number of the elution volume indicate peaks for the proteins of EPO, collection each fractions due to each peak , lyophilized until obtained a dry substance as a powder of EPO enzyme which is used in the following experiments .

Factors affecting EPO activity

To determine the optimal conditions of EPO enzyme several experiments had been designed including enzyme volume, reaction time, temperature, substrate concentration, pH and effect of some metal ions on peak I of EPO enzyme activity.

Results and Discussion

The cross sections for aortic artery for adult female mice (control) shows a three layers for the wall represent internal, middle and external layers empty from foam cell (Fig.1), whereas the cross sections for aortic artery for female mice treated with H_2O_2 (1 %) in drinking water showed a change in the tissue indicating a disease was occurred representing a thickness in the lining wall of the aorta with proliferation of vascular smooth muscle cells with the presence of foam cells (Fig. 2). This is an indication for lesion in the lining of the blood vessel due to oxidative stress induced with H_2O_2 that contribute to produce lipid peroxides which act to change permeability of membrane causing lesion internal during contribution of the oxidation of LDL particles and then produce atherosclerosis. [13]

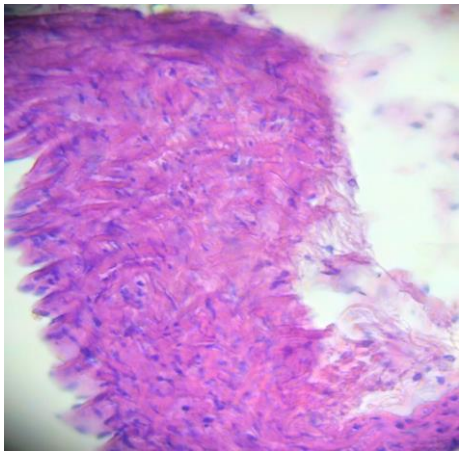

Figure 1. A three layers (internal, middle and external) in the aortic artery wall represent for normal female mice and empty from foam cells**.**

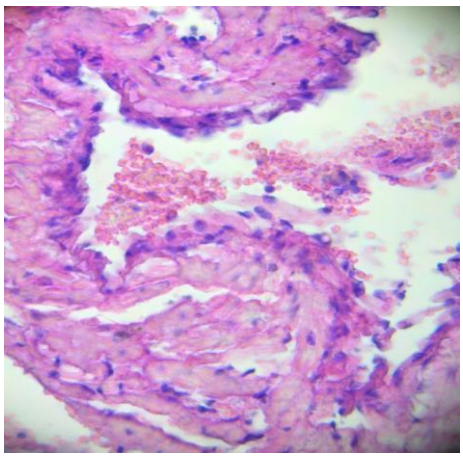

Figure 2. Thickness in the aortic lining wall (a) with proliferation of vascular smooth muscle cells (b) presence of foam cells (c).

Partial purification of EPO enzyme from hemolysate cells of the blood

Purification by dialysis

Results in Table 2 shows specific activity of EPO enzyme in hemolysate cells of the blood for normal mice was after dialysis process 0.016 unit mg $^{-1}$ protein i.e. increase 2.66 folds, 215.68 percent recovery compared to total activity of crude enzyme 100 % . The specific activity of EPO enzyme in hemolysate cells of the blood for atherosclerosis mice group was 0.037 unit mg $^{-1}$ protein after dialysis process, i.e. increased 2.46 folds before dialysis 0.015 unit mg $^{-1}$ protein and 202.5 % recovery compared to total activity of crude enzyme 100 % as indicated in (table 2).

Purification by ion- exchange chromatography

Results indicated in (Fig .3) presence of two peaks which have activity of EPO enzyme in hemolysate cells of the blood for normal mice as indicated in (Table 1). Peak I was appeared at elution volume 78 -132 ml with a specific activity 0.018 unit mg $^{-1}$ protein , i. e. increased 3 folds compared to specific activity of crude enzyme which have recovery percent about 58.23 %. Whereas peak II at elution volume 144- 186 ml, specific activity 0.02 unit mg $^{-1}$protein , i. e. more 3.33 folds than specific activity of crude enzyme which have recovery percent was 74.11 % compared to 100 % specific activity of crude enzyme (Table 2).

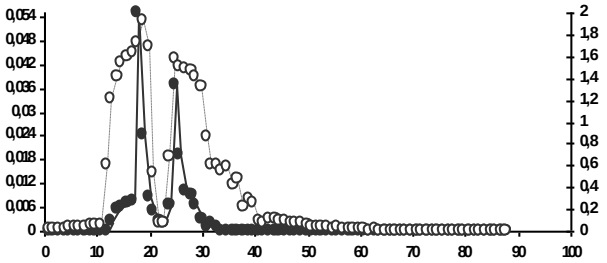

Figure 3. Recovery sample from purified enzyme EPO from hemolysate cells of the blood for normal mice by anion exchange chromatography using exchanger DEAE-cellulose packed separation column with dimensions (2.5 × 40 cm) at rate of flow of 1.2 ml min $^{-1}$ (72 ml h^{-1}).

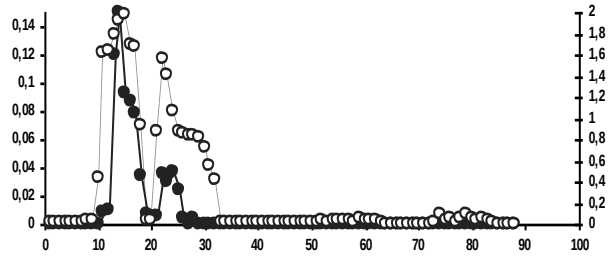

Figure 4. Recovery sample from purified enzyme EPO from hemolysate cells of the blood for induced atherosclerosis mice by anion exchange chromatography using exchanger DEAE-cellulose packed separation column with dimensions (2.5 × 40 cm) at rate of flow of 1.2 ml min $^{-1}$ (72 ml h^{-1}).

Table 2. Purification steps for EPO enzyme in hemolysate cells of the blood for normal mice.

Purification steps		Total volume, ml	Total protein, mg	*Activity (unit ml^{-1})	Activity in enzymatic unit		Purification folds	Reco-very,%
					Total	Specific		
Crude enzyme		10	169.37	0.102	1.02	0.006	1	100
Dialysis		9.2	132.25	0.24	2.2	0.016	2.66	9.2
Ion-exchange chromatography	Peak I	54	31.87	0.011	0.594	0.018	3	58.23
	Peak II	42	37.06	0.018	0.756	0.02	3.33	74.11

*Enzymatic unit (*U*) indicate to the amount of enzyme that oxidize one micromole of substrate in one minute.

Table 3. Purification steps for EPO in hemolysate cells of the blood for induced atherosclerosis mice.

Purification steps		Total volume, ml	Total protein, mg	*Activity, (unit ml^{-1})	Activity in enzymatic unit		Purification folds	Reco-very, %
					Total	Specific		
Crud enzyme		10	153.75	0.24	2.4	0.015	1	100
Dialysis		9	128	0.54	4.86	0.037	2.46	202.5
Ion-exchange chromatography	Peak I	48	25.02	0.066	3.16	0.126	8.4	131.66
	Peak II	30	23.77	0.025	0.75	0.031	2.06	31.25

*Enzymatic unit (*U*) indicate the amount of enzyme which oxidize one micromole of substrate in one minute.

The results in Fig. 4 was indicated two peaks present which also have an activity of EPO enzyme in hemolysate cells of the blood for induced atherosclerosis mice as shown in Table 3. Peak I appeared for the activity of EPO enzyme at elution volume 66-114 mL, its specific activity 0.126 unit mg $^{-1}$protein, i. e. increased about 8.4 folds over specific activity of crude enzyme which have 131.66 % recovery compared to total activity of crud enzyme . But peak II shows elution volume 132 -162 mL, its specific activity 0.031 unit mg^{-1} protein, i-e greater about 2.06 folds than for crude enzyme and 31.25 % recovery (Table 3).

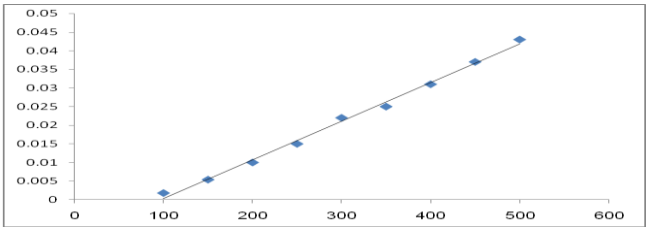

Figure 5. Effect of the enzyme extract volume on EPO enzyme activity

Study of the kinetic properties for EPO enzyme after partial purification of it from hemolysate cell of the blood in induced atherosclerosis mice.

To determine the optimal conditions of EPO enzyme in hemolysate cells of the blood in induced atherosclerosis mice. The following experiments had been designed including.

Effect of enzyme volume on EPO activity

The measurement for the activity of EPO enzyme in the presence of different volumes of the enzyme which was purified partially from hemolysate cells of the blood for induced atherosclerosis mice for peak I about 100- 500 µl . Fig. 5 shows the relationship between enzyme activity and volumes of enzyme with a constant other factors. It was shown that the rate of enzyme reaction increases with increasing the volume of enzyme reaches maximum at 500 µl. This results was in agreement with, [14] which shows the rate of enzymatic reaction increases with increase the volume of enzyme if substrate is sufficient with constant other factors.

Effect of buffer solutions on enzyme activity

The study of buffer solutions effect on the rate of enzymatic reaction of purified EPO isozyme I using different buffer solutions at a concentration 0.1M as follows:

1.Tris- HCl buffer	$C_4H_{11}NO_3$-HCl buffer.
2. Trisodium Citrate buffer	$C_6H_8O_7$-$C_6H_5O_7Na_3$ buffer.
3. Sodium bicarbonate buffer	Na_2HCO_3-Na_2CO_3 buffer.
4. Phosphate buffer	Na_2HPO_4-KH_2PO_4 buffer.
5. Phosphate buffer	Na_2HPO_4-NaH_2PO_4 buffer.
6. Sodium acetate	CH_3COONa.

The preferable enzyme activity were obtained for isozyme I which was purified from enzyme EPO was with sodium acetate buffer as indicated in Fig 6. This result is similar to the results obtained for purified enzyme EPO from uterus rat females.[15]

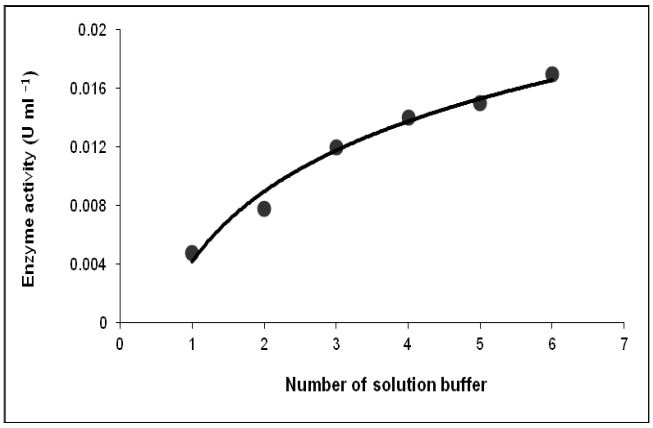

Figure 6. Effect of buffers solution on EPO enzyme activity

Effect of pH on EPO enzyme activity

The influence of pH upon the EPO activity was investigated using the sodium phosphate buffer solution with different pH (4, 4.5, 5, 5.5, 6, 6.5, 7, 7.5, 8) as shown in Fig. 7. We show that the EPO activity of peak I was maximum at 6 , thus in all further experiment incubation were carried out at this point. Other studies showed that optimum pH for EPO purified from uterus of female rat was 5.6 using the same buffer.[15]

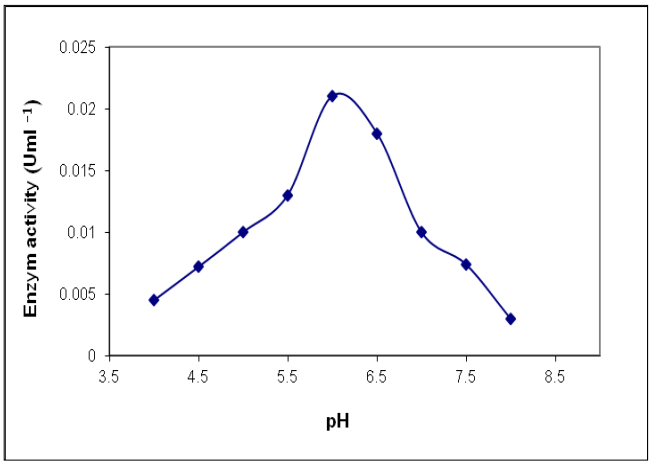

Figure 7. Effect of pH on EPO enzyme activity

Effect of time on enzyme activity

Maximum EPO activity observed after 21 minute of the reaction as shown in Fig. 8.

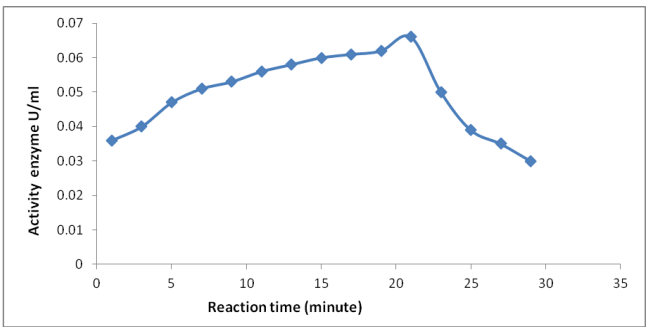

Figure 8. Effect of reaction time on EPO enzyme activity

Effect of Temperature on enzyme activity

It seems that by increasing temperature lead to increase EPO activity, the maximum activity of the enzyme showed at 30 °C followed by decreasing in enzyme activity as shown in Fig. 9 so that 30 °C used as optimal temperature to estimate EPO activity in the following experiments, Other studies [15] showed that the higher activity of EPO which was purified from uterus rat femals was at 37 °C. Also the results of isozyme I of EPO from hemolyzate cells of the blood showed a lost of enzyme activity at 60 °C for 10 minutes, this results indicated that EPO enzyme is unstable at high temperature more than that of optimum temperature .

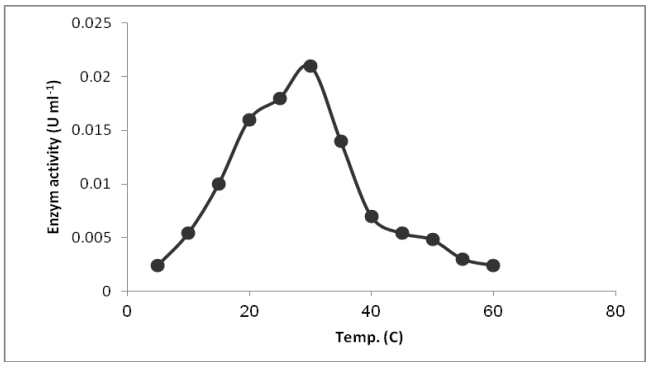

Figure 9. Effect of Temperature on EPO enzyme activity

Effect of some metal ions on enzyme activity

Effect of different cations Hg^{+2}, Mn^{+2}, K^{+}, Ca^{+2}, Na^{+}, Mg^{+2} were studied on the rate of enzymatic reaction of EPO at optimum conditions which was indicated before. The results shows all the positive ions for chloride salts of these metals which was added to a reaction mixture have catalytic effect on the activity of enzyme and the higher catalytic effect appeared when mercury ion was added, this increasing may be due to stabilization of the transition state by metal ions of the reaction between enzyme and its substrate .[16]

Table 3. Optimum conditions to evaluate peak I EPO activity partially purified from hemolysate cells of the blood for induced atherosclerosis mice.

Enzyme volume, µL	Type of solution buffer	pH	Reaction time, min	Temperature, °C	Metal ions	Substrate conc., µM
500	sodium acetate	6	21	30	Hg^{+2}	200

Table 4. Optimum inhibitory concentration of GE and DA on EPO enzyme activity purified from hemolysate cells of the blood in induced atherosclerosis mice.

GE concentration, µM	Activity, (U ml $^{-1}$) ×100	Percentage for inhibition %	DA concentration, µM	Activity (U ml $^{-1}$) ×100	Percentage for inhibition, %
Control without inhibitor	1.26	0	Control without inhibitor	1.14	0%
1	0.66	47.6	1	0.84	26.31
2	0.42	66.6	2	0.72	36.8
3	0.72	42.8	3	0.075	73.68
4	0.84	33.3	4	0.36	68.4
5	0.54	57.1	5	0.78	31.5
6	0.48	61.9	6	0.54	52.6

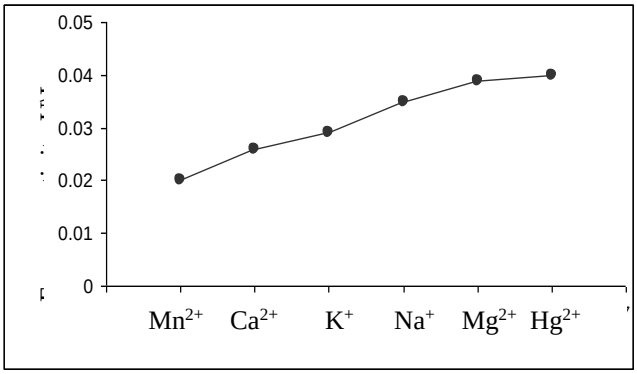

Figure 10. Effect of cation ions on EPO enzyme activity

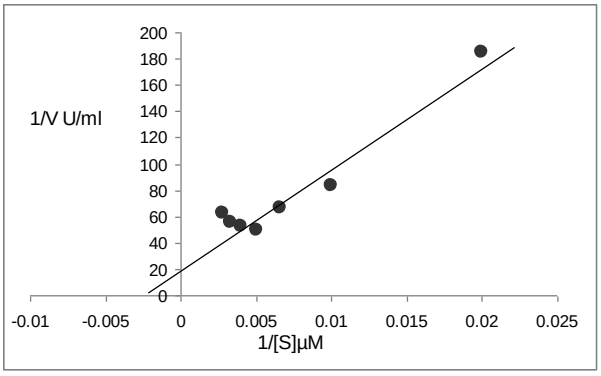

Figure 11. Effect of substrate concentration on EPO enzyme activity

Effect of substrate concentration on EPO enzyme activity

The activity of enzyme was measured in the presence of different concentrations of guaiacol as a substrate. It was found that the maximum activity obtained by using 200 µM of guaiacol.

Line Weaver-Burk plot as shown in Fig. 11. The maximum velocity (V_{max}) and Michaele's –Menten constant (K_m) were found to be 0.045 U ml $^{-1}$ and 400 µM respectively.

Other studies found K_m value for EPO enzyme separated from guinea pig bone marrow equal to 4 mM using guaiacol as substrate .[6]

From all the above experiments we can conclude that optimum conditions for peak I EPO enzyme isolated and partially purified from hemolysate cells of the blood for induced atherosclerotic mice as shown in (Table 3).

Inhibition Effect of isoflavone compounds on peak I for EPO enzyme

It was observed from(Table 4 and 5) that activity of peak I EPO enzyme purified from hemolysate cells of the blood in induced atherosclerosis femal mice decreased when using different concentration of isoflavone compound (GE, DA, BI, FO).

Table 5. Optimum inhibitory concentration of BI and FO on EPO enzyme activity purified from hemolysate cells of the blood in induced atherosclerosis mice.

BI concentration, µM	Activity (U ml $^{-1}$) ×100	Percentage for inhibition, %	FO concentration, µM	Activity (U ml $^{-1}$) ×100	Percentage for inhibition, %
Control without inhibitor	1.08	0	Control without inhibitor	1.14	0
1	0.54	50	1	0.24	78.94
2	0.9	16.6	2	0.18	84.21
3	0.66	38.8	3	0.3	73.68
4	0.42	61.1	4	0.18	84.21
5	0.96	11.1	5	0.42	63.15
6	1.02	5.5	6	0.36	68.42

It was found, that the concentration 2, 3, 4 µM for GE, DA, BI respectively posses more inhibition than other concentrations used in this experiment, whereas FO posses an inhibition concentration at 2 and 4 µM with a higher percent of inhibition 84.21 % than that produced by other isoflavones DA, GE, BI, these results of inhibition was indicated in (table 5). This enzyme inhibition may be due to the action of BI to inhibit phosphodiesterase enzyme which convert cAMP to AMP, therefore BI act to increase the level of cAMP which is decrease the total number of inflammation cells (Eosinophil and Basophil cells) lead to decreasing the level of EPO present in inflammatory Eosinophil cells [17]. Since other isoflavone compounds such as DA, FO have a similar structure to BI (fig .12), may be act similarly for inhibition for EPO enzyme as indicated by BI compound, also the inhibition of these compounds may be have a similar structure to estrogen hormone, where estrogen decreased the total number of inflammation cells. consequently this isoflavone compounds may be binding with estrogen receptors .[18]

Also the results obtained for GE isoflavone compound posses a competitive inhibition toward EPO enzyme.

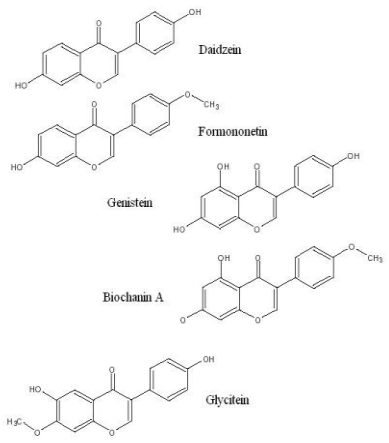

Figure 12. Chemical structure of different isoflavone compounds.

Type of inhibition for EPO enzyme by isoflavone compounds

The type inhibition of peak I EOP purified from hemolysate cells of the blood for induced atherosclerosis femal mice was carried out for isoflavone compounds (FO, BI, DA, GE) by measurement of the activity of enzyme with the presence of optimum concentration of inhibitor used as indicated in (Table 6).

The results showed a competitive inhibition was indicated for EPO enzyme with GE isoflavone compound according to Line Weaver- Burk plot (Fig. 13), whereas the inhibition were non competitive for DA, BI, FO isoflavone compounds according to Line Weaver- Burk plot also (figs. 14,15,16). The values of inhibition constant with these compounds GE, DA, BI, FO were 1.44, 4, 5, 3 µM respectively as indicated in Table 6.

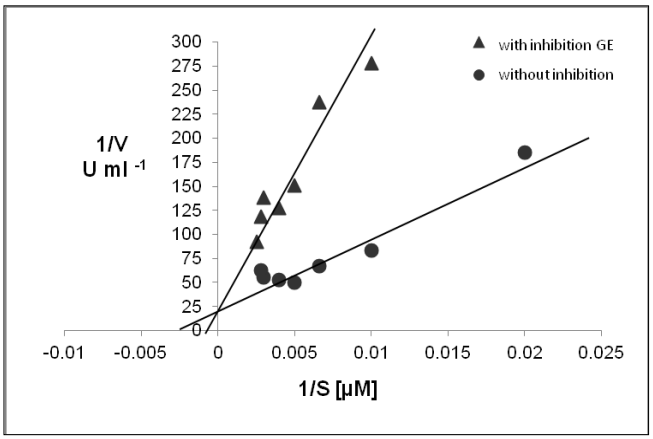

Figure 13. Inhibition enzyme activity from EPO purified of hemolysate cells of the blood for induced atherosclerosis mice by isoflavone compound GE.

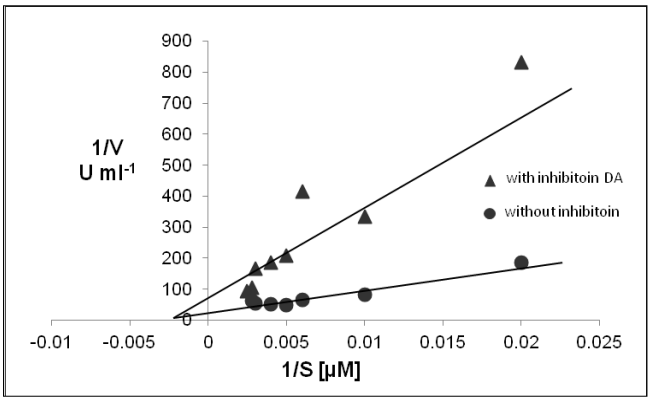

Figure 14. Inhibition enzyme activity from EPO purified of hemolysate cells of the blood for induced atherosclerosis mice by isoflavone compound by DA .

Table 6. Type of inhibition for EPO purified from hemolysate cells of the blood for induced atherosclerosis mice .

Optimum concentration (µM)	K_m (µM) without inhibitor	K'_m (µM) with inhibitor	V_{max} (unit ml^{-1}) without inhibitor	V'_{max} (unit ml^{-1}) with inhibitor	K_i (µM)	Kind of inhibition
(GE)2	400	833	0.045	0.045	1.44	Competitive
(DA)3	400	400	0.045	0.014	4	Non competitive
(BI)4	400	400	0.045	0.022	5	Non competitive
(FO)2	400	400	0.045	0.01	3	Non competitive

K_m - Michael's-Menten constant, K'_m - appearance Michael's-Menten constant, V_{max} - maximum velocity, V'_{max} - appearance maximum velocity, K_i - inhibition constant.

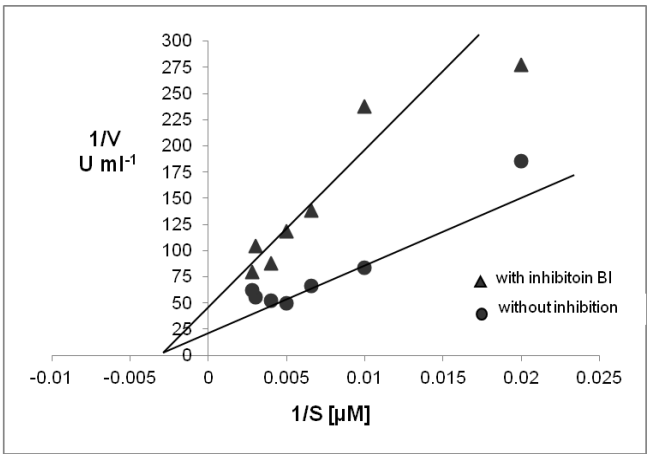

Figure 15. Inhibition enzyme activity from EPO purified of hemolysate cells of the blood for induced atherosclerotic mice by isoflavone compound BI.

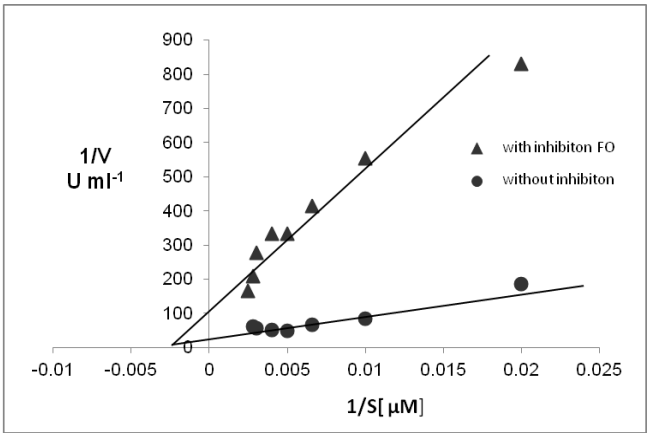

Figure 16. Inhibition enzyme activity from EPO purified of hemolysate cells of the blood in induced atherosclerotic mice by isoflavone compound FO.

REFERENCES

[1]Singh, A. K., Singh M ., Gupta, A. K. and Singh, P. K., *Uniq. J. Ayurved. Herbal Med.*., **2014,** *2(1)*, 1-5.

[2]Schuett, H., Luchtefeld M., Grothusen, C., Grote, K. and Bernhard, S., *Thromb. Haemost*., **2009**, *102*, 215-222.

[3]Olsen, L. R ., Syse, K., Little, C. and Christensen, B. T., *Biochem . J.*,**1985 ,** *229* ,779-784.

[4]Henderon, P .J., Byun, J ., Williams, V .M., Mccormick, L. M., Parks, C. W. and Ridnour, A .L., *Proc. Natl. Acad. Sci. USA*, **2001**, *98 (4)*,1631 – 1636.

[5]Mccormick, M. L., Roeder, T. L., Railsback, M. A. and Britigan, B. E., *J. Biol. Chem.*, **1994,** *269(45)*, 27914-27919.

[6]Keyhani, E., Zarei, M. A. and Lashgarblooki-Livani, T., *FEBS Letters.*, **1999,** *452*, 233 236.

[7]Vandelen, C. J. and Kettle, A. J., *Biochem. J.*, **2001**, *358*, 233-239.

[8]Rapoport, S. M., Schewe, T., Wiesner, R., Halangk, W. and Ludwig, P. *Eur. J. Biochem.*, **1979,** *99*, 545-561.

[9]Schacterle, G. R. and Pollack, J. K., *Biochem*., **1979,** *51*, 654-655 .

[10]Culling, C. F. A., Allison, R. T. and Barr, W. T., *Cellular Pathology Technique*. 4th Ed. Butterworth and Co. Ltd, **1985,** 641.

[11]Al-Haj, H. A. *Preparations microscopic optical theory and applications.* House march for publication and distribution, and printing the first edition, Amman Jordan, **2010.**

[12]Desser, R. K., Himmelhoch, S. R., Evans, W. H., Januska, M., Mage, M. and Shelton, E., *Arch. Biochem. Biophys.*, **1972,** *148*, 452.

[13]Devasagayam, T., Tilak, J. C., Boloor, K. K., Sane, S. K., Ghaskadbi, S. S. and Lele, R., *J. Assoc. Physicians India*, **2004 ,** *52*, 794-802.

[14]Ahmed, Y. and Hilali, L. A., *Biochemistry, Part I*, Dar Ibn Al Atheer for printing and publishing, conductor/Iraq, **2010,** 278.

[15]Olsen, R. L. and Little, C., *Eur. J. Biochem.*, **1979,** *101*, 333-339.

[16]Murray, R. K., Bender, D. A., Botham, K. M., Rodwell, V. W., and Weil, P. A., *Harpers' illustrated biochemistry*". **2009**, 28th. Ed., Mc Graw Hill company N.Y.

[17]Ko,W., Lin, L., Shen, H., Lai, C., Chen, C. and Shih, C., *Evidence-Based Compl. Altern. Med.*, Article ID *635058*, **2011,** pp 1-13.

[18]Shore, L. S. and Lyttle, R., *Pharm. Struct. Activity Relations.*, **1986,** 253-256.

Received: 04.06.2014.
Accepted: 29.09.2014.

SUBPLASMALEMMAL STRUCTURES OF EXCITABLE AND UNEXCITABLE CELLS IN CLINICAL AND EXPERIMENTAL STUDIES

N. S. Kukurtchyan[a]* and G. R. Karapetyan[a]

Keywords: Transmission electron microscopy, cardiomyocyte subsarcolemma thickness, hepatocytes subcytolemma thickness, inoculation by CCl_4, pulmonary arterial valve stenosis.

The phenomenon of plasmatic membrane (PM) thickness was seldom noted at investigation of cells in different organs. However just presence of such a phenomena was noted, but no valuation of its biological importance was given. In a basis of excitable and unexcitable cells plasmatic membrane thickness changes lays cell submembrane layer thickness alteration. Reversible and irreversible damages of its structures can be a key of cell dysfunction at pathology.

* Corresponding Authors: Karapetyan, G. R.
Fax: +374 -10-28 19 51
E-Mail: sapootraa_a@yahoo.com
[a] H. Buniatian Institute of Biochemistry, of National Academy of Sciences of Republic Armenia, Paruir Sevag str. 5/1, 0014, Yerevan, Republic of Armenia.

INTRODUCTION

Plasmatic membrane (PM) is arranged as a biomolecular layer of phospholipids with hydrophilic heads oriented toward extracellular and intracellular compartments. PM is organized into domains which differ in structure and function. Physicochemical properties of PM make it closer to a liquid than to a solid and point to the necessity of formation of inner shell which prevents waning of membrane. Changes in PM thickness as a form of its structure has been mentioned before.[1] PM ability to undergo fast reversible changes of its thickness was observed in the presence of high concentration of Ca^{2+} and phospholipasas.[2] PM local thickness of endotheliocytes of myocardium blood vessels of rat was observed in hypertrophy, while strongly increasing of osmophility and cardiomyocytes sarcolemmas thickness was observed at ischemia and hypoxia.[3,4] It has been shown earlier that during cardiac surgery, 15 minutes after connecting the apparatus of artificial circulation, sarcolemma became more electron-dense, and after another 15 minutes, it was degraded and replaced by large quantity of vesicles.[5] The thicking of cardiomyocytes sarcolemma was also observed in our earlier studies. Increase in PM electron density was shown to occur in cardiomyocytes, endotheliocytes, eritrocytes, connective tissues cells, shvane cells, acsolemmas of vegetative nerve endings of patients with rheumatic and congenital heart defects.[6]

We proposed a hypothesis, that changes in PM thickness on the cell, under different damaging influences, are a universal mechanism of adaptation of its cytoskeleton to the influence. Study of intracellular pressure and the excitable membrane of giant axon suggested, that cytoskeletal structure is involved in the mechanical support of the membrane. Most plausible source of the mechanical response is axsolemma itself.[7] The phenomenon of PM thickness has often been noted during investigation of different cells in different organs. However, just the presence of such a phenomenon has been noted, and no evaluation of its biological importance has been reported.

All data indicate the necessity of an investigation of the phenomenon of changes in the thickness of membrane. Investigations done by our group on the phenomena of changes in PM thickness both in clinic and experimental studies, over a prolonged period, also pointed the necessity of further study of submembrane layer.[8, 9]

Submembrane layers comprising of small cytoplasma area with a thickness up to 3-4 nm have links to PM inside. It is important to state that the above mentioned submembrane layer is not observed in all types of cells. Hyaloplasma confined in a narrow area is more adhesive and practically does not consist of any organelles. The structural elements of cytoskeleton are investigated here involve actin microphilamentous, as well as have more deeply located intermediate filaments and microtubules. Dense net of actin filaments associated with PM provide mechanical stability of cytoplasm surface layer. The association of actin filaments with febrile stabilizing proteins leads to formation of cross linking in the area of filaments crossing, which is responsible for the inflexibility of all submembrane layers. As mentioned earlier the alteration in the group of membrane compounds lipids and proteins depend on contractions generated by submembrane microphilaments. Such alterations take place by a energy requiring mechanism.[10] On the other hand actin filamentous net is able to contract because of short myosin aggregates.[11]

Proteins regulating the assembly kinetics of the cytoskeletal biopolymer F-actin are known to impact the architecture of actin cytoskeletal networks in vivo but the underlying mechanisms are not well understood.[12]

Some findings provide further evidence to support an emerging theme that cytoskeleton proteins play important roles not only for establishing membrane architecture and integrity but also for regulating the membrane protein constituents that influence the electrical properties of excitable cells.[13]

It must be noted that investigation of submembrane layer using only the method of immune fluorescence is not enough for studying structural organization of this layer as well as the structures alteration during pathological processes. The morphological studies of submembrane layer have become possible at electron microscopy resolution up to 10.000 – 20.000. Using the method of immune fluorescence microscopy, it was shown that this layer has an organized structure consisting of spherical structures, tubules and microfilaments nets.

MATERIALS AND METHODS

Reagents

Reagents used were crystalloid cardioplegic solution (Na 147 meq L^{-1}, K 19 meq L^{-1}, Ca 4 meq L^{-1}, Cl 155 meq L^{-1}, HCO_3 25 meq L^{-1}, glucose 0.2 % , pH 7.4, Mg 2 meq L^{-1}), powdered paraformaldehyde, OsO_4, Sodium cacodylate trihydrate, 96 % ethyl alcohol, acetone, Epon 812, Epon Hardener MNA, Epon Hardener DDSA, Epon accelerator DNP-30, uranyl acetate, sodium citrate, lead nitrate, photoplates. All reagent used were of analytical grade and purchased from Sigma Chemical Co. (USA).

Human Subjects

All procedures involving human subjects were approved by institutional review board/bioethical committee (Erevan State Medical University, RA) and conformed to the Legal Aspects of Research Ethics and Science in European Community directive (2001/20/EC), (IRB Approval YSMU Bioethical committee N7 by 26.04.2011).

In this study the myocardium of right atria of 10 patients with pulmonary arterial valve stenosis (PAVS) was investigated. The patients were divided into 3 groups depending on the systolic pressure of right ventricular: I group - mercury column pressure was up to 60 mm (2 patients); II group - mercury column pressure was from 60 to 100 mm (3 patients); III group - mercury column pressure was more than 120 mm (5 patients).

Biopsy material was collected during canulation process of cardiosurgical procedure of patients.

Animal studies

All procedures involving animals were approved by the Institutional Review Board\ Institutional Animal Care and Use Committee (H. Buniatian Institute of Biochemistry, Yerevan, NAS RA) and conformed to the European Communities Council directives (86\609\EC).

The material (dog myocardium) used in this study concerning PAVS was collected earlier.

For experiment involving inoculation by CCl_4, the liver of two-month-old male rates weighing 150-200 g was used. Liver toxicity was experimentally induced in Wistar male rat, weight 180-200 g, by intraventral injection of CCl_4 (3ml per each rat twice a week during 20 days).[14] The animals were maintained at the standard light and feeding conditions. A week after the last injection of CCl_4 animals were decapitated under light ether anesthesia.

Treatment of material

The bioptates taken during canulation (small pieces of the right atria) as well as at the end of experiment have immediately put in cold (4 ºC) mix of paraformaldehyde in a sodium cacodylate buffer and glutaraldehyde for 12 h with following post fixation in 1% OsO_4 solution for 2 h, dehydration in ascending series of spirits, saturation in a mixture of acetone and Epon resins of different proportions and pouring in gelatinous capsules into epon.

Obtaining of ultrathin slices and its treatment

The ultrathin slices (up to 500 Å) were made using ultracut LKB (Swedish) and Reichert (Austria). Ultrathin slices were double contrasted with uranyl acetate and sodium citrate and lead nitrate solutions.

Observation under TEM

The ultrathin slices were observed under the transmission electron microscope (Phillips CM 10) with a resolution x 20000.

Measurement of structures

The electronogramms the structures under investigation of patients and dog with valve stenosis of the pulmonary artery (VSPA), as well as the electronogramms of white rat inoculated by CCl_4 were measured by the Micro-ruler MR-1, Traceable and calculated by TED Pella ultrastructural size calculator.

Statistical analysis

Data were expresses as the mean ± S.E.M. All data were analyzed using a one-way analysis of variance (ANOVA) (SigmaStat 3.5 for Windows). Differences were considered as significant at $P < 0.05$.

RESULTS

Submembane layer of excitable cells, taken from cardiomyocytes of experimental animals, human myocardium during correction of congenital heart disease and liver hepatocytes of experimental animals, was taken as the objects for the investigation.

Examination under an electron microscope, with a resolution up to 20000, of cardiomyocytes of patients with congenital heart disease and valve stenosis of the pulmonary artery at a developed stage of disease where the process of hypertrophy takes place at the end of cytotomia process, showed the presence of three not very-large structures. These structures are in close contact to the

formed sarcolemma and to each other. Two of these structures are round-oval shaped with unchanged surface layer composed of thick filaments, each one of which in turn consists of up to three parallel thin filaments. The third structure lay between the first two and looks like leptofibrilla (Figure 1).

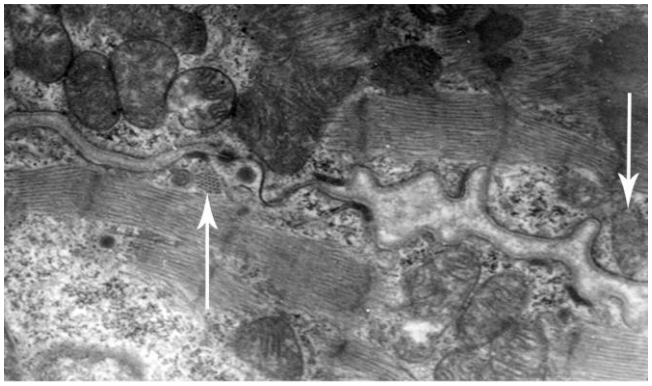

Figure 1. The ultrastructure of subplasmalemma of cardiomyocytes cytotomia of patients with VSPA**.** The presence of leptofibrilla in the centre between two round oval structures, supporting sarcolemma's arcade, is seen (x 10000).

An investigation of sarcolemma of two forming cells revealed the presence of thick short singular filaments in some parts of it, which could be residual networks.

As the destructive changes of CMC took place, the sarcolemma of scalloped windings and arcades with the destructively changed round-oval shaped structures lays one after another. These structures afforded basis for sarcolemma for its arcades and scalloped windings (Figure 2).

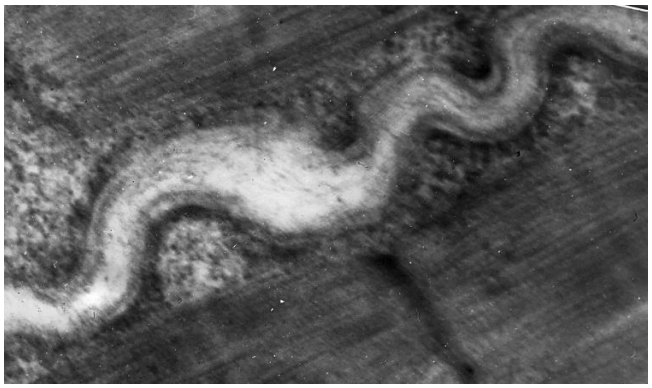

Figure 2. The ultrastructure of cardiomyocytes of patients with VSPA. The enlarged tubules with short vertical structures inside are presented. In sarcolemma's arcades are observed round-oval structures support sarcolemma (x 20000).

It must be mentioned that these structures have ability to change their sizes both in length and in width. The measurement of dimension of such structures was earlier reported.[15] It has been already shown, by TEM resolution up to 10000-20000, that these structures differ in size, depending on the injuring influence, leading to alternation in subsarcolemma layer thickness. In CMC of the above-mentioned heart disease these oval structures are up to 100-280 nm high.

At the same time small tubules are found in subsarcolemma layer of CMC closely connected to sarcolemma and composed of different short vertical structures as well as residues nets of thick filamentous. These tubules change their thickness, which in turn influence on the total thickness of subsarcolemmal layer (depending on pathological influence). The width of tubules ranges between 100-150 nm.

The experimentally induced stenosis of pulmonary arteries of dogs exhibited the presence of T-system's tubules in submembrane layer as well as noticeable alterations of thickness of T-system's tubules (Figure 3). The submembrane layer thickness varies from 50 to 100 nm.

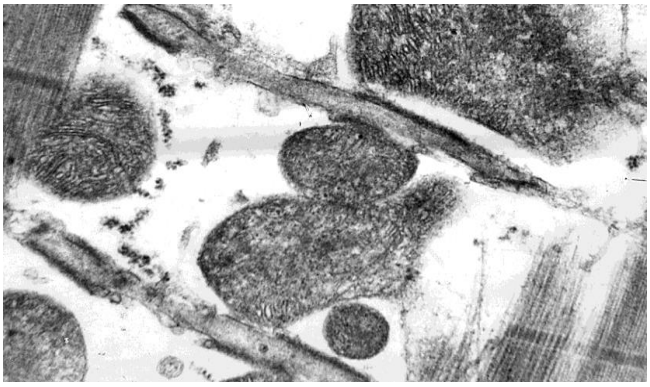

Figure 3. Ultrastructure of cardiomyocytes T-system in experimentally induced stenosis of pulmonary artery on dog model. The thickness of subplasmalemma of T-tubules is significant, as well as the presence of tubules (x 20000).

Studies of different type of cells (muscular and non muscular) have shown that as a response to pathological influence, there is a change in the thickness of submembrane layer. Such changes could be noted at electron microscope resolution up to 10000.

Inoculation by CCl_4 results in noticeable changes in hepatocyte submembrane layer thickness (Figure 4) as well as destruction of intracellular organelles resulting in the formation of shapeless aggregates consisting of mitochondria.

Figure 4. Rat liver hepatocytes inoculated by CCl_4. Significant increase in subcytolemma thickness are visible. Large round-oval structures as well as spherical structures are present (x 10000).

After repeated inoculation (twice per 20 days) of white rat liver by intraventricular injection of CCl_4, the round structures are found in submembrane layer, consisting of column of thin filaments stitched vertically by thick filaments. These structures are bound from outside by thick filaments (Figure 5). It could be suggested that a group of Mch are observed by us, however it is not like that.

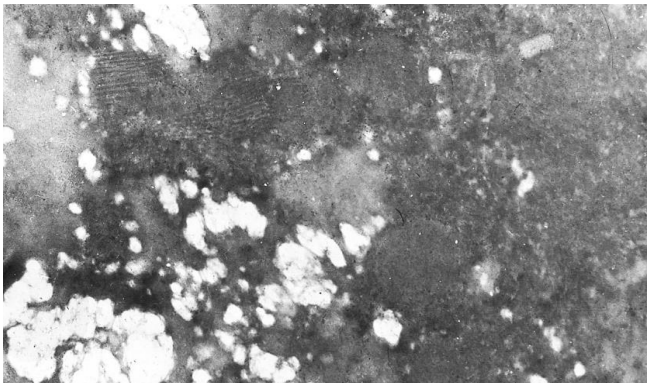

Figure 5. Rat liver hepatocytes inoculated by CCl_4 .Significantly enlargement of round oval structures are seen in large numbers (x 10000).

Prolongation of thin filaments from one side to another of the structure observed here is quite different from Mch cristae. These structure are about 480-650 nm in size. It must be noted that in hepatocytes the oval structures of the same size, as well as the shapeless masses consist of Mch, which are transformed by cristae into a type of honeycomb were found.[16]

ATP-ase activity of Mch in hepatocytes strongly decreased.[14] In the process of lyses of hepatocytes, intracellular organelles the subcytolemma layer is quite thick. The oval round structures different in size are found here. The size of these structures is up to 120-320 nm. The tubules and spherical structures consist of thick filamentous.

In a group with sodium thiosulfate injection before CCl_4 injection, the structures mentioned above up to 250-320 nm in size were also found. However the thickness of subcytolemma layer was not changed in equal measure. It could be explained by the fact that spherical structures composed of thick filaments are bigger in size compared to oval structures and are more sensitive to damaging influence.[17]

DISCUSSION

The basis of function of high specialty cardyomyocyts is the process of electromechanical linking. The coordination of all phases of contraction and relaxation of cardiomyocytes is provided by an ion transportation system. The main compounds of such system are - sarcolemma, sarcoplasmatic reticulum and mitochondria.[18] The structure of cardiomyocyte corresponds its main function. The process of electromechanical linkage takes place in it followed with further mobilization of all organelles used in this process. [19]

The data obtained from our previous studies have shown that sarcolemma's submembrane layer thickness changes primarily looks like an increasing of its electron density. Investigation of the comparison of electron high density and blurring areas of sarcolemma by the all perimeter of CMC of patients with different stages of CMC injures have shown that in a case when the prolongation of high electron density area is about 60% of sarcolemma's total length, some damaging processes are found in CMC organelles. Decreasing of this area's prolongation from 60-40% was accompanied by moderate destruction of organelles. When about 40% of total length of sarcolemma is thickened and the length of blurring areas is increased it leads to prolonged destructive changes of CMC.[20]

The cardiomyocyte has an intracellular scaffold, the cytoskeleton, which has been implicated in several cardiac pathologies including hypertrophy and failure.

The essential role of the submembrane cytoskeleton for membrane protein and cellular function is clearly illustrated by dysfunction in cytoskeleton elements in human disease.

It was earlier supposed that lateral part of cardiomyocyte salcolemma is free and that fixing of the free surface part of sarcolemma of cardiomyocyte to myofibril's on Z-line level is due to scalloped bulging at cell contraction.[19] However our studies of clinical and experimentally induced pathology have shown that submembrane layer of sarcolemma observed structures are usually not viewable at normal resolution of microscope (10000-20000), but are present in pathological samples.

These oval-round structures lay close to Z lines as well as could be observed in a space until M line. By the electron microscopic study singular structures are observed in a high quantity in sarcolemma in close contact with each other. The presence of such structures helps sarcolemma to move to scalloped bulging at cardiomyocyte contraction to form arcades at pathology.

These structures have ability to change their size which is mostly seen in reversible damages of cardiomyocytes caused by pathology.[15] As it was shown earlier defects in components of cytoskeleton affect the ability of the cell to compensate at both functional and structural levels in the long term.[21] The cytoskeleton plays the role in modulating both the electrical activity (through ion channels and exchangers) and mechanical (or contractive) activity of the adult heart. The limited visual data available suggests that the subsarcolemmal actin cytoskeleton is sparse in the adult myocyte. Cytoskeletal modulate an electro-mechanical activity in cardiac myocytes.[22] These filaments are likely to have important roles in mechanical support of ion channel function.[23]

Within epithelial cells, filamentous actin is concentrated at the plasma membrane. Its functions include structural support of the plasma membrane, establishing and maintaining cell polarity, regulation of membrane protein distribution and activity, and enhancing membrane vesicle trafficking. The actin cytoskeleton contributes the cellular pathogenesis in a number of disease states, it has been found to contribute significantly to cholangiocyte function and disease initiating structural and functional alterations in

ischemic bile ducts. The actin cytoskeleton plays a central role in the physiology and diseases of the intrahepatic bile duct.[24, 25] The important parts of choleostasis pathogenesis is decrease of hepatocyte membrane transporter, inhibition of Na^+, K^+-ATFaza and the membrane permeability, as well as destroying of hepatocyte cytoskeleton and interruption of vesicular transport.[26]

For current research of subplasmalemma layer of excitable and unexcitable cells at pathological process were chosen with different pathological conditions such as chronic pathology – narrowing of human pulmonary artery outlet and its experimental engineering on animal model, engineering of acute-chronic pathological process at rat liver using high toxical drug. As have shown the results of our study independently on pathology type both on human and animal models, submembrane layer responded by its thickness alteration and changes its structures size. The obtained data indicate that round oval structures and tubules are more stable structures compare with nets and are formed by thick filaments. At the same time it must be mentioned that under toxic influence the rate of change of size of round oval structures are more than that with the use of TiNa, which does not let the big reversal of these structures. It must be noted that at observed changes of subplasmalemma layer thickness, as well as returning of its structure to normal size need great amount of energy. However, if it takes place during the decrease of ATP-ase activity, as it was in inoculation by CCl_4, it will lead to subplazmalemma layer function disorder.[14] The process of reversibility of submembrane layer depends on energy status of cell, which can underline pathological process at tissue and organ as well.

CONCLUSION

At the bottom of the excitable and unexcitable cells plasmatic membrane thickness alteration lays changes of cell submembrane layer. Reversible and irreversible damages of its structures could be a key component in cell function disorders during pathological processes.

ACKNOWLEDGEMENT

Current work was performed by support of H. Buniatian Institute of Biochemistry Natl. Acad. Sci. of RA.

REFERENCES

[1]Avtsin, A. P., Shakhlamov, W. A., *M. Medicine*, **1979**

[2]Trump, B. F., Arstilla, A. U., *in: Principlet of Pathobiology*, Laria, M. T., Hill, R. B. (Ed) Oxford, University Press, Oxford **1971**, 955.

[3]Davidenko, O. A., *Abstract book on the issue of Histo-hematic barriers, All Union Meeting of Cardiology, Moskow*, **1978**, 255.

[4]Tsagareli, Z. T., *The book*: *Ultrastructural analysis of cardiac activity*, Ganatleba, Tbilisi, **1977**, 92.

[5]Sheremet'eva, G. F., *Abstract of Doctoral Thesis*, M., Moscow, All Union Scientific Center of Surgery) **1983**.

[6]Kukurtchyan, N. S., Aglintsian, T. S., *J. Blood Circ.*, Yerevan, **1990**, 23, 1.

[7]Terakawa, S., *Metabolic Regulation of Membrane Function, Armenian Academy of Sciences Publisher*, Yerevan, **1990**, 140.

[8]Karapetyan, G. R., Kukurtchyan, N. S., Kevorkian, G. A., *J. Hepatol. Int.*, **2011**, *5*, 333.

[9]Kukurtchyan, N., Karapetyan, G., Hovhannisyan, V., *10th Ann. Conf. Armenian Electron Microsc. Soc.*,, Yerevan, Armenia, **2001**, 70.

[10]Fulton, A., *EE Media*, 1987

[11]Molitoris, B. A., *Kidney Int.*, **2004**, *66*, 871–883.

[12]Falzone, T. T., Oakes, P. W., Sees, J., Kovar, D. R., Gardel, M. L, *J. Biophys.*, **2013,** *104*, 1709**.**

[13]Stagg, M. A., Carter, E., Sohrabi, N., Siedlecka, U., Soppa, G. K., Mead, F., Mohandas, N., Taylor-Harris, P., Baines, A., Bennett, P., Yacoub, M. H., Pinder, J. C., Terracciano, C. M. *Circ. Res.*, **2008,** *103*, 855.

[14]Margaryan, A. S., Badalyan, R. B., Abramyan, S. S., Simonyan, L. A., Batikyan, I. G., Simonyan, A. L., *Int. Symp. UNESCO "Problems Biochem., Mol. Radiat. Biol. Genetics,"* Yerevan, **2007**, 40.

[15]Kukurtchyan, N. S., Karapetyan, G. R., *Eur. Chem. Bull*, **2013**. *2*, 999.

[16]Karapetyan, G. R., *J. Med. Sci. Armenia*, **2008**, *48*, 60.

[17]Karapetyan, G. R., Kukurtchyan, N. S., Kevorkian, G. A., *FEBS Congress*, **2013**, 23.

[18]Novitski, A., *The way: Medical blog*, **2011**

[19]Bratus', W. W., Gawrish, A. S., *Manual of Cardiology.* Ed. by Kovalenko, V. N., Morion, Ukraine, **2008**.

[20]Kukurtchyan, N. S., *Int. Conf. Surgical Centre*, Yerevan, Armenia, **1994**, 48.

[21]Vatta, M., Faulkner, G., *Future Cardiol.*, **2006**, *2*, 467.

[22]Calaghan, S. C., Le Guennec, J. Y., *Prog. Biophys. Mol. Biol.*, **2004**, *84*, 29.

[23]Kee, A. J., Gunning, P. W., Hardeman, E. C., *J. Muscle Res. Cell Motility*, **2009**, *30*, 187.

[24]Doctor, R. B., Fouassier, L., *Semin. Liver Diseases*, **2002**, *22*, 263.

[25]Lee, H. T., Park, S. W., Kim, M., D'Agati, V. D., *Lab. Invest.*, **2009**, *89*, 196.

[26]Podimova S. D., *J. Clin. Perspect. Gastroenterol. Hepatol.*, **2010**, *3*, 17.

Received: 16.09.2014.
Accepted: 09.10.2014.